Physical Properties of Shear Oriented Cocoa Butter

by

Sarah E. Guthrie

A thesis
presented to the University of Waterloo
in fulfillment of the
thesis requirement for the degree of
Doctor of Philosophy
in
Physics

Waterloo, Ontario, Canada, 2008

I hereby declare that I am the sole author of this thesis. This is a true copy of the thesis, including any required final revisions, as accepted by my examiners.

I understand that my thesis may be made electronically available to the public.

ABSTRACT

Cocoa butter is a highly complex system of triacyglycerides which has been shown to crystallize in a markedly different fashion under the application of shear.

A rheometer insert was developed to enable the intact extraction of sheared samples for study of melting properties, crystal orientation and breaking stress[1].

Samples were created by ramping from 50°C at three different cooling rates (0.5, 1 and 2°C/min) to three different end point temperatures (16, 18 and 20°C), creating nine different temperature sets. Viscosities of the cocoa butter samples under shear were recorded during sample creation and large jumps in viscosity were identified as form II and form V crystallization. Comparison of crystallization times for the nine different temperature profiles allowed for the conclusion that over a shear range of 90 – 1000 s^{-1} there was no further appreciable shear acceleration of the form V transformation for the 16 and 18°C temperatures and only a slight increase up to 500 s^{-1} for the 20°C temperature.

Sheared samples were also examined with differential scanning calorimetry. Samples were examined for peak melting temperature on each of day 0, day 1, day 7 and day 28. Six of the nine different temperature conditions examined yielded a critical shear rate, above which the melting points of the samples were dramatically different than for low shear and no shear samples. For the day 0 and day 1 samples, above 500 s^{-1} the melting temperatures were ~2°C higher than for 360 s^{-1} and below. For the day 7 and day 28 samples, above 500 s^{-1} the peak melting temperatures were ~2°C lower than for the lower shear and no shear samples.

The orientation of sheared samples was also examined using x-ray diffraction. In all of the nine temperature sets, orientation was present for shear rates of 360 s^{-1} and higher.

Breaking stress measurements were performed on sheared and non-sheared samples. These tests showed results remarkably similar to those seen in the DSC tests, with a critical shear rate existing in six of the nine temperature sets, above which an increase in the breaking strength occurs.

Examination of samples on either side of the critical shear rate with x-ray diffraction yielded two distinct x-ray patterns leading to speculation that the application of high shear rates causes a change in the crystallization of cocoa butter leading to selective crystallization and the formation of a compositionally different form V crystal with fewer defects than its lower/no shear counterparts.

Acknowledgements

The author would like to gratefully acknowledge the following people for their guidance and assistance.

Stefan Idziak

Alejandro Marangoni

Gianfranco Mazzanti

James Benson

Table of Contents

Table of Figures

Glossary:

α	form II	
a	width of beam	m
β	Form V and VI	
b	distance between plates	m
β'	forms III and IV	
β-MPT	(β-memory point temperature	
β_V	form V	
C_S	Heat capacity	J/(kg°C)
d	interplanar spacing	Å
DSC	Differential Scanning Calorimeter	
$E_y(z)$	Young's modulus	Pa
Φ	real heat flow	J/s
F	Force	N
FWHM	Full width at half maximum	degrees
γ	form I	
$\dot{\gamma}$	shear rate	s^{-1}
g	gravity	m/s^2
h	distance between two plates/2	m
I	intensity of transmitted beam	
I	geometric moment of inertia	kg m^2
I_o	intensity of the incident beam	
λ	Wavelength	Å
L	length of beam	m
μ	linear absorption coefficient	1/m
M	bending moment	Nm
P	Pressure	
POP	1,3-palmitoyl-2-oleoylglycerol	
POS	1-palmitoyl-2-oleoyl-3-stearoylglycerol	
q	scattering angle in reciprocal space	Å $^{-1}$
θ	scattering angle	degrees
SOS	1,3-stearoyl-2-oleoylglycerol	
τ	shear stress	N/m^2
T	Temperature	C
t	thickness of beam	m
TAG	triacyglycerol	
U	velocity of upper plate	m/s
u	X component of velocity	m/s
v	Y component of velocity	m/s

w	Z component of velocity	m/s
ω	angular velocity	rad/s
x	thickness which x-ray beam passes through	m
y	position in y axis	
z	distance of element section dz from neutral plane.	m
η	Visocisty	Pa s
ρ	radius of curvature	m
σ	normal stress	Pa

1.0 Introduction

Cocoa butter, a highly complex system of triacyglyerols and other more minor components, has the distinction of being the main ingredient in one of the world's most beloved foods – chocolate. As such, there has been a great deal of research into its properties, both thermal and sensory. Published works date back to the early 1900s classifying up to six different polymorphic forms by means of thermal and x-ray analysis [2-7]. These different crystallographic structures vary in stability with the material gradually transitioning through unstable, lower melting temperature polymorphs over time to reach more stable forms.

The most favorable polymorphic form of cocoa butter for chocolate is called the form V polymorph. It will produce chocolate with a suitable melting temperature, high gloss and good snap[8]. Cocoa butter will reach the form V state if crystallized from the melt and left alone at room temperature, but it will take days and the size of the crystals formed will be very large. Chocolatiers know that stirring (the application of shear), along with a heating and cooling cycle will help the chocolate to enter a form V structure much more quickly. It is only in more recent times, however, that this qualitative knowledge has been quantified analytically[9-18].

It has been demonstrated through the use of x-ray accessible shear cells that the application of shear during a cooling ramp does indeed cause cocoa butter to accelerate its transition into the more stable form V structure[10, 11]. However, the shear rates and temperature ramps employed in some of these studies have differed considerably from those generally used for production purposes. That fact, as well as the use of x-ray diffraction, has led to the discovery that under certain conditions the cocoa butter

crystallites can be induced to align with one another, creating an oriented crystalline material[10]. Up to a point, the higher the shear rate, the higher the degree of orientation.

Thus, while the creation of a form V structure in a considerably reduced time would be very desirable, the effect of crystal orientation on the morphology and mechanical properties of a chocolate product is unknown.

Up to this point shear cells used to create aligned cocoa butter samples did not allow for samples to be extracted without melting. Therefore in order to investigate this shear induced orientation, a Couette insert for a rheometer was designed to be capable of splitting into two pieces, allowing for the intact extraction of a crystallized oriented sample[1].

During sample creation in the rheometer, viscosity data for a large number of shear rates, cooling rates and end point temperatures can be recorded. The viscosity data can be used to further examine the shear acceleration effect over a large range of temperature conditions and elucidate the effect of shear on the acceleration of the phase transformation. Once the sample is removed intact, pieces of it can be analyzed for melting temperature by using a differential scanning calorimeter, and then the orientation of all of the planes can be examined using x-ray diffraction techniques. The breaking stress of the samples can also be tested by use of a three-point bending apparatus.

In this way, the effects of orientation and shear on the physical properties of cocoa butter can be examined.

In this thesis background material on the composition and structure of cocoa butter as well as a brief survey of the literature in the field is presented, as well as

summaries of the relevant techniques of rheology, differential scanning calorimetry, x-ray diffraction and three-point bending.

A presentation and discussion of viscosity data attained in the split couette cell leads the results section. The samples are cooled from 50°C to 16, 18 or 20°C at 0.5, 1 or 2°C/min, creating nine different temperature conditions.

This is followed by peak melting temperature analysis over a period of 28 days. Melting temperature data for each shear rate is presented for day 0, day 1, day 7 and day 28 for each temperature condition.

The melting data is followed by the x-ray orientation studies, x-ray diffraction patterns of low and high shear samples and finally the peak breaking stress data.

A summary of the work and discussion of its implications and resulting working theories concludes the thesis.

1.1 Background

Interest in chocolate has been ongoing for over three millennia, yet the understanding of the physical structure of cocoa butter, its main component, is in its infancy. Since techniques of chocolate manufacture have been guarded with the utmost secrecy, it is difficult to gauge what is known and when the knowledge was acquired.

Published works date back to as early as 1900, when it was noted that there are large variations in melting temperature[19]. By 1940 it was known that cocoa butter has at least one stable and one unstable form[20]. Up to that point, the concept of studying a system of pure components to better understand the behaviour of cocoa butter had not been developed. However, parallel investigations into pure triacyglycerols, the main

component of cocoa butter, had been underway for some time. In fact, as far back as 1852, three different forms were reported for tristearin as well as other glycerides[21].

It is well known that the physical and chemical properties of vegetable fats principally depend on their triacyglycerol (TAG) components. The TAG composition, in conjunction with hydrocarbon chain length, fatty acids saturation and melting point give rise to a highly complex thermal behaviour.

Melting and crystallization of fats are phase transitions and for a fat such as cocoa butter the transition is generally explained in terms of fat polymorphism. Polymorphism in fats is defined as the capacity of the lipids to crystallize into several forms differing in structure and melting temperature.

Polymorphic variability of lipids, TAG in particular, is quite diverse. Generally, a simple, broad classification can be made according to three main forms, usually given as α, β and β'. It has also been found, however, that there are some cases where additional classification of a low stability form γ occurs, as well as subclasses of structures within a main form e.g. β_1 and β_2. Formation of these polymorphs for a given lipid material is mainly dependent on the temperature at which crystallization takes place, although other factors such as shear, cooling rate and fat content also play a role.

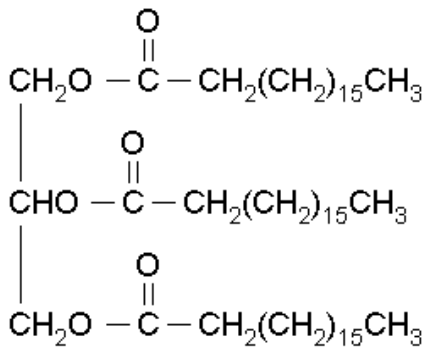

Figure 1: Typical TAG formation with a glycerol backbone and attached fatty acids. The TAG shown is triolein (OOO)

In cocoa butter 80% of the TAG fraction is monounsaturated, of which 95% is the sum of POP (1,3-palmitoyl-2-oleoylglycerol), SOS (1,3-stearoyl-2-oleoylglycerol) and POS (1-palmitoyl-2-oleoyl-3-stearoylglycerol). Each polymorphic form has a different typical x-ray diffraction pattern. This is due to the fact that the polymorphism itself results from the different possibilities of lateral packing of the fatty acid chains and the longitudinal stacking of molecules in lamellae. There are two main types of longitudinal stacking of TAG molecules corresponding to two or three (2L or 3L) fatty acid lengths.

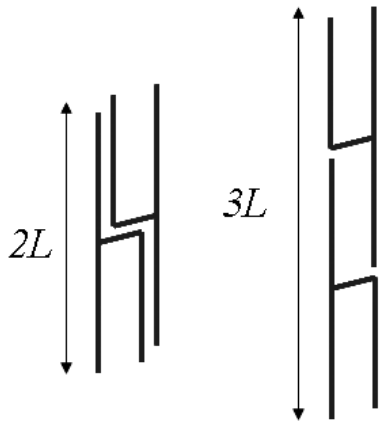

Figure 2: Representation of the two different types of longitudinal stacking for TAGs – the 2L and 3L fatty acid lengths.

The three main types of lateral packing modes for TAGs are illustrated in Figure 3. The α form has a hexagonal unit cell, the β' form has an orthorhombic unit cell and the β form was thought to be triclinic unit cell[22]. Recently however, the structures for the form V and VI of cocoa butter have been solved, and the β form has been shown to have a monoclinic structure – the difference being that the angles α and β are equal to 90° [23, 24].

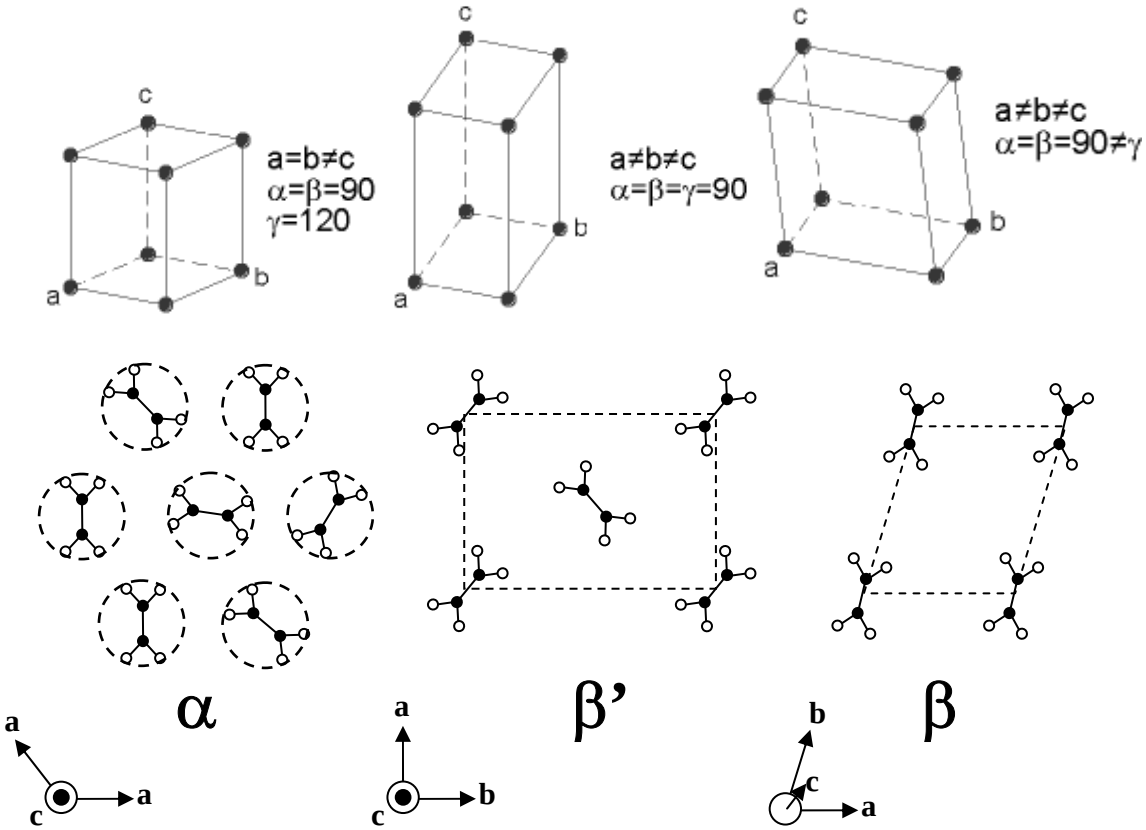

Figure 3: On the top from left to right, hexagonal, orthorhombic and monoclinic unit cells. Across the bottom two rows it is shown how TAGs pack into the unit cells [25].

The x-ray patterns are typically divided into two areas – low *q* (long spacings) and high *q* (short spacings). The short spacings relate to the small distances between the fatty acid hydrocarbon chains of the TAG. These spacings help define the polymorph since

differences originate from the different possibilities of lateral packing of the fatty acid chains. The long spacings relate to the longitudinal packing of molecules in lamellae (layers), making them merely the repeat distances in the direction roughly perpendicular to the lamellae.

Much work has been done to characterize the polymorphism of cocoa butter in particular, due to its huge importance to the chocolate industry. Obviously a great deal of knowledge about the thermal properties and phase behaviour is necessary to optimize production and product quality. There is, however, still a great deal of debate in many areas of the research. In 1951 Vaeck[2] proposed that while the three main polymorphs are α, β' and β sub-cells, in order of their increasing thermal stability, there is also a fourth crystalline form, often called γ, which is less stable than the α form. Again, in 1960 Vaeck proposed the same four polymorphs only with slightly different melting temperatures[20]. However, in 1966 it was proposed by Wille and Luton[4], through the use of x-ray diffraction in conjunction with DSC, that there were actually six different polymorphic forms I – VI, where I is the γ, II is the α, III and IV are both β' and V and VI are both β. The later works of Huyghebaert and Hendrickx[26], as well as Lovegren[27], also confirm six different forms using DSC techniques.

Form I (or γ) is extremely unstable and is obtained by cooling rapidly to very low temperatures[4]. At 0°C this form is stable for less than a minute, before beginning to change into form II.

Form II (or α) can be obtained by cooling at 2°C/min or by keeping form I at 0°C for over 15 minutes. Once formed, it will persist at 0°C for approximately 5 hours before changing to form III and has a melting temperature in the range 17-22°C. A range is

given due to cocoa butter composition variability, resulting in each cocoa butter having a slightly different melting temperature for each polymorph. Typical x-ray data shows strong identifying peaks at 49Å and 4.25 Å.

Form III (β') is formed, according to Wille and Lutton[4], by either crystallizing at 5-10°C or transforming the form II by storage at 5-10°C for 16 hours. Once formed it persists for 5 days at 5°C or less than 4 hours at 16°C, before transforming into form IV. Typical x-ray data shows identifying x-ray peaks at 49 Å, 4.25 Å and 3.86 Å.

Form IV (β') is achieved either via transformation from form III, or from solidification of the melt at 16-21°C. It is identified by strong x-ray peaks at 45 Å, 14.8 Å and 4.35 Å as well as two other medium intensity peaks at 4 Å and 3.8 Å. An accepted melting range for forms III and IV is 20-27°C.

Form V (β) can be identified by a large shift in 001 x-ray diffraction peak position to 63 Å, indicating a transformation from a double chain (2L) to a triple chain (3L) structure. It can be obtained via transformation from a less stable form. General methods involve cooling the melt to 25-28°C, reheating to 31-33°C and then either crystallizing at this temperature, or dropping again to lower temperatures. Wille and Lutton[4] also employed agitation of the sample to aid in crystallization. Once formed, the form V will persist for months if stored at normal room temperatures.

While form VI (β) has an almost identical x-ray pattern to form V, with subtle differences coming in the high q range only, there is a very noticeable change in melting temperature. Form VI is also the only form which cannot be crystallized directly from the melt. It forms only via a solid state transition from form V. An accepted melting range for forms V and VI is 29-34°C.

While these six polymorphic forms have, over the years, been confirmed by other authors[7, 26-29], debate still exists as to the validity of the distinction between the two β' forms III and IV, as well as the two β forms V and VI. Wille and Lutton[4] themselves admitted that they were unsure about form III, since an examination of a system comprised of the three largest TAG components failed to achieve a pure form III. Likewise, Chapman et al.[7], were not able to obtain a pure form III and merely extrapolate the data. Wille and Lutton[4] are, however, quite certain about the distinct form VI, citing evidence that a pure sample of POS behaved in a similar fashion[4].

In 1980, Merken and Vaeck[30] once again report only 4 polymorphic forms in cocoa butter, citing form III as being a mixture of II and IV and form VI being just form V, lacking the liquid TAG fraction. They claim that the DSC peaks allotted to other forms can be caused by various phenomena such as: separation of a solid solution in two phases, thermal inertia of equipment and exothermic transformations interfering with endothermic phenomena of fusion [30].

Support for this position has been steadily, if slowly, growing. While not all authors are ready to abandon form VI, many have at least begun to question the validity of a form III[6, 31-36]. Schlichter-Aronhime and Garti[31] for example have shown that depending on the cooling rate in a DSC experiment, different melting temperatures are achieved for a crystal structure thought to be form III. In fact, the slower the cooling rate, the higher the melting temperature - a temperature not corresponding to any known polymorph. As the melting point rises, the enthalpy value should increase, since it is dependent on temperature. However, under conditions of very slow cooling, the melting

curve does not show an increase in enthalpy. This implies that forms II and IV form a mixture with varying composition according to aging or cooling conditions[31].

The thermal characteristics of forms I to VI, as quoted previously, were determined by DSC (differential scanning calorimetry) heating curves. Many of these studies have been attempted, not only to classify the melting temperatures of the different polymorphs [4, 7, 26, 27, 30, 37, 38], but also to verify polymorphs and define the 'recipes' for making the different polymorphs, i.e., determining which forms the cocoa butter goes through on its way to becoming a form V, or under what conditions a form I appears [7, 12, 28-30, 32, 39-44].

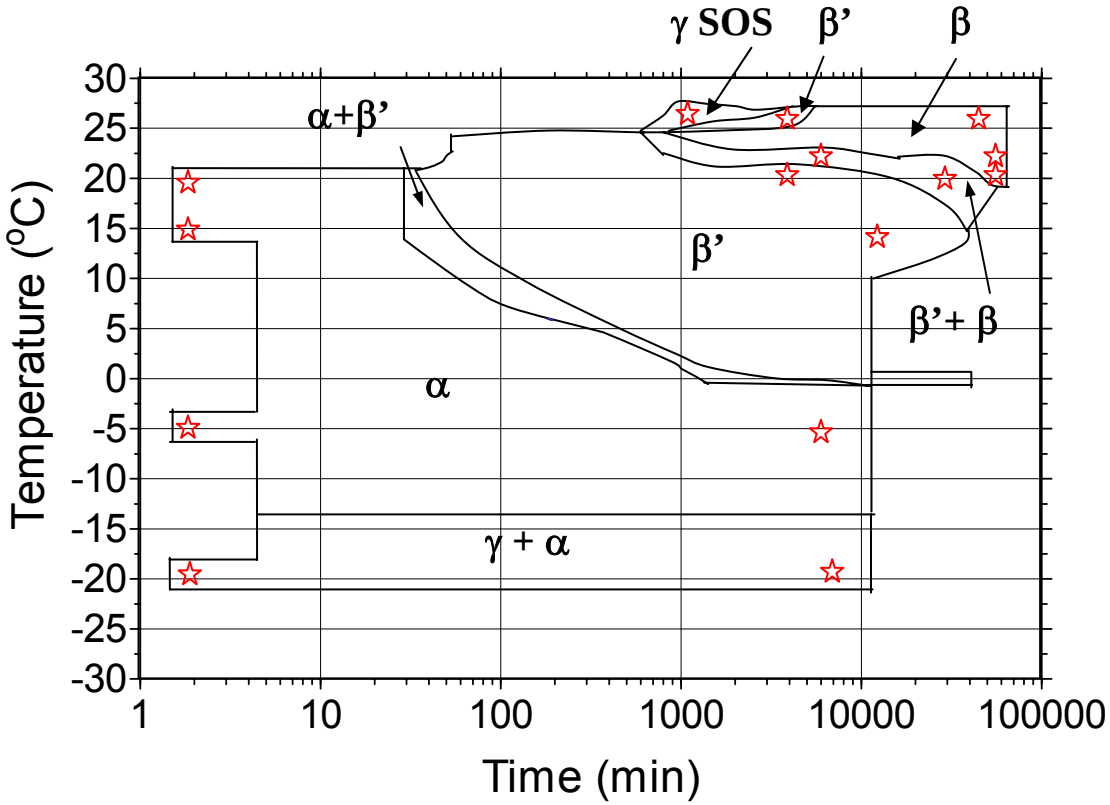

Figure 4: Time – temperature state diagram for the polymorphism of statically crystallized cocoa butter taken from Marangoni & McGauley [44]

A time-temperature state diagram can be seen in Marangoni and McGauley [44] (Figure 4) and a very similar state diagram is shown in van Malssen et al.[34]. Comparison of these figures demonstrates very aptly the differences in opinion of the degree of complexity found. While the basic structure of the diagrams is the same, Marangoni and McGauley [44] show many areas of mixed polymorphs, which are not present in the work of van Malssen et al.[34]. Van Malssen et al.[34] show the persistence of the γ, or form I, briefly above 0°C and also persisting for hours at –5°C. This clearly contradicts the work of Marangoni and McGauley[44] who show the γ only existing well below –10°C and then only in a mixed state.

A similar temperature-cooling rate state diagram was extrapolated by Spigno et al.[40] from x-ray work done by van Malssen et al.[36]. This state diagram shows the dependence of the polymorph on not only time and temperature, but also on the cooling rate. Van Malssen et al.[36] conclude that the polymorph is dependent on the final temperature of the cooling, only so long as the cooling rate is fast enough. If the cooling rate is too slow, higher melting temperature polymorphs are allowed to form.

Not only is there debate about the number of polymorphic forms and the methods of obtaining them, there is also a certain degree of variation in reported x-ray data and melting temperatures. This has been explained as being due to the large compositional variation between cocoa butters produced in different regions of the world[45]. In recent years melting temperatures have been adopted as a range, rather than a specific value, to incorporate this variation A large body of work is available which well defines this range [4, 7, 20, 30, 37].

Dating back to Wille and Lutton[4], very comprehensive x-ray data have also been gathered; due to the variations, however, a certain amount of cross referencing is required to decide which data are the most accurate. Tables 2-4 in Appendix 1 compare x-ray studies of the different polymorphs over the past 38 years. These tables include small q values (long spacings). While the high q range (referred to as the short spacings) are used more commonly, recently there has been more interest in the whole region[10, 29, 33, 46]. The short spacings are referred to as the fingerprint region, since the polymorphic form can be determined easily with these peaks alone. However, the long spacings are also useful, since they can also be used to identify the polymorph in most cases and may present valuable information about the different polymorphs and their phase transitions [33]. Appendix 2 shows typical synchrotron x-ray diffraction patterns of forms II-VI.

A key area of disagreement in the literature, with regard to x-ray identification, seems to be the identification of the form VI polymorph. While there are those who dispute its existence as a distinct polymorph[30-32, 35, 47], the transition to this state holds some importance to bloom studies (bloom being the disfiguration of chocolate's surface with a white growth) and hence identification still has some relevance. The literature also contains varying short spacing diffraction images of form VI. A figure in van Langevelde et al. [45] shows short spacings of different polymorphs. Forms III and IV are not listed separately since this author agrees with Schlicher-Aronhime[31] and believes it to be only one phase. Form VI is shown as it is typically identified elsewhere[4, 5, 33, 43, 48-50], however van Malssen et al.[34] present a comparison of a form V and VI that shows a remarkably different form VI. Forms V and VI (β_V and β_{VI})

do not generally differ from each other anywhere other than the short spacings, yet here, peaks above 5 Å are markedly different, while the short spacings themselves do not differ significantly from each other. Hence, the form VI depicted here more closely resembles a form V than a form VI.

This discrepancy in identifying form VI may be explained, in part, by considering the work of van Langevelde et al. [45]. This work compared the form VI of a wide variety of different cocoa butters from around the world. It was found that, depending on the origin of the cocoa butter; the x-ray pattern of a form VI could very easily resemble that of a typical form V, leaving the melting point as the only way to distinguish it as a form VI. The same work also demonstrated that the x-ray pattern also changes depending on the crystallization method used. That is to say, samples reached via the memory effect or the isothermal method had different x-ray patterns for form VI within the same cocoa butter sample. Form V was also seen to be different, although less so. They conclude that it is then impossible to achieve a form VI that can be considered to be typical of all cocoa butters.

Another comment of some interest is made by Adenier et al.[50], who state that it is impossible to have a pure form VI, that is form V will always be present. An examination of the x-ray patterns of these two forms shows that, indeed, the peaks of form V are always contained within form VI.

Other authors have also undertaken, for the purpose of bloom studies, to show the process of transformation between forms V and VI. To this end they have either mathematically[45] or physically[49, 51] combined different combinations of forms V and VI to achieve x-ray diagrams showing the progression of the change. These works

elucidate the possibility that some of the form VI data found in the literature may in fact more closely resemble a mixture of forms V and VI.

A discrepancy, perhaps related, can be seen in the work of Loisel et al. [29], which shows a form V x-ray image depicting a comparison of cocoa butter, to both its high melting fraction (composed of those TAGs contained in cocoa butter with a high melting point) and its low melting fraction (low melting point TAGs). While a very large x-ray diffraction peak can be seen at 44.4 Å ($q = 0.143$ Å^{-1}) for the high melting fraction, a definite peak is still apparent in the pattern shown for the regular cocoa butter sample. This peak is unusual since it has never been previously reported in a form V, but has been seen repeatedly by this author in form VI. They also report a higher than usual melting point for this structure (37°C), and explain it as being possibly due to a lipid segregation or phase separation, stating that the peak position corresponds to a tristearin (SSS) peak.

Mazzanti et al.[11] also report possible phase separation of the β_V under conditions of low shear. They show a peak appearing at $q=0.179$ Å^{-1}, which they claim to be the 002 peak of a spacing 70.2 Å, which would be consistent with a phase separation rich in SOS and POP[11].

These phase separations do much to underscore the comments of Merken and Vaeck[30] and Schlichter-Aronhime[31], showing that fractionation is a very real occurrence and cannot be overlooked in studies of polymorphism.

Another interesting phenomenon in cocoa butter polymorphism is called the memory effect. Without it, form V (β) is generally only obtained via a phase transformation from form IV (β'). It has been demonstrated, however, that it is possible to have the β_V easily obtained from the melt if there is a "β-memory effect". This is due

to the fact that if the cocoa butter is not melted sufficiently, even a few form V or VI crystallites persisting in molten cocoa butter are capable of causing complete form V solidification of the sample [4, 7, 33, 35, 45]. While studies by Chapman et al.[7] observe a form IV crystallizing from the melt due to the memory effect, most have seen the emergence of the form V [4, 7, 33, 35, 45].

Work by van Malssen et al. [35] defines the β-MPT (β-memory point temperature) as the temperature to which cocoa butter has to be heated to prevent recrystallization into the β_V within 45 minutes when cooled to 25°C (recall that the β melting range is 25-28°C). The authors present results for a wide variety of different cocoa butters which suggest that the highest of the β-MPT is 38°C. This result draws attention to the huge range of values used throughout the literature to guard against the memory effect. Some authors heat their samples to as high as 110°C for up to 2 hours[37, 52, 53], some to 80°C for 20[16] or 30 minutes[54], some to 70°C for 10 minutes[38], others to 50°C for 1 hour[55] and others to only 10°C above the melting point of the specific polymorph[56].

This inconsistency in the literature and the lack of acceptance of a lower melting temperature can, perhaps, be linked to the work being done on seed crystals[37, 47, 52, 57-60]. In 1989, Davis and Dimick[61] said that some minor components such as glycolipids, phospholipids and saturated triacyglycerols, may serve as seed crystals and promote the crystallization of the cocoa butter. They also showed that the seed crystals have a very high melting temperature (above 60°C) and concluded that a unique composition was responsible, rather than a different polymorph[37]. In 1991 Arruda et al.[57] showed that if the very first seeds of crystal growth are extracted from the melt

and isolated, those crystals are different in composition from the original cocoa butter and have a melting temperature of up to 70°C. They focused on the phospholipid composition of the cocoa butter and showed that the seed crystals contained 4% phospholipids while the original cocoa butter contained 0.34%. Their explanation for this is that a phospholipid head contains about 10 water molecules. Below a certain energy level these heads will be drawn together to form nucleation sites[57]. Looking also at the TAG content, Chaiseri and Dimick[52] saw that early seed crystals had high concentrations of complex lipids, saturated TAGs, saturated fatty acid rich diacylglycerols and monoacylglyercols and that the rapidly nucleating seed crystals had higher concentrations of SOS than their original cocoa butter.

These studies make it clear that there are parts of the cocoa butter which may not melt at the β-MPT of 38°C given by van Malssen et al.[35], and their condition of "preventing recrystallization into the β_V within 45 minutes when cooled to 25°C" may not be applicable in all conditions.

Accelerating the transition into the β or form V via the memory effect, and other means, is part of another large area of cocoa butter research. Form V has always been a huge part of research into cocoa butter due to its importance to the chocolate industry. This form has the desired melting temperature, mouth feel, and glossy appearance. Achieving the desired form V in as little time as possible has always been a goal of research into the polymorphism of cocoa butter.

As far back as the 1950s, it was observed that applying shear (or agitation) to chocolate or cocoa butter causes it to crystallize at a much faster rate[1, 9-18, 20, 62-65].

Dating back to 1985, Ziegleder [13] observed that by applying shear to cocoa butter, it was induced to convert from form IV to form V. This work has been continued more recently by several different groups[1, 9-12, 14-18, 63].

Stapley et al. [12] use a temperature controlled shear cell before reheating samples enough to transfer them to a DSC. They report that high melting point forms were achieved as long as the shear rates were high enough, the tempering time was long enough and the re-warming temperature was low enough. Due to the nature of their experiment, this seems to indicate that form V was achieved in the shear cell, and then reformed in the DSC via the memory effect.

Bolliger et al. [14, 15] use a rotor to apply shear to chocolate as it is tempered. They report that in a comparison of methods, the same quality of chocolate crystallization can be achieved much more quickly by applying shear. They also report that changes in shear significantly influence viscosity and melting enthalpy.

MacMillan et al. [9] report that the use of shear shortens the length of time to reach form V by allowing form IV to be bypassed and form V reached from form III. The highest shear rate used was 12 s^{-1}, but the trend observed was that an increase in shear shortened the induction time.

Mazzanti et al.[10, 11], however, report shear rates of 90 to 1440 s^{-1}. While they also report a shortened induction time via a transition directly from form II to form V, it is surprisingly in a longer time than that reported by MacMillan et al. [9] (20 minutes as compared to 2 minutes). This can, in part, be explained by differences in sample volume and vast differences in cooling rate.

The difference in induction times between the work of Mazzanti et al.[10, 11] and MacMillan et al.[9] could also, perhaps, be related to the work of Savage and Dimick[53]. They show that the induction time of cocoa butters vary depending on their origin. MacMillan et al. [9] list their cocoa butter as being of Ghanian origin, while the origin of the Mazzanti et al.[10, 11] cocoa butters are unknown. It can be seen in the more recent work of Mazzanti et al.[10, 11] however, that the two different cocoa butter samples they employed also behaved differently from each other.

It should also be noted that while MacMillan et al. [9] report no orientation due to shear, a very obvious orientation, in both forms II and V, is apparent in the work of Mazzanti et al [10, 11]. The different planes examined in the two different experiments explain this discrepancy, since orientation was not observed by Mazzanti et al. [10, 11] in the plane examined by MacMillan et al. [9]

Mazzanti et al. [66] also expand on their shear work and develop a descriptive model. They propose that the crystallites grow layer upon layer of slightly different composition and that the shear rate and temperature applied define these compositions. Simultaneously, the shear and temperature would define the crystalline interface area available for secondary nucleation by promoting segregation and affecting the size distribution of the crystallites. The combination of these factors – composition, area and size distribution – favours dramatically the early onset of β_V under shear and determines the proportions of forms II, IV and V after the transition.

Also investigating the effects of shear are Toro-Vasquez et al.[16]. They use DSC techniques in conjunction with rheology to monitor the crystallization process under shear. While no conclusive x-ray data is offered, they report a shear rate effect that

favored β crystallization at temperatures of 19, 22, and 26.5°C, for rpm values of 120 and 400 rpm[16].

The work of Sonwai et al. [18] shows, among other things, work done with a microscope shear cell. Shear rates of 3-500s^{-1} with a ramp of 50 to 20°C at 5°C/min were examined and a decrease in the size of the crystallites as well as an increase in their number was reported. This means that the application of shear acts to decrease the size of crystals formed, yet increases the number of nucleation events.

The work of Dhonsi et al. [17] investigated shear rates of 1-50s^{-1} and crystallization temperature of 13, 17, 20 and 23°C. The found that for the lower temperatures, crystallization was fast, independent of shear rate. Only the highest temperature of 23°C yielded a shear dependency of the crystallization time, with these samples crystallizing faster than those sheared at 20°C.

Another method of accelerating the formation of form V is the application of ultrasonics. Higaki et al. [67] report that the application of ultrasonics (20 Hz, 100W) accelerates the formation of form V. A 3 second sonication raised the temperature of the sample from 32.3 to 32.9°C and when cooled to 20°C and examined with x-rays showed form V. A 9 second application, on the other hand, raised the sample temperature to 34.3°C and caused the formation of both forms II and V. A 15 second application raised the temperature to 36.2°C and resulted in a sample of only form II. While the sonication process does accelerates the formation of form V, it does so only for very short application times, since the use of ultrasonics raises the temperature of the cocoa butter through acoustic energy and causes the formation of mixed polymorphs.

Work with seed crystals to accelerate the transition had begun by the 1960s [3]. The basic concept of the research is that crystals are added to the melt and are then used as nuclei for crystal growth, similar to what happens with the memory effect. Giddey and Clerc[3] showed in 1961 that crystals of SOS and POS could be used to seed cocoa butter and accelerate the transition into a stable form. Later, Koyano et al. [60] experimented with adding seed crystals of a fine crystal powder to dark chocolate. They conclude that the addition of the β_2 form of BOB (1,3-dibehenoyl-2-oleoyl-glycerol) accelerates the transition to form V. Hachiya et al.[58] have also demonstrated that the addition of seed powders of form III, V and VI greatly accelerate the transition to form V, with powders of form VI being the most effective. They do, however, caution that the polymorphic form of the cocoa butter was more greatly influenced by the crystallization temperature than the seed crystal[58].

The six forms of cocoa butter, have been extensively studied visually via microscopy[2, 20, 28, 39, 42, 44, 47, 50, 54, 68-73]. The work of Hicklin et al.[28] for example, not only characterizes the six polymorphs via x-ray diffraction, but also shows images of them all. From these works it is clear that all six forms have a distinct visual structure.

Hicklin et al.[28] show that form I has no distinct morphology, form II has ordered lamellae, form III has protruding tubular crystals, form IV has densely packed needle-like crystals, form V has multilayered crystals, regular in shape and form VI has crystals protruding from a matrix of more regularly shaped crystals[28].

Marangoni and McGauley[44] on the other hand clearly demonstrate that the visual appearance of many of the polymorphic forms is highly dependent on the

crystallization temperature and the amount of time allowed for crystallization. They show that the γ and the α are granular in appearance regardless of the length of crystallization time or crystallization temperature. The microstructure of the β' polymorph, on the other hand, varied substantially depending on the crystallization time and temperature. Generally, the higher the temperature and the longer the time, the more deviation was seen from the granular structure, with first crystal clustering and then ~25μm crystallites with a needlelike appearance. Thus, both temperature and thermal history will affect the microstructure of the β' form. The β polymorph also displayed different microstructures. After incubation for 4-5 weeks at 20 and 22°C the sample no longer displayed uniform morphology – large microstructures (600 μm to 2 mm) were also observed. After 4 weeks at 20°C, a granular morphology was the predominant structure of the continuous phase, but the larger microstructures had a featherlike appearance and were visible to the naked eye. It was concluded that the phase transition from the β' form to the β polymorph usually leads to the formation of the large microstructures [44].

The mechanical properties of cocoa butter[54, 74-76] are also extremely important as the hardness of a fat is strongly influences the perceived texture of a food product[54]. When crystallizing, cocoa butter forms a three-dimensional crystal network stabilized by van der Waals forces[77]. The strength of this network has been related to several different properties. DeMan noted in 1976 that the solid fat content (SFC) will strongly influence the mechanical behavior of a fat[78]. Further to that, he later notes that the macroscopic properties of the network are influenced also by its chemical composition, the polymorphic state, the crystallite size and shape and the spatial

distribution of the mass of the network[77]. Brunello et al. [54] confirm that the mechanical properties of cocoa butter are not only governed by the amount of solid fat present in the crystal network, but also by the structure of the network. Polymorphism was found to strongly influence the mechanical properties indirectly via its effects on the microstructure of the material[54]. The work of Campos et al.[79] with milk fat and lard also makes these points, but goes on to show that networks with large particles and more heterogeneously distributed mass are softer fats, whereas smaller particles and a more homogenous distribution of mass result in a firmer fat.

Clearly, while there is huge body of research into many aspects of cocoa butter properties and polymorphism, understanding of the mechanisms and underlying processes is limited in part due to the wide diversity in the composition of different cocoa butter samples and the complicated interactions of the many different TAGs contained therein.

As cocoa butter research progresses, it is clear that while many questions can and have been answered, the answers themselves lead us into a much more complicated, multidimensional world of cocoa butter polymorphism. We can see that the cooling rate, shear rate, temperature, time and composition lead to different phase separations and polymorphs, and all play a role in defining morphology and structure.

1.2 Rheology

1.2.1 Fluid Mechanics

If we consider a system of a Newtonian fluid contained between two infinite parallel plates, one at rest and one moving with velocity *U*, the fluid will not slip at the walls and if the pressure is constant then the velocity distribution is a linear one,

$$u = U\frac{y}{b} \qquad \textbf{(1)}$$

where *u* is the velocity at a given y position and b is the distance between the plates. The situation of one moving wall and one stationary wall is known as Plane Couette Flow.

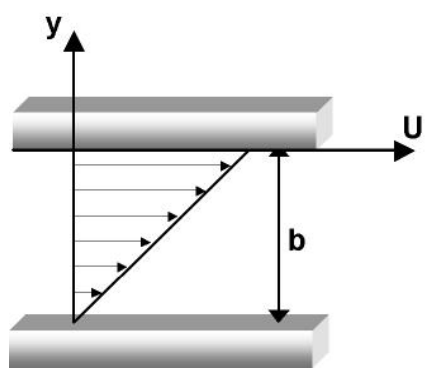

Figure 5: Linear velocity distribution for Newtonian fluids between parallel planes, one of which moving with velocity U

The shear stress is then defined as

$$\tau = \eta\frac{U}{b} \qquad \textbf{(2)}$$

or more generally

$$\tau = \eta \frac{\partial u}{\partial y} \tag{3}$$

where η is the shear viscosity. The shear rate is defined as

$$\dot{\gamma} = \frac{U}{b} = \frac{\partial u}{\partial y} \tag{4}$$

and shear viscosity is defined as

$$\eta = \frac{\tau}{\dot{\gamma}} \tag{5}$$

Equation (5) applies for a Newtonian fluid, but complex fluids (fluids involving larger molecules than Newtonian fluids) have a viscosity which is shear dependent. The shear stress for a non-Newtonian fluid depends on the applied shear rate causing a steady-state shear viscosity dependent on shear.

$$\eta(\dot{\gamma}) = \frac{\tau(\dot{\gamma})}{\dot{\gamma}} \tag{6}$$

To incorporate viscous fluid effects into the differential analysis of Newtonian fluid motion we must incorporate shearing stresses (a shear stress is a stress component that acts tangentially). The normal differential equations of motion are

$$\rho g_x + \frac{\partial \sigma_{xx}}{\partial x} + \frac{\partial \tau_{yx}}{\partial y} + \frac{\partial \tau_{zx}}{\partial z} = \rho\left(\frac{\partial u}{\partial t} + u\frac{\partial u}{\partial x} + v\frac{\partial u}{\partial y} + w\frac{\partial u}{\partial z}\right) \tag{7}$$

$$\rho g_y + \frac{\partial \tau_{xy}}{\partial x} + \frac{\partial \sigma_{yy}}{\partial y} + \frac{\partial \tau_{zy}}{\partial z} = \rho\left(\frac{\partial v}{\partial t} + u\frac{\partial v}{\partial x} + v\frac{\partial v}{\partial y} + w\frac{\partial v}{\partial z}\right) \tag{8}$$

$$\rho g_z + \frac{\partial \tau_{xz}}{\partial x} + \frac{\partial \tau_{yz}}{\partial y} + \frac{\partial \sigma_{zz}}{\partial z} = \rho\left(\frac{\partial w}{\partial t} + u\frac{\partial w}{\partial x} + v\frac{\partial w}{\partial y} + w\frac{\partial w}{\partial z}\right) \tag{9}$$

where σ is the normal stress (a stress component that acts perpendicularly) and τ is the shear stress. The first subscript indicates the direction of the normal to the plane the stress is acting on and the second indicates the direction of the stress. g_x, g_y and g_z are components of gravity; ρ is the density of the fluid element; and u, v, and w are components of velocity in the x, y and z directions respectively.

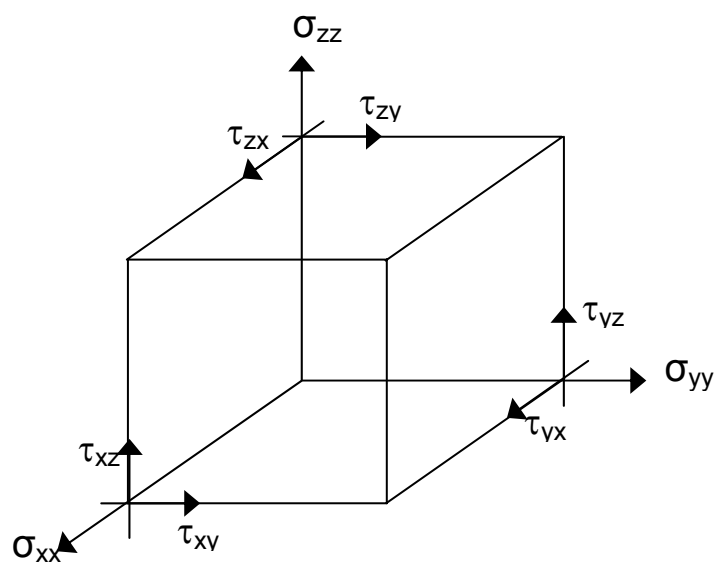

Figure 6: Three-dimensional stress components on a fluid element

For incompressible, viscosity-constant, Newtonian fluids, the normal and shear stresses are

$$\sigma_{xx} = -\mathrm{P} + 2\eta \frac{\partial u}{\partial x} \quad \textbf{(10)}$$

$$\sigma_{yy} = -\mathrm{P} + 2\eta \frac{\partial v}{\partial x} \quad \textbf{(11)}$$

$$\sigma_{zz} = -\mathrm{P} + 2\eta \frac{\partial w}{\partial x} \quad \textbf{(12)}$$

$$\tau_{xy} = \tau_{yx} = \eta\left(\frac{\partial u}{\partial y} + \frac{\partial v}{\partial x}\right) \quad \textbf{(13)}$$

$$\tau_{yz} = \tau_{zy} = \eta\left(\frac{\partial v}{\partial z} + \frac{\partial w}{\partial y}\right) \quad \textbf{(14)}$$

$$\tau_{zx} = \tau_{xz} = \eta\left(\frac{\partial w}{\partial x} + \frac{\partial u}{\partial z}\right) \quad \textbf{(15)}$$

where P is the pressure and η is the viscosity.

When these stresses are substituted into the normal differential equations of motion they result in the Navier-Stokes equations, using the simplifying continuity equation $\frac{\partial u}{\partial x} + \frac{\partial v}{\partial y} + \frac{\partial w}{\partial z} = 0$.

$$\rho\left(\frac{\partial u}{\partial t} + u\frac{\partial u}{\partial x} + v\frac{\partial u}{\partial y} + w\frac{\partial u}{\partial z}\right) = -\frac{\partial P}{\partial x} + \rho g_x + \eta\left(\frac{\partial^2 u}{\partial x^2} + \frac{\partial^2 u}{\partial y^2} + \frac{\partial^2 u}{\partial z^2}\right) \quad \textbf{(16)}$$

$$\rho\left(\frac{\partial v}{\partial t} + u\frac{\partial v}{\partial x} + v\frac{\partial v}{\partial y} + w\frac{\partial v}{\partial z}\right) = -\frac{\partial P}{\partial y} + \rho g_y + \eta\left(\frac{\partial^2 v}{\partial x^2} + \frac{\partial^2 v}{\partial y^2} + \frac{\partial^2 v}{\partial z^2}\right) \quad \textbf{(17)}$$

$$\rho\left(\frac{\partial w}{\partial t} + u\frac{\partial w}{\partial x} + v\frac{\partial w}{\partial y} + w\frac{\partial w}{\partial z}\right) = -\frac{\partial P}{\partial z} + \rho g_z + \eta\left(\frac{\partial^2 w}{\partial x^2} + \frac{\partial^2 w}{\partial y^2} + \frac{\partial^2 w}{\partial z^2}\right) \quad \textbf{(18)}$$

This can be simplified to

$$\rho\frac{D\vec{V}}{Dt} = -\vec{\nabla}P + \rho\vec{g} + \eta\nabla^2\vec{V} \quad \textbf{(19)}$$

where

$$D = u\frac{\partial}{\partial x} + v\frac{\partial}{\partial y} + w\frac{\partial}{\partial z} + \frac{\partial}{\partial t} \quad \textbf{(20)}$$

If we now consider flow between two horizontal infinite parallel plates, then in this geometry we regard the flow to be in the x direction, parallel to the plates with no

velocity in the y or z direction. It then follows from the continuity equations that $\frac{\partial u}{\partial x} = 0$. So, we can see that there would be no change in velocity, u, in the z direction for infinite planes and for steady flow $\frac{\partial u}{\partial t} = 0$. Therefore u = u(y).

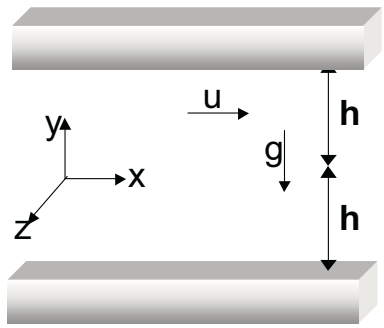

Figure 7: Geometry involved in flow of fluid through two parallel plates

If these conditions are then used in the Navier-Stokes equations, they reduce to

$$0 = -\frac{\partial P}{\partial x} + \eta\left(\frac{\partial^2 u}{\partial y^2}\right) \quad \textbf{(21)}$$

$$0 = -\frac{\partial P}{\partial y} + \rho g \quad \textbf{(22)}$$

$$0 = -\frac{\partial P}{\partial z} \quad \textbf{(23)}$$

with g_x and g_z set to zero and g_y set to –g.

Solving these equations, keeping in mind the boundary conditions, gives the velocity distribution as

$$u = \frac{1}{2\eta}\left(\frac{\partial P}{\partial x}\right)(y^2 - h^2) \quad \textbf{(24)}$$

This is called Poiseuille flow. If the flow is due to the motion of the plate only then the flow is called Couette flow.

We can expand on this and consider flow between concentric cylinders. We will use the cylindrical version of the Navier Stokes equations and we can consider that there is no velocity in the r or z directions, and the velocity is in the theta direction only. So if we take the theta component of the Navier Stokes equation:

$$\begin{aligned}&\rho\left(\frac{\partial v_\theta}{\partial t}+v_r\frac{\partial v_\theta}{\partial r}+\frac{v_\theta}{r}\frac{\partial v_\theta}{\partial \theta}+v_z\frac{\partial v_\theta}{\partial z}+\frac{v_r v_\theta}{r}\right)\\&=-\frac{1}{r}\frac{\partial P}{\partial \theta}+\eta\left(\frac{\partial^2 v_\theta}{\partial r^2}+\frac{1}{r}\frac{\partial v_\theta}{\partial r}+\frac{1}{r^2}\frac{\partial^2 v_\theta}{\partial \theta^2}+\frac{2}{r^2}\frac{\partial v_\theta}{\partial \theta}-\frac{v_\theta}{r^2}\right)\end{aligned} \tag{25}$$

Then we can reduce it to

$$0=\frac{\partial^2 v_\theta}{\partial r^2}+\frac{1}{r}\frac{\partial v_\theta}{\partial r}-\frac{v_\theta}{r^2} \tag{26}$$

or

$$\frac{d^2 v_\theta}{dr^2}+\frac{d}{dr}\left(\frac{v_\theta}{r}\right)=0 \tag{27}$$

Integrating twice will then give

$$v_\theta=\frac{A}{2}r+\frac{B}{r} \tag{28}$$

We can then apply boundary conditions. In our Couette cell, the inner cylinder is kept fixed, hence at $r=r_1$, $v_\theta=0$ and at $r=r_2$, $v_\theta=r_2\omega$. Therefore we can find that

$$A=2\frac{r_2^2\omega}{r_2^2-r_1^2}\text{ and }B=-\frac{r_1^2 r_2^2\omega}{r_2^2-r_1^2} \tag{29}$$

So, this gives a velocity distribution of

$$v_\theta = \frac{r_2^2 \omega}{r_2^2 - r_1^2}\left[r - \frac{r_1^2}{r} \right] \tag{30}$$

The shearing stress on the inner cylinder can also be calculated from

$$\tau_1 = -\left[\eta r \frac{d}{dr}\left(\frac{v_\theta}{r} \right) \right]_{r=r_1} = -\frac{2\eta r_2^2 \omega}{r_2^2 - r_1^2} \tag{31}$$

1.2.2 Rheometry

Rheology can be defined as the study of the flow and deformation of matter. Sir Isaac Newton found that when a pressure was applied to a fluid, it flowed at a precise rate and that the rate was proportional to the magnitude of the applied pressure. This is the essence of rheology and is expressed in Newton's Law, which states that the shear stress, τ, is proportional to the strain rate (the rate of change of strain with respect to time), $\frac{d\gamma}{dt} = \dot{\gamma}$. Here strain is defined as a deformation of a material under an applied force. The constant of proportionality is the viscosity η and

$$\tau = \eta \dot{\gamma} \tag{32}$$

From this equation it can be seen that the viscosity is readily obtainable by measuring the shear stress and strain rate.

The Advanced Rheometry Expansion System (or ARES) from TA Instruments is a controlled strain rheometer which is capable of subjecting a sample to either a dynamic (sinusoidal) or steady (linear) shear strain, then measuring the resultant torque exerted by the sample in response to the strain. Strain is applied by the motor and a transducer measures the resulting torque.

For our experiments only the steady shear strain is used, with the outer cylinder of the couette cell constantly rotating and subjecting the sample to a steady shear rate for the duration of the experiment. The measured torque is then converted into shear stress and combined with the shear cell geometry and applied strain to produce a measurement of viscosity.

1.3 Differential Scanning Calorimetry

Differential Scanning Calorimetry (DSC) is a technique for measuring the difference between the heat flow rate to a sample and to a reference sample while they are subjected to identical temperature environments of heating or cooling [80].

The measurement of the difference in heat flow rate can only be accomplished during a heating or cooling ramp since, barring chemical reaction heat flow rates, a temperature ramp is required for a heat flow.

There are two basic types of DSCs: the Heat Flux DSC and the Power Compensation DSC. In power compensation DSC the temperatures of the sample and the reference are controlled independently using two different furnaces. The temperatures are made identical by varying the power input to the two furnaces. The energy required to do this is then a measure of the enthalpy or heat capacity change in the system. In heat flux DSC, the sample and the reference are connected by a low resistance heat flow path and the assembly is enclosed in a single furnace. Enthalpy or heat capacity changes in the sample cause a difference in its temperature relative to the reference. The temperature difference is recorded and related to enthalpy change in the sample using calibration experiments.

The particular DSC we use is a TA Instruments Q100. This is a heat flux DSC with a turret-type measuring system. In this system the heat exchange takes place via small hollow cylinders which serve as elevated sample supports. This is a relatively new design which allows for large heating and cooling rates with a small sample volume. A more common type of DSC is the disk-type where the heat exchange takes place via a disk which serves as a solid sample support. The disk-type is a simple and easily built design with a high sensitivity, allowing for small sample volumes, however the heat exchange between the furnace and the sample is limited, allowing for only medium heating and cooling rates.

A turret-type system has the advantages of a very small system size combined with a low thermal mass, a very short heat conducting path, a direct connection between the sample and the furnace and no interference between the sample and the reference. These things combine and result in a smaller furnace and a quicker thermal response time than the disk-type system[81]. This allows for faster heating and cooling rates.

For a steady-state measurement, the real heat flow Φ of the sample is directly proportional to the measurement signal ΔT. (ΔT is simply the difference between the temperature of the sample and the reference) The conditions of constant heat consumption are achieved when the sample and reference have different, temperature-independent heat capacities. In this way, a greater amount of heat will always flow into the sample whose heat capacity is higher, in order to maintain the steady-state heating rate. When the heat capacity of the sample is greater than the reference then the real heat flow is directly proportional to the difference in sample temperatures.

$$\Delta\Phi_{SR} = -K' \cdot \Delta T \quad \textbf{(33)}$$

However, there is no steady-state condition for measurement during a transition or reaction. Where there is a quasi-steady state then the following is valid in approximation

$$\Delta\Phi_{SR} = \beta(C_S - C_R) \quad \textbf{(34)}$$

$$\beta(C_S - C_R) = -K' \cdot \Delta T \quad \textbf{(35)}$$

This relation describes the baseline and is the basic equation for determining the heat capacity C_S. For an empty reference crucible $C_R = 0$ and

$$C_S = -K' \cdot \frac{\Delta T}{\beta} \quad \textbf{(36)}$$

Integration of the measured curve with the baseline subtracted gives the heat of transition or reaction. The heat equals the enthalpy of reaction or transition only if the heat capacity is constant during the transformation. Otherwise the enthalpy of transition is a function of temperature. As a consequence the peak area is an integral mean value of the enthalpy change within the temperature regime of the peak.

1.4 X-ray Diffraction

The peaks in an x-ray diffraction pattern are directly related to the atomic distances. Let us consider an incident x-ray beam interacting with the atoms arranged in a periodic manner as shown Figure 8.

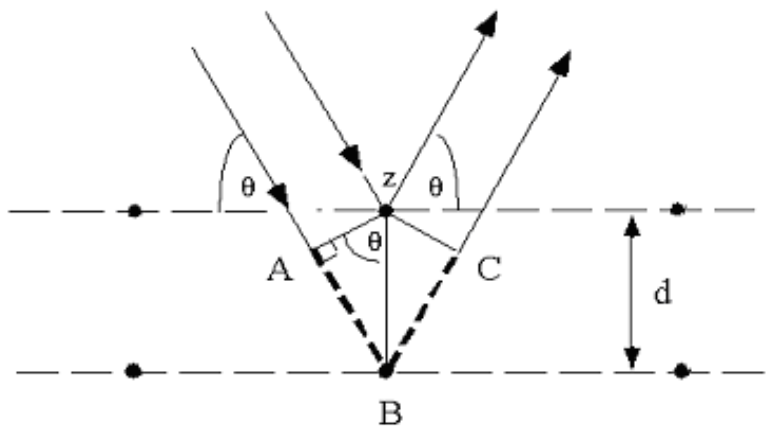

Figure 8: Crystal planes diffracting x-rays at angle θ, where the distance A to B is dsinθ or nλ/2

When an x-ray beam strikes a crystal, most of the beam travels straight through. Some of the x-rays do, however, interact with the electrons of each atom, causing them to emit and 'scatter' x-rays in all directions. In a crystal most of the scattering is cancelled out by destructive interference, but there are some directions where it will add through constructive interference to produce a diffracted beam

The atoms, represented as spheres in the diagram, can be viewed as forming different sets of planes in the crystal. For a given set of lattice plane with an inter-plane distance of d, the condition for a diffraction (peak) to occur can be simply written as

$$n\lambda = 2\ d\ \sin\theta \qquad \textbf{(37)}$$

which is known as the Bragg's law. In the equation, λ is the wavelength of the x-ray, θ the scattering angle, and n an integer representing the order of the diffraction peak.

It is important to point out that although we have used atoms as scattering points in this example, Bragg's Law applies to scattering centers consisting of any periodic distribution of electron density. In other words, the law holds true if the atoms are

replaced by molecules or collections of molecules, such as colloids, polymers, proteins and virus particles.

The difference in angle between the incoming beam and the outgoing beam is measured as 2θ. When examining x-ray diffraction data is it often convenient to look at the diffraction measurement in terms of the reciprocal space value q rather than the diffraction angle 2θ. They are related by:

$$q = \frac{4\pi}{\lambda} \sin\theta \tag{38}$$

And therefore:

$$q = \frac{2\pi}{d} \tag{39}$$

Therefore, the value of q is independent of experimental parameters such as wavelength, and diffraction patterns taken at different wavelengths can be compared directly.

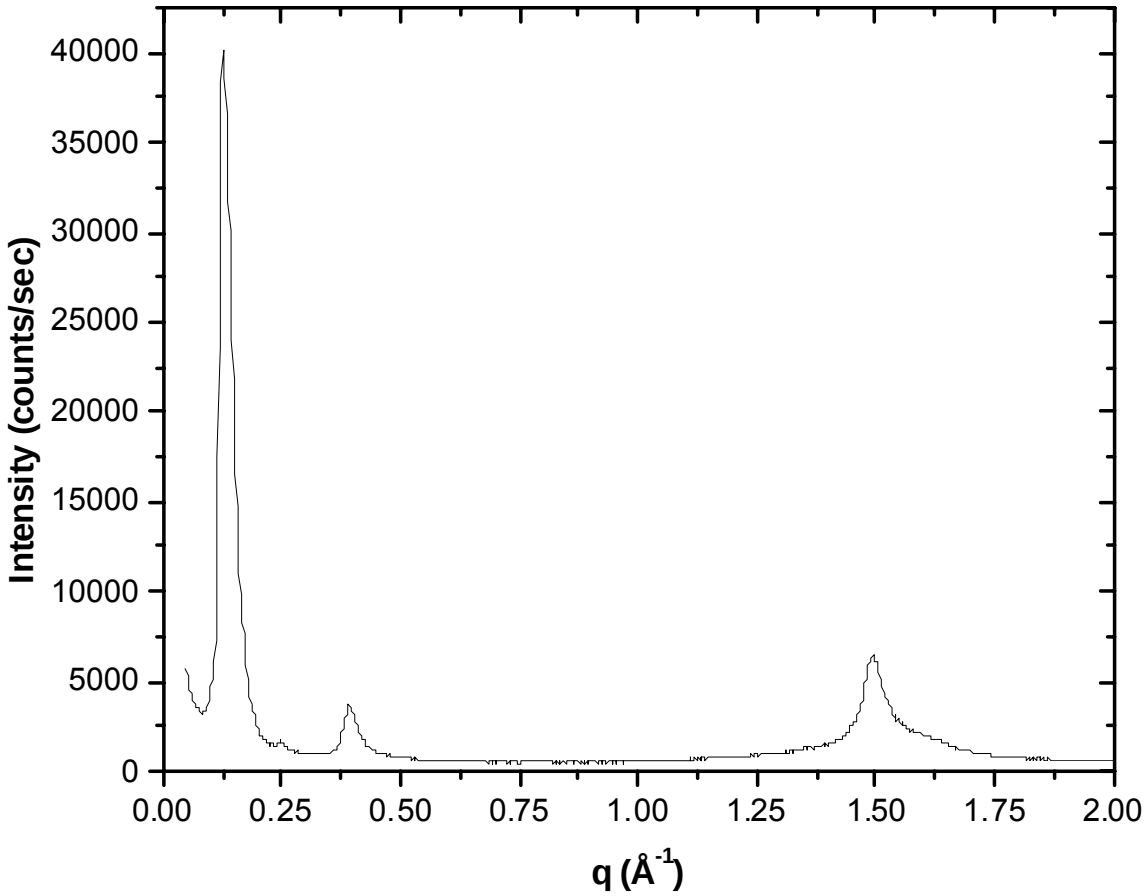

Figure 9: X-ray diffraction pattern of the form II (α) structure of cocoa butter in terms of q

Figure 9 shows a diffraction pattern of the α form of cocoa butter, where λ is 0.8911Å. Each peak is produced by a reflection from a certain plane within the crystal structure.

Absorption is another concept which is important. When x-rays encounter any form of matter they are partly transmitted and partly absorbed. The fractional decrease in the intensity I of an x-ray beam as it passes through an homogeneous substance is proportional to the distance traveled. It can be given as:

$$I = I_o \exp(-\mu x) \qquad \textbf{(40)}$$

where I is the intensity of the transmitted beam, I_o is the intensity of the incident beam, μ is the linear absorption coefficient and x is the thickness the beam passes through.

Orientation within a crystalline material such as cocoa butter can be described as having all of the crystal platelets lined up in the same direction. The effect of orientation on a diffraction pattern can be seen in Figure 10. This is a 2-dimension diffraction pattern, showing a ring of diffraction. The diffraction intensity is higher at the sides than at the top and bottom indicating a preferred orientation within the material.

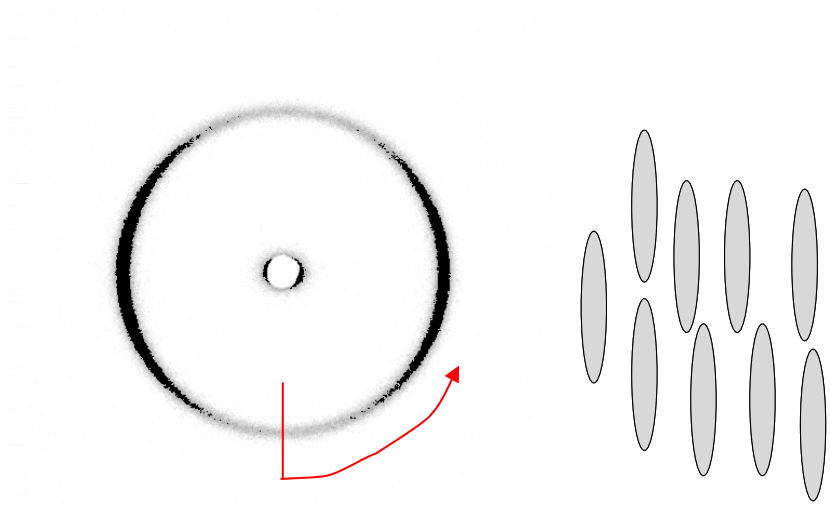

Figure 10: On the left, Figure 5-7 taken from Mazzanti [25] showing a 2-dimensional diffraction pattern of an oriented sample with the arrow indicating the 0 position and the direction of the mosaic scan. On the right, a depiction of oriented crystals

If we convert the diffraction pattern in Figure 10 into a one dimensional representation we get something like Figure 11, which is a representation of the intensity around the diffraction circle. This can also be referred to as a mosaic scan.

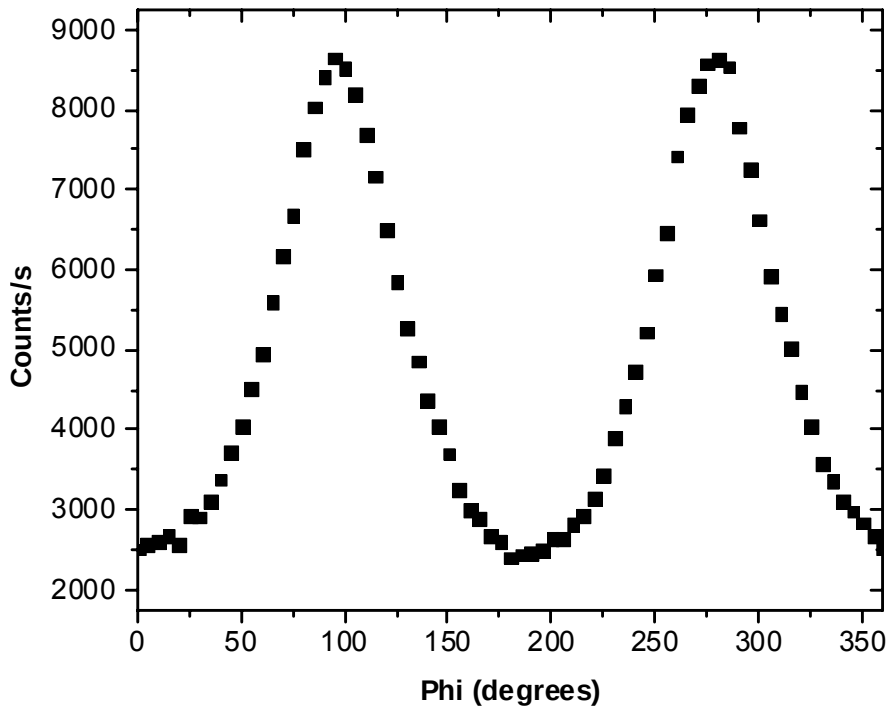

Figure 11: Diagram depicting diffraction intensity orientation scan

Figure 11 can also be achieved using a one dimensional detector. The detector can be moved to the 2θ angle of a diffraction peak and then the sample itself can be rotated in a plane as shown in Figure 12.

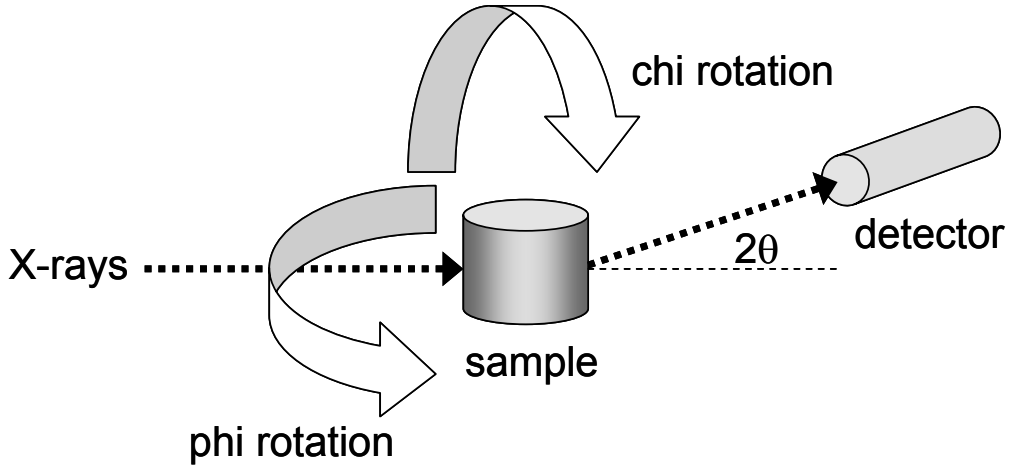

Figure 12: Diagram showing the sample rotation planes of ϕ and χ

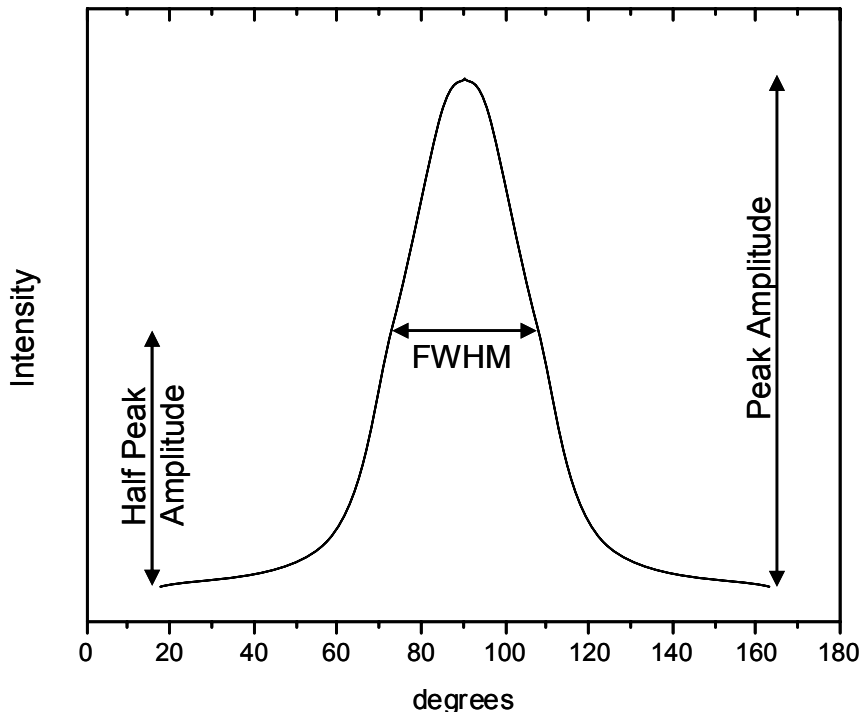

Figure 13: Diagram showing the position of a Full Width Half Maximum (FWHM) measurement

In order to extract information from Figure 11 about the amount of crystallite orientation, the peaks can be fit and the Full Width at Half Maximum amplitude (FWHM) can be determined (Figure 13).

1.5 Mechanical Properties

1.5.1 Bending

Bending is a tensile process at small deflections: the outside of the bend is stretched, the inside is compressed and, in between, there is a neutral axis, which does not experience any tensile stress at all. In a homogeneous, symmetrical material the neutral axis will be at the geometric centre. It should be noted that at bigger deflections shear forces come into play and the process is no longer simple bending.

When bending occurs, it is usual to describe it mathematically in terms of the radius of curvature at each point on the "beam".

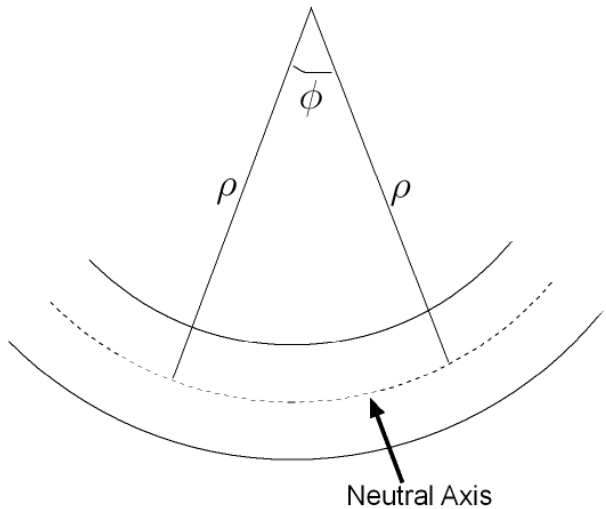

Figure 14: Diagram showing the bending of a beam

Consider an element of beam where the radius of curvature of the neutral axis is ρ and the element includes an angle ϕ at the centre of curvature. An incremental lamina distance z from the neutral axis has length $(\rho \pm z)\ \phi$, so the extension/compression of the lamina is $\pm z\phi$ and the strain is $\pm z/\rho$, $\phi = \pm z/\rho$.

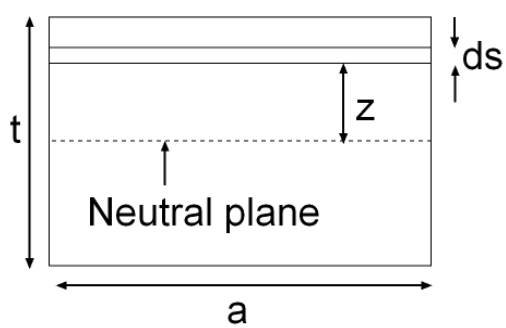

Figure 15: Section of a beam

Now consider a symmetrical beam, which is pointing towards us, as shown in Figure 15, with thickness t and width a. When the beam bends, the rectangle shown above will be rotated and we can calculate the bending moment needed for this by considering the tensile forces involved. We know that the strain on the element dz caused by bending is ±z/r, so we can calculate the stress and the force required to achieve this:

$$F = E_y(z)\left(\frac{\pm z}{\rho}\right)a \cdot dz \qquad \textbf{(41)}$$

where $E_y(z)$ is Young's modulus, which is, in general, a function of z because it varies through the thickness of the beam in many cases. The moment of this force about this slice of the neutral plane is:

$$F \cdot z = \frac{\pm E_y(z)z^2 a \cdot dz}{\rho} \qquad \textbf{(42)}$$

The total bending moment on this slice is the sum of the moments on all the elements dz:

$$BendingMoment = \frac{a}{\rho}\int_{-\frac{1}{2}t}^{\frac{1}{2}t} E_y(z)z^2 dz \qquad \textbf{(43)}$$

and this will be equal to the applied moment at each point in the beam (which will depend on the applied force and its distance from this point).

Equation (43) leads to the general expression for Bending Stiffness, which is the bending moment per unit width and per unit curvature required to bend the beam:

$$S_b = \int E_y(z)z^2 dz \qquad \textbf{(44)}$$

and to the Geometric Moment of Inertia, I, which describes the effect of the shape of the beam cross-section:

$$I = \int az^2 dz \tag{45}$$

For a simple, symmetrical beam, made from a homogeneous material, equation (43) for Bending Moment becomes:

$$BendingMoment = \frac{a}{\rho} E_y \int_{-\frac{1}{2}t}^{\frac{1}{2}t} z^2 dz = \frac{a}{\rho} E_y \left[\frac{z^3}{3} \right]_{\frac{-t}{2}}^{\frac{t}{2}} = \frac{E_y a t^3}{12\rho} \tag{46}$$

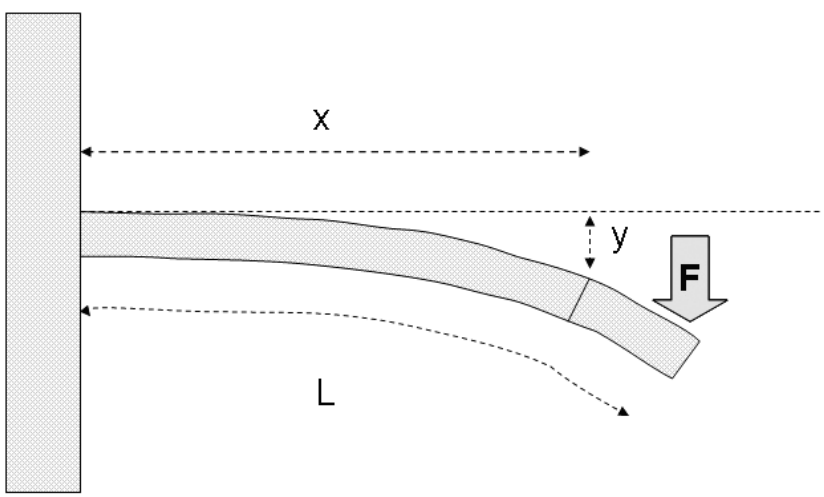

Figure 16: Cantilever beam, fixed at one end while a force is applied to bend the other

Now, consider the cantilever beam in Figure 16. It is length L, fixed at one end, width a, thickness t. It is homogeneous and symmetrical and has a constant value of E_y. A force F is applied to the free end and we want to know about the deflection y at a distance x from the fixed end.

The radius of curvature (ρ) is the radius of a circle with the curvature centred at the current point. Curvature can be defined by the first and second differentials of the curve, that is, radius of curvature is the radius of the circle having the same values for

dy/dx and d^2y/dx^2 as the current point. The value of ρ can be calculated by manipulating the equation for a circle:

A circle with centre (a,b) and radius r has equation:

$$(x-a)^2 + (y-b)^2 = r^2 \tag{47}$$

If we differentiate with respect to x:

$$2(x-a) + 2(y-b)\frac{dy}{dx} = 0 \tag{48}$$

Which, when rearranged and after substituting r back in gives

$$\frac{dy}{dx} = -\frac{\left(r^2 - (y-b)^2\right)^{\frac{1}{2}}}{y-b} \tag{49}$$

Differentiating a second time

$$2 + 2\left(\frac{dy}{dx}\right)^2 + 2(y-b)\frac{d^2y}{dx^2} = 0$$

$$(y-b) = \frac{-\left(1+\left(\frac{dy}{dx}\right)^2\right)}{\frac{d^2y}{dx^2}} \tag{50}$$

If we substitute (50) into (49), rearrange and simplify then we find

$$\frac{1}{r} = \frac{\frac{d^2y}{dx^2}}{\left(1+\left(\frac{dy}{dx}\right)^2\right)^{\frac{3}{2}}} \tag{51}$$

So, the radius of curvature, ρ, is defined as

$$\frac{1}{\rho} = \frac{\frac{d^2 y}{dx^2}}{\left(1 + \left(\frac{dy}{dx}\right)^2\right)^{\frac{3}{2}}} \tag{52}$$

But for small deflections

$\frac{dy}{dx}$ is small and $\left(\frac{dy}{dx}\right)^2 << 1$ so

$$\frac{1}{\rho} = \frac{d^2 y}{dx^2} \tag{53}$$

The bending moment at distance x from the wall equals the applied bending moment. Using equations (44), (45) and (53):

$$BendingMoment = E_y I \frac{d^2 y}{dx^2} = F(L - x) \tag{54}$$

Integrating, we get

$$\frac{dy}{dx} = \frac{F}{E_y I}\left(Lx - \frac{x^2}{2}\right) + K \tag{55}$$

There is a boundary condition that, at x=0, dy/dx = 0, so K =0.

Integrating a second time:

$$y = \frac{F}{E_y I}\left(\frac{Lx^3}{2} - \frac{x^3}{6}\right) + K' \tag{56}$$

There is a boundary condition that, at x = 0, y = 0 so K' = 0. So at x = L:

$$y_L = \frac{FL^3}{3E_y I} \tag{57}$$

And the bending stiffness is

$$S_b = \frac{E_y I}{a} = \frac{FL^3}{3E_y I} \tag{58}$$

This situation is considered to be a two-point bending test.

1.5.2 Three Point Bending

A three-point bending test is similar to the above, but is calculated as if there were two side by side two-point tests.

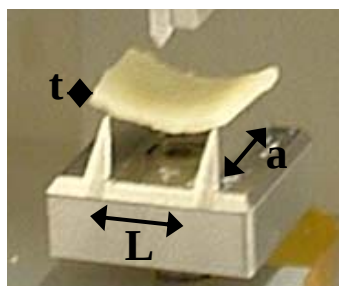

Figure 17: Close-up of three point bending stage with dimensions shown

In this case we can find that the bending moment simplifies from equation **(54)** at x=L/2 to

$$M = \frac{F}{2}(L - x) = \frac{FL}{4} \tag{59}$$

For a rectangular beam

$$I = \frac{at^3}{12} \tag{60}$$

So, if we consider the stress at y=h/2

$$\sigma = \frac{-My}{I} = \frac{3FL}{2at^2} \tag{61}$$

The Young's Modulus is

$$E = \frac{F}{\delta}\frac{L^3}{4at^3} \tag{62}$$

Where δ is the deflection of the beam. If we consider a graph of force vs deflection then

$$E = slope \times \frac{L^3}{4at^3} \tag{63}$$

1.5.3 Curved Beams

Since the cocoa butter samples we are examining are curved, we must adapt the bending theory to be applicable to curved beams. The sketch below shows a curved section subject to a bending moment M. We can see that the neutral axis r_n has moved away from the central axis r_c. This is the primary difference between a straight beam and a curved beam.

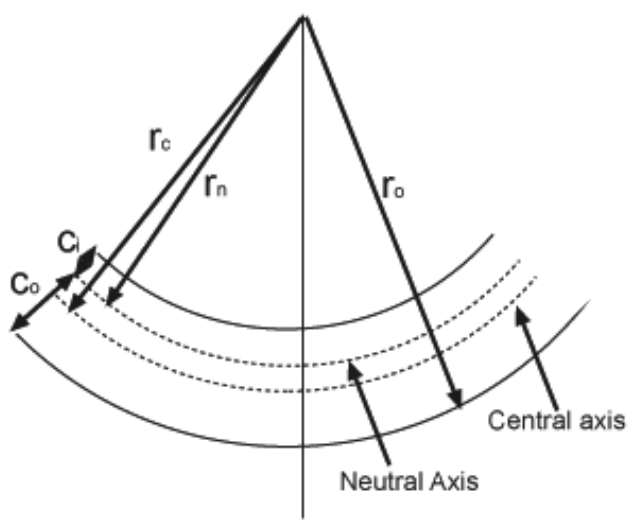

Figure 18: Diagram of a curved beam

The strain is given by

$$\varepsilon = (r - r_n)\frac{d\phi}{r\phi} \tag{64}$$

The strain is 0 when r is at the neutral axis and is maximum when r is the outer radius of the beam ($r = r_o$)

Using the relationship of stress/strain = E the normal stress is simply

$$\sigma = E\varepsilon = E(r - r_n)\frac{d\phi}{r\phi} \tag{65}$$

The location of the neutral axis is obtained by summing the product of the normal stress and the area elements over the whole area and setting it to 0

$$\int_A \sigma \cdot dA = \frac{Ed\phi}{\phi}\int_A \frac{r - r_n}{r} dA = 0 \tag{66}$$

This reduces to

$$A - r_n \int_A \left(\frac{dA}{r}\right) = 0 \tag{67}$$

And so for a rectangle,

$$r_n = \frac{A}{\int_A \left(\frac{dA}{r}\right)} = \frac{(r_o - r_i)}{\ln\left(\frac{r_o}{r_i}\right)} \tag{68}$$

where r_i is the inner radius and r_o is the outer radius.

The stress resulting from an applied bending moment is derived from the fact that the resisting moment is simply the integral over the whole section of the moment arm from the neutral axis (y) multiplied by σdA (= dF). It reduces to

$$M = \frac{r\sigma A(r_c - r_n)}{(r - r_n)} \tag{69}$$

And so

$$\sigma = \frac{M(r - r_n)}{A(r_c - r_n)r} \tag{70}$$

The maximum stress will occur at either the inner or the outer surface.

The curved beam flexure formula is in reasonable agreement with the straight beam formula for beams with a ratio of curvature to beam depth of $r_c/h > 5$. As the beam curvature/depth radius increases the difference between the maximum stress calculated by curved beam formula and the normal beam formula reduces. If the ratio is about 10 then a maximum stress error of only about 4% results from using the straight beam formulae.

2.0 Experiment

2.1 Split Rheometer Couette Cell

2.1.1 Split Couette Cell Design:

Simple temperature controlled shear flow can be achieved with a rheometer quite easily by employing a water bath for temperature control and concentric cylinders for applying shear. With a TA Instruments ARES-RFS strain controlled rheometer (Figure 19(a)), a cylindrical 'cup' is rotated, while a stationary 'tool' or 'bob' is held within the cup and connected to a sensor above. In this manner a sample is contained between two surfaces and sheared between one stationary and one moving surface, the traditional Couette geometry. The bob sensor measures normal force and torque, allowing for continuous monitoring of the crystallization process within the sample. The temperature of the system is monitored via a sensor at the bottom of the sample cup set into the water bath.

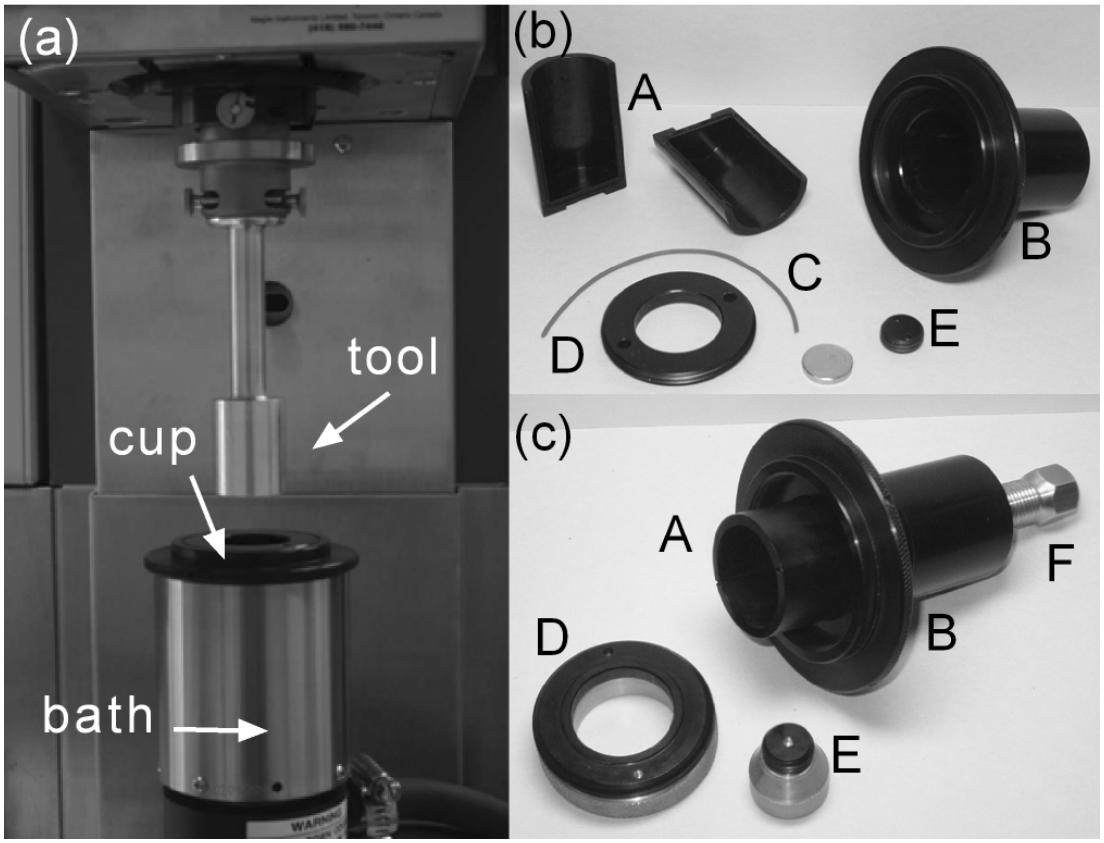

Figure 19: (a) A TA Instruments ARES-RFS showing the split Couette attachment inserted into the water bath and the tool attached to the sensor. (b) and (c) The split rheometer Couette attachment, shown (b) disassembled and (c) partially assembled.

However, conventional concentric cylinders designed for a rheometer give the same dilemma as with an x-ray accessible Couette shear cell[10, 11]. Once the cocoa butter sample has been cooled and crystallized, it cannot be extracted from the system without melting away part of the structure.

In order to accomplish the extraction of a sheared sample of cocoa butter intact, I developed a modification to the concentric cylinder system[1]. Two cups were manufactured, as shown in Figure 19b and Figure 19c, which fit snugly inside one another. The outer cup (B) has an inner diameter of 33.6 mm and the inner cup (A) has an inner diameter of 27.8 mm. The outer cup (B) is designed to screw into the water bath

of the rheometer. The inner cup (A) was cut into two pieces lengthwise and an o-ring grove machined into each piece, allowing for the installation of a sealing o-ring (C). This provided a tight seal between the two pieces when the inner cup (A) was reassembled and placed within the outer cup (B). A ring (D) is then screwed into the top of the cylinders to hold the inner cup securely in place. A bob was also manufactured, having an outer diameter of 25.8 mm, thus creating a gap size of 1mm. This bob is also designed to have a conical bottom surface, to minimize flow distortion at the bottom of the cup. Once assembled, the split rheometer cup behaves in the same manner as a solid cup.

Once a sample of cocoa butter has been solidified inside the split cup under controlled temperature and shear conditions, the bob can be detached from the upper sensor and then the entire cup and bob removed intact from the water bath. The retaining ring (D) can then be unscrewed to allow the removal of the inner, split cylinder (A). In the bottom of the outer cylinder (B), a small plug (E), which was installed to allow good thermal contact with the rheometer's temperature sensor, can then be removed to allow for the insertion of a threaded rod (F) which applies pressure to the bottom of the inner cylinder (A), forcing it out of the outer cup (B). This leaves the bob surrounded by the two halves of the cylinder (A) with the cooled and solidified sample of cocoa butter still intact in the gap between them. A sharp tap to the seam of the cylinder (A) causes it to split apart with the cocoa butter remaining attached to either the bob, or the inner surface. This can be seen in Figure 20. The cocoa butter can then be removed in large pieces for further study.

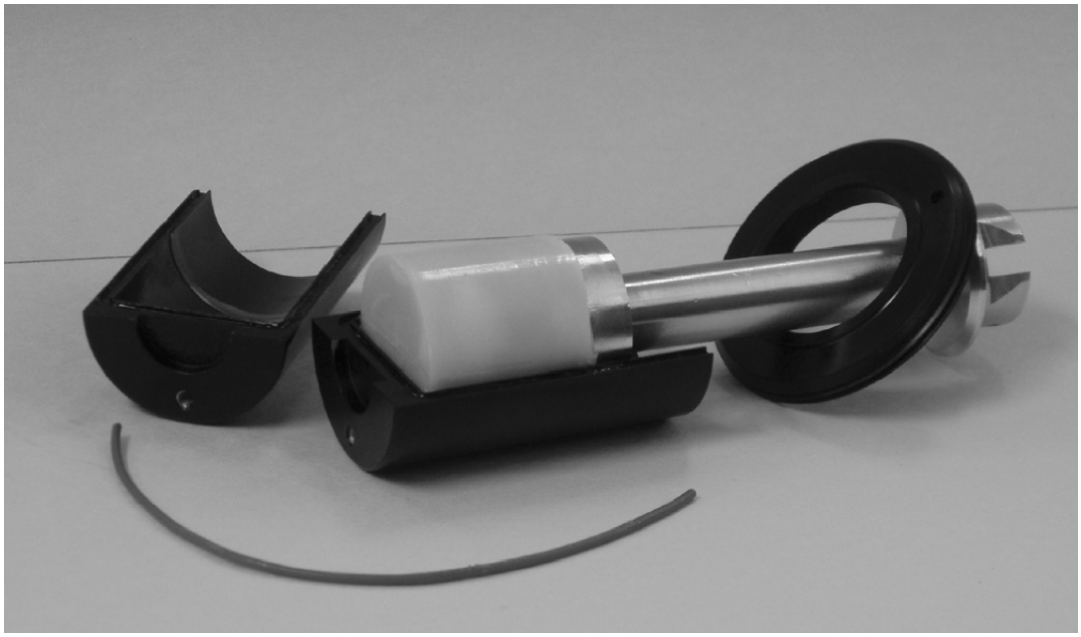

Figure 20: The split Couette attachment with a sample of cocoa butter having been cooled from 50 to 18°C at 0.5°C/min while sheared at $500s^{-1}$.

A typical rheometer sample run for the split Couette attachment is shown in Figure 21. A sample of cocoa butter (2.8mL) is put into the sample cup. The bob is lowered to create a gap of 0.6mm between the bottom of the bob and the bottom surface of the cup. The sample is held in a melted state at 50°C for a period of 30 minutes before a shear rate of $360s^{-1}$ is applied, simultaneously with the temperature beginning to decrease at a rate of 0.5°C/min from 50°C to 18°C. Once 18°C is reached, the temperature plateaus and two separate crystallization events occur. The first event is the transition from the melt to crystal form II [11]. The second event is the transition from form II to form V [11]. X-ray diffraction of such a sample confirms the presence of a mixed structure consisting of forms II and V, with the amount of form V increasing proportionally to the applied shear rate[25]. That is, the higher the shear rate, the more form V present in the sample.

To assess the ability of the split Couette insert to accurately measure viscosity a comparison was done with the standard cup and bob provided with the rheometer. The attachment has an inner cup diameter of 34mm and a bob diameter of 32mm, thus creating a 1mm gap. A large sample volume of 15mL is required. The bob features an indent at the bottom to minimize end effects. Figure 21 shows a comparison of the two different Couette attachments. Clearly these two results are quite comparable, yet there are differences in both the viscosity and the time to onset of crystallization. The differences in viscosity can be accounted for by considering that there would be a lag in cooling the larger sample volume, while the difference in the onset time of crystallization is only slight and certainly within reasonable limits for our instrument given the degree of temperature control that is attainable.

The temperature of the top and bottom of the sample was also closely monitored during an experiment to assess temperature lag within the sample volume. At the end of the fastest cooling ramp of 2°C/min the top of the cell was found to be only 0.2° warmer than the bottom of the cell.

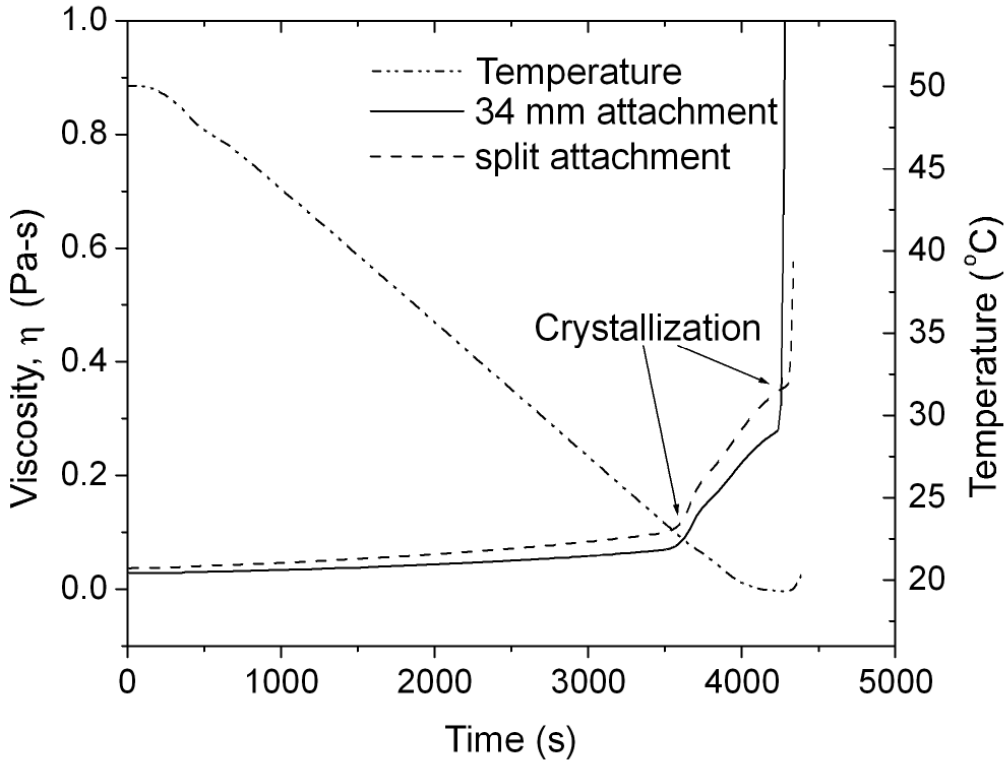

Figure 21: Comparison of crystallization viscosity curves for the split Couette attachment and the 34mm standard Couette attachment.

The crystallization events indicated in Figure 21 are revealed as large sudden changes in viscosity. In order to confirm our assumption that this change corresponds to a crystallization event, a comparison can be done with x-ray diffraction data from an x-ray accessible couette cell[25].

Figure 22 is taken from Mazzanti[25]. Shown is the integrated intensity of the α peak for temperatures 17.5°C and 20°C at 90 and 1440s^{-1} for a cooling ramp of 0.5°C/min from 50°C. The initial onset of the α crystallization seems to be only temperature dependent. A comparison can be done with similar temperature and shear conditions in the split couette cell. In Figure 22 crystallization begins at ~ -5mins for the

17.5°C data and at ~0mins for the 20°C data. Looking ahead to Figure 27 and Figure 30, these values are very similar and confirm our assumption as to the α transition being the first large sudden jump in viscosity.

The second crystallization event is assumed to be shear dependent and as such a comparison to x-ray data will be presented in the next section.

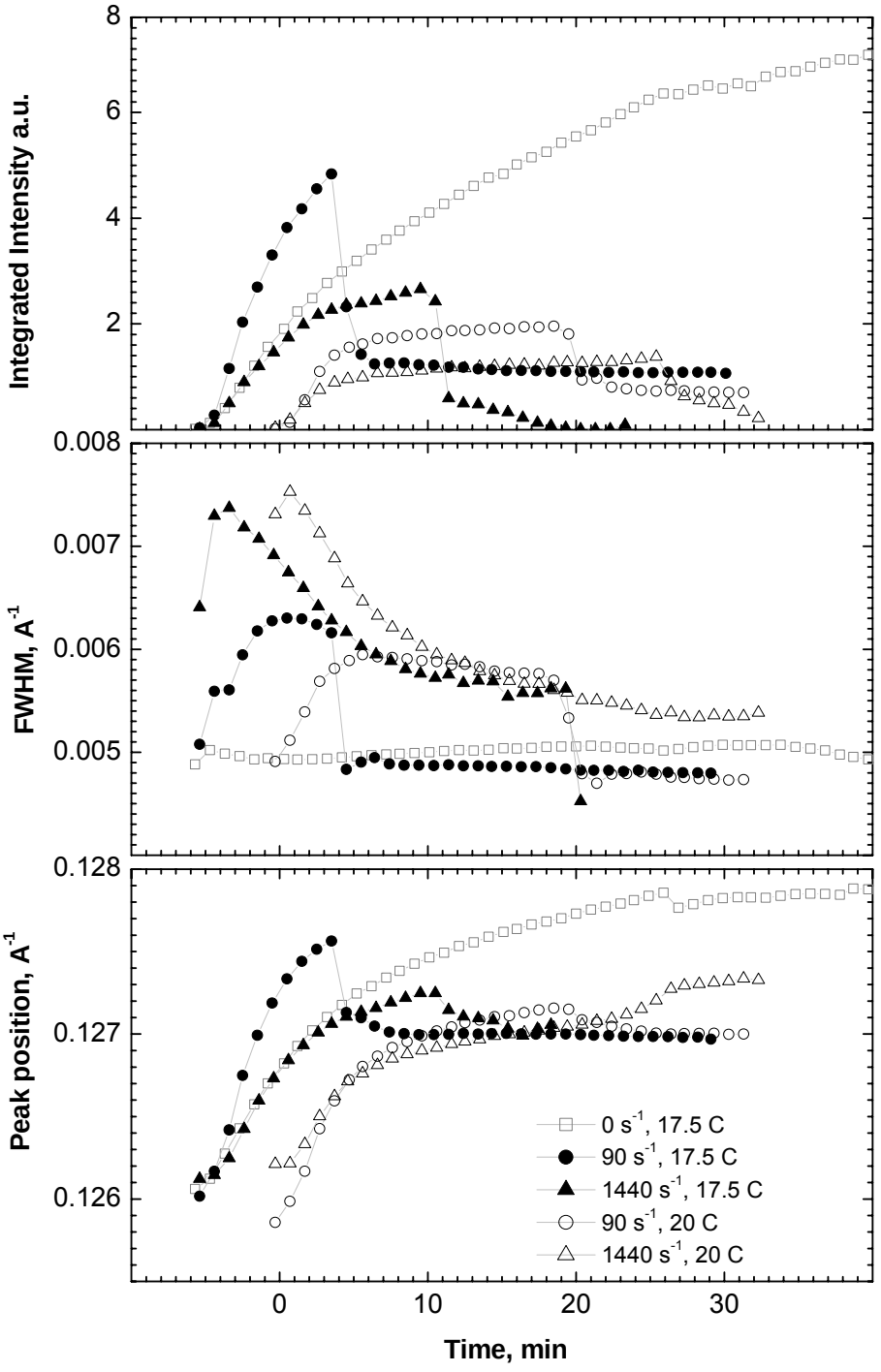

Figure 22: Figure 6-28 taken from Mazzanti[25] depicting x-ray diffraction data of the α peak taken in an x-ray accessible couette cell at the slow cooling rate of 0.5 C/min.

2.2.2 Split Couette Experiments:

Cocoa butter was obtained from Barry-Callebaut (Belgium). A volume of 4mL was placed into the Couette cell. This volume was changed from the previously shown results (Figure 21) in order to have a volume which just submerged the bob. This was done to eliminate any effect of a change of density in the material due to crystallization and temperature (I.e,. a change in density of the material would change the volume and thus height of the sample in the cup, effectively changing the contact area. Submerging the bob means the contact area remains constant regardless). This submersion also eliminated edge effects. A cap was also placed on the top of the cell to help minimize heat flow from or to the surroundings.

The cocoa butter, once loaded into the cell, was heated to 50°C for 30 minutes before being subjected to a cooling ramp. This initial hold time was used to make sure that the sample was fully melted. The water bath surrounding the outer cylinder was employed to cool the system with three different cooling rates (0.5°C/min, 1°C/min and 2°C/min) to three different end point temperatures (16°C, 18°C, and 20°C). Viscosity and temperature as a function of time were recorded by the rheometer until the cocoa butter had crystallized to a point where the torque on the inner cylinder was sufficient to cause the system to shut down to protect the sensor.

The cocoa butter was then extracted from the sample cup in two half cylinder pieces and stored in an incubator set to the end point temperature until needed.

2.2.3 Split Couette Data:

Rheometry plots of viscosity (Pa-s) vs time (s) for the 9 different temperature profiles are shown in Figure 23 to Figure 32.

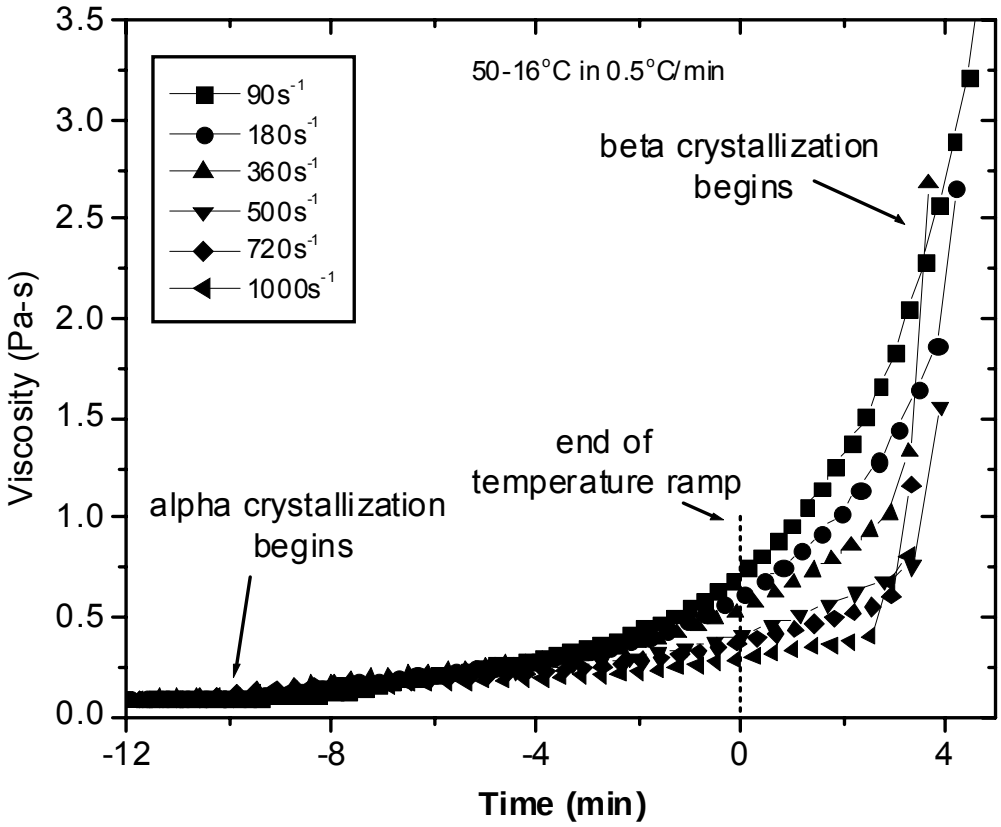

Figure 23: Cocoa butter ramped at 0.5°C/min from 50°C to 16°C whilst sheared in the split couette rheometer attachment at shear rates of 90 – 1000s^{-1}.

The first data set consists of a ramp at 0.5°C/min from 50°C to 16°C. The cocoa butter is sheared in the rheometer as it is cooled and the viscosity is monitored as shown in Figure 23. The temperature profile is continuous at 0.5°C/min and thus is not shown in the figure. The x-axis has been normalized so that 0 min on the time axis occurs when the minimum temperature is reached. To help focus on the crystallization events towards the end of the experiment time, only the viscosity data beginning shortly before the end

point temperature is reach is shown. The omitted data show a gradual increase with temperature prior to the onset of large scale crystallization.

There are several features of Figure 23 which are immediately apparent. Firstly, the viscosity of the cocoa butter at the point of β crystallization is different for each different shear rate. As the shear rate is increased, the viscosity at β crystallization is lower. This observation is consistent with the idea that the application of shear causes a decrease in the size and quantity of crystallites formed during the initial crystallization process. Fewer crystals would be represented by a lower solid fat content and a therefore a lower viscosity. However it is also consistent with shear thinning (a reduction in viscosity due to the application of shear). Since we know that some degree of shear thinning will occur in this situation[82] there is no way to make any conclusions as to crystal size and amount from these data alone. In fact, it has been shown that increasing the size ratio of particles in a suspension will enhance shear thinning characteristics[83].

Secondly, we can see that increasing the shear rate does not necessarily reduce the time taken to reach the β_V crystallization. While the sample sheared at 1000 s^{-1} is the fastest to crystallize here, there is not a large margin between the crystallization times of any of the shear rates. While the total time taken for crystallization to the β_V form is much shorter than reported for static samples, a static sample can not have its viscosity monitored with the rheometer, and can not, therefore, be directly compared. In theory, an oscillatory test could have been done, but while close to static, a certain amount of mixing must take place. Therefore, the only direct evidence that can be offered here is that static samples created under the same temperature ramp conditions had to be left in the cell for a period of at least 4 hours in order to be solid enough to be removed intact,

whilst the sheared samples could be removed immediately. A phase diagram of static work can however be found in Marangoni and McGauley [44] (Figure 4).

We should also note that the two separate crystallization events shown in Figure 21 are much more difficult to pinpoint here. The second event is still quite obvious; however the α transition is much more ambiguous. An event seems to take place at ~ -10 minutes. On this scale it is hard to differentiate, however if we focus, for example, on the $1000s^{-1}$ shear rate on the original scale as shown in Figure 24 it becomes much more apparent. In this particular data set of 50-16°C in 0.5°C/min, the low final temperature allows for a very large range in viscosities between the shear rates as at lower temperature, more fat will crystallize and that fat will have a higher solid fat content due to the lower temperature.

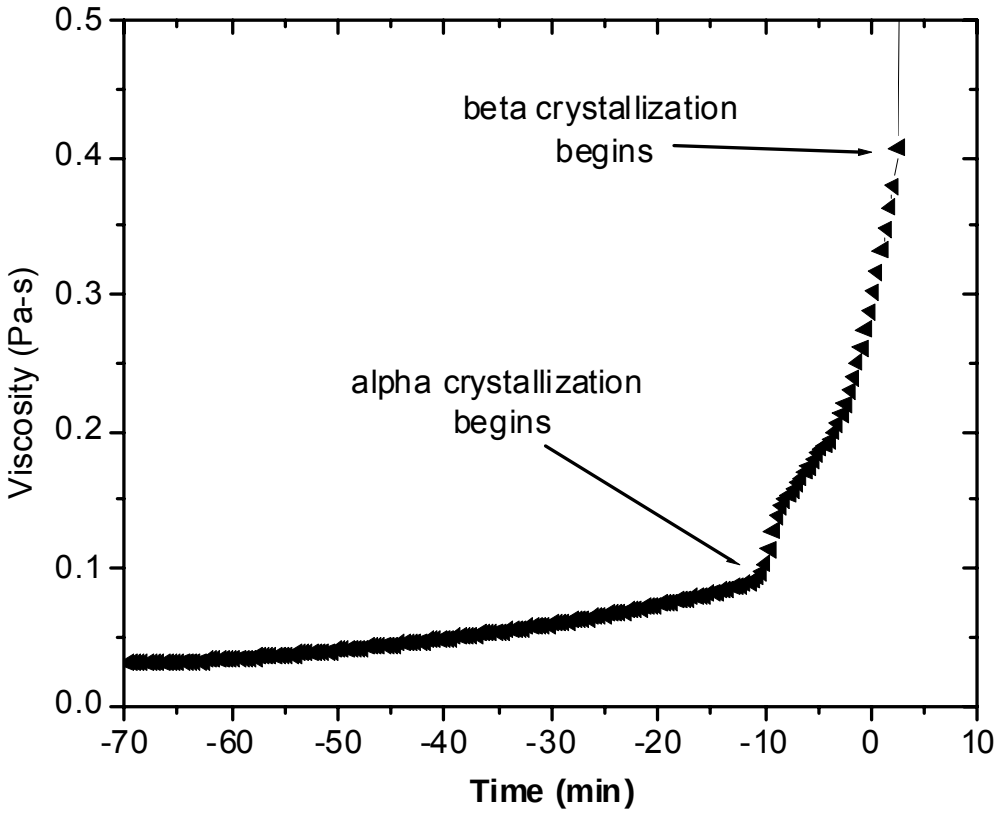

Figure 24: Cocoa butter ramped at 0.5°C/min from 50°C to 16°C whilst sheared in the split couette rheometer attachment at a shear rates of $1000s^{-1}$.

Moving now to look at the same end point temperature, but with a slightly faster cooling ramp (Figure 25), we notice that the main differences between it and Figure 23 are the larger spread between the viscosities of the different shear rates, the shape of the curves and the final crystallization time.

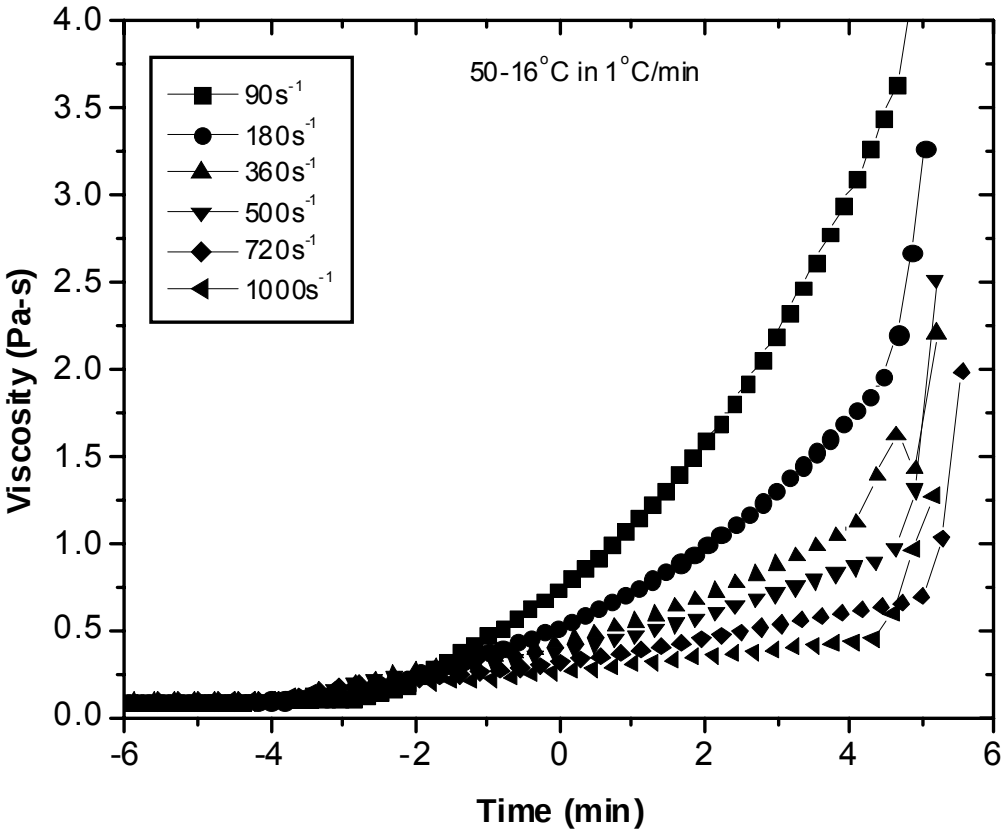

Figure 25: Cocoa butter ramped at 1°C/min from 50°C to 16°C whilst sheared in the split couette rheometer attachment at shear rates of 90 – 1000s^{-1}.

The β_V crystallization times shown in Figure 25 clearly illustrate a lack of acceleration of the β_V event between the lowest and highest shear rates. In fact, this particular data set shows the lower shear rates crystallizing faster than the higher shear rates. This could be explained as due to viscous heating as outlined in Appendix 3.

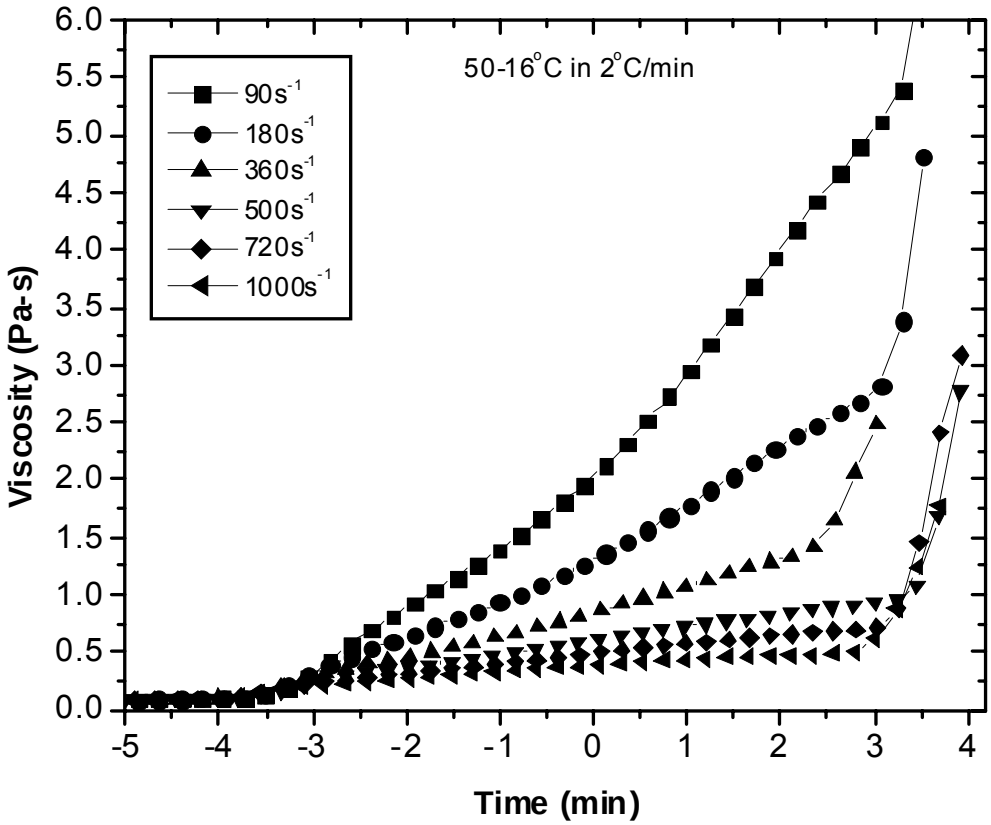

Figure 26: Cocoa butter ramped at 2°C/min from 50°C to 16°C whilst sheared in the split couette rheometer attachment at shear rates of 90 – 1000s^{-1}.

Looking now at Figure 23 to Figure 32 (excluding Figure 24) in sequence, we can see that the shape of the curves between the two crystallization events gradually changes. It starts as a curve reminiscent of exponential growth, and then changes to a more linear growth. By the time we look at Figure 28 we see an initial sharp increase followed by a linear region, giving the appearance of a shoulder. This linear region then gradually flattens until by Figure 31 and Figure 32, it is more of a plateau.

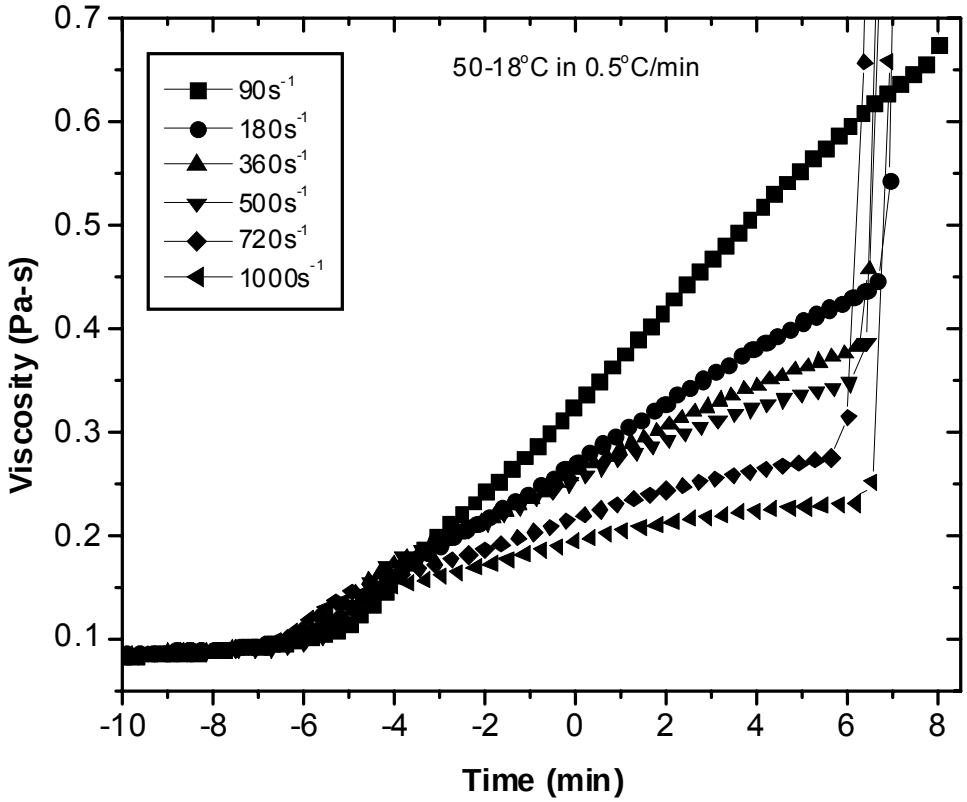

Figure 27: Cocoa butter ramped at 0.5°C/min from 50°C to 18°C whilst sheared in the split couette rheometer attachment at shear rates of 90 – 1000s^{-1}.

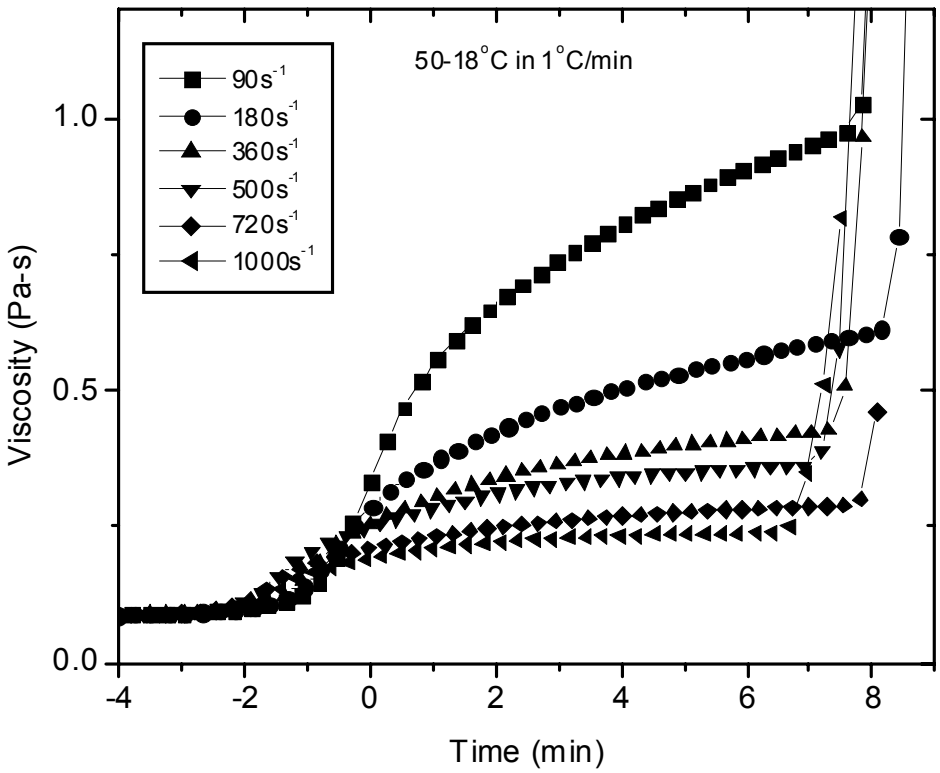

Figure 28: Cocoa butter ramped at 1°C/min from 50°C to 18°C whilst sheared in the split couette rheometer attachment at shear rates of 90 – 1000s^{-1}.

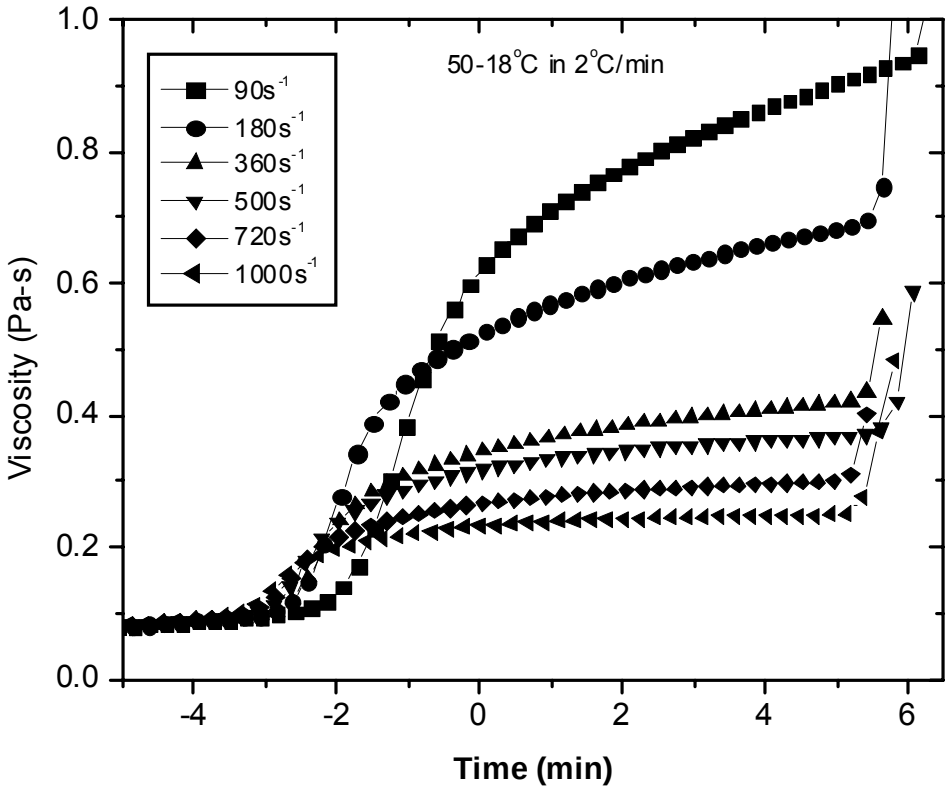

Figure 29: Cocoa butter ramped at 2°C/min from 50°C to 18°C whilst sheared in the split couette rheometer attachment at shear rates of 90 – 1000s^{-1}.

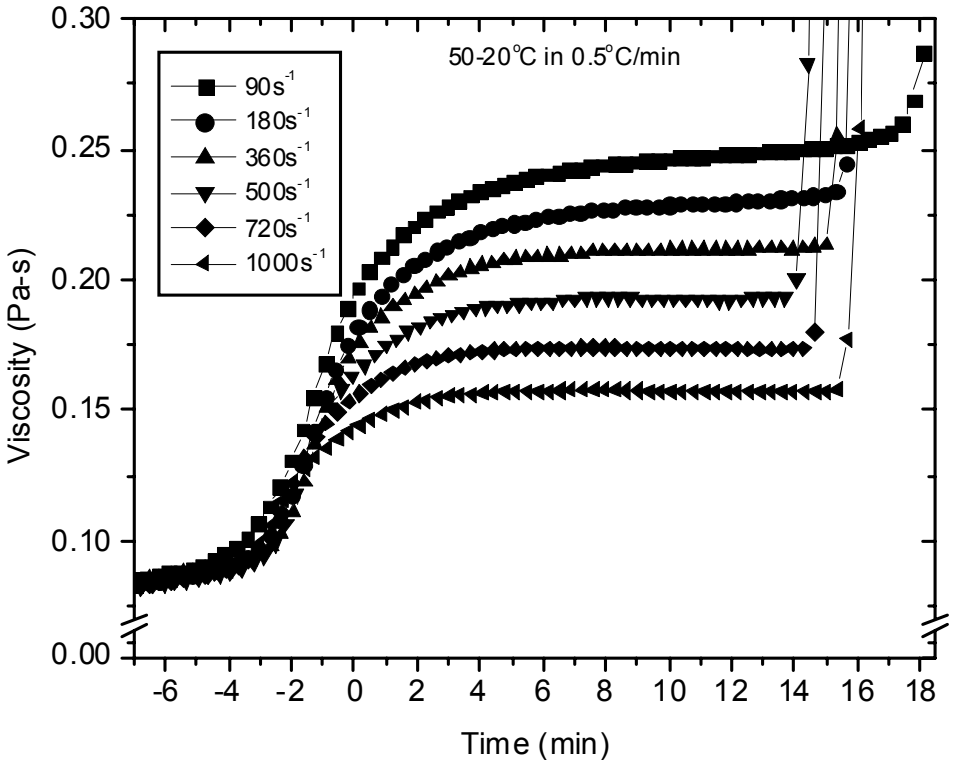

Figure 30: Cocoa butter ramped at 0.5°C/min from 50°C to 20°C whilst sheared in the split couette rheometer attachment at shear rates of 90 – 1000s^{-1}.

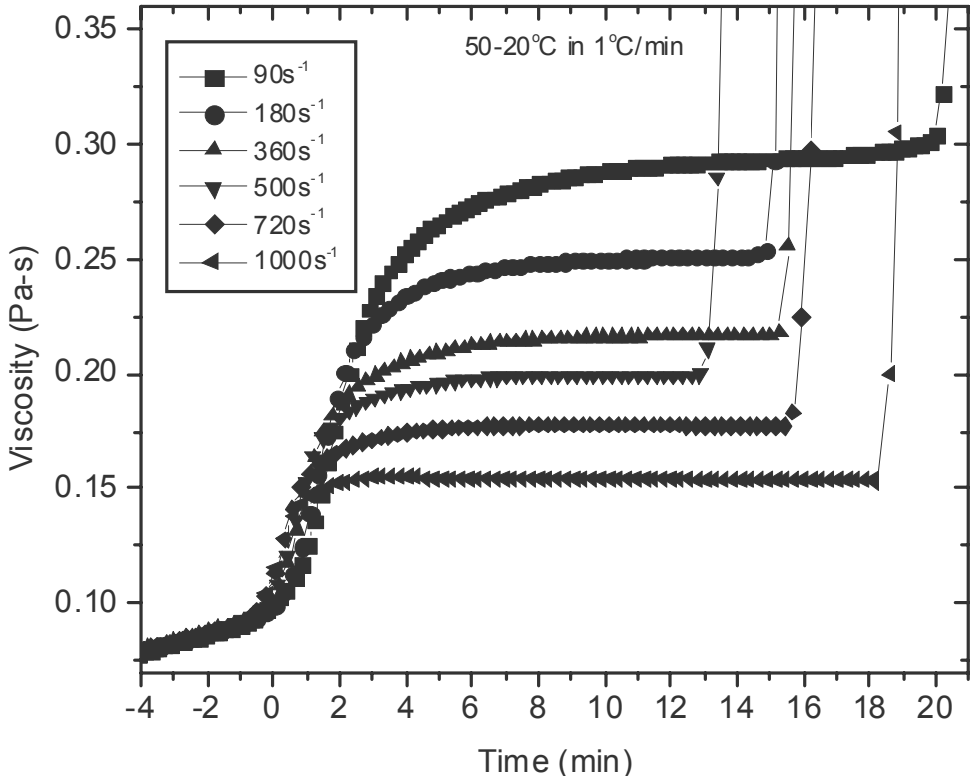

Figure 31: Cocoa butter ramped at 1°C/min from 50°C to 20°C whilst sheared in the split couette rheometer attachment at shear rates of 90 – 1000s^{-1}.

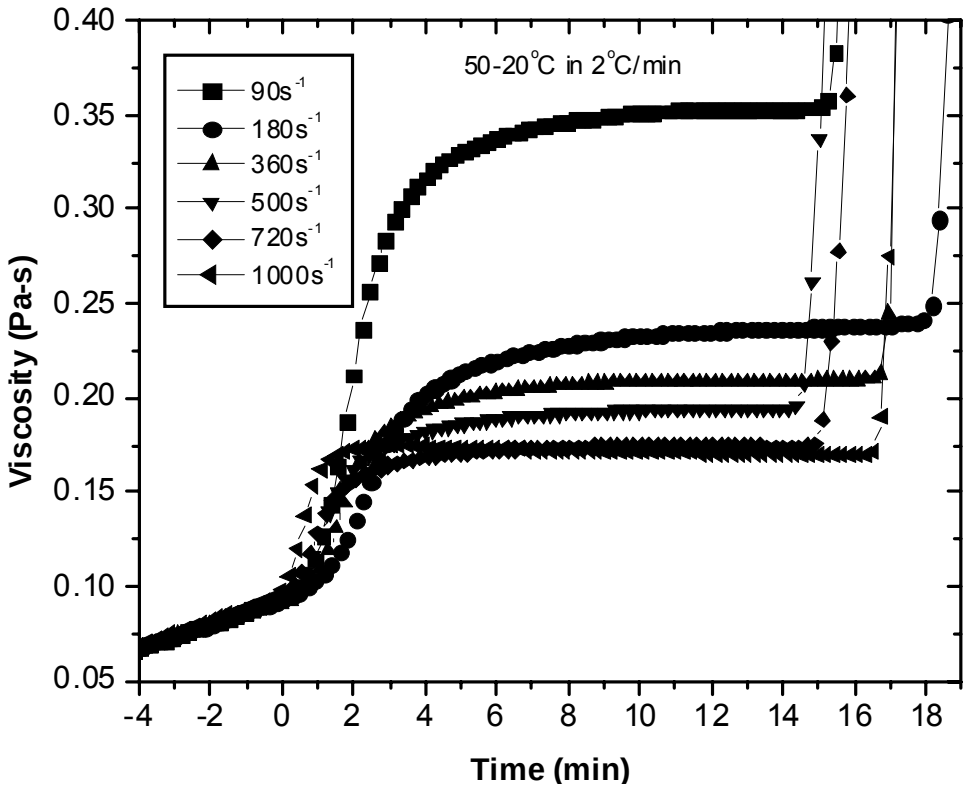

Figure 32: Cocoa butter ramped at 2°C/min from 50°C to 20°C whilst sheared in the split couette rheometer attachment at shear rates of 90 – 1000s^{-1}.

This plateau region (as seen in Figure 31 and Figure 32) occurs exclusively in the highest end point temperature (20°C) data. This is consistent with the much longer static crystallization time of a 20°C sample. At 20°C, cocoa butter crystallization into an α form takes much longer than at cooler temperature. The 20°C crystallization curve looks much flatter than those for the 16 and 18°C samples due to the fact that at 20°C a much smaller percentage of the α crystallization was accomplished before the β_V transformation occurred. This is also reflected in the lower viscosities at the β_V transition in the 20°C samples, as compared to the 16°C and 18°C samples. Thus the change in shape of the viscosity curves can be accounted for completely by the end point temperatures. If this is the case, that the shape is due to the temperature alone, one can

speculate that the shape of the viscosity curves of static samples under these cooling conditions would be very similar, although this assertion is impossible to verify.

The cooling ramp also has a very obvious effect on the shape of the crystallization curves. The slowest cooling rate of 0.5°C/min allows the crystallization process to begin at higher temperatures. At these higher temperatures crystallization is a naturally slower process and the change is viscosity is very gradual. This results in the beginning of the viscosity curve having a slow increase. This happens to a lesser extent with the 1°C/min ramp also. The differences in the end point temperatures, as already stated, is that the 16°C temperature creates a much larger impetus for crystallization, which causes a very fast crystallization rate and hence a rapid increase in viscosity. Crystallization at 18°C is ~2 minutes slower and a further ~10 minutes slower at 20°C. Thus, the change in shape between the curves can be fully explained. The exponential shape at 16°C is due to the very fast crystallization at the endpoint with a variable length of initial slower growth due to the slower crystallization ahead of the endpoint temperature. At 18°C this effect is less apparent due to the endpoint crystallization itself happening much more slowly, and by 20°C the crystallization ahead of the endpoint temperature has minimal effect.

It can also be seen that the α transition time is not always at the same time for each temperature set. While Figure 32 is an exception, it is generally the case that if there is a deviation in a data set, it is because the lowest shear rates are making their α transition slightly later. This could indicate a slight acceleration of the α transition due to shear for the higher temperature end points. We can examine this further by looking at a plot of the α transition times (Figure 33). These times can be easily extracted by eye, however the values were confirmed using derivative edge detection techniques. This

technique uses the second derivative of the curve and yields a peak whose position is easily determined at the point of increase. It should also be noted that in normalizing the α crystallization times to the end of the ramp, actual temperatures of the sample were used rather than the temperature of the water bath. A certain amount of temperature lag is expected between the water bath and the sample. This lag increases with a lower end point temperature. Thus for example, the 0.5 °C/min temperature ramps for 20°C, 18°C and 16°C will not be offset from each other in time by exactly 4 minutes as would be expected. The difference between the data sets will increase with decreasing temperature.

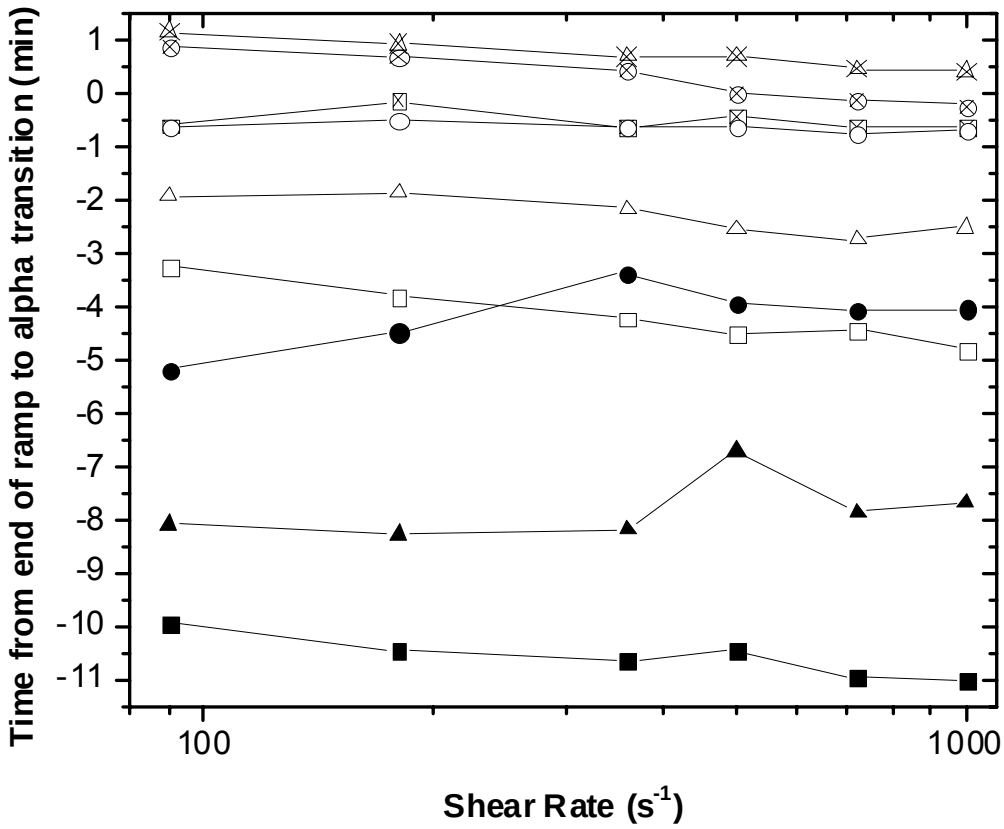

Figure 33: Graph of time taken to the onset of α crystallization from the end of a temperature ramp vs shear rate, for cocoa butter ramped at 0.5°C/min to 16°C(—■—), 18°C (—▲—) and 20°C (—●—); 1°C/min to 16°C (—□—), 18°C (—△—) and 20°C (—○—); and 2°C/min to 16°C (—⊠—), 18°C (—⊠—) and 20°C (—⊗—) whilst sheared in the split couette rheometer attachment at shear rates of 90 – 1000s^{-1}

A general decrease in the α transition time with shear can be seen in some of the data sets. It should be noted, however, that for most of these data sets, the α transition time occurs before the final temperature is reached. The 0.5°C/min ramps in particular have an α transition time before even 20°C is reached. Therefore we would expect that all of the 0.5°C/min data should look exactly the same since they should all have been subjected to exactly the same conditions leading up to α crystallization. These are all of

the solid symbols. While they have been normalized to the end of the ramp time and are offset from each other accordingly, the shape and deviation of these curves should be the same. Clearly they are very different from each other in shape with the 20°C and 18°C data varying by ~2 minutes and the 16°C data varying only within ~1 minute between shear rates.

Therefore, we can only conclude that the events leading up to α crystallization are not constant and that the error in Figure 33 can be on the order of minutes in some cases. (This is much larger than any experimental errors reasonably assumed and so error bars are not included). As such, any acceleration effects shown in the α crystallization data could be explained as within error. These differences between individual data sets should only affect comparison of the α crystallization time since β_V crystallization can be normalized to the α time.

The effects of viscous heating should also be considered when looking at the α crystallization times. This is examined in appendix 3.

If we examine the effect of shear rate on the acceleration of the α to β_V transition time, we can quantitatively analyze what we have already noticed qualitatively: that there is no large decrease in crystallization time due to shear for the shear rates examined. The α and β_V crystallization times can be extracted from the viscosity curves and used to create a graph showing the time between the α and β_V crystallizations plotted vs shear rate (Figure 34).

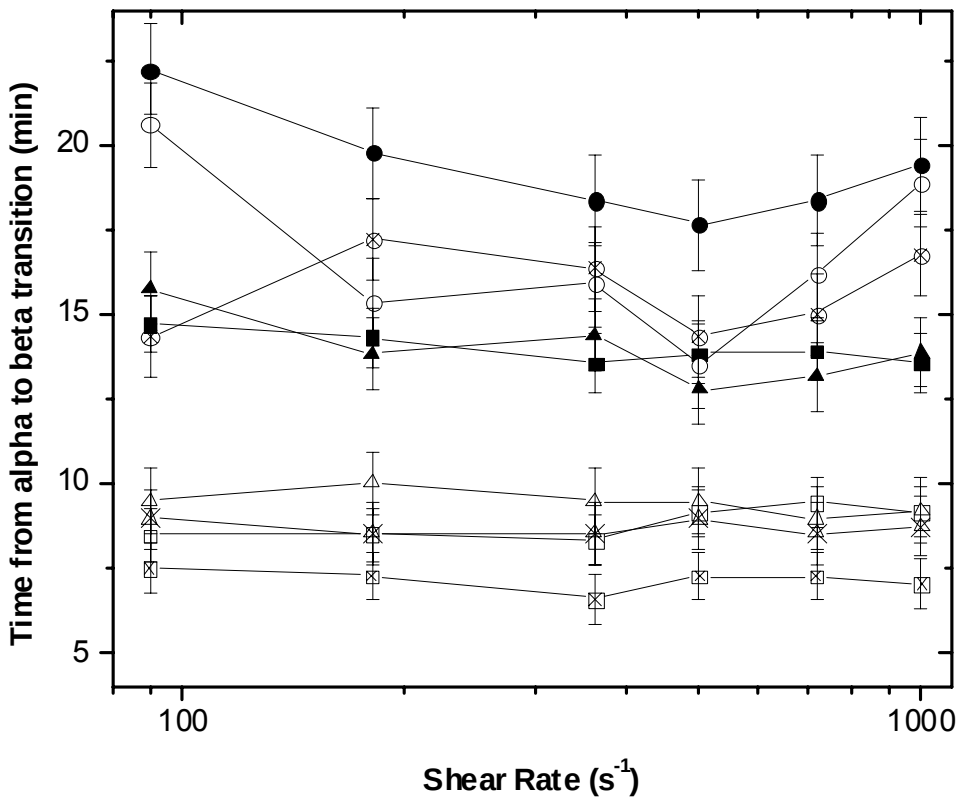

Figure 34: Graph of time taken from onset of α crystallization to the onset of β_V crystallization vs shear rate for cocoa butter ramped over 9 different cooling profiles of 50°C cooled at 0.5°C/min to 16°C (—■—), 18°C (—▲—) and 20°C (—●—); 1°C/min to 16°C (—□—), 18°C (—△—) and 20°C (—○—); and 2°C/min to 16°C (—⊠—), 18°C (—⋇—) and 20°C (—⊗—) whilst sheared in the split couette rheometer attachment at shear rates of 90 – 1000s^{-1}

Before Figure 34 is examined in depth, we can first confirm our assumption that the second large jump in viscosity is indeed a crystallization event where form V is produced.

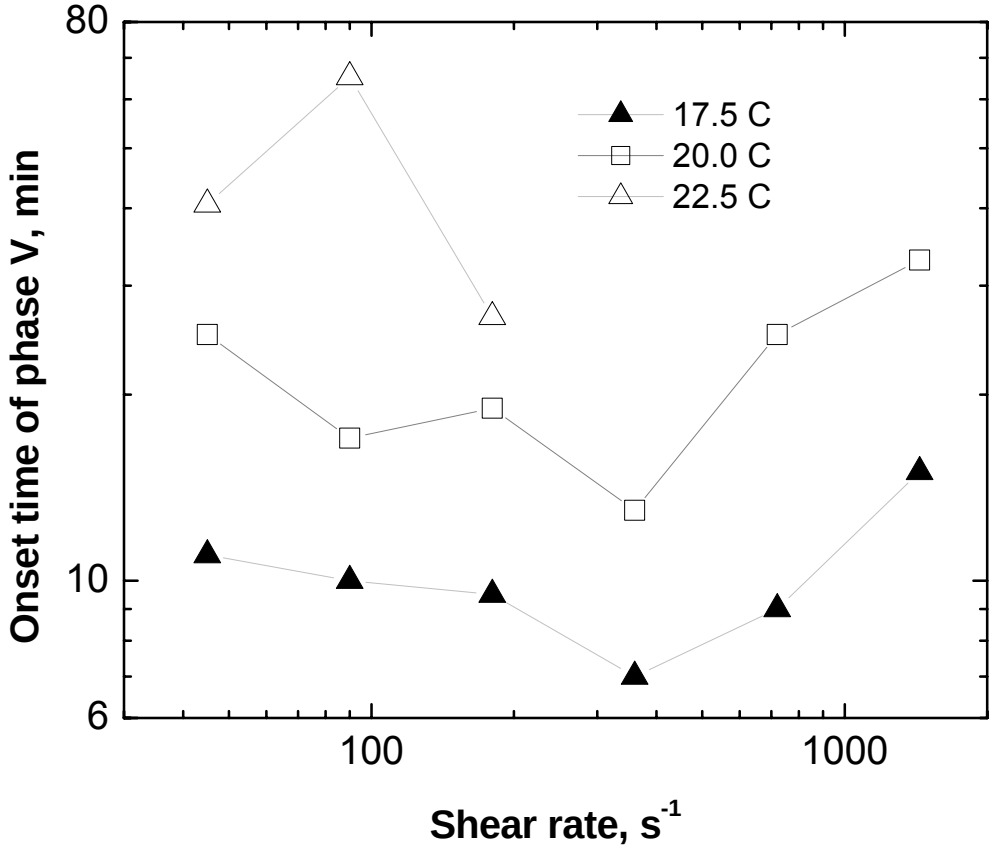

Figure 35: Figure 6-19 taken from Mazzanti[25] depicting the onset times of β_V extracted from x-ray diffraction data taken in an x-ray accessible couette cell at a cooling rate of 3°C/min.

Figure 35 is taken from Mazzanti[25]. It shows onset times similar to those shown in Figure 34, for a cooling ramp of 3°C/min and end point temperatures 17.5, 20 and 22.5°C. For 17.5°C a value of ~10 minutes can be extracted at $90s^{-1}$, while for 20°C a value of ~18 minutes can be extracted for $90s^{-1}$. These values can be compared to data in Figure 34. While the difference in cooling rate would make a great deal of difference in the α to β_V transition time we can see that the time for the 50-18 °C in 2°C/min data set is ~9 minutes and for the 50-20°C in 2°C/min is ~14 minutes. These values are very close despite the large difference in conditions and confirm our assumption that the second large jump in viscosity is a β_V crystallization event.

From Figure 34, the greatest effect of shear is seen in the 20°C endpoint data, where there is a general decrease in time between crystallization events up to $500s^{-1}$ where presumably the effects of viscous heating begin to overshadow the acceleration effects of the shear. We can also see the effects of the cooling rate and end point temperature on the crystallization process. The lowest temperature and fastest cooling rate is clearly the fastest to crystallize. However, we can see that the 16°C and 18°C runs with the slowest ramp speed fall together with the 20°C runs, behind the rest of the 16°C and 18°C data. This can be explained by the fact that the α crystallization event happened, as already noted, before the 20°C temperature was reached and thus the slower ramp speeds have much in common with the 20°C data runs. The apparent lack of acceleration of the α to β_V transition time may seem to contradict previous reported works[9, 25]; it is, however, consistent. A certain amount of acceleration is seen for the 20°C data, but if we look again at Figure 34 and exclude the first and last data points, there is an acceleration of no more than 3 minutes. This small difference in results can be explained by taking into account the difference in sample volume, cooling systems and ramp rates. For example, the cooling system employed in [25] allowed a certain amount of overshoot in cooling before compensating. This would cause the sample to crystallize faster than would normally be seen for that end point temperature otherwise. Clearly the majority of the acceleration effect can be seen in very low shear rates and past that point, greater increase in shear will no longer further accelerate the transition.

Also to be considered is the viscous heating from Appendix 3:. Clearly the premise that viscous heating could be causing a retardation of the crystallization process in the faster shear rates is valid. It is also quite reasonable to speculate that if the

temperature of the system could be maintained with the friction energy removed through adequate cooling it is possible that crystallization time would continue to decrease with an increase in applied shear.

We can also examine and compare the viscosity at the onset point of β_V crystallization. Figure 36 shows this viscosity plotted against shear rate for the 9 different cooling profiles. It should be noted that error bars are not included as the error is less than 0.2 Pa s in general.

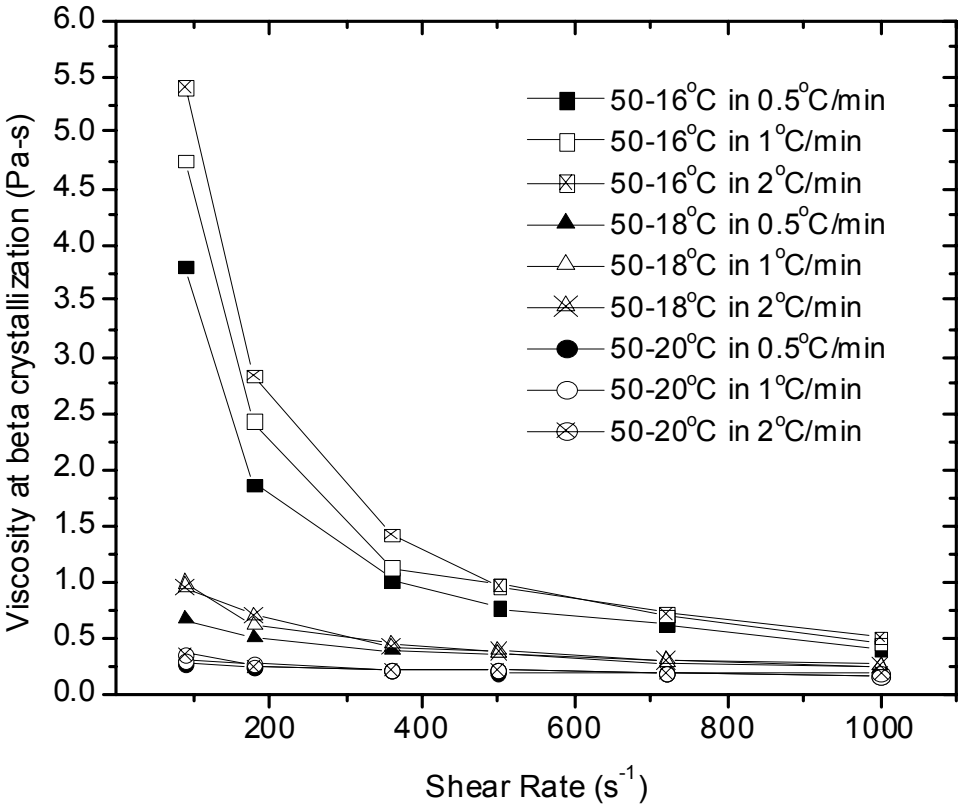

Figure 36: Graph of viscosity at the onset of β_V crystallization vs shear rate for cocoa butter ramped over 9 different cooling profiles whilst sheared in the split couette rheometer attachment at shear rates of 90 – 1000 s^{-1}.

Immediately apparent from this figure is the grouping of the data sets into end point temperature sets, with the highest viscosities being for the lowest temperature

(16°C) as one would expect due to the lower temperature having a higher solid fat content. We also notice that at the lowest shear rates there is a much larger spread in the data and as the shear rate increases the data sets for a given end point temperature converge. The explanation for this could be twofold. Firstly it could be that the effects of the ramp speed are very influential on the size of the crystals formed and as the shear rate is increased the crystal size becomes more dependant on the shear rate and the difference in the data sets between the different ramps is eliminated. It could also be explained as the effect of shear thinning reaching a maximum amount. This would seem to be a likely scenario, but to it we can also add the fact that as the shear rate is increased a component of viscous heating is added, which we have already speculated would explain the increase in crystallization time shown in Figure 34.

Since the spread between the ramp rates seemed to be larger at the lower temperature, a quick experiment was undertaken at 15°C for a ramp of 1°C/min and 2°C/min as shown in Figure 37. At this temperature the high viscosity caused the torque while shearing to be at the limits of the rheometer's capabilities. The $90s^{-1}$ data point is missing for the 1°C/min ramp due to the rheometer's protection limits shutting down the experiment before β_V crystallization was reached. This data set, does, however support the previous conclusions of convergence due to viscous heating, as it shows the same convergence seen in Figure 36.

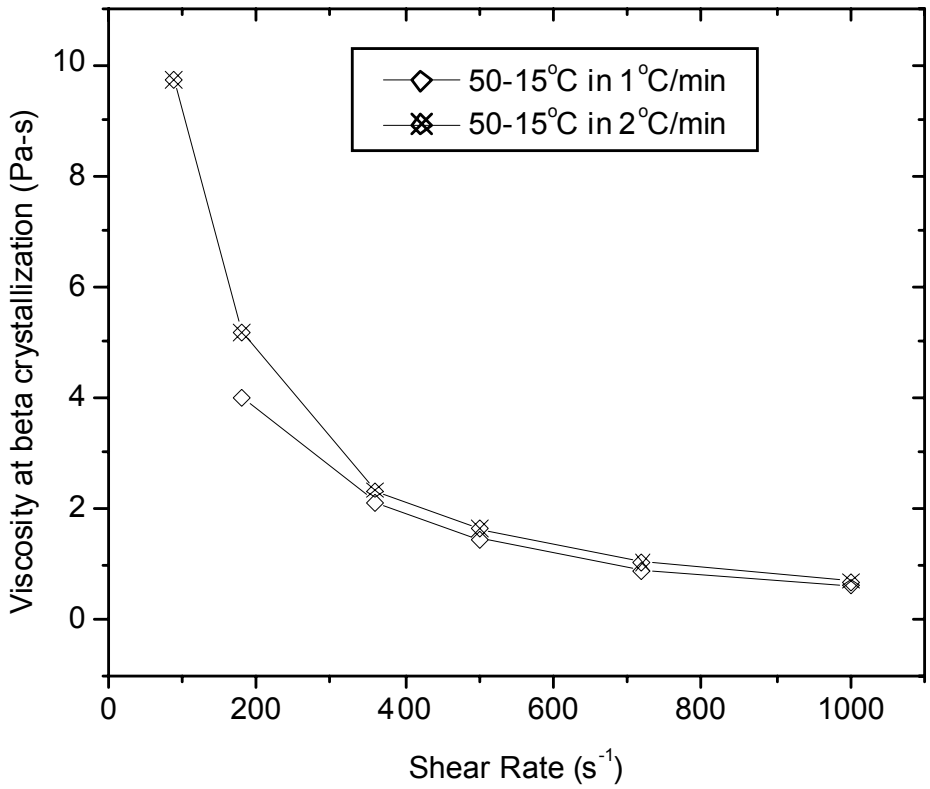

Figure 37: Graph of viscosity at the onset of β_V crystallization vs shear rate for cocoa butter ramped from 50-15°C at 1°C/min and 2°C /min whilst sheared in the split couette rheometer attachment at shear rates of 90 – 1000s^{-1}.

It should also be noted that while these data sets represent only one data run per temperature, ramp and shear conditions, multiple data runs were done for each. In most cases the viscosity curves replicated almost exactly, however, there were instances of dramatic deviations.

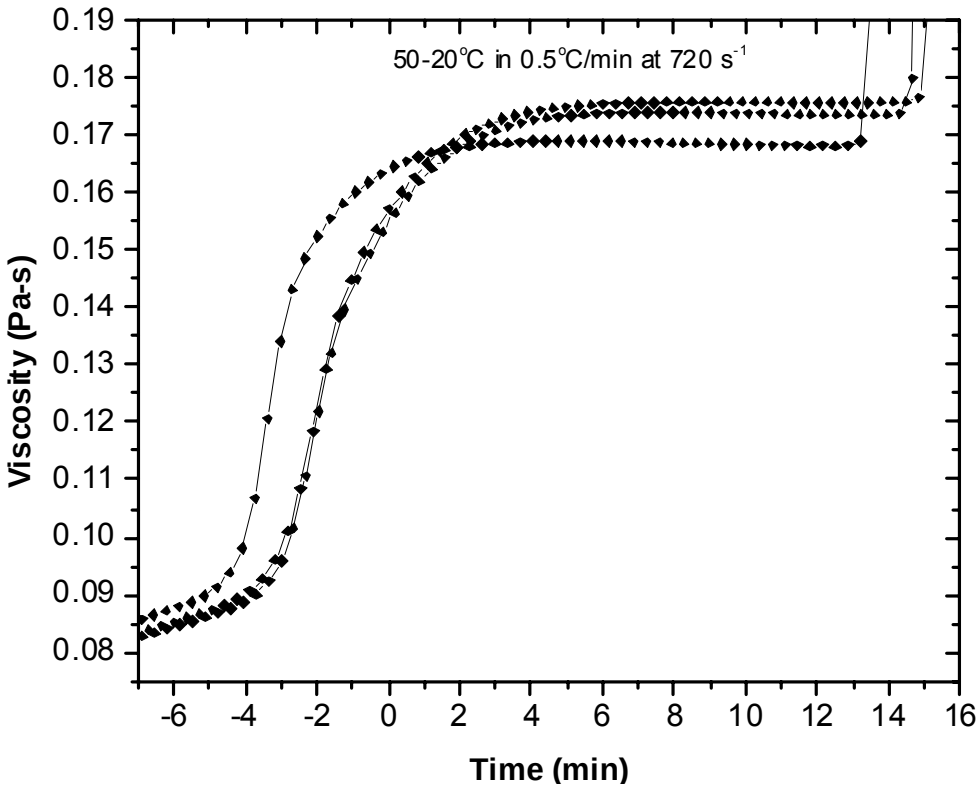

Figure 38: Three repeated data runs of cocoa butter ramped at 0.5°C/min from 50°C to 20°C whilst sheared in the split couette rheometer attachment at a shear rate of $720s^{-1}$ illustrating deviations in repeatability.

Figure 38 shows three repeated experiments of 50°C to 20°C in 0.5 °C/min at a shear rate of $720s^{-1}$. Clearly two of the data runs are very similar while the third is somewhat different in both α crystallization time and plateau viscosity.

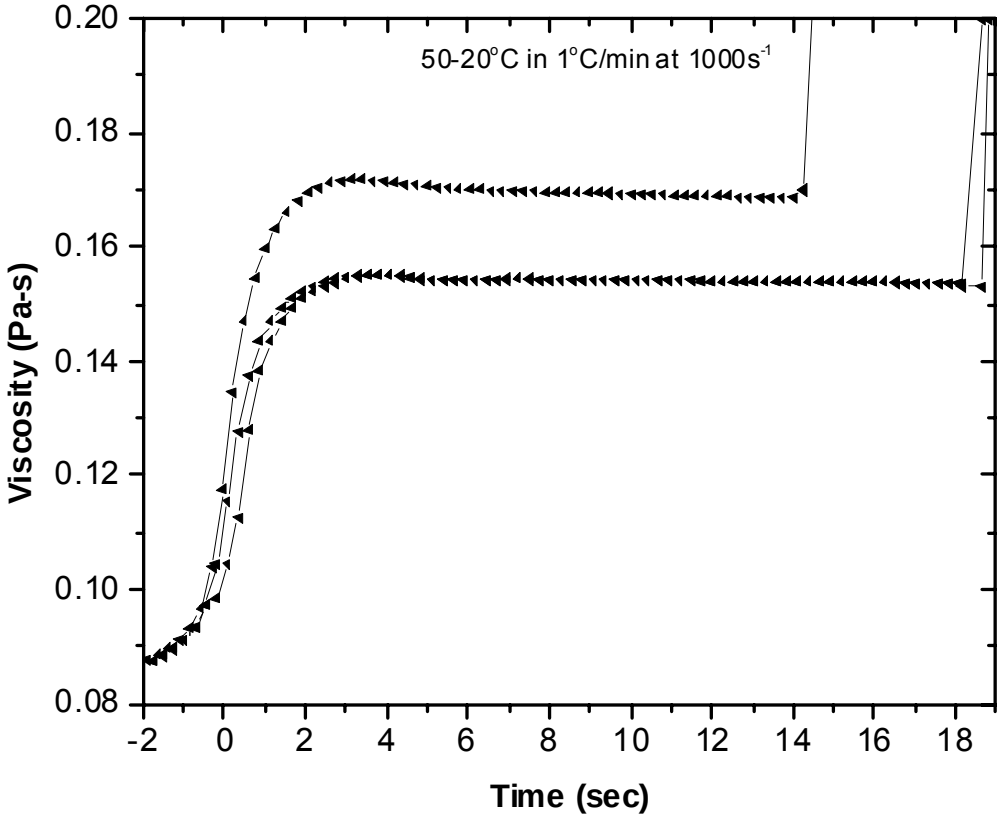

Figure 39: Three repeated data runs of cocoa butter ramped at 1°C/min from 50°C to 20°C whilst sheared in the split couette rheometer attachment at a shear rate of $1000s^{-1}$ illustrating deviations in repeatability

Likewise, Figure 39 shows another interesting deviation. It shows three separate data runs of 50°C to 20°C in 1°C/min at a shear rate of $1000s^{-1}$. Once again, two of the data sets are very similar, while the third is, in this case, very different.

An explanation for such large deviations in one data set is difficult, since their occurrence might be considered random. However, the largest of these discrepancies (as shown in Figure 38 and Figure 39) occur in the highest endpoint temperature data runs and at the higher shear rates. Thus we can speculate that a disruption in the shear field through brief wall slipping could be responsible for the difference in crystallization behaviour. These very different data sets were rare and were excluded from the analysis.

To summarize, the investigation of the effects of shear on the viscosity of cocoa butter when subjected to various temperature conditions yielded some unexpected results. Previous work[25] with similar shear rates and temperature had shown a decrease in the β_V crystallization time up to a shear rate of $360s^{-1}$ for a cooling ramp of 3°C/min. This investigation, however, shows no appreciable acceleration in the transition time over a range of 90 – $1000s^{-1}$ for all but the 20°C end point data. There is, however, a very large decrease in the crystallization time as compared to static conditions[25]. This difference can be explained as due to the difference in cooling rate, end point temperature, and sample size. These things would all have a noticeable effect on the crystallization of the cocoa butter sample and can explain the difference in the results.

2.2 Differential Scanning Calorimetry Measurements

In order to assess the differences inherent in a sheared cocoa butter sample, the melting points of samples created at different cooling and shear rates were monitored over a period of 28 days. Three different cooling rates (0.5°C/min, 1°C/min and 2°C/min) and three different end point temperatures (16°C, 18°C, and 20°C) were used, for a set of 9 different temperature profiles. A static shear rate of $0s^{-1}$ was also used for all of the different temperature profiles so that the melting temperature of unsheared cocoa butter created under the same temperature conditions could be compared.

After the sample of crystallized cocoa butter had been created and extracted, as described in Section 2.1, twelve small pieces of the cylindrical samples were cut and placed in hermetic aluminum DSC pans. The pieces were taken from the same section of the cocoa butter cylinder each time, approximately 1 cm from the bottom of the sample cup.

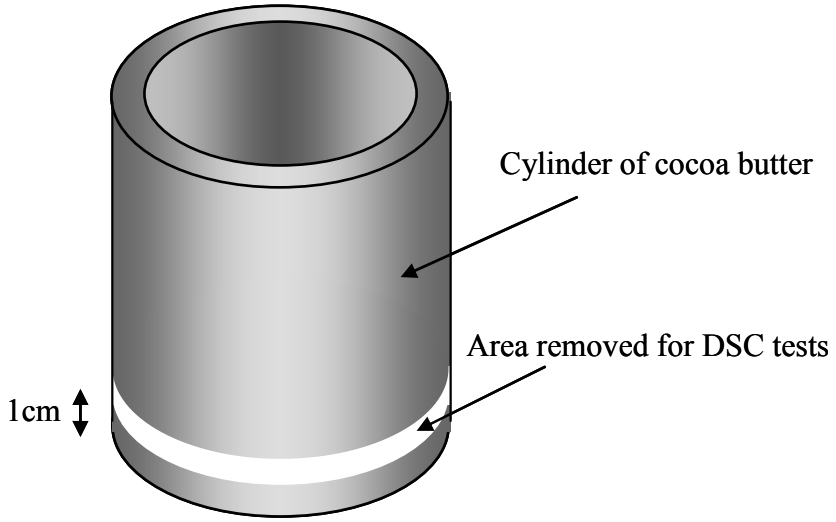

Figure 40: Diagram showing location of the DSC samples in relation to cocoa butter cylinder

The size of the piece was judged so that it just filled the bottom of the DSC pan – a sample weight of approximately 8mg.

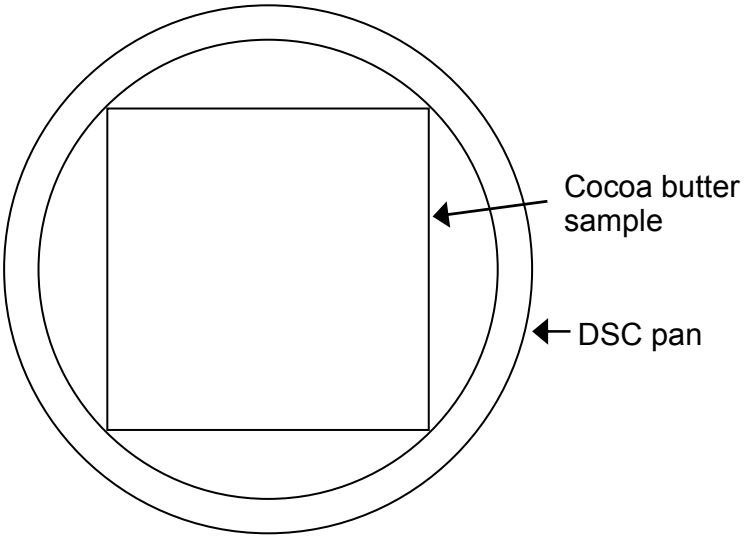

Figure 41: Depiction of the size and placement of a cocoa butter sample in a DSC pan.

Three of these pans were examined in a TA Instruments Q100 DSC to assess their peak melting temperatures on each of day 0, day 1, day 7 and day 28 in the 28 day period, heating at 5°C/min. Prior to measurements, the pans were stored at their final ramp temperature. A typical day 28 melting curve is shown in Figure 42.

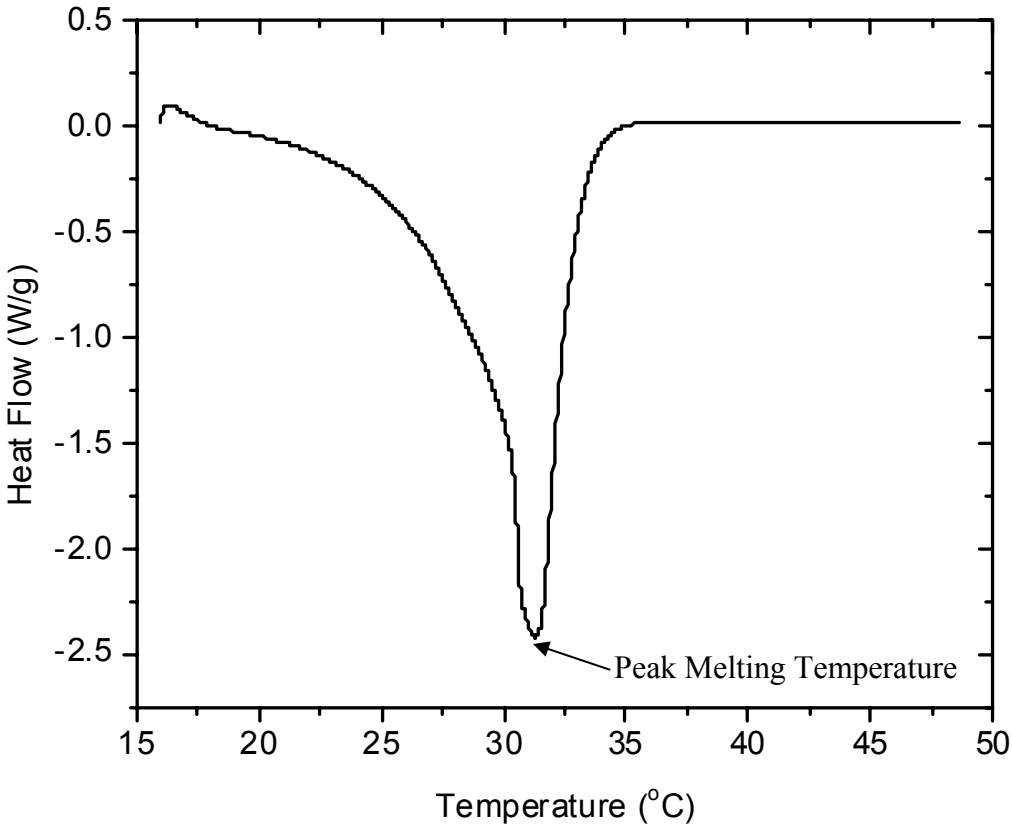

Figure 42: Differential scanning calorimetry graph of heat flow(W/g) vs temperature (°C) for a sample of cocoa butter created under a shear rate of $1000s^{-1}$ whilst cooled from 50-16°C in 2°C/min and stored for 28 days at 16°C.

The peak melting temperature is judged to be the temperature at the peak of the enthalpy curve. In the case of Figure 42 that temperature is 31.3°C.

2.2.1 Differential Scanning Calorimetry Data

Differential scanning calorimetry (DSC) data for the 28 days has been collected together into graphs for each of the 9 different temperature profiles. These figures (Figure 43-Figure 51) show the peak melting temperature for each of day 0, day 1, day 7 and day 28 plotted against shear rate. The error bars reflect the range of values in the

three different repetitions, with the data point representing the average of these three values. All of the data these figures were extracted from can be found in Appendix 4.

The first data set consists of a ramp at 0.5°C/min from 50°C to 16°C (Figure 43). Immediately apparent is the difference in melting temperature between sheared and unsheared samples. The application of any of the shear rates above $90s^{-1}$ cause an increase in melting temperature for the day 0 and day 1 samples. This has been previously reported and reflects the results from x-ray and rheometry studies showing that shear will accelerate the transformation of the cocoa butter into the form V polymorph. The sheared samples will contain varying quantities of crystallites of β_V, while the unsheared samples will be form II, III and IV crystallites only. During storage the remaining non-β_V crystallites will transform to β_V causing the gradual increase in melting temperature over time. Figure 43 also shows that aside from the change between sheared and unsheared samples, there is no noticeable change in peak melting temperature with shear rate for this particular end point temperature and ramp rate.

Figure 43 also shows some data points with large error bars. If we want to look for instance at the day 7, $90s^{-1}$ point, we look at the day 7 graph of Figure 84 (Appendix 4). We can see that the large error bar results from the cocoa butter transitioning between two different melting temperature structures and the double peaks result in a large range of values.

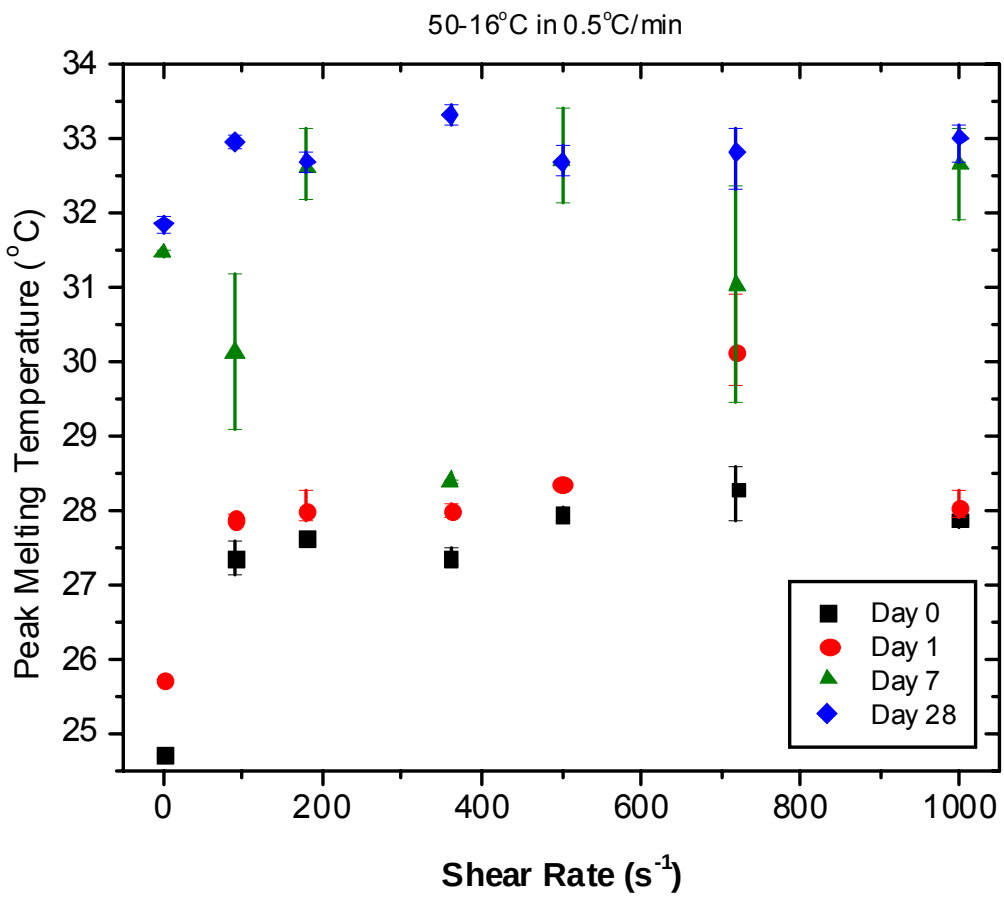

Figure 43: Graph showing peak melting temperature extracted from DSC melting curves for a sample of cocoa butter created under shear rates of 0-1000s^{-1} whilst cooled from 50-16°C in 0.5°C/min

If we move on now and look at the next data set, 50-16°C in 1°C/min (Figure 44), we can see that the slight increase in cooling ramp rate creates a very dramatic shear rate dependence. Once again we have the initial increase with the application of shear as compared to the 0s^{-1} sample. However, now we also have a transition between a shear rate of 360 and 500s^{-1}. For 360s^{-1} and below the melting temperatures are very similar to those seen in Figure 43 for the 0.5°C/min ramp rate. For shear rates of 500 s^{-1} and above, however, the melting temperatures for day 0 and day 1 are increased by 1.5 to 2°C compared to the lower shear rates.

For the day 7 and the day 28 samples there is also a transition for 500s^{-1} and above. Instead of an increase in peak melting temperature, as with the day 0 and day 1 samples however, here we see a decrease in the peak melting temperature as compared to the lower shear rates.

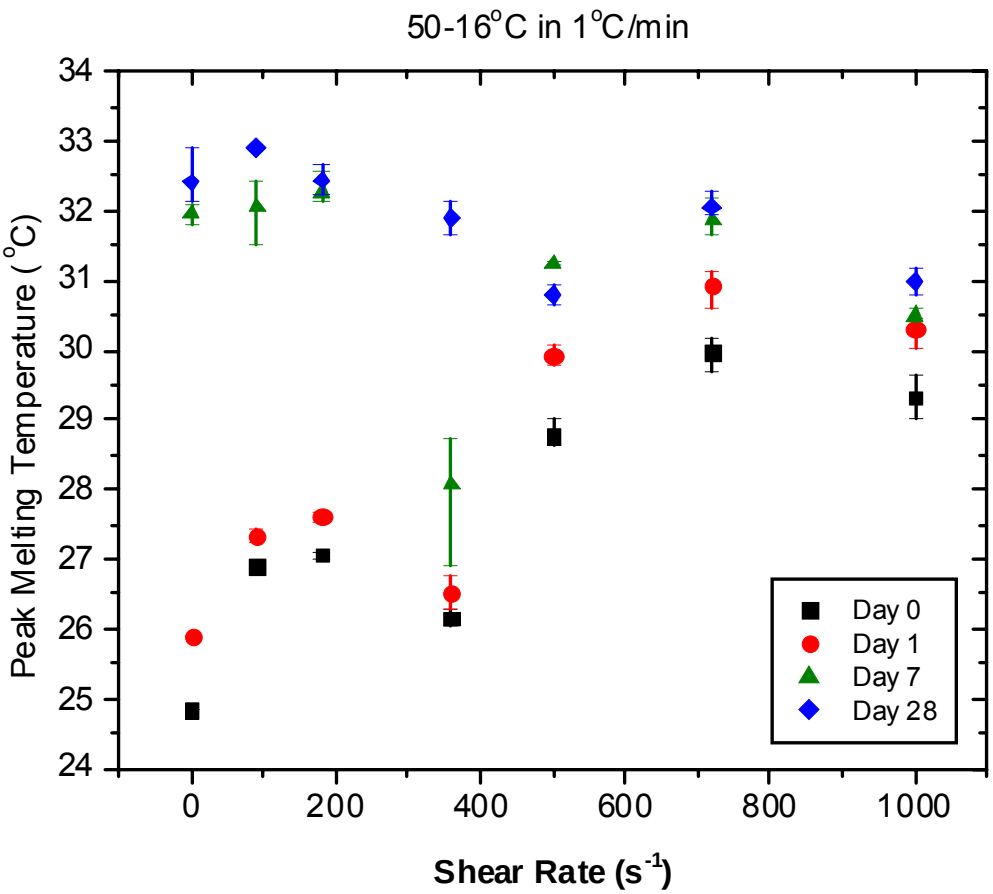

Figure 44: Graph showing peak melting temperature extracted from DSC melting curves for a sample of cocoa butter created under shear rates of 0-1000s^{-1} whilst cooled from 50-16°C in 1°C/min

The next data set (Figure 45) once again shows data for the same end point temperature, but again a faster ramp rate – this time 2°C/min. This data set is very similar to the 1°C/min ramp (Figure 44) with the exception that here the transition is between 500 and 720 s^{-1}.

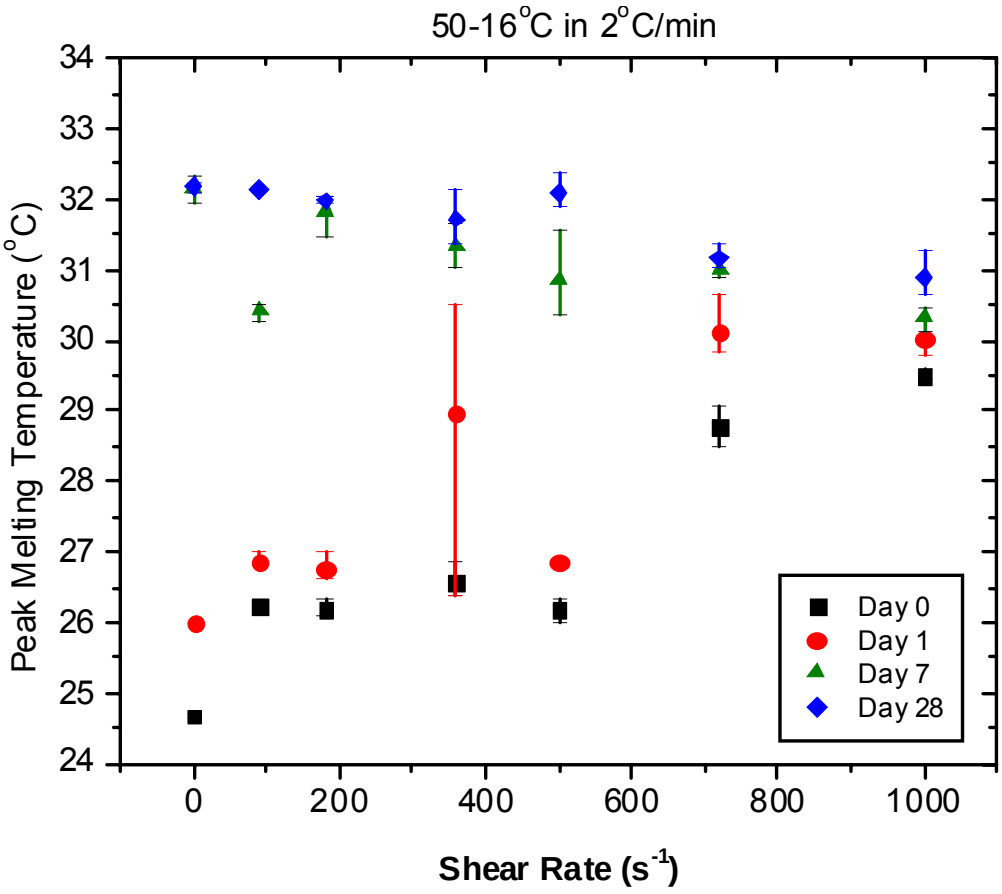

Figure 45: Graph showing peak melting temperature extracted from DSC melting curves for a sample of cocoa butter created under shear rates of 0-1000s^{-1} whilst cooled from 50-16°C in 2°C/min

The remaining 6 temperature sets are shown in Figure 46-Figure 51. The majority of these data sets exhibit the same temperature transition point that is seen for the 1 and 2°C/min ramps to 16°C. The only exceptions to this are the 0.5 and 2°C/min ramps to 18°C, meaning that only the 20°C sample shows a transition with the 0.5°C/min ramp. Figure 52 represents graphically the occurrence of the shear transition depending on temperature and ramp conditions.

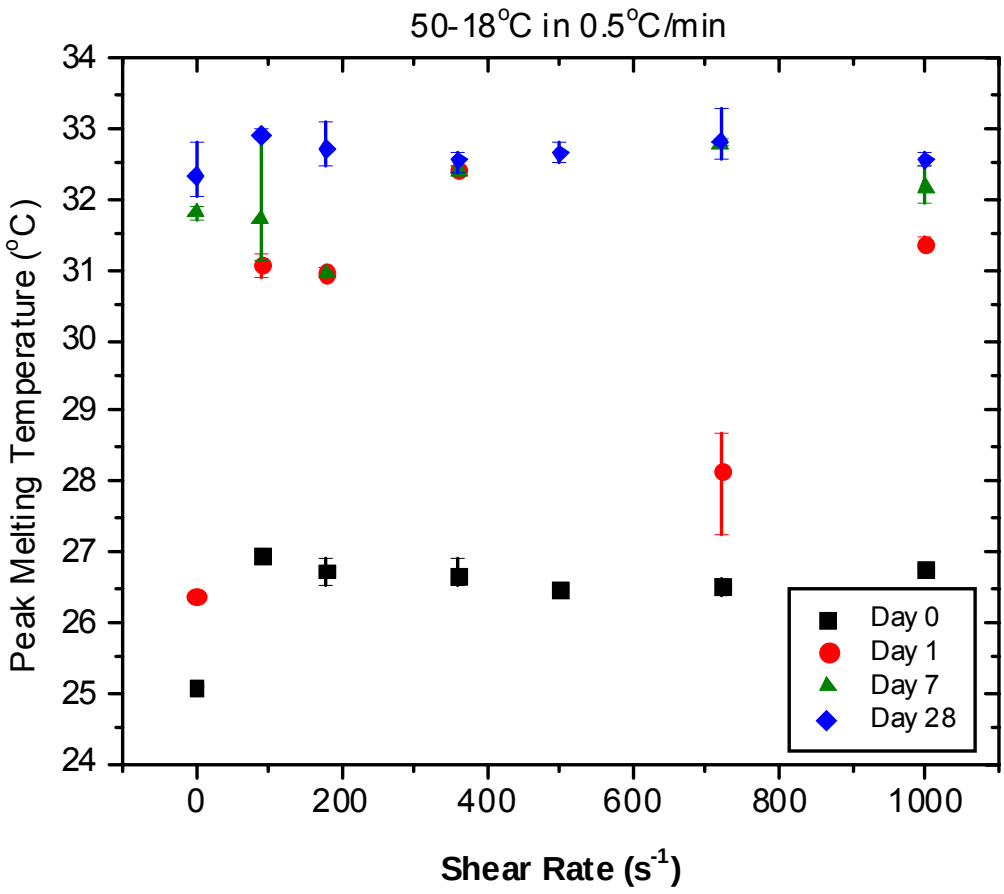

Figure 46: Graph showing peak melting temperature extracted from DSC melting curves for a sample of cocoa butter created under shear rates of 0-1000s^{-1} whilst cooled from 50-18°C in 0.5°C/min

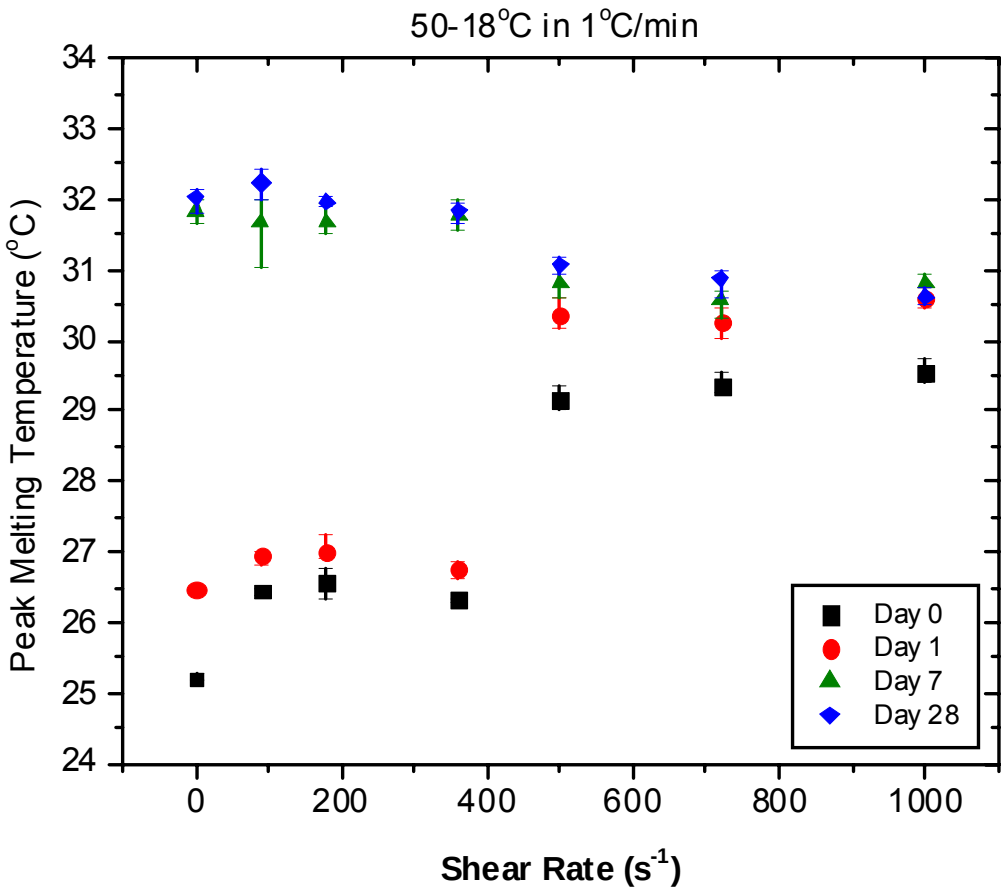

Figure 47: Graph showing peak melting temperature extracted from DSC melting curves for a sample of cocoa butter created under shear rates of 0-1000s^{-1} whilst cooled from 50-18°C in 1°C/min

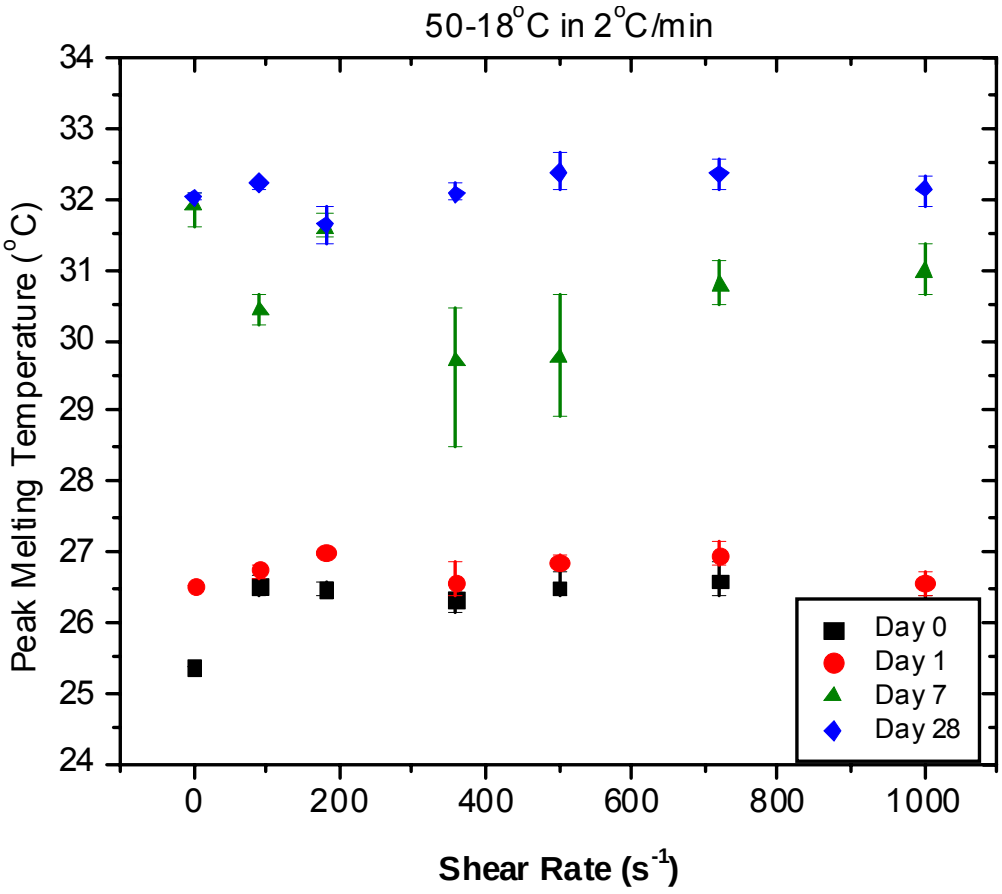

Figure 48: Graph showing peak melting temperature extracted from DSC melting curves for a sample of cocoa butter created under shear rates of 0-1000s^{-1} whilst cooled from 50-18°C in 2°C/min

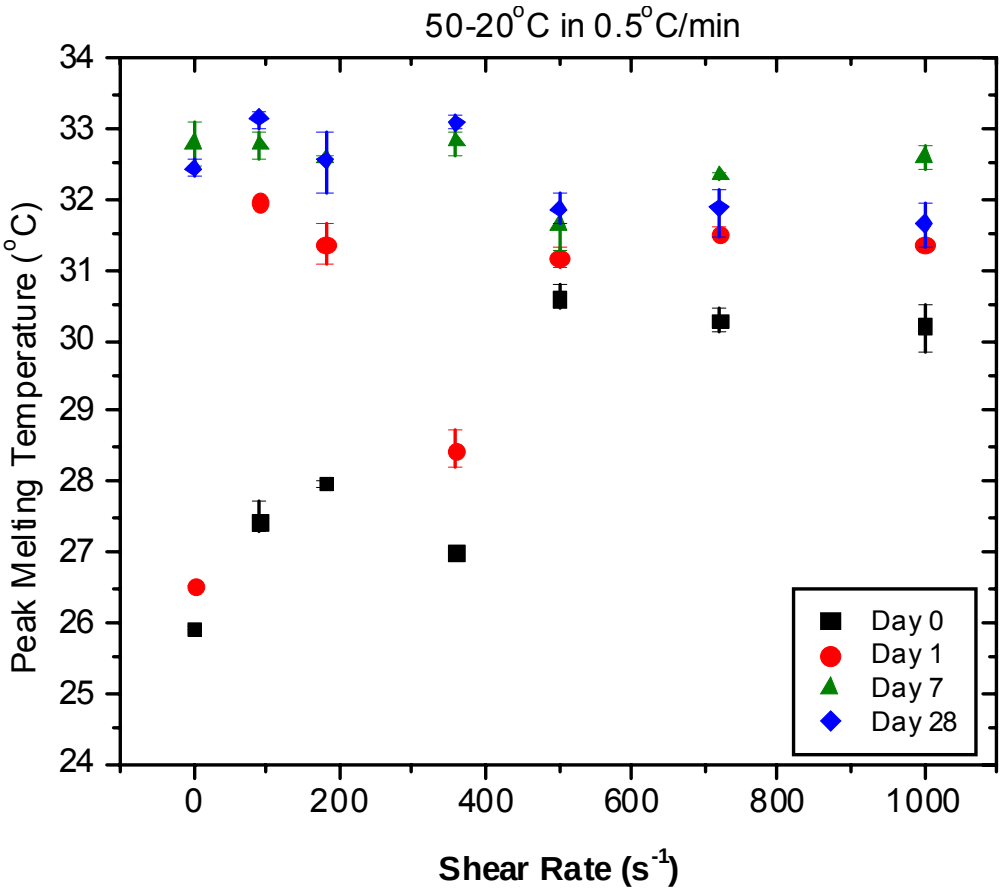

Figure 49 Graph showing peak melting temperature extracted from DSC melting curves for a sample of cocoa butter created under shear rates of 0-1000s^{-1} whilst cooled from 50-20°C in 0.5°C/min

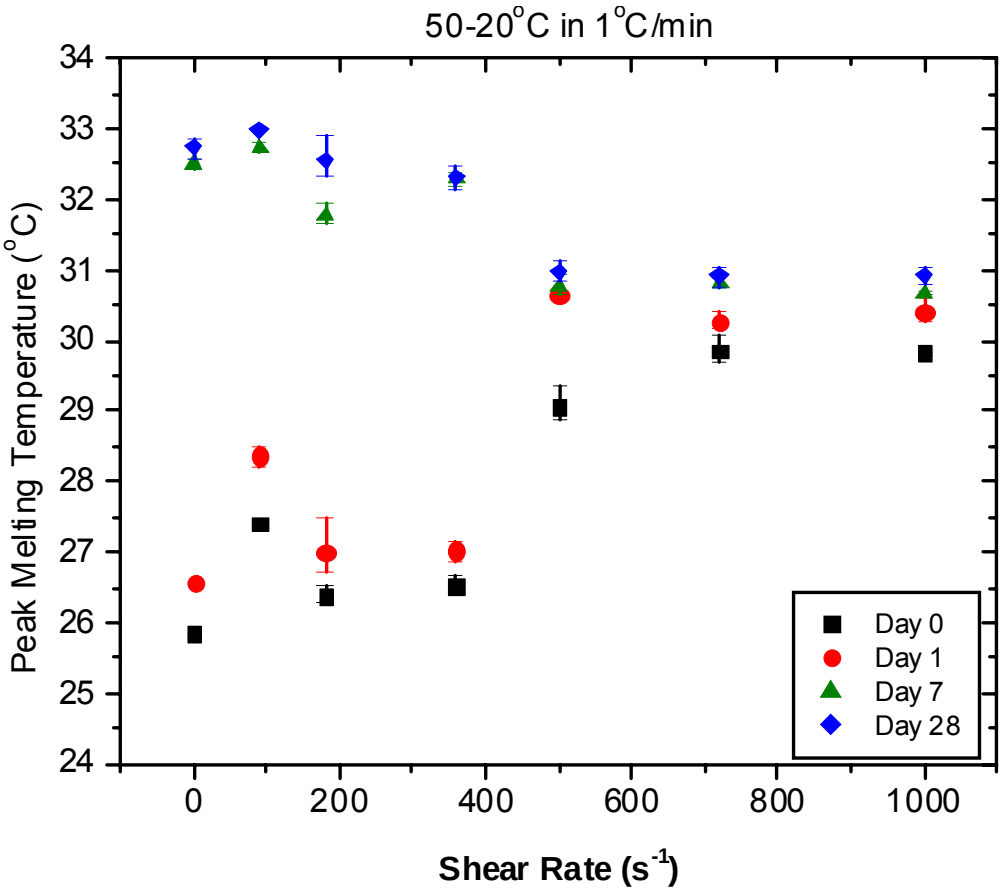

Figure 50: Graph showing peak melting temperature extracted from DSC melting curves for a sample of cocoa butter created under shear rates of 0-1000s^{-1} whilst cooled from 50-20°C in 1°C/min

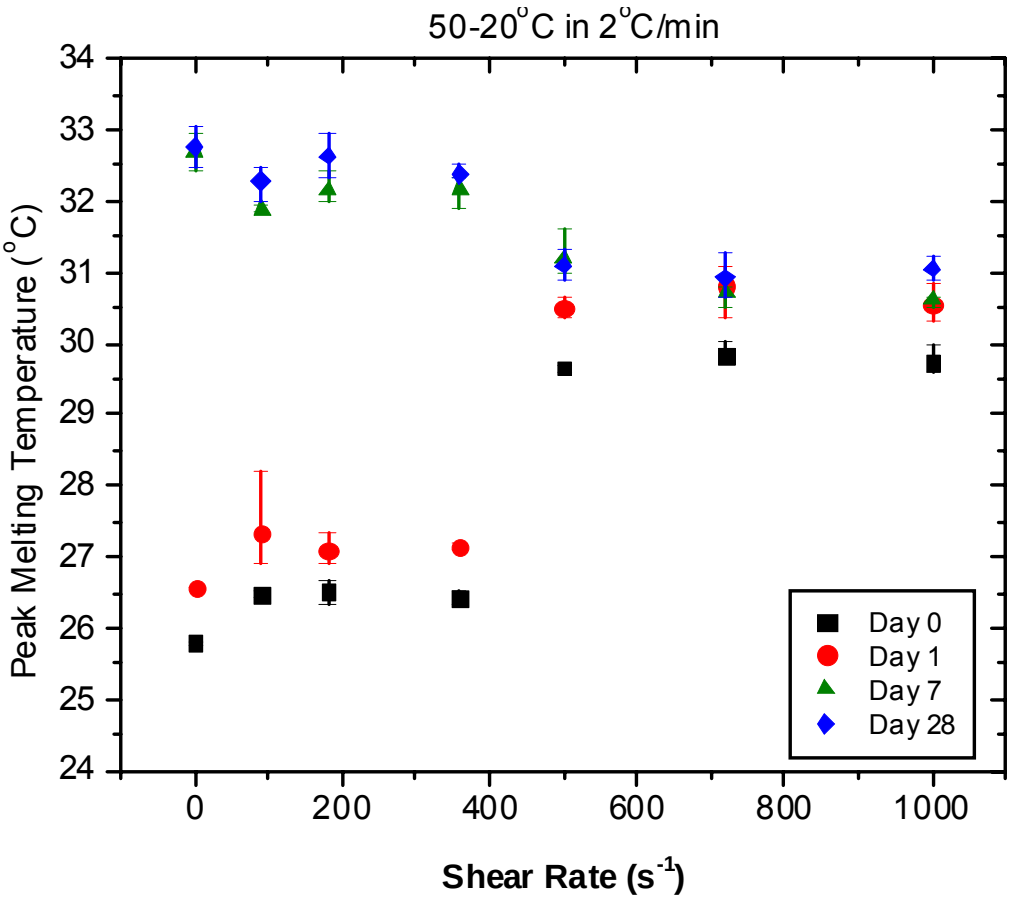

Figure 51: Graph showing peak melting temperature extracted from DSC melting curves for a sample of cocoa butter created under shear rates of 0-1000s^{-1} whilst cooled from 50-20°C in 2°C/min

Therefore we can see, barring the three exceptions out of the 9 temperature sets examined, there is generally a temperature transition shear rate, above which the peak melting temperature of the sheared cocoa butter is immediately elevated by approximately 2°C.

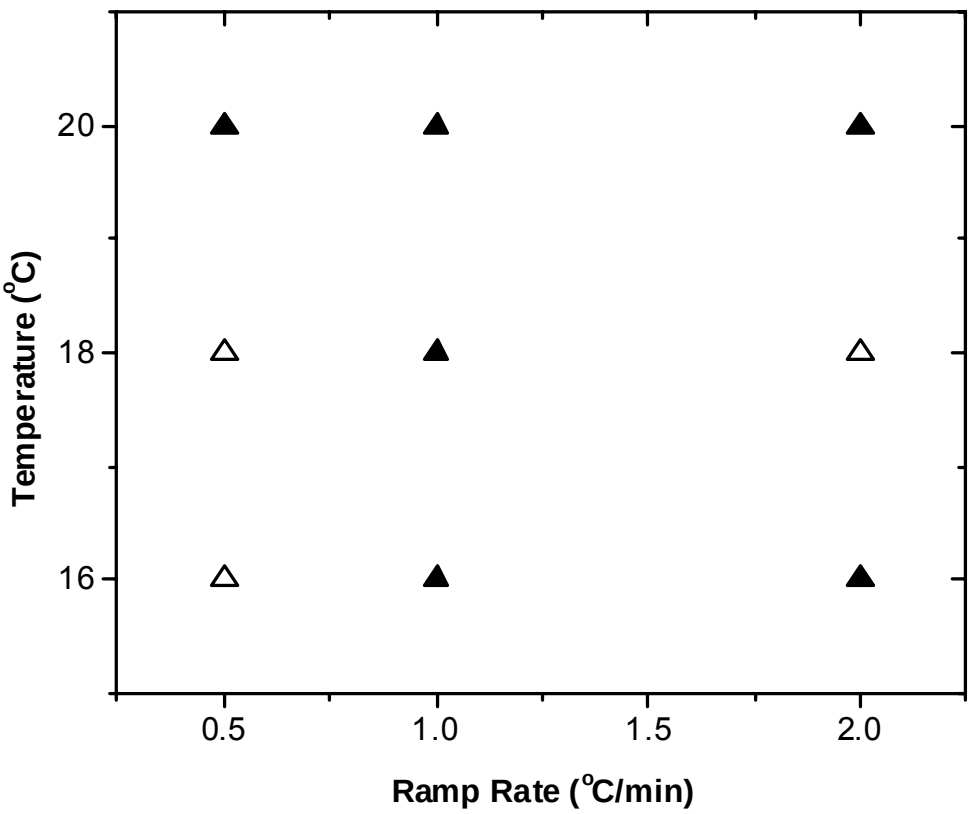

Figure 52: Figure depicting the occurrence of a shear transition in the DSC data. (△) represents no transition in a given data set, while (▲) represents a transition occurring.

To examine this transition more closely, we can take the 360 and 500 s^{-1}, day 0 data from Figure 51 and plot the heat flow curves together in Figure 53.

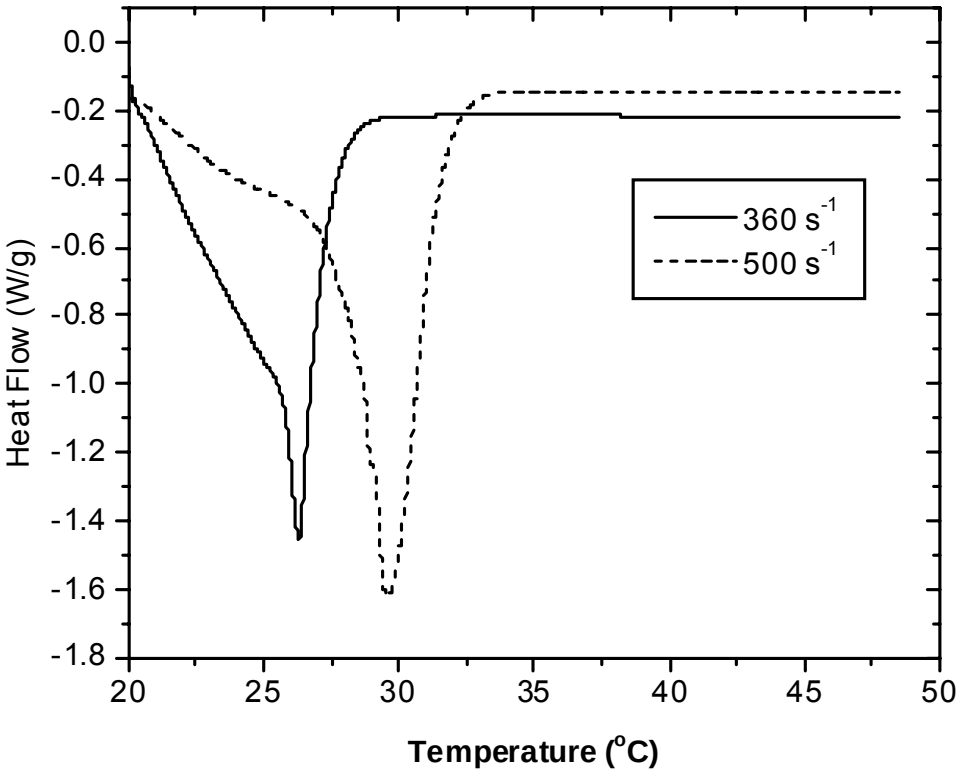

Figure 53: Heat flow vs temperature taken on day 0 for cocoa butter sheared at 360 and 500 s^{-1} whilst ramped from 50-20°C at 2°C/min

From this comparison we can see that there is a small amount of material contained with the $500s^{-1}$ sample which is melting over the range of the $360s^{-1}$ sample, however there is no complimentary higher melting component contained within the $360s^{-1}$ sample. Clearly there is a very large difference between these two melting curves.

We can also examine the difference between the day 28 melting curves for these two different samples (Figure 54).

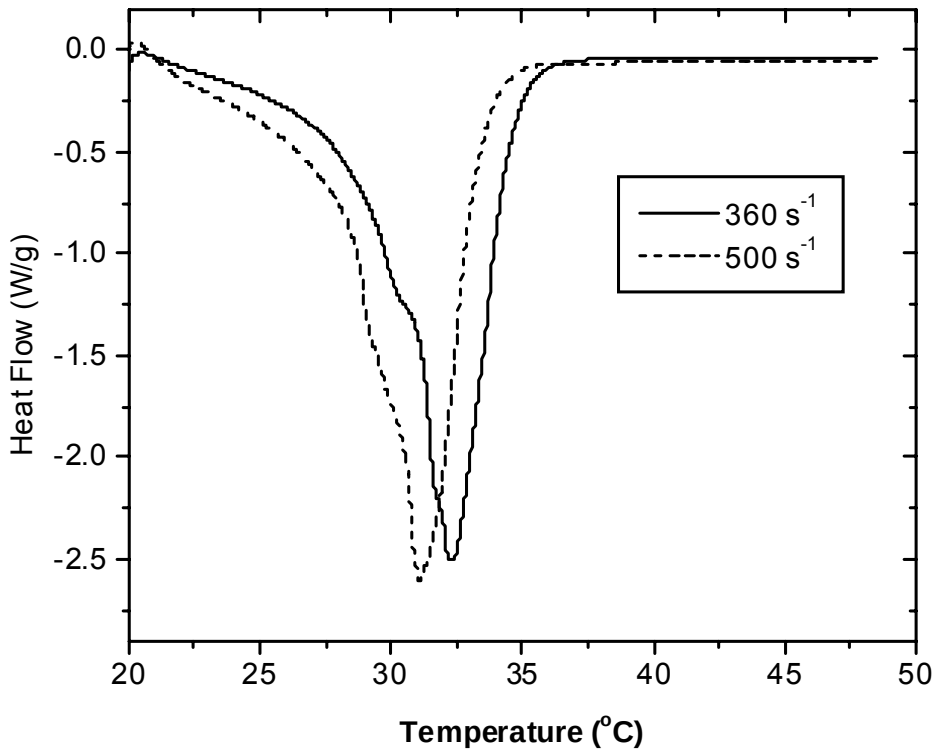

Figure 54: Heat flow vs temperature taken on day 28 for cocoa butter sheared at 360 and 500 s^{-1} whilst ramped from 50-20°C at 2°C/min

Figure 54 shows that the difference between the 360 and 500s^{-1} samples at day 28 is reversed from the day 0 effects, with the 500 s^{-1} sample now having the lower peak melting temperature by approximately 2°C. Unlike the day 0 data, these peaks seem very independent with neither seeming to contain a component of the other. They are both of similar width and amplitude. We can note though, that for these two graphs (Figure 53 and Figure 54) the value of peak heat flow is larger for the 500s^{-1} sample in both cases.

To see if there is a general trend in the dependence of the size of the heat flow peak on the shear rate and if that corresponds to the same shear transition as seen in the peak melting temperature graphs, we can construct graphs showing the area under the

heat flow peaks (enthalpy) and plot that against shear rate for the day 0, day 1, day 7 and day 28 samples. These plots can be found in Appendix 5 (Figure 138 to Figure 146).

Figure 138 to Figure 146 are considerably noisier than Figure 43 to Figure 51, however they show convergence above $500s^{-1}$ for the same samples. That is, for the transition shear rate of between 360 and 500 s^{-1}, there is an increase in the enthalpy for the day 0 and day 1 compared to values below the shear transition. The general noisiness of the data shows a general increase in the random error of the data. While these values incorporate error due to measurement of the mass of the samples, the variability also indicates that the amount of crystallization is much more variable than the melting temperature of those crystals.

We can note from the melting data that the melting temperatures observed at the higher shear rates are in fact lower that that generally seen for a β_V polymorph in this cocoa butter. In fact, as we have already noted, it is almost 2°C lower that that of the lower shear rate β_V forms produced. From this, as well as the fact that this lower melting temperature persists throughout the whole 28 days, it seems reasonable to conclude that the jump in melting temperature at higher shear rates is caused by crystallization of either a different polymorph or of predominantly lower melting temperature TAGs crystallizing into a β_V structure. This will be discussed further in section 3.

While the difference in melting temperature alone does seem very clear, obviously x-ray analysis is required for confirmation (and can be found in section 2.3.2) and supports the theory of selective crystallization.

Still to be discussed, however, is the reason behind the certain data sets which do not exhibit the shear transition. These data sets are the 50-16°C in 0.5°C/min, the 50-

18°C in 0.5°C/min and the 50-18°C in 2°C/min. There are a few possibilities for the explanation. Firstly, there may simply be no transition for those conditions. The slow cooling rate of 0.5°C/min for examples allows for a much slower crystallization and more α crystallites to form before a β_V transition. The presence of a larger amount of α crystallites could impede the transformation into the chemically altered β_V form.

Secondly, we have seen that the transition need not occur at $500s^{-1}$, it has been seen at $720s^{-1}$, and therefore it is possible that a transition occurs off the scale, above $1000s^{-1}$. Unfortunately the rheometer limitations make this impossible to test.

The third possibility is a function of the experimental variability. It was seen over the course of these measurements that a given data point above the shear transition could show no change in temperature for one sample, yet for a repeated sample created under exactly the same conditions with a very similar viscosity profile, there would be a change in temperature. While unlikely due to the number of repetitions done for the three data sets, it is possible that a transition is merely less likely, but still possible under those conditions.

If we consider what the data sets have in common, we can see that the 0.5°C/min ramps are more likely explained by the lack of a transition point simply due to the presence of a large amount of α crystallites which remain through the β_V transition. The 18°C in 2°C/min data set seems more likely to be explained as either having a higher transition shear rate or merely having an erroneous $1000s^{-1}$ data point.

We must still consider why such a transition with shear would occur in the first place. First, however, the x-ray and mechanical data should be examined to provide a fuller picture of the situation. A more detailed discussion will follow in section 3.

2.3 X-ray Measurements of Sheared Cocoa Butter

Once a sample of cocoa butter has been extracted from the split couette apparatus (Section 2.1), x-ray diffraction studies can be done to assess the orientation of the sample. A fixed target CuK_α source was utilized with a focusing graphite monochromator crystal and a Bicron point detector. This gives a beam with a wavelength of 1.54 Å. One set of slits before the sample was used to further collimate the x-ray beam and two further pairs on either end of a helium filled flight path after the sample helped cut out background scatter. The resulting beam has a resolution $\Delta q = 0.03$ Å^{-1}. The sample is mounted in a Huber 4-circle diffractometer.

In order to minimize the effects of sample size on the orientation scans, the sample needs to be as uniform as possible. If this was not the case then the effects of attenuation though varying amounts of cocoa butter could mimic orientation. Since the thickness of the cocoa butter is 1mm, a sample is created which is roughly a cylinder of diameter 1mm and height 1mm. The cocoa butter cylinder can then be mounted on a wire and placed in the x-ray beam whose size is larger than the sample. Thus, the entire sample volume is encompassed by the beam. By rotating the detector through a scan in the theta plane, a diffraction image can be achieved (such as those shown in Appendix 2). Since the application of shear accelerates the appearance of the form V structure, only orientation in that structure was investigated as it persisted over the course of all of the measurements. A typical orientation, or mosaic, scan of the (002) diffraction peak of the β_V crystal is shown in Figure 55. The (002) peak was selected since it was a clearer peak, away from the interference of the direct beam on the data

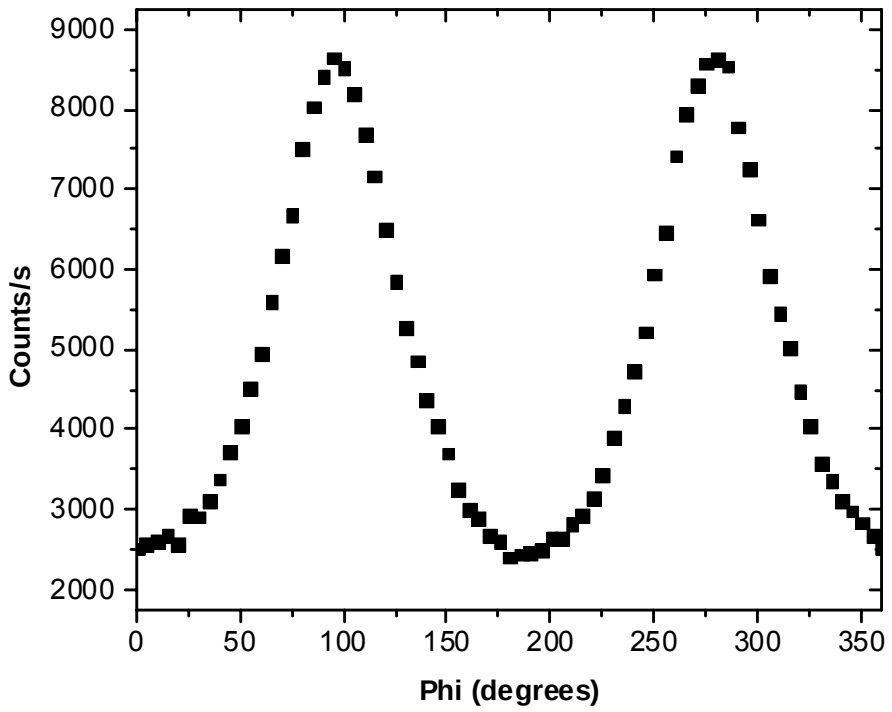

Figure 55: Graph showing x-ray intensity values as a function of Phi rotation for a 1mm^2 piece of cocoa butter created in the split couette attachment by ramping from 50-20°C in 2°C/min, whilst shearing at 1000s^{-1}

Figure 55 is a scan in the phi plane. The chi plane is similarly oriented, however the placement of the mounting wire causes attenuation of the x-ray reflection in that plane. To find the correct degree of orientation the phi scan must be done whilst the chi angle is at a peak maximum. To accomplish this, a phi scan can be done and the phi angle moved to one of the two peaks (from Figure 55 this would be either 90 or 270 degrees). Then a chi scan (with phi fixed at either 90° or 270°) can be done and the chi angle moved to one of the two peak intensities determined from that scan. The process is then iterated to produce the most accurate values for orientation.

This process is very time consuming, but it can be sped up due to the discovery that the peak orientation was always in line with the plane of the applied shear. When the

sample is place in the Huber 4-circle diffractometer and centred it can also be oriented in the chi plane by eye, through the use of a telescope. This method was found to be accurate within 0.5 degrees and had a negligible effect on the orientation FWHM. In this way, only a phi scan need be done to determine degree of sample orientation.

The phi data can then be fit with a Gaussian model to determine FWHM.

2.3.1 X-ray Diffraction Data

The orientation data recorded for the 9 different temperature profiles are all fairly straightforward. Orientation was detected for all data sets starting at either $180s^{-1}$ or $360s^{-1}$. Following that there is a general decrease in the FWHM, or increase in degree of orientation, after which there is either a plateau or a slight increase. The data can be found in Figure 56, Figure 57 and Figure 58. Error bars reflect data variation.

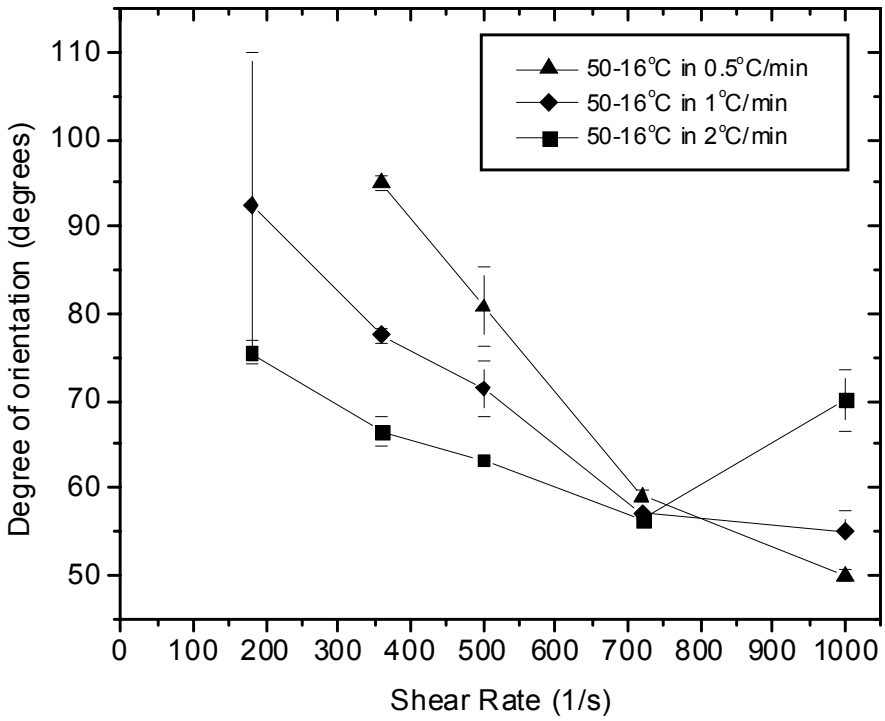

Figure 56: Orientation FWHM of phi scans done of cocoa butter ramped from 50-16°C at 0.5, 1 and 2°C/min whilst sheared at 0 – 1000s^{-1}. Data points not shown do not have orientation.

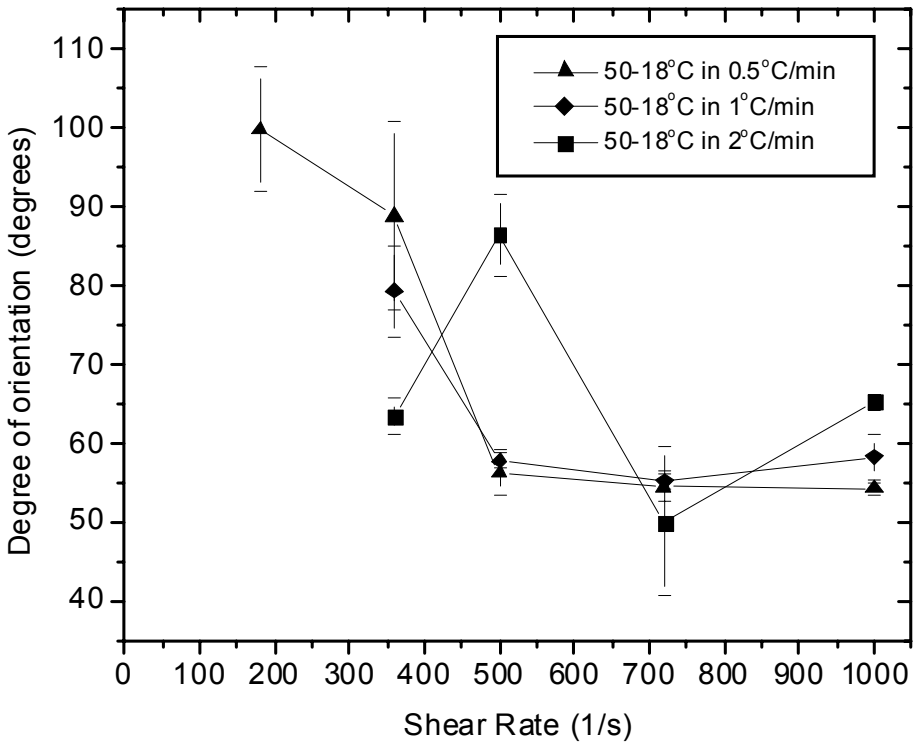

Figure 57: Orientation FWHM of phi scans done of cocoa butter ramped from 50-18°C at 0.5, 1 and 2°C/min whilst sheared at 0 – 1000s^{-1}. Data points not shown do not have orientation.

The general increase in the degree of orientation is expected from previous results[25], which showed an increase in the degree of orientation with shear rate. The few points which appear to be discrepancies in this trend would perhaps be eliminated with an increased sampling.

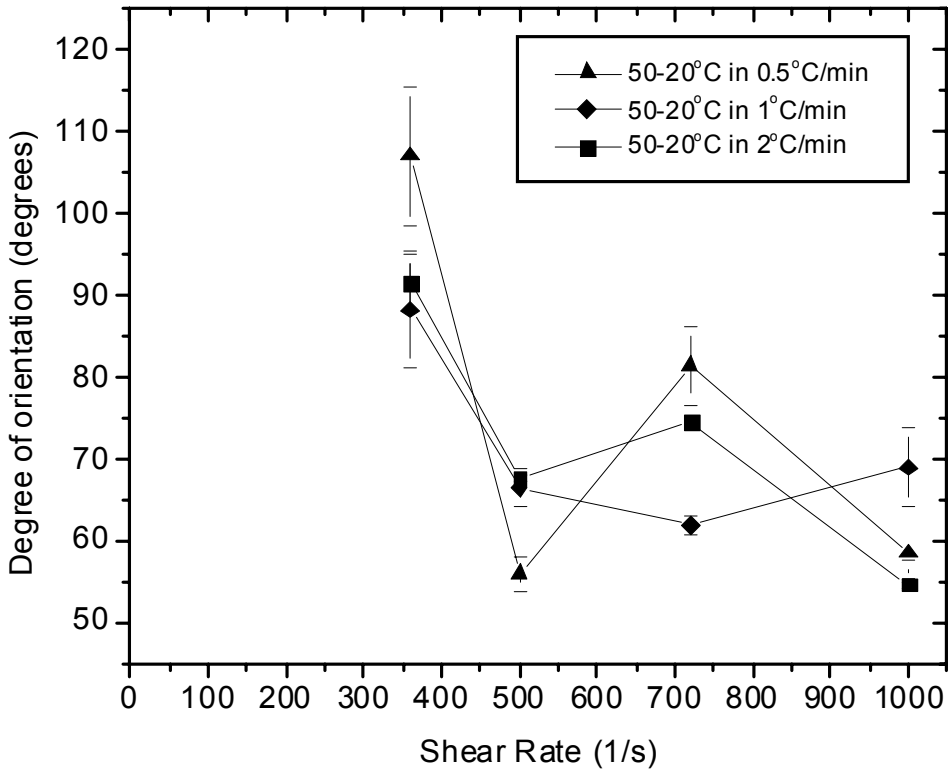

Figure 58: Orientation FWHM of phi scans done of cocoa butter ramped from 50-20°C at 0.5, 1 and 2°C/min whilst sheared at 0 – 1000s^{-1}. Data points not shown do not have orientation.

Clearly the x-ray diffraction data confirms our expectation from previous work that orientation of the crystallites occurs with high shear rates and that the orientation increases up to a point before either plateauing or decreasing again slightly due perhaps to the effects of viscous heating.

2.3.2 X-Ray structure examination

In order to further examine the effect seen in the DSC results, samples of 50-20°C in 2°C at 360s^{-1} and 500s^{-1} were chopped into a fine powder and placed in 1.5mm glass capillaries. A scan in q was then done over a range of q=0.05 to 2$Å^{-1}$ at time intervals similar to those done in the DSC experiments, i.e., day 1, ~day 7 and ~day 28. Exactly the same x-ray lineup was used for both samples and they were stored together.

Figure 59 shows data for the 360 s^{-1} sample on each of day 1, day 8 and day 34. The day 1 pattern shows a mixture of form V with at least one of the other polymorphs of forms II, III and IV (see Appendix 2). The day 8 and day 34 data are almost identical however, with a clear form V pattern.

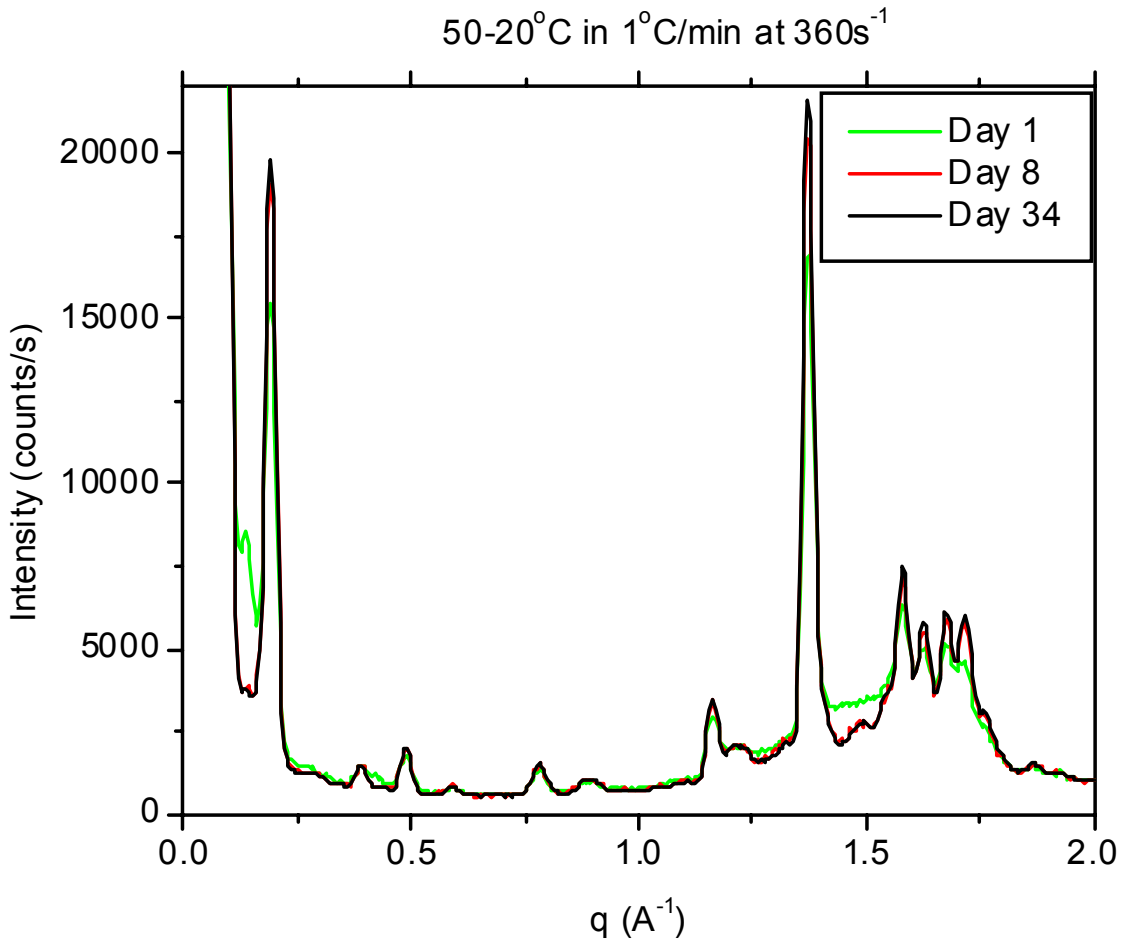

Figure 59: X-Ray diffraction patterns in q of a capillary of a chopped sample of cocoa butter created with a temperature ramp from 50-20°C in 1°C/min whilst shearing at 360s^{-1} on each of day 1, day 8 and day 34.

Figure 60 shows data for the 500 s^{-1} sample on each of day 1, day 8 and day 33. The day 1 sample here does not show any signs of being a mixture of any of form II, III or IV as concluded from the DSC results. It is, however, less intense than the day 8 and day 33 data, indicating less material scattering, hence we can conclude a smaller amount

of β_V material is present. We can also note that the shape of the peaks in the region of q=1.5 to 1.8Å^{-1} appear different from those in a normal β_V pattern.

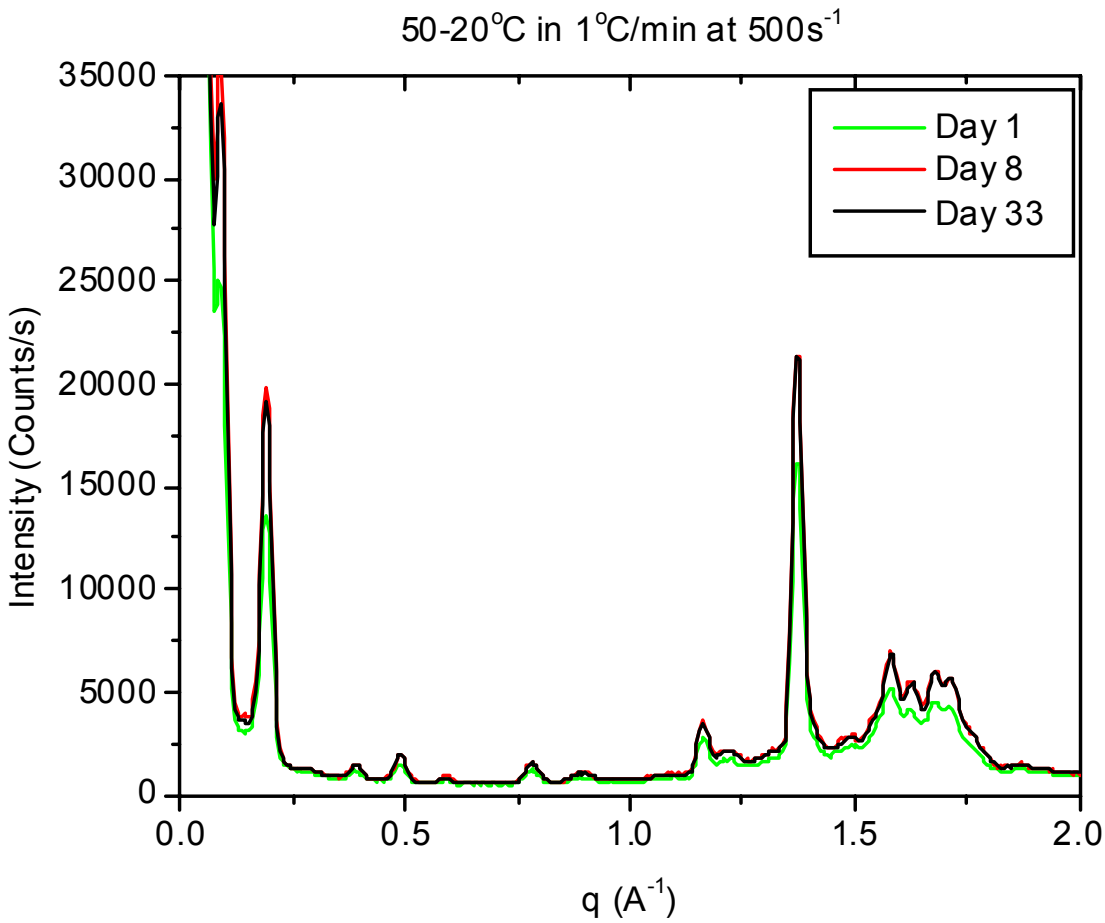

Figure 60: X-Ray diffraction patterns in q of a capillary of a chopped sample of cocoa butter created with a temperature ramp from 50-20°C in 1°C/min whilst shearing at 500s^{-1} on each of day 1, day 8 and day 33.

Figure 61 shows a comparison of the q=1.5 to 1.8Å^{-1} region of the 360 and 500s^{-1} data on day 34 and 33. While the rest of the data is almost an exact match, this area shows deviations. If we consider the four peaks shown, then the height of the 1st, 2nd and 4th peaks are quite different, with the 360s^{-1} sample having more intensity. The troughs between these peaks are also of different heights. Overall the 360s^{-1} sample has much sharper, more intense peaks.

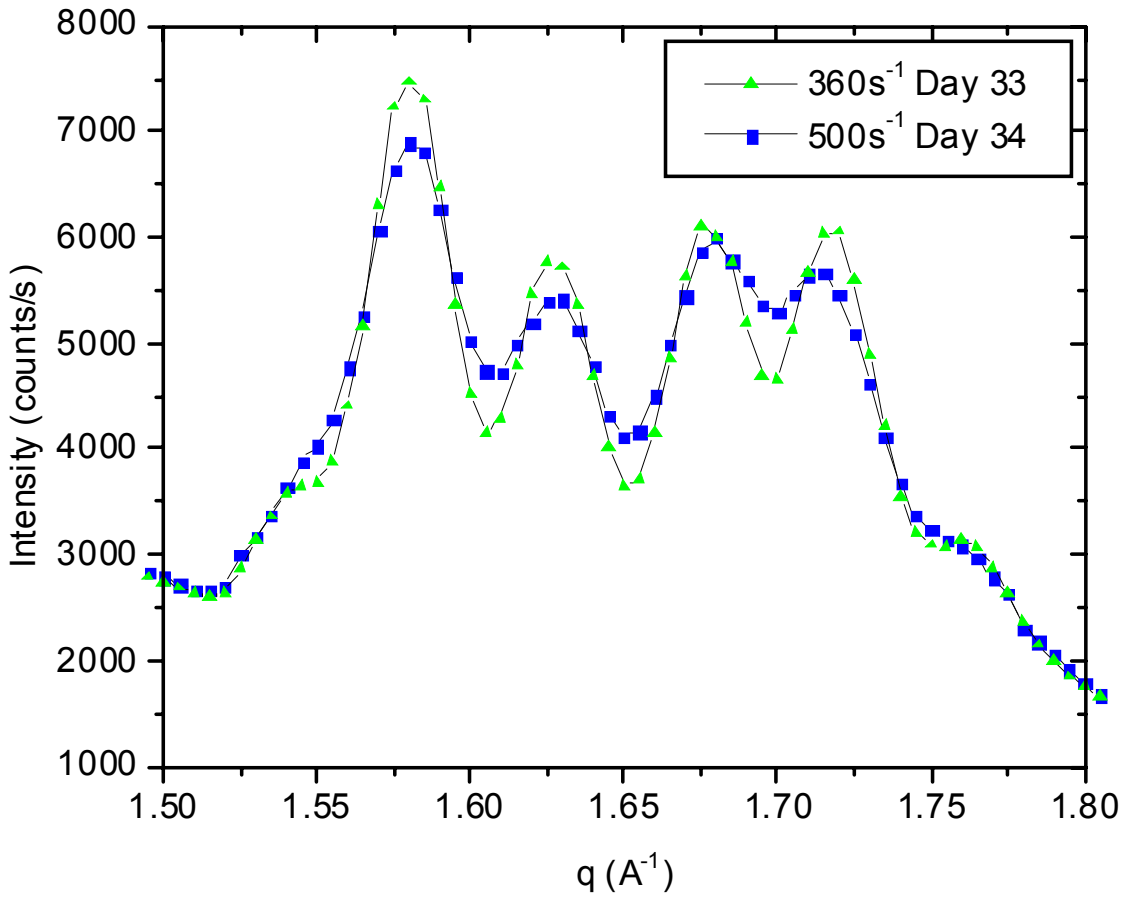

Figure 61: Comparison of x-ray diffraction patterns in q of a capillary of a chopped sample of cocoa butter created with a temperature ramp from 50-20°C in 1°C/min whilst shearing at $360s^{-1}$ and $500s^{-1}$ on day 34 and 33 respectively.

It should also be noted that this is also the area which shows the main differences between forms V and VI [84]. Figure 62 is taken from high resolution synchrotron data in Guthrie et al. [84] and shows the q=1.5 to 1.8$Å^{-1}$ range for a comparison of forms V and VI. We notice that for form VI there are peaks between the main 4 peaks of the form V pattern. Now, if we look again at Figure 61 we see that there in an increase in intensity at those places for the $500s^{-1}$ sample.

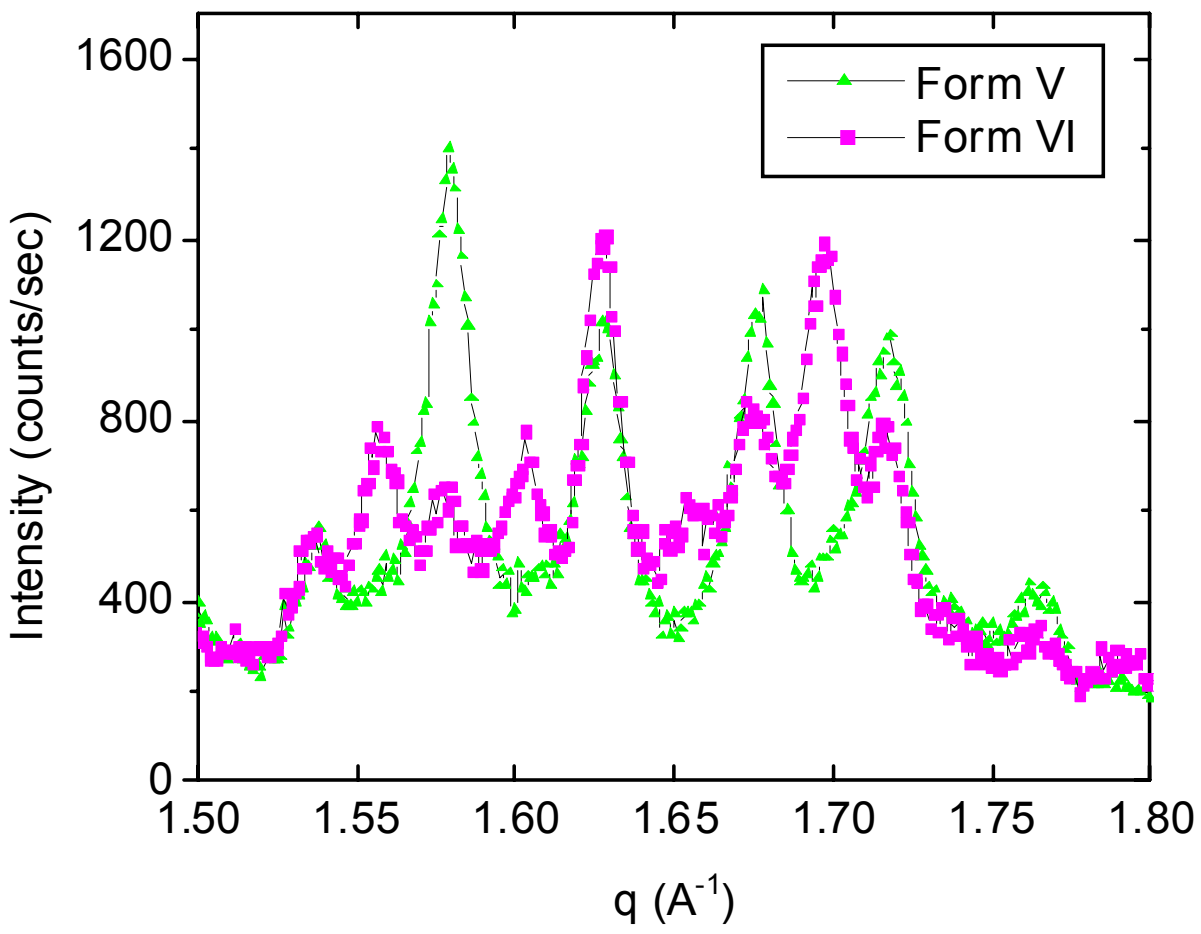

Figure 62: Comparison of form V and VI high resolution x-ray patterns taken from Guthrie et al. [84]

If we were to consider this data alone, we might conclude that the $500s^{-1}$ sample is a mixture of forms V and VI. However, if we take into account the DSC peak melting data we realize that the melting temperature of the $500s^{-1}$ sample is several degrees *below* what a mixture of forms V and VI would produce. Clearly this is evidence to support the hypothesis that lower melting temperature TAGs are predominantly crystallizing. This would allow for a structure with a mixture of form V and VI to have a lower melting temperature.

An attempt was made to assess whether the $500s^{-1}$ data was actually a combination of β_V and β_{VI} by data fitting. The high resolution data shown in Figure 62

was taken as a sample of β_V and β_{VI}. Since it is higher resolution than the data shown in Figure 61 it would be hard to compare in its current format. Consequently a convolution of the data with a Gaussian needed to be performed to artificially lower the resolution of the data sets.

A convolution is an operator which takes two functions f and g and produces a third function that, in a sense, represents the amount of overlap between f and a reversed and translated version of g. Said another way, it is an integral that expresses the amount of overlap of one function g as it is shifted over another function f. It therefore blends one function with another. Mathematically, it is defined as:

$$f * g \equiv \int_0^t f(\tau)\, g(t-\tau)\, d\tau,$$

Thus, a convolution of the β_V and β_{VI} data sets was performed with a Gaussian function which had a FWHM of 0.01. Code for performing this operation can be found in [85].

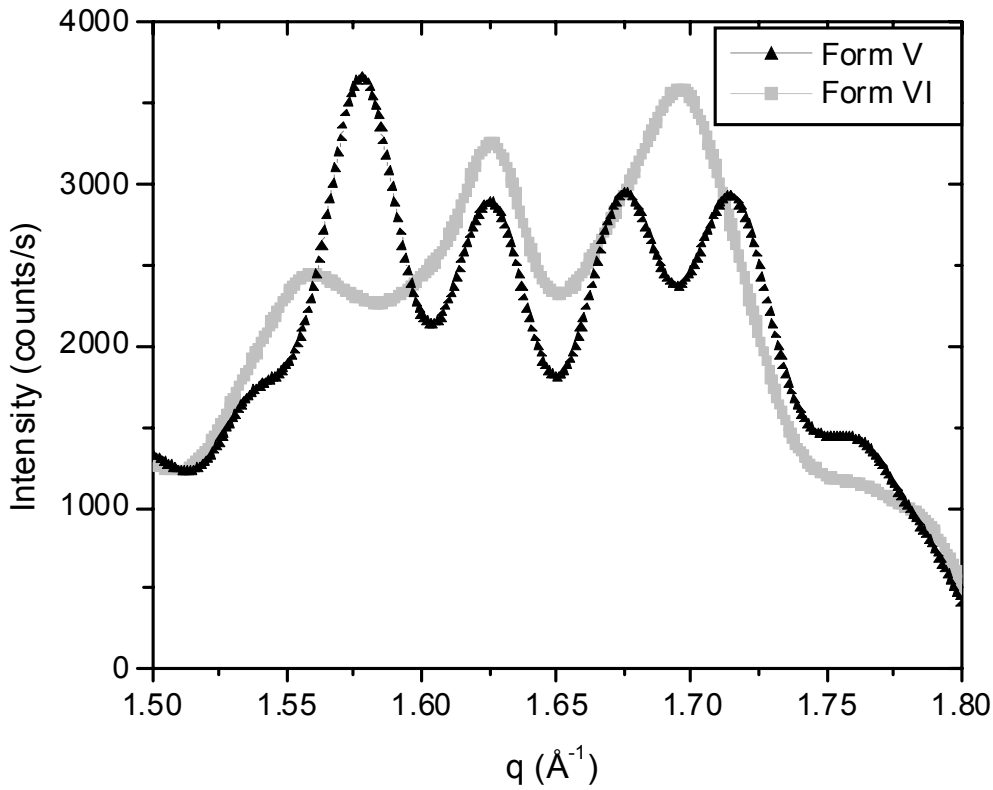

Figure 63: Form V and VI high resolution x-ray patterns taken from Guthrie et al. [84] and convoluted with a Gaussian of FWHM 0.01 to effectively decrease the resolution of the x-ray patterns

The results of the convolution can be seen in Figure 63. After the convolution is performed the data can be combined to see which mixture of β_V and β_{VI} fit the 500s^{-1} data the best.

The formula used was $\beta_V * x + \beta_{VI} * (1-x) = Y$, where Y represents the 500s^{-1} data set and x is varied to produce the closest fit. The value achieved for x was 0.701 with a χ^2 of 1.96. Thus a sample with approximately 70% β_V fit the 500s^{-1} data the best.

From Figure 64 we can see that this result, while crude, yielded a substantially higher peak at the 1.625 position for the fit line. While by no means definitive, it is evidence against this modified structure being partially form VI.

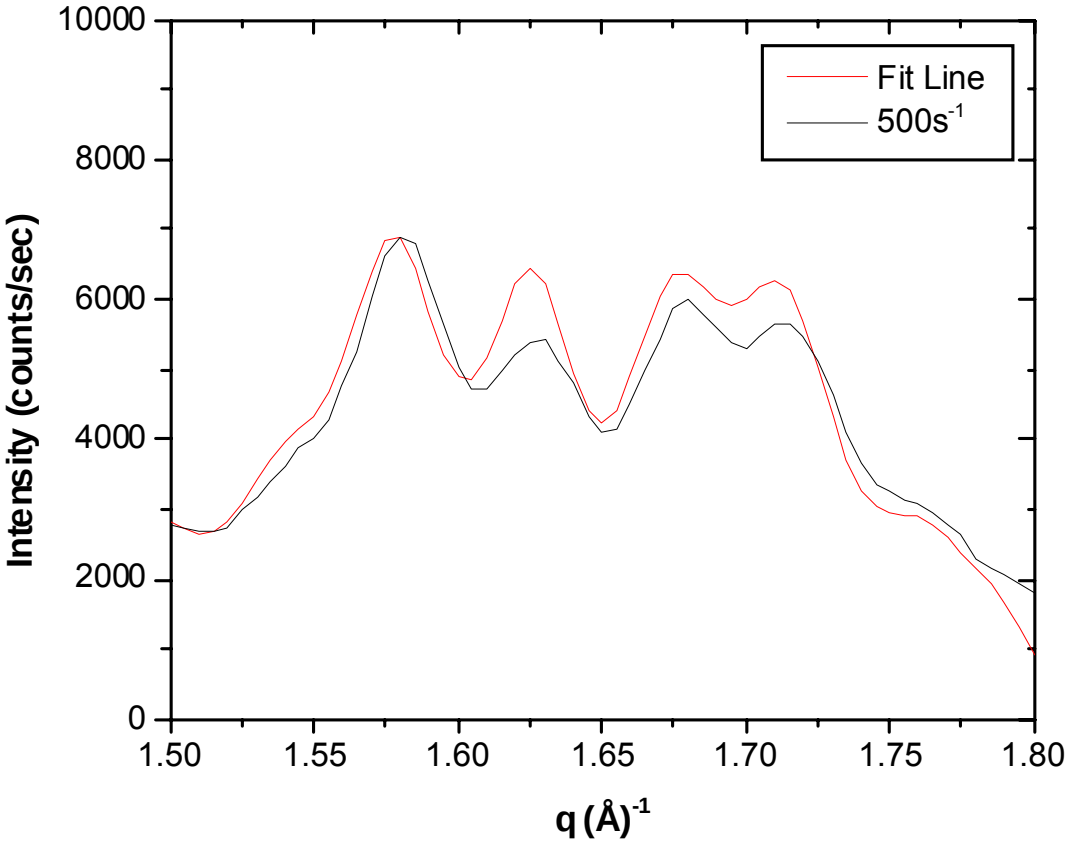

Figure 64: Figure showing x-ray diffraction patterns in q of a capillary of a chopped sample of cocoa butter created with a temperature ramp from 50-20°C in 1°C/min whilst shearing at $500s^{-1}$ on day 33 compared with a fit line generated from a combination of 70%β_V and 30% β_{VI} .

2.4 Mechanical Testing

In order to measure the strength of the oriented cocoa butter samples a simple apparatus was designed incorporating a Transducer Techniques 50 mN load cell and a 3-point bending attachment (Figure 65).

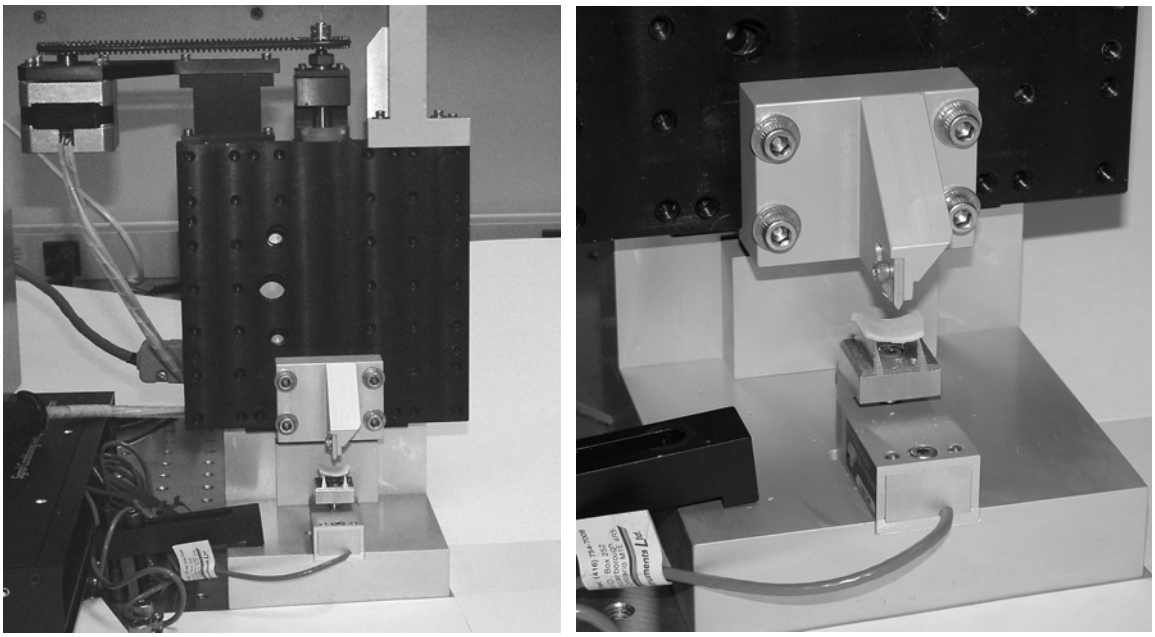

Figure 65: Three point bending apparatus.

A motor is attached to a simple translation stage mounted in a vertical position. A MicroE optical encoder is attached to the stage to accurately measure its movement. The upper blade of the three point bending system is also attached to the stage, while the lower two blades are mounted on the load cell. The entire system is controlled via a LABVIEW program. As the motor is commanded to move at a steady rate, the optical encoder is monitored and the position is recorded. A sample of cocoa butter is placed on the lower two blades of the three-point bending system, which sits on the load cell. This load cell is a force sensor and as the upper blade makes contact with the cocoa butter

sample, the load cell measures the applied force and it is recorded as a function of the optical encoder position (Figure 66). As the motor continues to move the blade downwards, the force applied to the cocoa butter continues to increase until the sample breaks and the measured force returns to zero. A sample force versus position graph is shown in Figure 66.

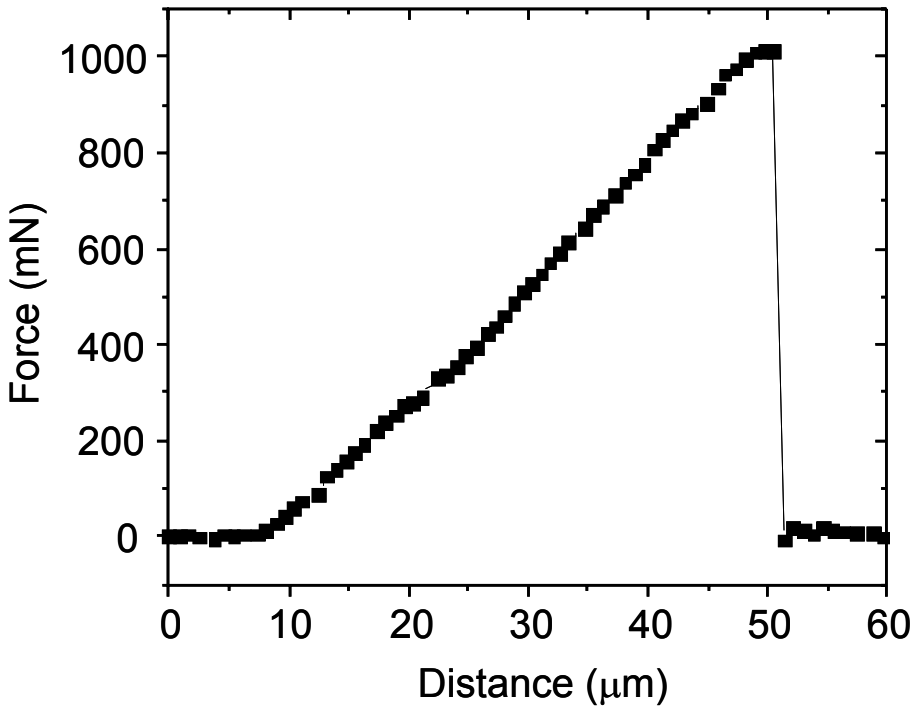

Figure 66: Sample force versus position graph for 50-20°C in 2°C/min at $1000s^{-1}$

The value of peak breaking force can then be recorded and converted into peak breaking stress as outline in section 1.5.2. The force versus position graphs can also be fit and the slopes converted into Young's modulus values via equation (63).

2.4.1 Mechanical Testing Data

Graphs of peak breaking stress versus shear rate for the 9 different temperature profiles are shown in Figure 67 to Figure 69. The results are very strikingly similar to those seen in section 2.2 for the DSC values.

For those samples which exhibited a transition in melting temperature between 360 and 500s^{-1} (50-16°C in 1°C/min and 2°C/min; 50-18°C in 1°C/min; 50-20°C in 0.5°C/min, 1°C/min and 2°C/min) we can see that there is also a transition in peak breaking stress with the shear rates above the transition showing an increase in breaking stress.

Figure 67 is perhaps the least clear of the three end point temperatures reflecting the fact that there is a higher solid fat content (SFC) in the samples at the lowest temperature of 16°C and hence the peak breaking stress is already higher than for the other two samples. Despite this we can see that there is an increase for the 1 and 2°C/min samples with shear rate, but not for the 0.5°C/min sample. Any increase seen there is within the range of error.

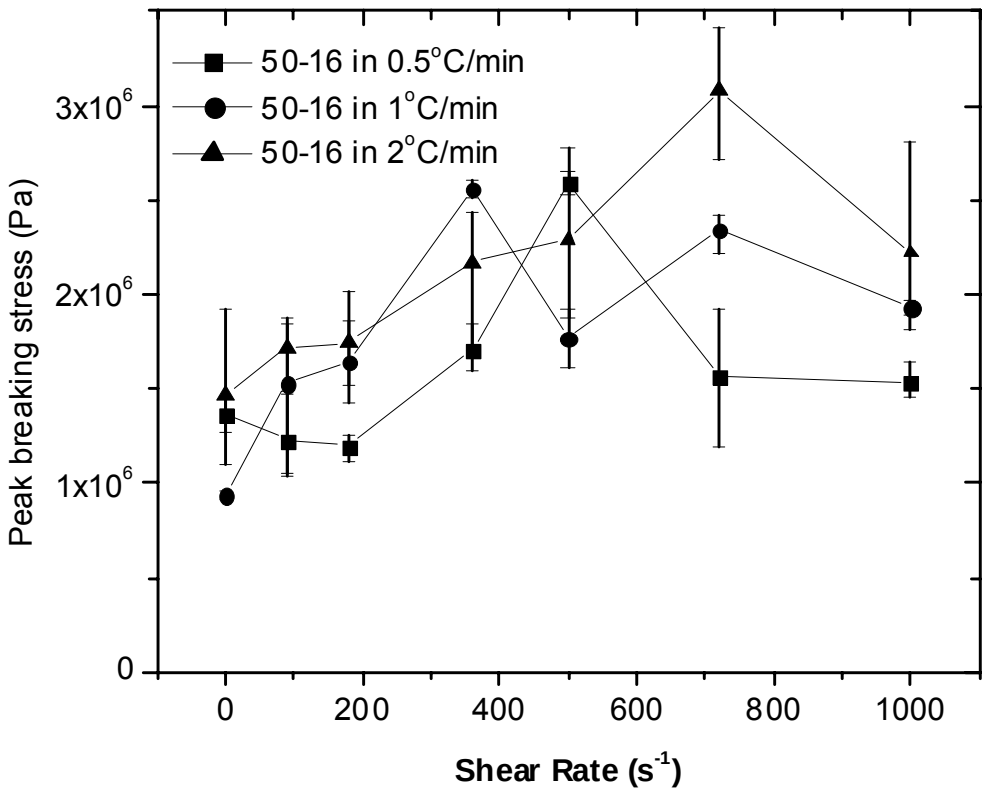

Figure 67: Graph showing peak breaking stress values for a sample of cocoa butter created under shear rates of 0 – 1000s^{-1} whilst cooled from 50-16°C at 0.5, 1 and 2°C/min

The two higher end point temperatures of 18°C and 20°C seen in Figure 68 and Figure 69 have a much clearer transition. For Figure 68 the only temperature transition was seen in the 1°C/min ramp and here there is clearly a jump to higher breaking stress for 500s^{-1} and above. There is an anomalous data point for 1000s^{-1} in the 2°C/min ramp data. The data set does not show a transition in DSC, yet seems to show the hint of a transition here between 720 and 1000s^{-1}. It was previously suggested that this sample might have a transition which is either at or above 1000s^{-1} and not seen in the DSC experiments. This could be supporting evidence of that.

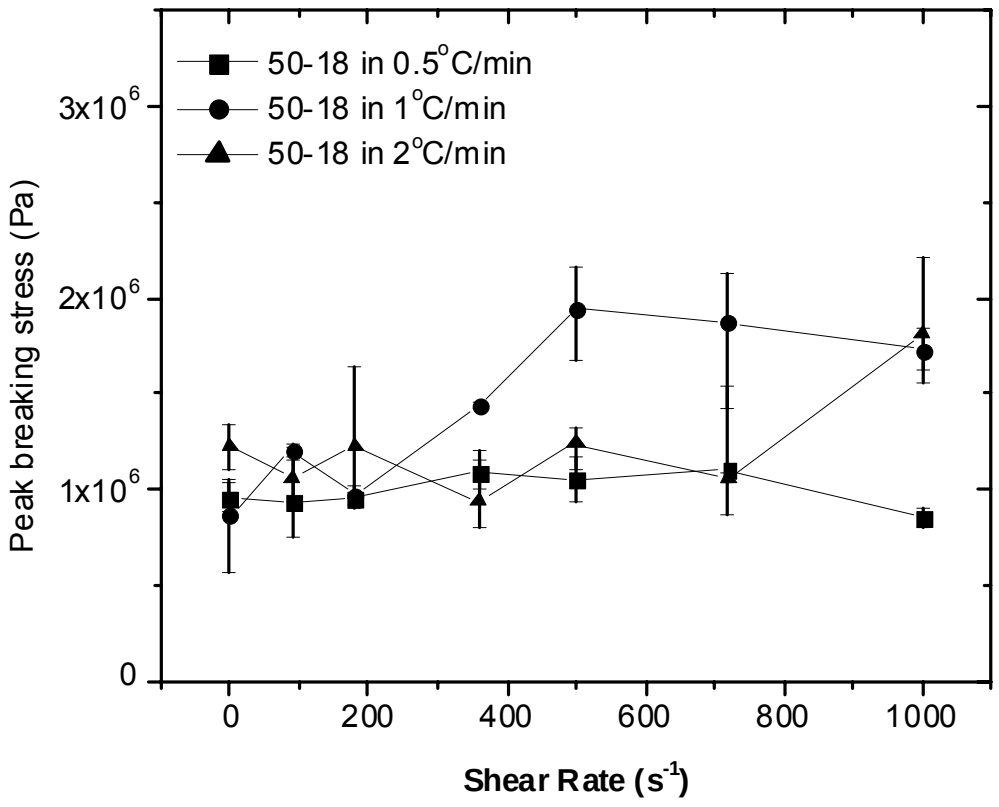

Figure 68: Graph showing peak breaking stress values for a sample of cocoa butter created under shear rates of 0 – 1000s^{-1} whilst cooled from 50-18°C at 0.5, 1 and 2°C/min

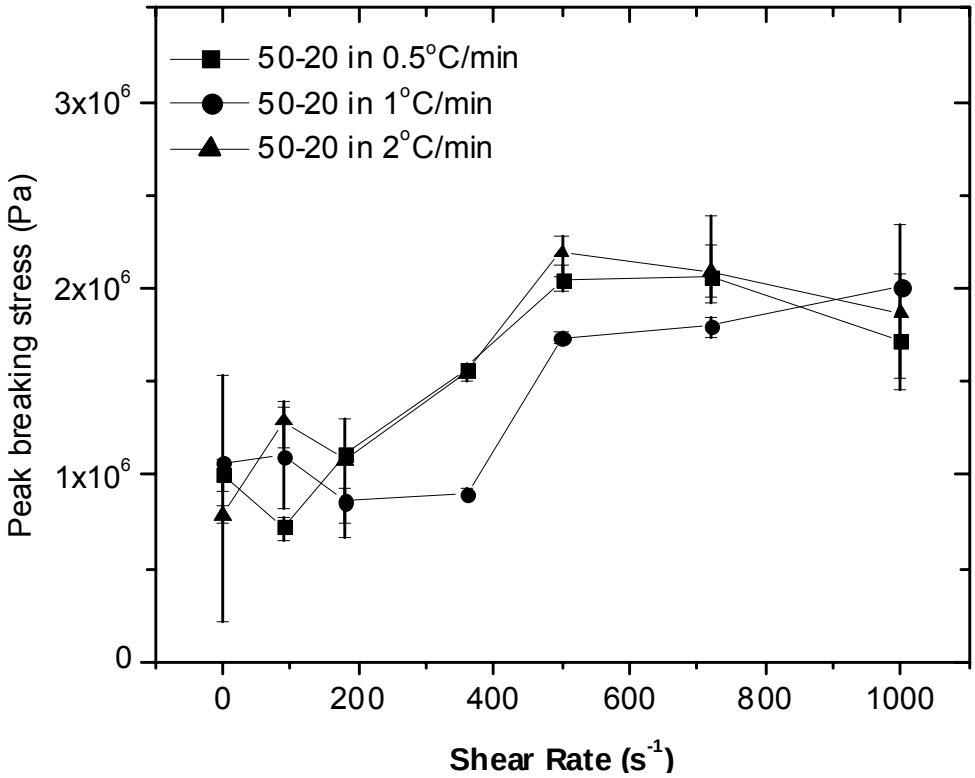

Figure 69: Graph showing peak breaking stress values for a sample of cocoa butter created under shear rates of 0 – 1000s^{-1} whilst cooled from 50-20°C at 0.5, 1 and 2°C/min

For Figure 69 which shows the highest end point temperature of 20°C, the transition is also very clear, with all shear rates of 500s^{-1} and above showing increased breaking stress values.

The results shown are for samples oriented as in Figure 17, with the upper blade in the trough of the curve. Data was also collected in the other plane at 90°, with the upper blade contacting the edges of the trough (Figure 70). These results were virtually identical (with those shown) within the range of error and are not shown.

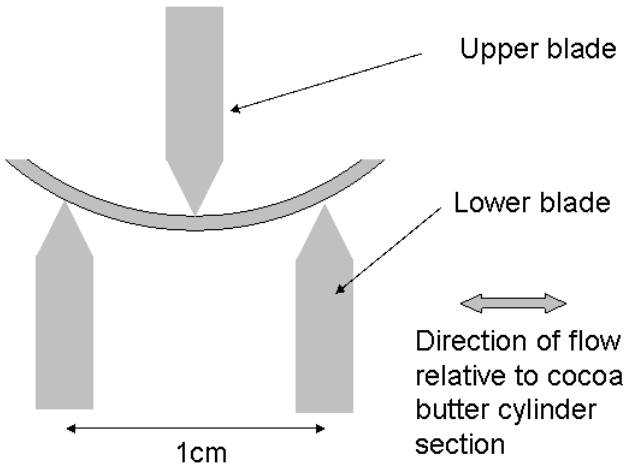

Figure 70: Diagram showing orientation of cocoa butter cylinder section in 3-point bending apparatus

The third dimension was never adequately tested due to the very small 1mm thickness. Samples of 1mm x 1mm x 10mm rectangles were attempted but the error involved for such small samples caused the attempt to be abandoned.

There are a few theories which could explain increased breaking stress: there could be a decrease in the grain size; or there could be an increase in the SFC; or a decrease in the number of defects in the crystal structure. Any or all of these explanations could be responsible for these results, however the matter will be further discussed in section 3.

The Young's Modulus of the samples can also be calculated through the slope of the breaking curves via equation (63)**.** These values can be found graphed in Figure 71, Figure 72 and Figure 73.

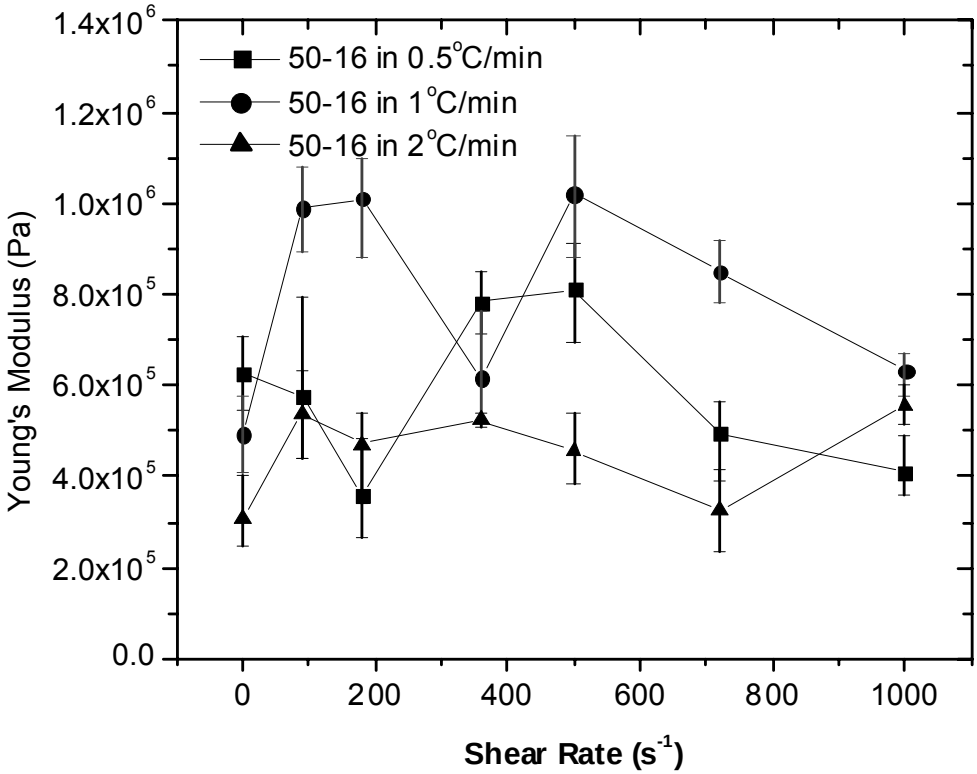

Figure 71: Graph showing Young's Modulus values for a sample of cocoa butter created under shear rates of 0 – 1000s^{-1} whilst cooled from 50-16°C at 0.5, 1 and 2°C/min

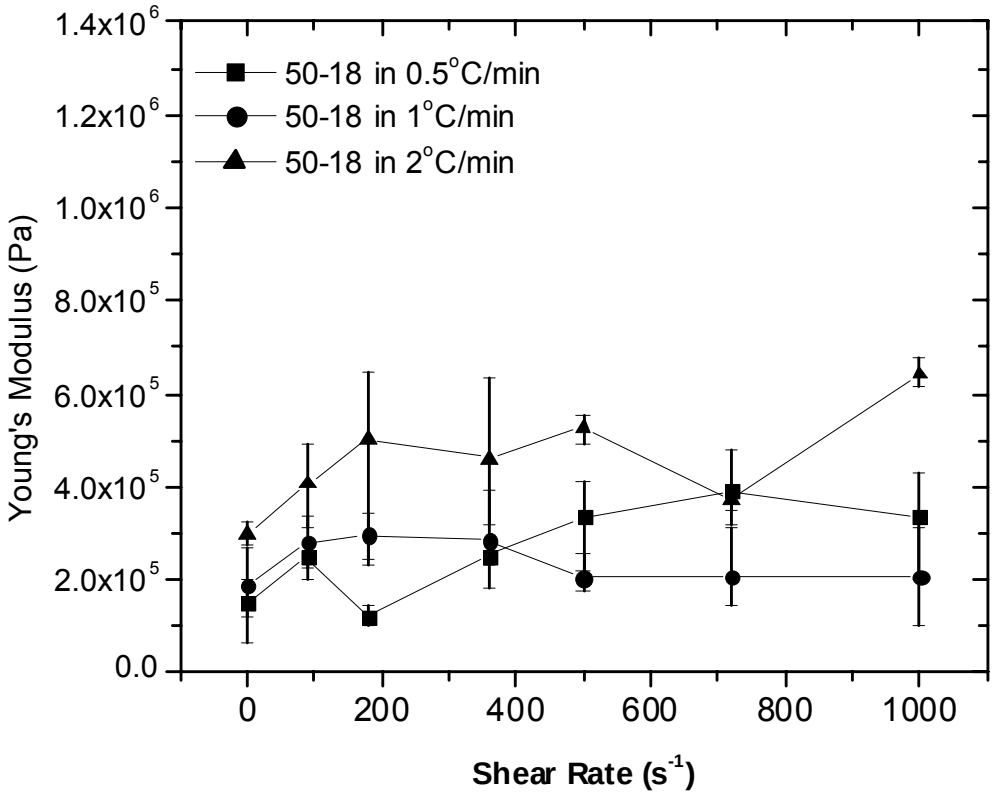

Figure 72: Graph showing Young's Modulus values for a sample of cocoa butter created under shear rates of 0 – 1000s^{-1} whilst cooled from 50-18°C at 0.5, 1 and 2°C/min

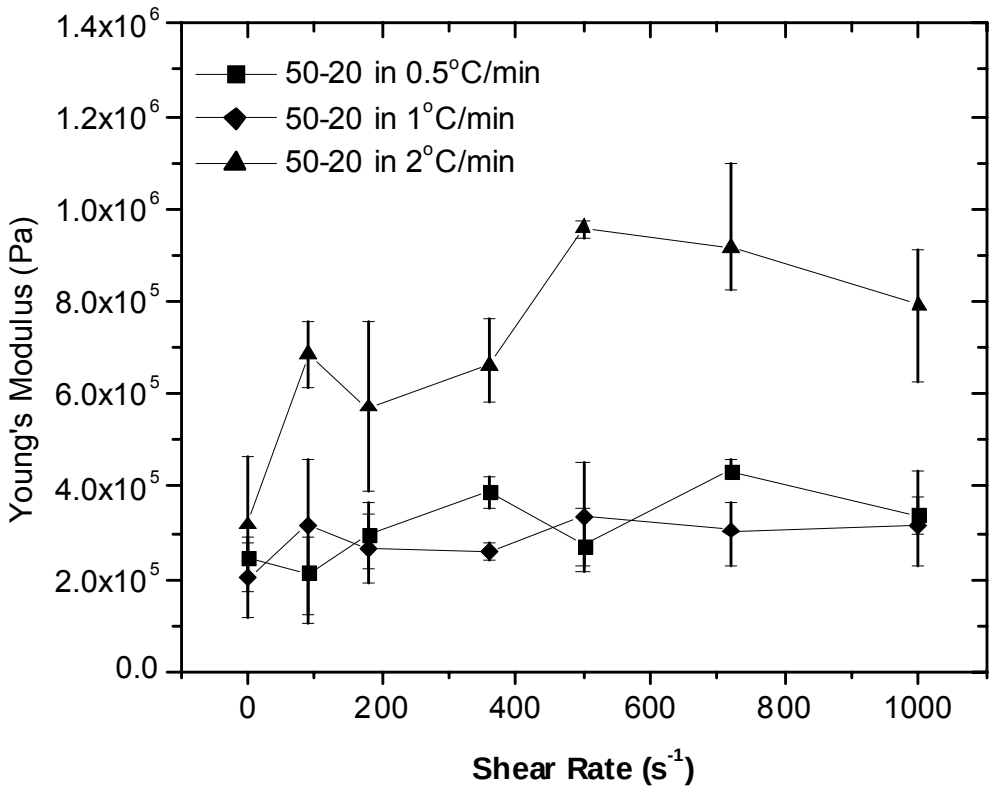

Figure 73: Graph showing Young's Modulus values for a sample of cocoa butter created under shear rates of 0 – 1000s^{-1} whilst cooled from 50-20°C at 0.5, 1 and 2°C/min

Clearly the Young's modulus data does not show the same trend that is seen in the DSC and the breaking point data. Only the data set of 50-20 in 2°C/min shows a transition between 360s^{-1} and 500s^{-1}. We also see a general decrease in the value of the Young's modulus with an increase in end point temperature. This would be consistent with the decrease in SFC with an increase in temperature.

As with the DSC results we see that there is a clear increase in breaking stress for higher shear rates with a transition occurring between 360 and 500s^{-1} for most temperature conditions. There are also instances of data sets with no change in breaking stress. These data sets are the same as those which showed no change in melting temperature for higher shear rates.

3.0 Discussion

Many different types of experiments were carried out to test the physical properties of cocoa butter, resulting in large quantities of information to be interpreted.

In order to simplify the discussion of the results of these different experiments the 20°C end point case can be discussed first. This temperature should result in the slowest kinetics of transformation with the 18 and 16°C endpoints being much faster, more chaotic and less clear in their interpretation.

Cocoa butter was sheared in the specially designed split couette cell to allow for the extraction of fully crystallized sheared samples. As the sheared cocoa butter samples were being created viscosity data was collected which can be interpreted to give the time of α and β_V crystallite formation. In this way the effect of shear on the α-β_V transition time can be fully examined for a large number of shear rates, temperatures and cooling rates. This allows for further examination of the previously reported shear acceleration of the β_V transition.

The viscosity data for the 50-20°C at 0.5°C/min, 1°C/min and 2°C/min ramps all show a more complicated relationship between shear and α-β_V crystallization time than a mere shear acceleration effect. In fact, a general decrease in crystallization time is seen only until $500s^{-1}$ when the crystallization time begins to increase again due to viscous heating.

The melting temperature of the material is also very important and is used in determining the crystal structure and composition of a material, with clear melting ranges being given for different crystal forms. Results of this investigation can help us to see if

orientation affects the melting properties or the application of shear alone affects the melting properties.

From the melting (DSC) data there is an obvious change in melting temperature between the $360s^{-1}$ and $500s^{-1}$ shear rates. Above $500s^{-1}$ there is an increase in the day 0 melting temperature by ~ 4°C and a decrease in the day 28 melting temperature by ~ 2°C. While the lower shear rates contain a mixture of forms and thus have a lower melting point, above the transition the melting temperature is immediately elevated. More remarkable however is that this elevated temperature is not consistent with a form V polymorph. After a period of 28 days this temperature has still not moved significantly and remains at least 2°C lower than a typical form V polymorph melting temperature in this cocoa butter.

Taking this information about the melting temperature and using it to evaluate the rheometry data we don't see any distinct change in the viscosity data above $500s^{-1}$ to account for such a large change in melting temperature. That is, there is no delineation between the $0\text{-}360s^{-1}$ data set and the $500\text{-}1000s^{-1}$ data set for any of the cooling ramps.

The creation of sheared samples which can be extracted intact from the apparatus also allows for examination of the previously reported shear alignment/orientation of the cocoa butter crystallites. Once the samples are extracted, x-ray diffraction allows for the degree of orientation associated with each shear, temperature and cooling rate point to be mapped out, allowing for further conclusions to be drawn about the conditions required for shear induced alignment to occur.

The orientation data shows orientation occurring at $360s^{-1}$ and declining to a plateau for the 500-1000 s^{-1} shear rates in to 50-20°C samples. Clearly this orientation plateau coincides with the change in melting temperatures.

X-ray diffraction can also be used to examine any structural changes brought about by shear or shear induced orientation. X-ray peak positions can be used to identify the different crystal forms and small changes in position and intensity of these peaks can show changes in composition and fractionation.

X-ray structure examination of two samples on either side of the transition (a $360s^{-1}$ sample and a $500s^{-1}$ samples for 50-20°C in 1°C/min) reveal obvious differences yet show them to both be of the β 'family'.

A comparison of the x-ray peak positions of the $500s^{-1}$ and a high resolution form VI pattern show remarkable similarities to a transition to a form VI structure. i.e. a strengthening at ~1.55, 1.6, 1.65 and 1.7 Å, along with a weakening at ~ 1.575, 1.675 and 1.725 Å. While this can be considered as evidence for the $500s^{-1}$ sample containing some form VI, we know that this structure would have an even higher melting temperature than a form V structure, rather than the lower one observed.

It is true, however, that small changes in chemical composition of the crystallites could also be responsible for the changes in peak intensity. High resolution x-ray diffraction studies of these samples would be required to more accurately assess the differences between the two x-ray patterns

Finally the breaking strength of the shear samples can be examined with a three point breaking apparatus. The breaking strength is dependent on temperature due to changes in solid fat content associated with storage temperature (i.e, the lower the

temperature, the higher the breaking stress); however the dependency on shear and orientation can also be examined. Grain size and domain size will also have an effect on breaking strength and the link between shear, temperature and cooling rate on these properties can also be examined.

A look at the peak breaking stress for the different shear and cooling rates shows a transition point again between 360 and 500 s^{-1} to higher breaking values.

In order to understand the reason behind the "transition point" we can first reconsider the properties of the high shear cocoa butter

As has been speculated previously, these DSC and X-ray results in particular clearly indicate the presence of an alternate chemical composition and structure above the transition point. These high shear samples have a lower 28 day melting temperature, yet an apparent contradictory mixture of forms V and VI, as well as elevated breaking stress values.

To explain this, we can consider the process occurring during crystallization. Firstly we can say that under static conditions large α crystallites will form with a small number of nucleation sites. This has been observed numerous times through microscopy[44]. Under static conditions, as the material cools, certain TAGs will selectively crystallize first and then be locked away from the crystallization process, thus changing the chemical composition of the remaining melt. This will create an 'onion' effect where the chemical composition of a crystallite will change radially.

Now, if we apply shear to the same system of α crystallizing cocoa butter, it will limit the crystal size and increase the number of nucleation sites. It will also promote

mixing and allow for a distribution of smaller crystals. This has been previously reported by both Mazzanti[25] and Sonwai et al.[18].

It seems reasonable to speculate that this trend cannot continue indefinitely with increased shear. Above a certain value of shear the size of the crystals will reach a minimum size and a constant distribution.

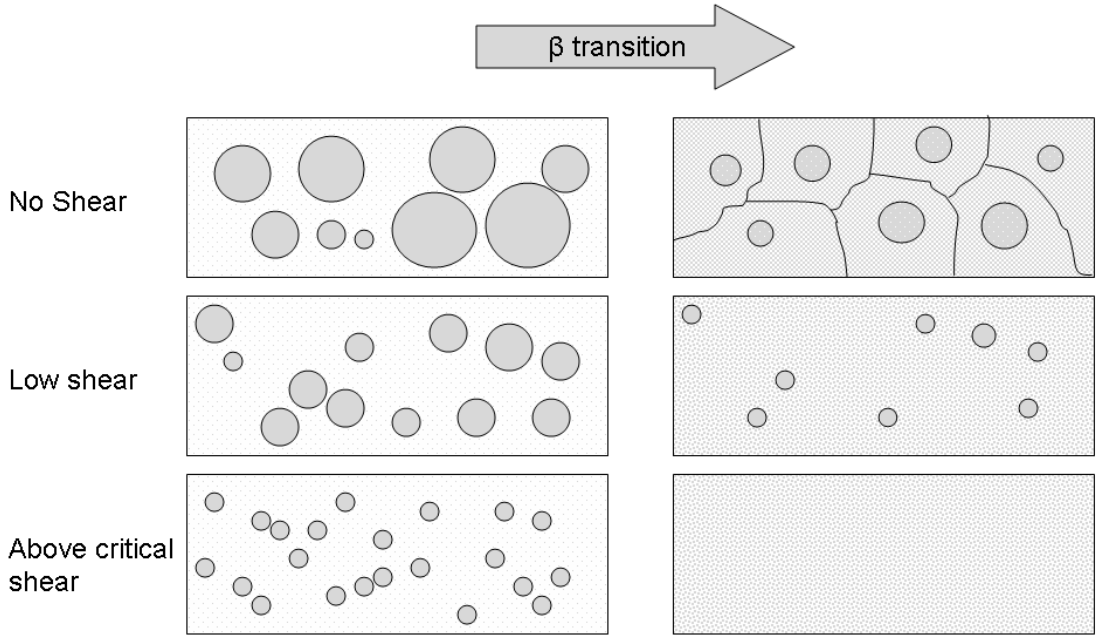

Figure 74: Diagram depicting theory of critical shear rate above which all α crystals melt leaving β_V free to have a completely uniform, defect free microstructure

Now, when the phase transition to β_V occurs, there is a release of energy associated with it. This energy (or heat) causes melting of the α material which is already crystallized. For the lower shear and static conditions where the crystallites are larger, only the outer surface of the α crystallites will be melted. In the higher shear conditions the small size of the crystallites will mean that most or all of the α crystallites will melt in the transition. A model proposed by Mazzanti[25] and Mazzanti et al.[66] has a similar hypothesis.

What this means for the β_V crystallization is that above a certain critical shear rate, the α crystallites will be small enough that the release of heat energy at the β_V transition will be enough to completely melt all of the α material. This would mean that at the point of initial β_V crystallization, form V has access to all of the material which would normally have been locked away in α crystallites. That is, above the critical shear rate, TAGs previously inaccessible have now become available for crystallization and the degree of mixing due to shear allows for β_V crystallization to occur selectively, i.e., the crystallization process can select the TAGs most favourable for crystallization. This crystallization process could then result in a β_V form which is composed of TAGs of a lower melting temperature.

The lack of residual α in this structure as well as the larger number of nucleation sites caused by increased mixing due to shear would allow for a more uniform network of crystals to form from the beginning, without defects caused by α crystallites which would later transform into β_V crystals. This uniform network of small crystals will then result in a structure of higher breaking stress[86-88].

An examination of the x-ray peak widths would be able to yield information about the coherence length of the samples. If the higher shear structures did indeed contain fewer defects then the peak widths would be narrower in q. Unfortunately the resolution of the in-house setup is not high enough to allow for such small differences to be apparent. Data found in Mazzanti[25] (Figure 75) acquired with an x-ray accessible shear cell at a synchrotron facility and with much higher resolution does show a decrease in peak width. High resolution studies of the samples would be very informative both for

an examination of the peak widths as well as a better look at the changes in the short spacings.

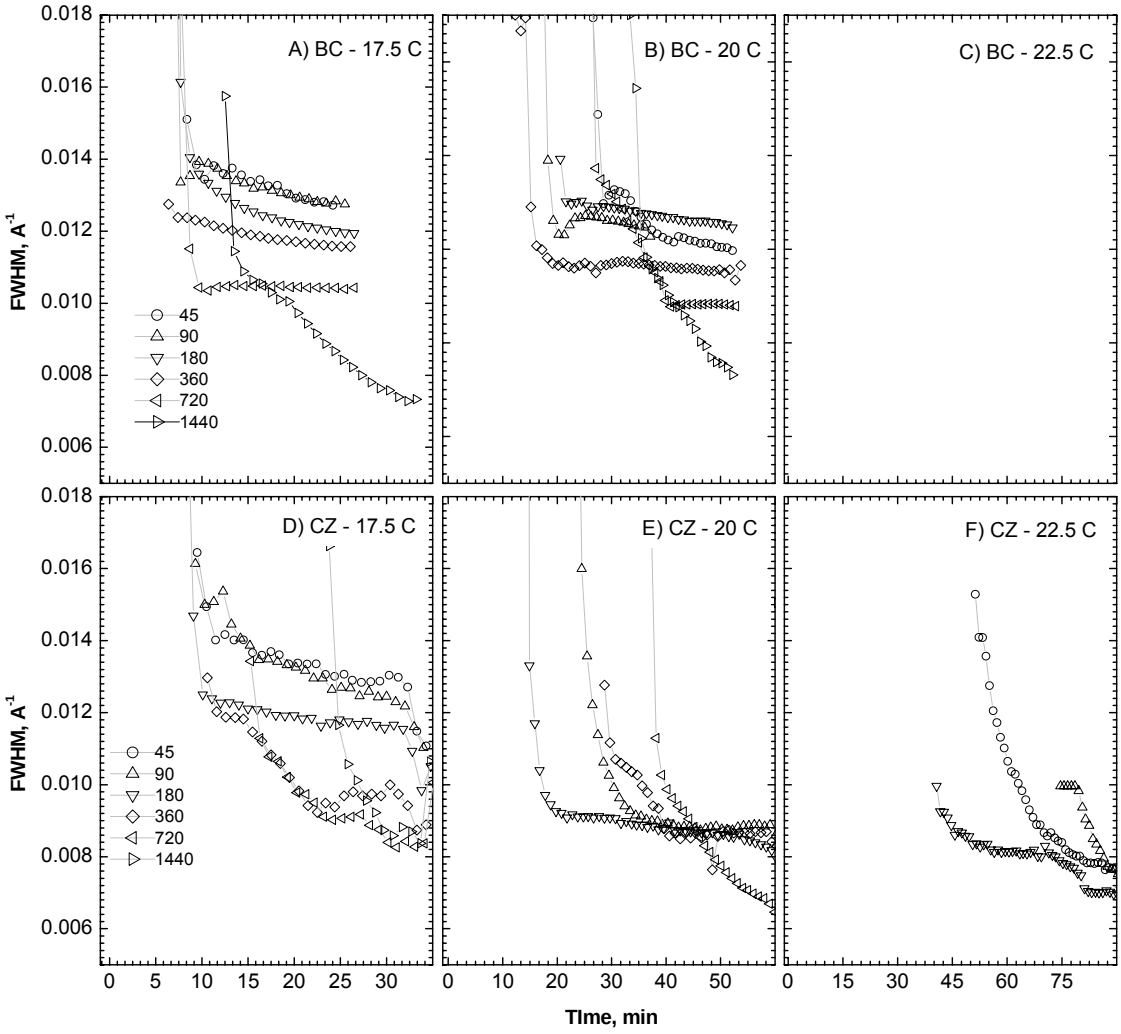

Figure 75: Figure 6-17 taken from Mazzanti showing FWHM data extracted from diffraction images of form V taken in an x-ray accessible shear cell at a cooling rate of 3°C/min showing the FWHM decreasing with shear.

This theory explains the 50-20°C data well. The 50-18 and 16°C data, as stated earlier is much more chaotic due to the faster crystallization times involved, however the same basic trends can be observed. The 18°C data set in particular is missing the transition point in the 0.5 and 2°C/min data sets. These data sets do, however exhibit

orientation, which leads to the conclusion that while orientation might help to make the transition possible, it is not the sole cause of the different melting and mechanical properties.

The missing transition in the 0.5°C/min data sets for 18°C and 16°C is easily explained. For the lower temperatures, more α is formed than in the 20°C case. Therefore for the lower temperatures there is more α to melt at the transition and more remains unmelted through the transition. This would impede the access of the selective crystallization process causing no transition in these data sets. The missing 2°C/min transition in the 18°C temperature data set can also be easily explained as occurring above the examined shear range, as discussed in section 2.

The hypothesis of selective β_V crystallization rests on the assumption that there is a critical shear rate above which the size of the α crystallites are such that they will melt completely upon the β_V transition energy release. Obviously microscopy evidence would be invaluable as confirmation.

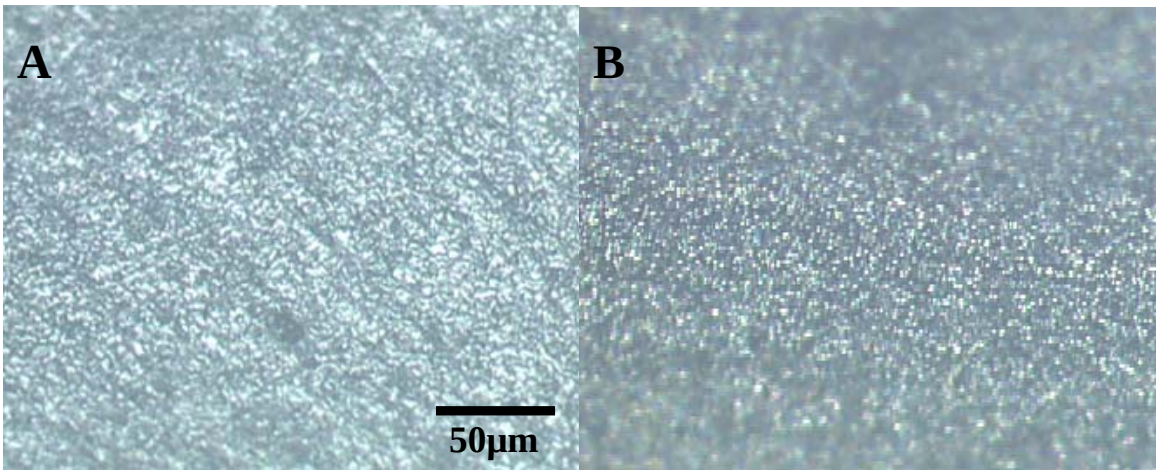

Figure 76: Micrographs of cocoa butter crystallized from 50-20°C in 2°C/min at a) $360s^{-1}$ and b) $500s^{-1}$

Figure 76 shows micrographs of the cocoa butter samples from either side of the transition. The images are of a broken edge of the sample under 10x magnification. The poor quality of the images is due to the uneven nature of the edge, but it was felt that any attempt to create a smooth edge would result in destruction of the crystallites. Even so we can see that the crystal sizes are very similar with the $500s^{-1}$ sample appearing slightly smaller.

Microscopy can also be done to confirm the decrease in particle size proposed, however a change in the method for sample creation may yield a sample more suitable for microscopy. A microscopy accessible shear cell would be ideal where the crystallization process could be viewed under shear and the melting of the crystallites in the β_V transition observed and confirmed. Such a shear cell is described in Sonwai et al.[18] which is commercially available. Experiments described therein do show a reduction in particle size with shear rate, however data was taken for a fast cooling rate and only up to $500s^{-1}$. An examination of shear rates on either side of a transition point shearing constantly would be invaluable for theory confirmation.

Chemical analysis may also be attempted with the 'shear changed' samples. A separation of the crystallites from the liquid fat might be attempted for the lower SFC samples. A study of a higher temperature such as 22°C might yield a slow enough crystallization process to make that possible.

The aging of the 'shear changed' samples can also shed light on its properties. Samples which had been stored for two years were examined to assess the permanence of the shear induced changes. Differential scanning calorimetry revealed a significant melting temperature jump as compared to the day 28 values. For a sample of 50-20°C in

2°C/min at 500s^{-1} the melting temperature changed to 33.9°C (Figure 77) as compared to 31.1°C for the day 28 value. The 2 year melting value can also be compared to the average 28 day melting temperature (32.5°C) for the lower shear samples in the data set. This value of 33.9°C is 1.4°C higher than the form V melting temperatures and is consistent with a form VI structure in this cocoa butter.

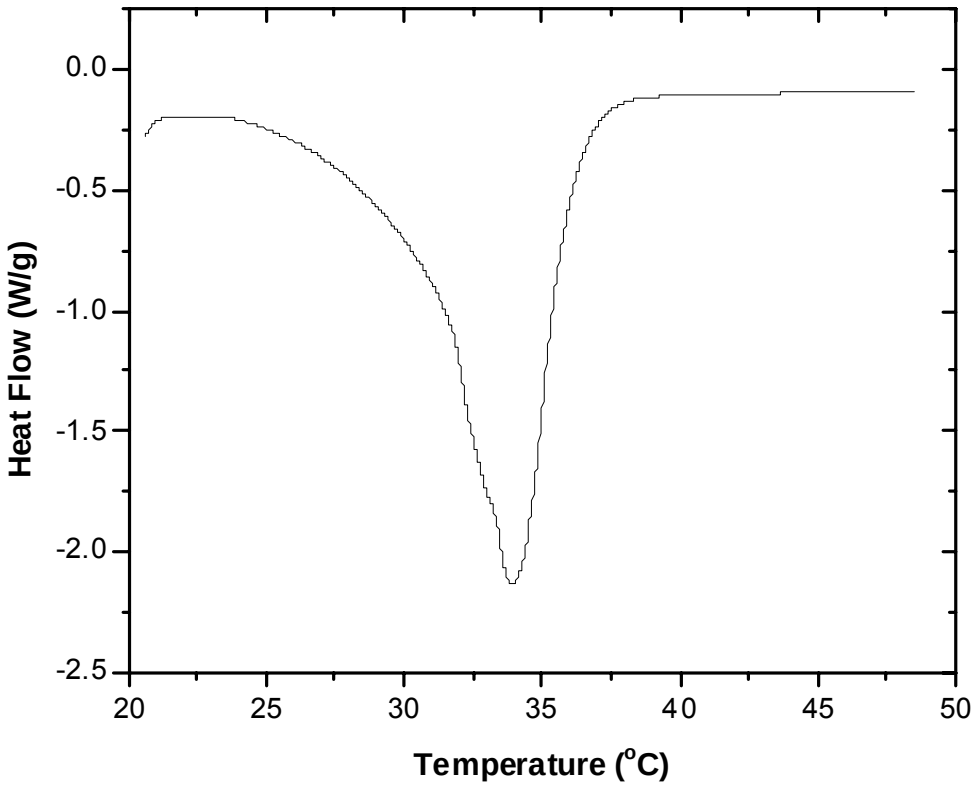

Figure 77: Differential scanning calorimetry graph of heat flow(W/g) vs temperature (°C) for a sample of cocoa butter created under a shear rate of 500s^{-1} whilst cooled from 50-20°C in 2°C/min and stored for 2 years at 20°C.

This means that whatever the change induced by the application of shear, the change in the melting properties is not permanent. If we believe that the high shear causes the formation of a chemically altered form V and VI combination then over time the remaining material must be incorporated as the structure matures into a form VI. The

solid fat content of the material would increase if that were the case. Thus a much longer study following the aging of the 'shear changed' samples would allow for measurement of SFC to help confirm the theory.

X-ray analysis of the two year old samples showed no change in orientation showing that once created the aging of a sample into a form VI has no effect. X-ray structure analysis was not done of an aged sample, but would also provide invaluable information.

The mechanical testing of the aged sample also showed retention of the elevated breaking stress in the 'shear changed' samples. This lends credence to the theory that fewer defects and smaller grain cause the increase in breaking stress.

To conclude, the application of shear to cocoa butter during crystallization causes acceleration of the α to β_V transition time for any applied shear rate as well as preferred orientation of crystallites above a certain shear rate. There is also a critical shear rate for certain cooling conditions which results in the formation of a chemically altered β_V structure, exhibiting altered melting properties and enhanced breaking strength.

4.0 Conclusions

In this investigation of the changes in properties of cocoa butter due to the application of shear, many interesting discoveries were made.

Viscosities of the cocoa butter samples under shear were recorded during sample creation, resulting in a data set showing the influence of shear, temperature and cooling rate on viscosity and crystallization time. Large jumps in viscosity were identified by comparison with x-ray diffraction data as α and β_V crystallization events. Comparison of $\alpha - \beta_V$ crystallization times for the nine different temperature profiles allowed for the conclusion that over a shear range of 90 - 1000 s^{-1}, there was no further appreciable shear acceleration of the form V transformation for the 16 and 18°C temperatures and only a slight increase up to 500s^{-1} for the 20°C temperature.

Sheared samples were also examined with differential scanning calorimetry. Samples were examined for peak melting temperature on each of day 0, day 1, day 7 and day 28. Six of the nine different temperature conditions examined yielded a critical shear rate, above which the melting points of the samples were dramatically different than for low shear and no shear samples. For the day 0 and day 1 samples, above 500s^{-1} the melting temperatures were ~2°C higher than for 360s^{-1} and below. For the day 7 and day 28 samples, above 500s^{-1} the peak melting temperatures were ~2°C lower than for the lower shear and no shear samples.

The orientation of sheared samples was also examined using x-ray diffraction. In all of the nine temperature sets, orientation was present for shear rates of 360s^{-1} and higher.

Breaking stress measurements were performed on sheared and non-sheared samples. These tests showed results remarkable similar to those seen in the DSC tests, with a critical shear rate existing in six of the nine temperature sets, above which an increase in the breaking strength occurs.

Taking the DSC and mechanical evidence of a shear dependent transition in samples properties, an examination of samples on either side of the critical shear rate was done with x-ray diffraction yielding two distinct x-ray patterns of the β_V family, leading to the conclusion that the higher shear sample was of a different chemical composition.

We can speculate then that the application of high shear rates causes a change in the crystallization of cocoa butter leading to selective crystallization and the formation of a compositionally different form V crystal with fewer defects than its lower/no shear counterparts. That is, there exists a shear transition point exists for some temperature conditions above which a transformation into this chemically altered β_V polymorph takes place. This form has a stable melting temperature ~2°C lower than its lower shear counterpart, a distinct x-ray fingerprint and enhanced breaking properties.

Appendix 1:

Table 1: X-ray Data of I – IV polymorphs of Cocoa Butter (Values in Å. Intensities: VW – very weak, W – weak, M – medium, S – strong, VS – very strong)

1966 Wille & Lutton [4]	1969 Witzel & Becker[5]	1970 Riiner[6]	1971 Chapman[7]	1985 Hicklin[28]	1999 Van Malssen[34]	1998 Loisel[29]	Guthrie
I 55.1 W		β' 2 57 M	I 54 S	I	I	I 52.6	
34 M		37 M		34 W			
26.8 W		28 W	27 M				
13.8 W							
						4.22	
4.19 VS		4.19 VS	4.17 S	4.19 VS		4.19	
3.7 S		3.72 M	3.87 M	3.7 S		3.77	
II 49 VS	α 46.2	α 50 S	II 51 VS	II 49 VS	II	II	
	23.85						
16.3 S	16	16 W	16.3 M	16.6 M			
9.6 VW							
4.24 VS	4.21	4.25 S	4.24 VS	4.25 S			
III 49 VS	β' 1 47.2		III 51 VS	III 49 VS	III	III	III 50
24.6 VW	22.1		25 VW				24.29
16.35 S	16		16.5 M	16.6 S			16.17
15.24 W	14.49			15.24 M			14.93
4.92 VW							
4.62 W	4.66			4.63 M			4.63
	4.33						4.31
4.25 VS	4.22		4.2 VS	4.25 S			4.22
3.86 S	3.86		3.87 W	3.87 M			3.85
IV	β' 2 46.43	β' 1 46 S	IV 49 VS	IV 46 VS	IV	IV	IV
45 VS	44.45						44.94
22.64 VW							
	16.05						
14.87 S	14.75	15 W	14.8 W	14.9 S			14.81
8.93 W							
	4.58						
4.35 VS	4.33	4.61 S	4.32 S	4.35 VS			4.33
4.15 W	4.16		4.13 S	4.17 W			4.15
3.97 M		3.9 W	3.88 W				3.98
3.81 M		3.77 W	3.75 M				3.79

Table 2: X-Ray Data of β_V polymorphs of Cocoa Butter (Values in Å. Intensities: VW – very weak, W – weak, M – medium, S – strong, VS – very strong)

1966 Wille & Lutton[4]	1969 Witzel & Becker[5]	1970 Riiner[6]	1971 Chapman[7]	1985 Hicklin[28]	1999 Van Malssen[34]	1998 Loisel[29]	Guthrie
V 63.1 M	pre β 64	β 65 W	V 66 S	V 66 S	V	V 64.8 VS	V 65.04
						44.4 VW	
32.2 VS	32.17	34 W	33 S	34 S		32.4 S	32.12
21.02 W	21.57						
16.05 W	16.05		16.2 VW	16.2 W		16.2 VW	16.02
12.8 S	12.76		12.8 M	13.15 W			12.86
10.64 M	10.6						10.71
9.4 VW	9.3						
8.04 M	8.1		8.1 M	8.08 W			8.07
7.1 W	7.06		7.1 VW				
5.4 M	5.42		5.38 M	5.43 M			5.41
5.15 W			5.13 VW				
4.58 VS	4.59	4.61 S	4.58 VS	4.6 VS	4.59	4.58	4.58
4.23 VW	3.98		4.22 W				4.52
			3.98 S	3.99 M	4	3.98	3.98
3.87 M	3.85	3.9 W	3.87 M	3.88 W	3.87	3.89	3.86
3.75 W	3.76	3.77 W	3.73 M	3.76 M	3.77	3.77	3.75
3.67 W	3.67		3.65 S	3.68 W	3.68	3.67	3.66
3.39 VW							

Table 3: X-Ray Data of the β_{VI} polymorphs of cocoa butter – form VI (Values in Å. Intensities: VW – very weak, W – weak, M – medium, S – strong, VS – very strong)

1966 Wille & Lutton[4]	1969 Witzel & Becker[5]	1970 Riiner[6]	1971 Chapman[7]	1985 Hicklin[28]	1999 Van Malssen[34]	1998 Loisel[29]	Guthrie
VI 63.1 VS	β 63.6		VI 63 S	VI 66 S	VI	VI	VI 64.38
							44.59
32	32.2		31 S	35 S			31.16
21.25 VW	21.3						21.44
16 W	15.91		15.9 VW		15.81		16.03
12.76 S	12.73		12.7 MW	13.2 W	12.68		12.83
10.62 W	10.6				10.6		10.72
9.2 VW							
7.96 M	8.07		8 MW	8.18 W			8.05
					7.63		
7.08 M	7.06		7 W				7.09
					5.96		
5.43 M	5.44		5.37 M	5.47 M			5.41
5.15 W			5.09 VW	5.16 W			5.14
4.59 VS	4.59		4.53 VS	4.6 VS	4.59		4.57
4.27 VW			4.21 W	4.28 W			4.23
4.04 W	4		4.01 W	4.04 M	3.96		4.03
							3.91
3.86 M	3.86		3.84 M	3.88 S	3.87		3.85
					3.77		3.79
3.7 S	3.7		3.67 S	3.71 S	3.68		3.7
3.36 VW							

Appendix 2:

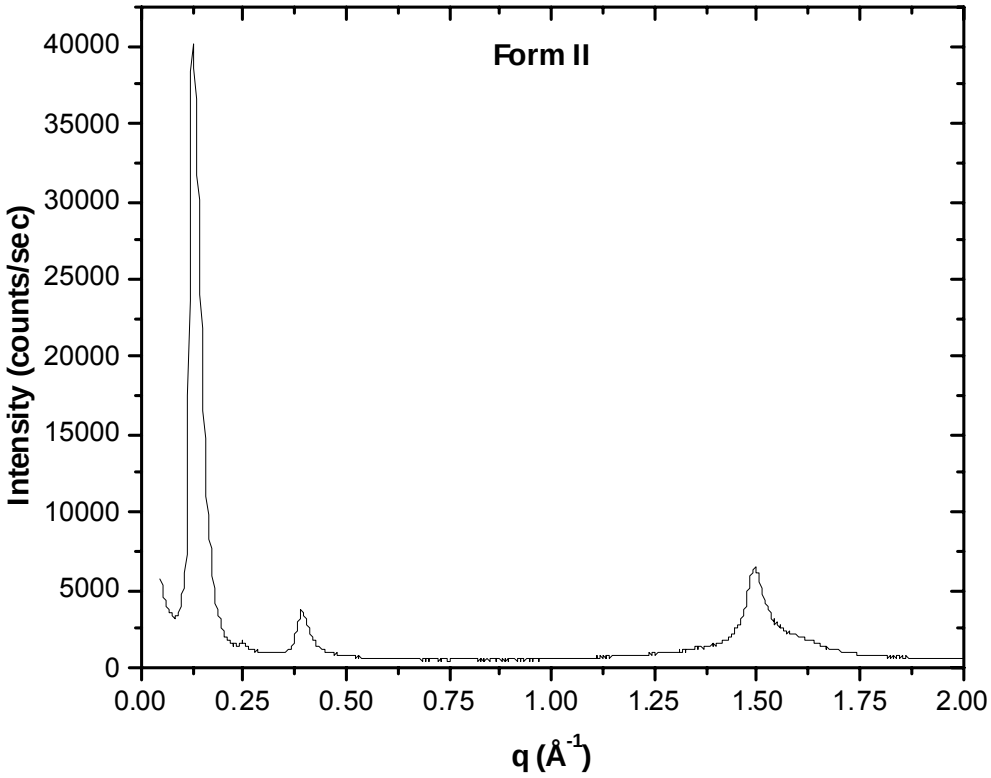

Figure 78: Syncrotron x-ray diffraction data of cocoa butter in a form II crystal structure

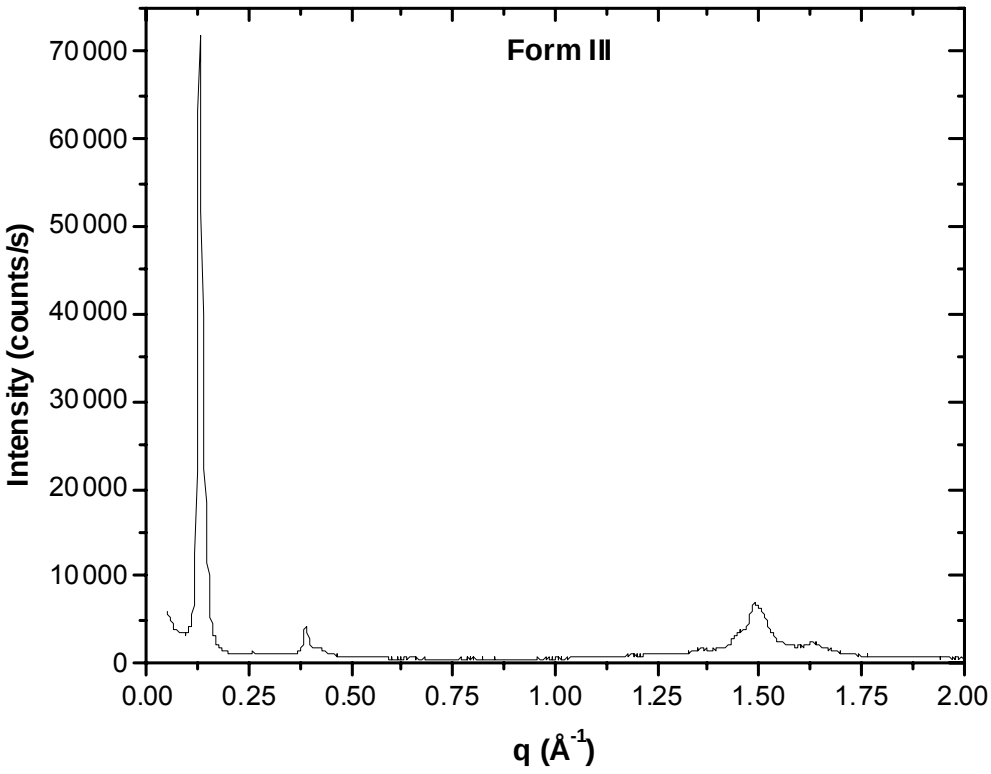

Figure 79: Syncrotron x-ray diffraction data of cocoa butter in a form III crystal structure

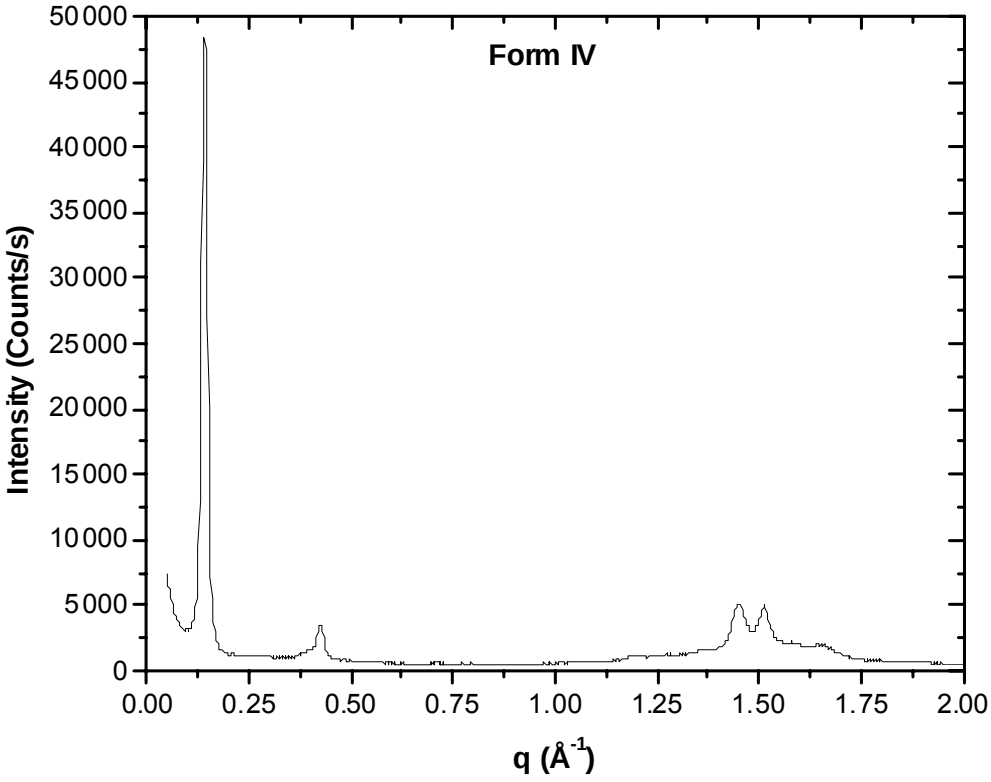

Figure 80: Syncrotron x-ray diffraction data of cocoa butter in a form IV crystal structure

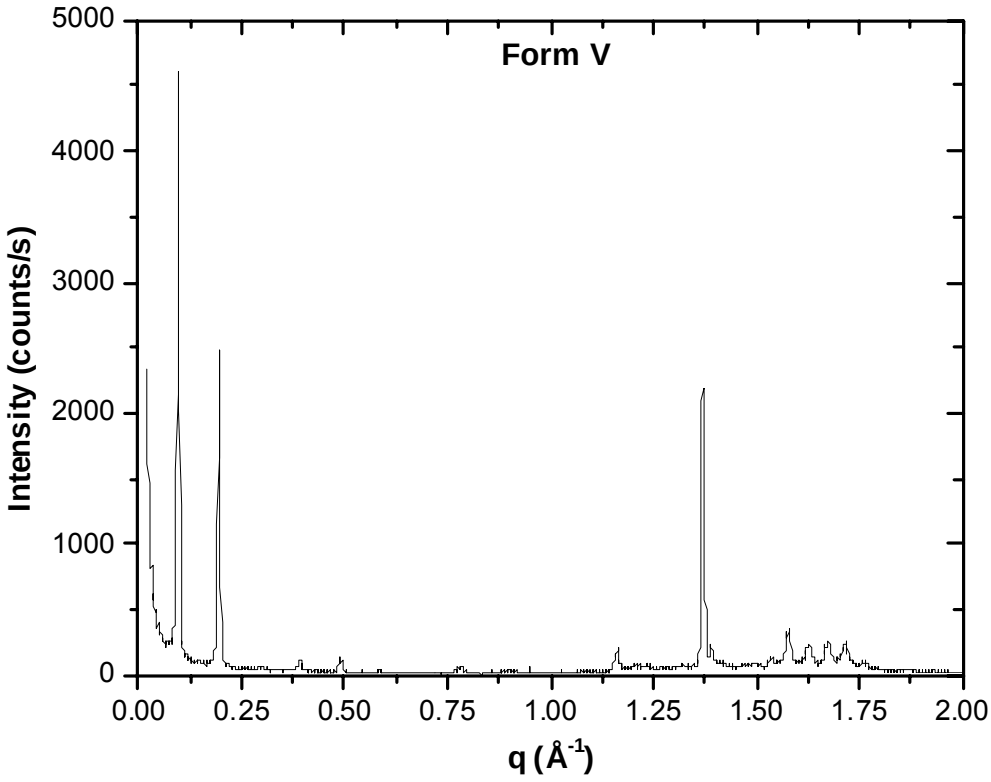

Figure 81: Syncrotron x-ray diffraction data of cocoa butter in a form V crystal structure

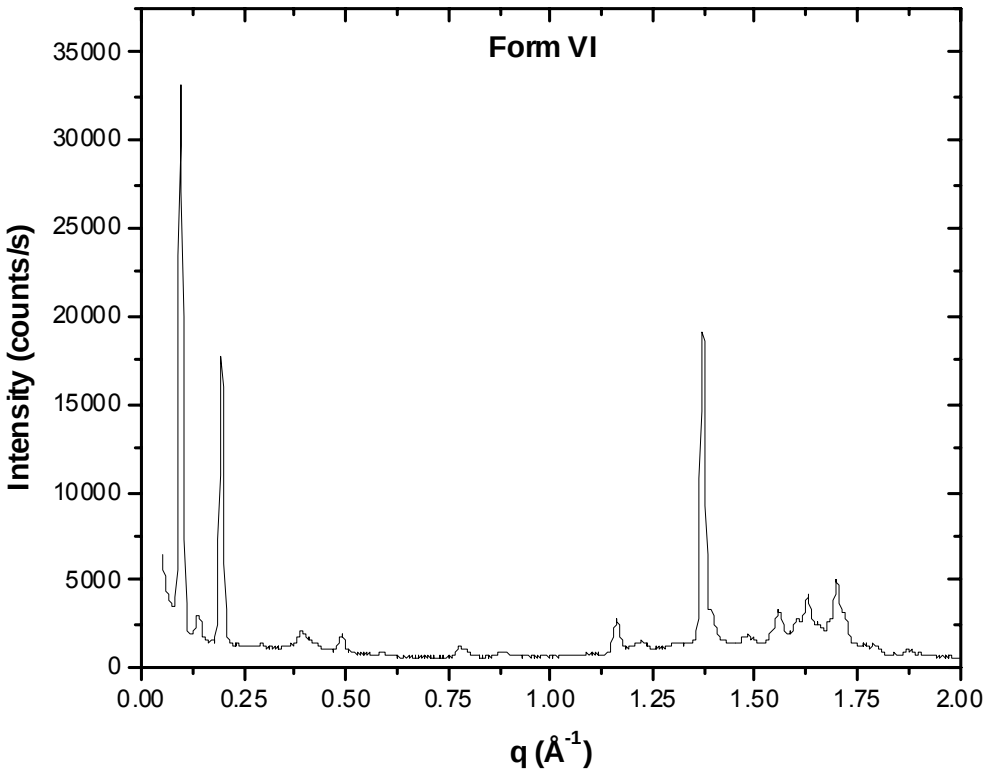

Figure 82: Syncrotron x-ray diffraction data of cocoa butter in a form VI crystal structure

Appendix 3:

The effects of viscous heating should also be considered when looking at the α crystallization times. The cooling of the system was controlled using the water bath's built in controller to minimize the effects of overshooting and have a better repeatability in the ramp. As such, no attempt was made by the system to compensate for the rise in temperature due to any heating effects. Therefore the recorded temperature of the system shows the effects of the viscous heating as well as any heat of crystallization. If we look at the actual recorded temperature data for 50-18°C in 2°C/min we can see the effects of the viscous heating on the system temperature. The lowest shear rate is a full half degree cooler than the highest shear rate (Figure 83). This is true for all of the temperature conditions examined.

.

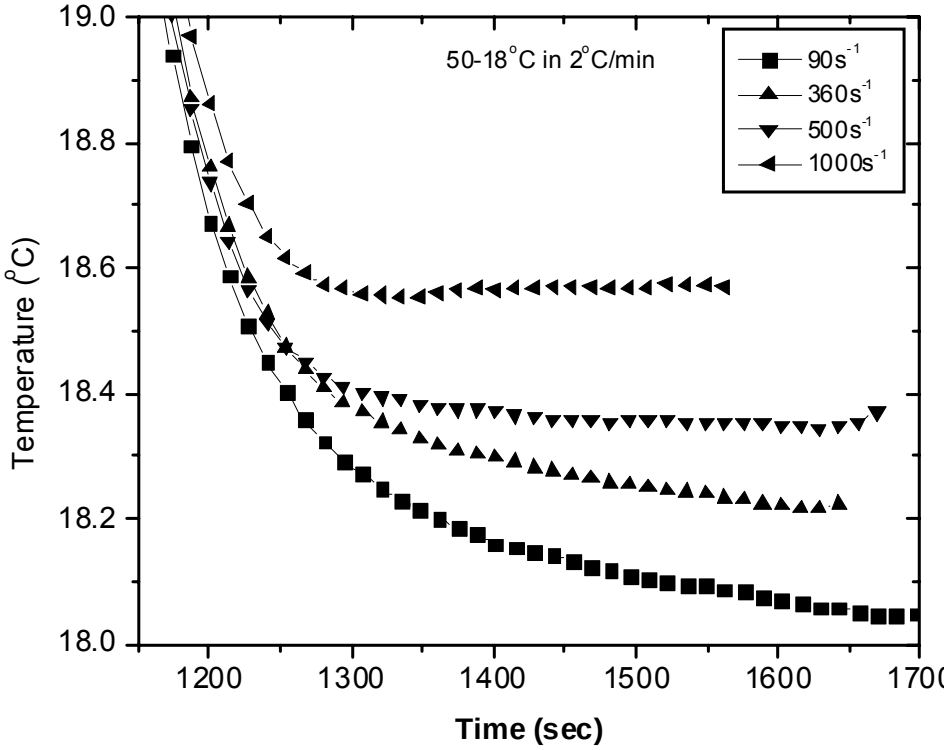

Figure 83: Graph showing temperature corresponding to Figure 29 for cocoa butter ramped at 2°C/min from 50-18°C at a shear rate of 90, 360, 500 and 1000s^{-1}

Clearly the temperature differences will have an effect on the α crystallization time, but would theoretically cause a retardation of the crystallization and would certainly not explain the more complicated crystallization behaviour seen.

Appendix 4:

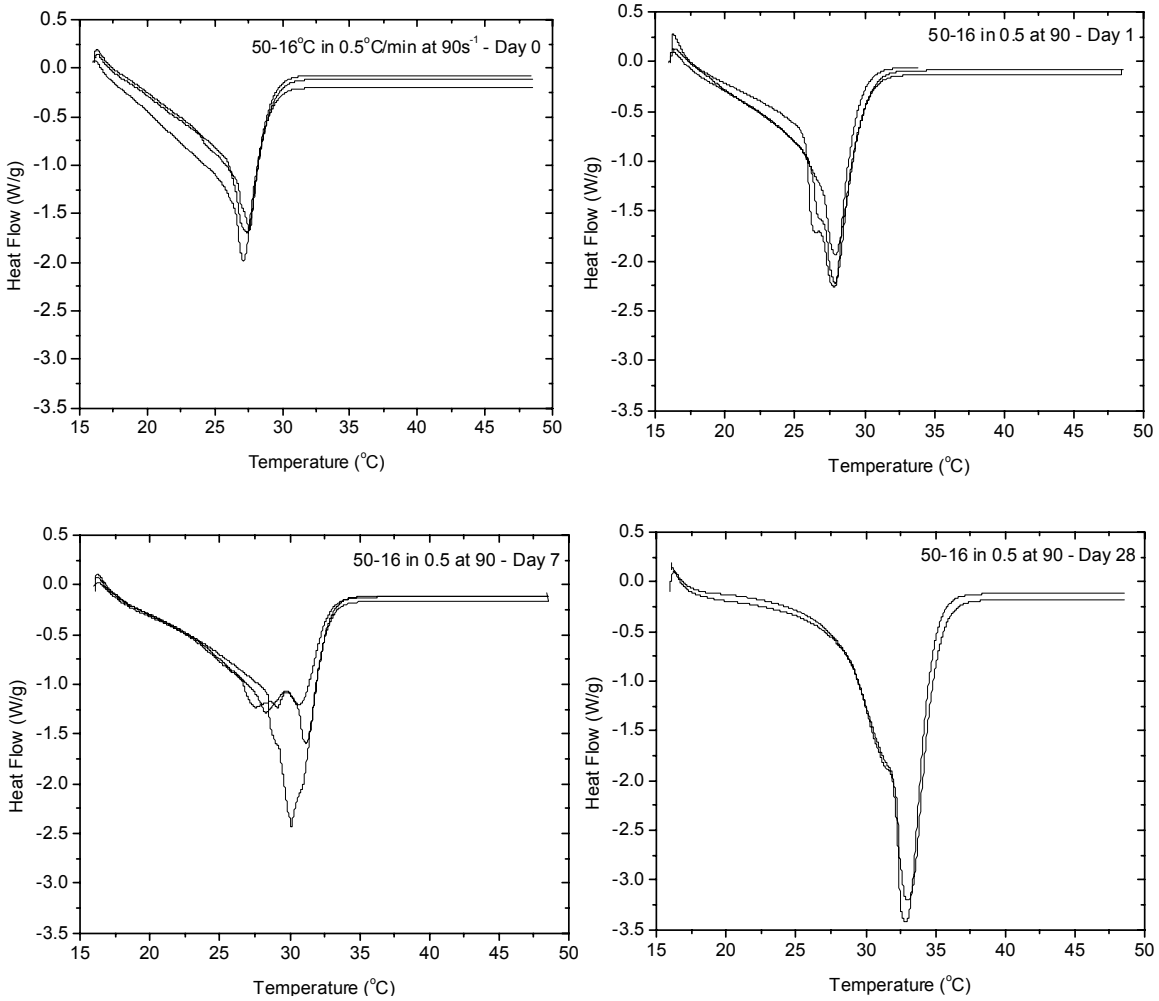

Figure 84: Heat flow curves of samples created by being cooled from 50 to 16°C at 0.5°C/min whilst shearing at a rate of $90s^{-1}$. The four graphs shown are sample repetitions carried out on day 0, day 1, day 7 and day 28.

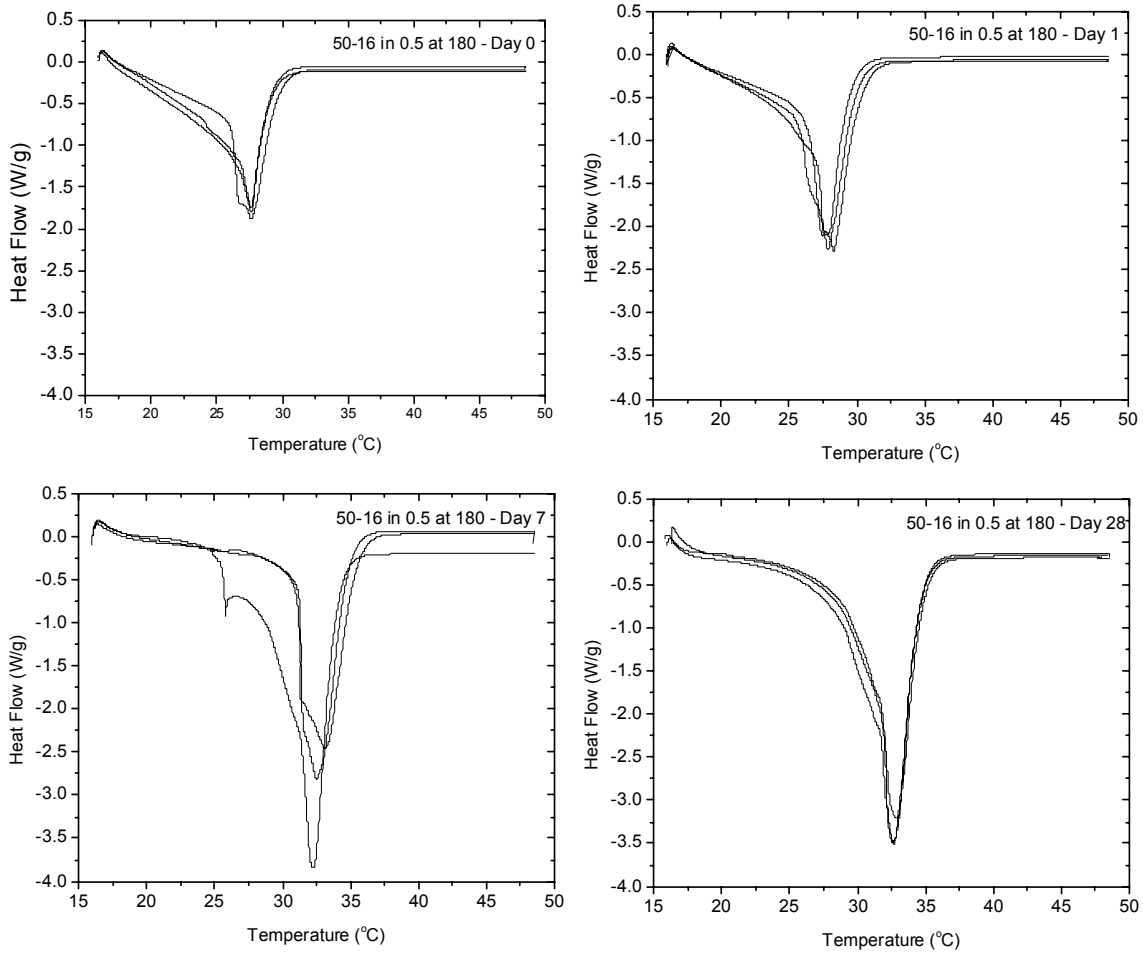

Figure 85: Heat flow curves of samples created by being cooled from 50 to 16°C at 0.5°C/min whilst shearing at a rate of $180s^{-1}$. The four graphs shown are sample repetitions carried out on day 0, day 1, day 7 and day 28.

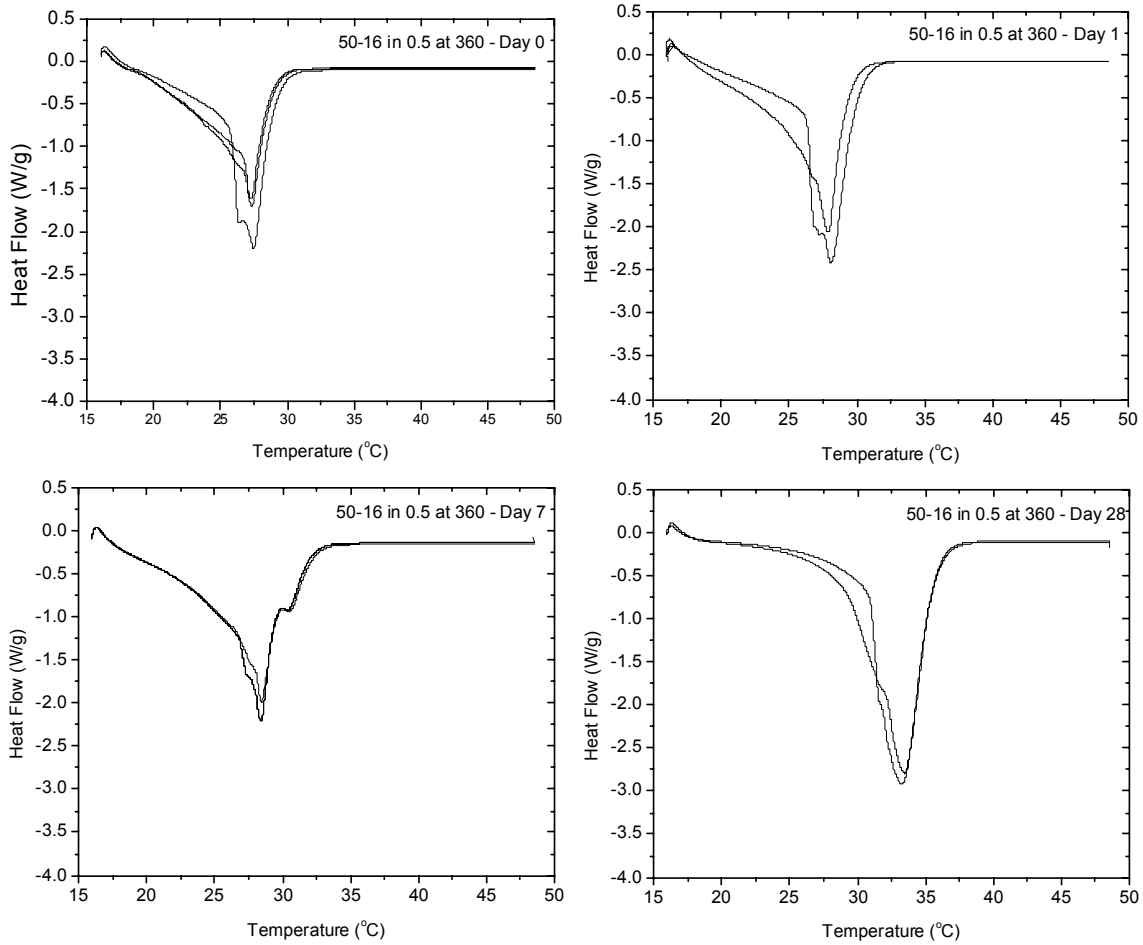

Figure 86: Heat flow curves of samples created by being cooled from 50 to 16°C at 0.5°C/min whilst shearing at a rate of $360s^{-1}$. The four graphs shown are sample repetitions carried out on day 0, day 1, day 7 and day 28.

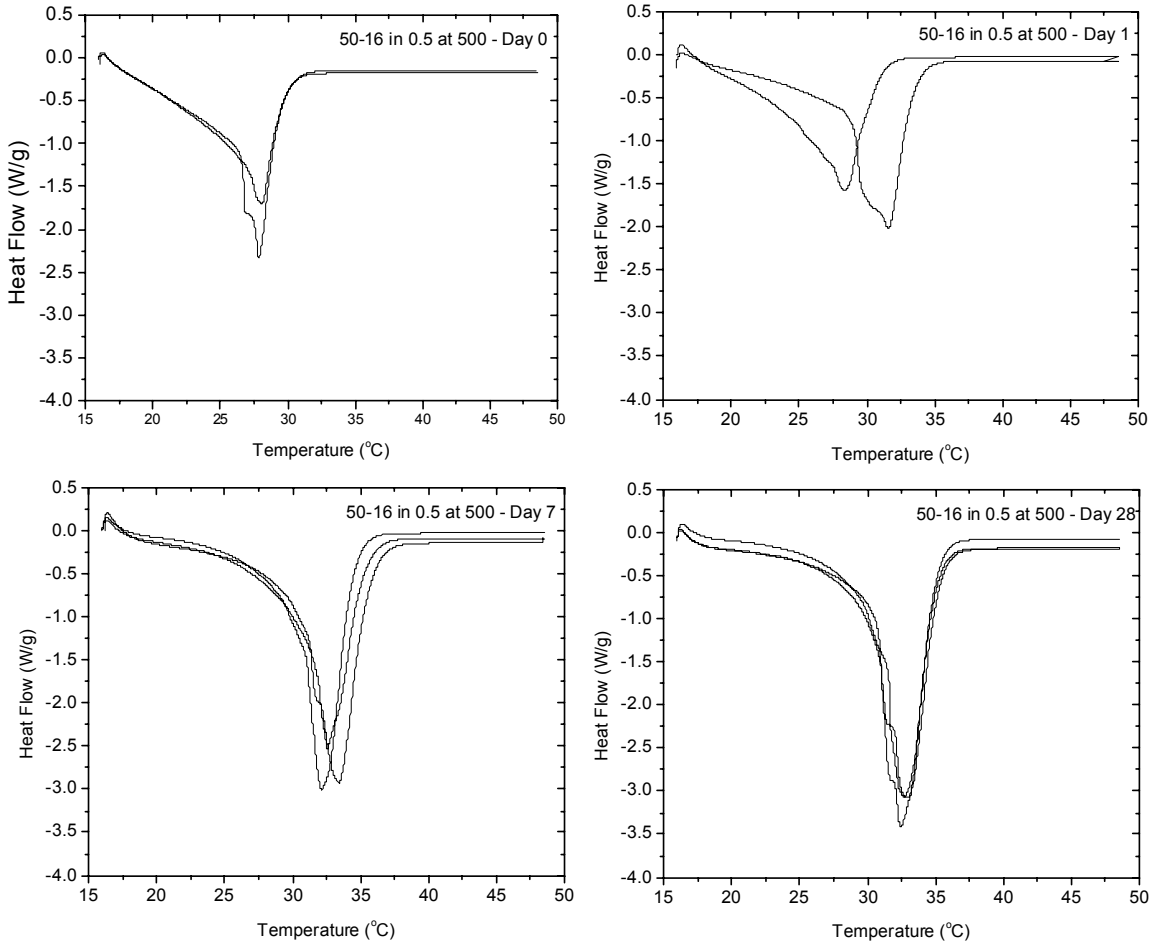

Figure 87: Heat flow curves of samples created by being cooled from 50 to 16°C at 0.5°C/min whilst shearing at a rate of $500s^{-1}$. The four graphs shown are sample repetitions carried out on day 0, day 1, day 7 and day 28.

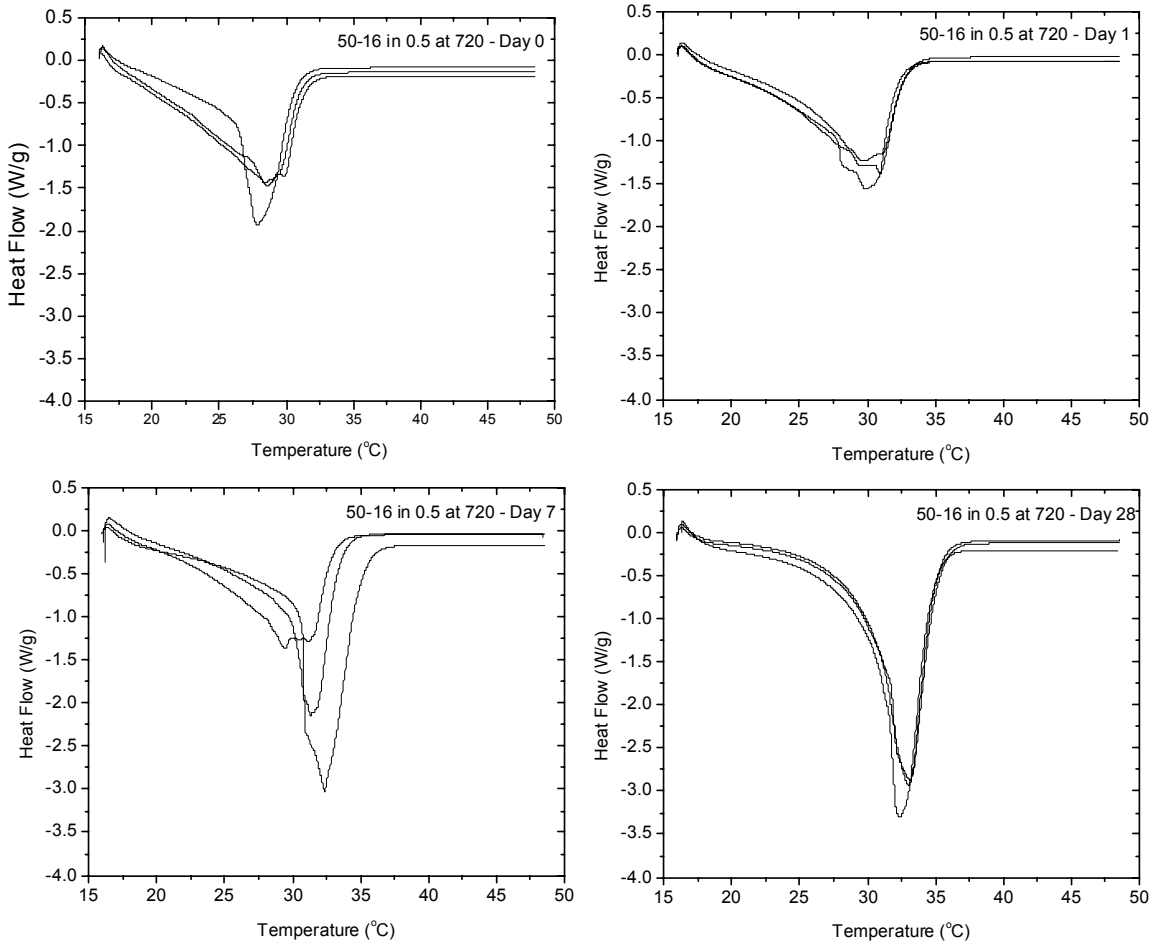

Figure 88: Heat flow curves of samples created by being cooled from 50 to 16°C at 0.5°C/min whilst shearing at a rate of 720s^{-1}. The four graphs shown are sample repetitions carried out on day 0, day 1, day 7 and day 28.

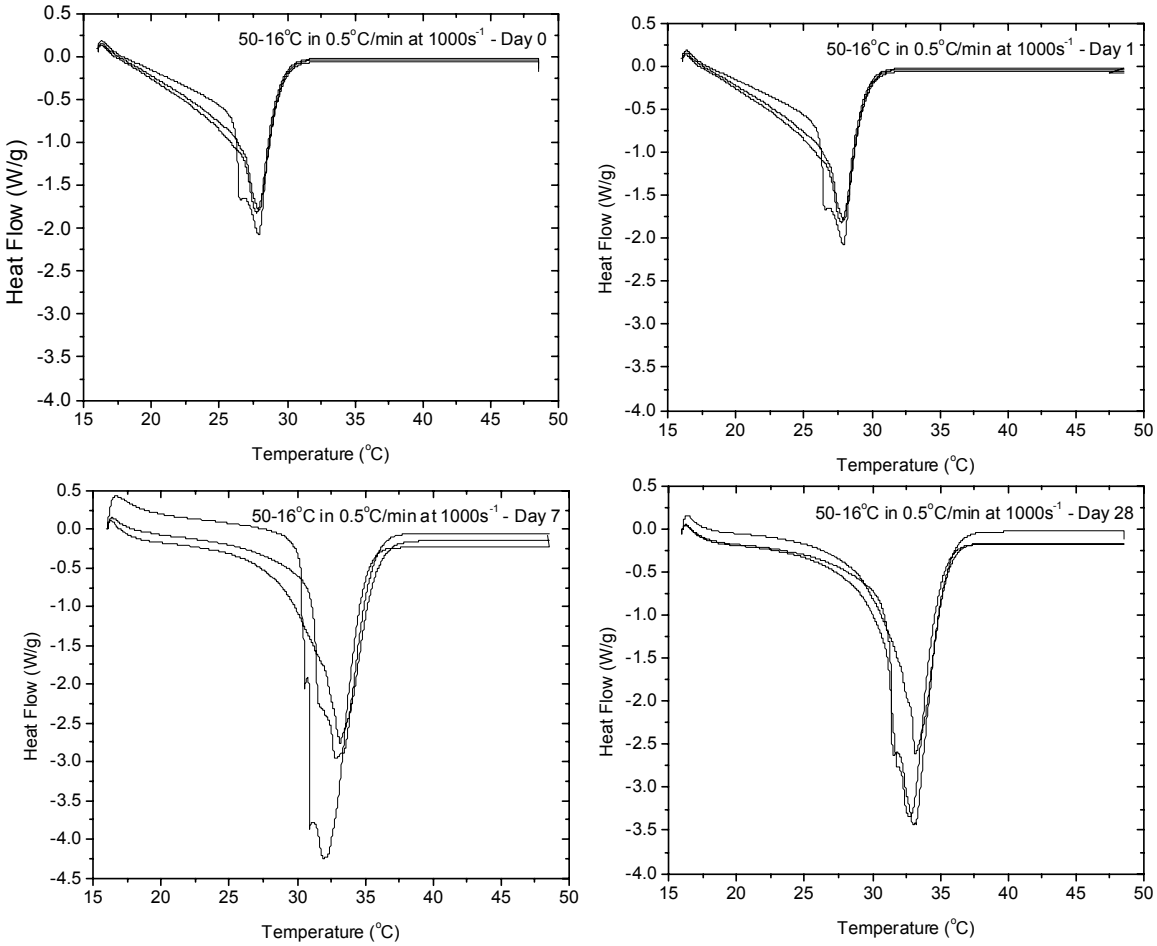

Figure 89: Heat flow curves of samples created by being cooled from 50 to 16°C at 0.5°C/min whilst shearing at a rate of $1000s^{-1}$. The four graphs shown are sample repetitions carried out on day 0, day 1, day 7 and day 28.

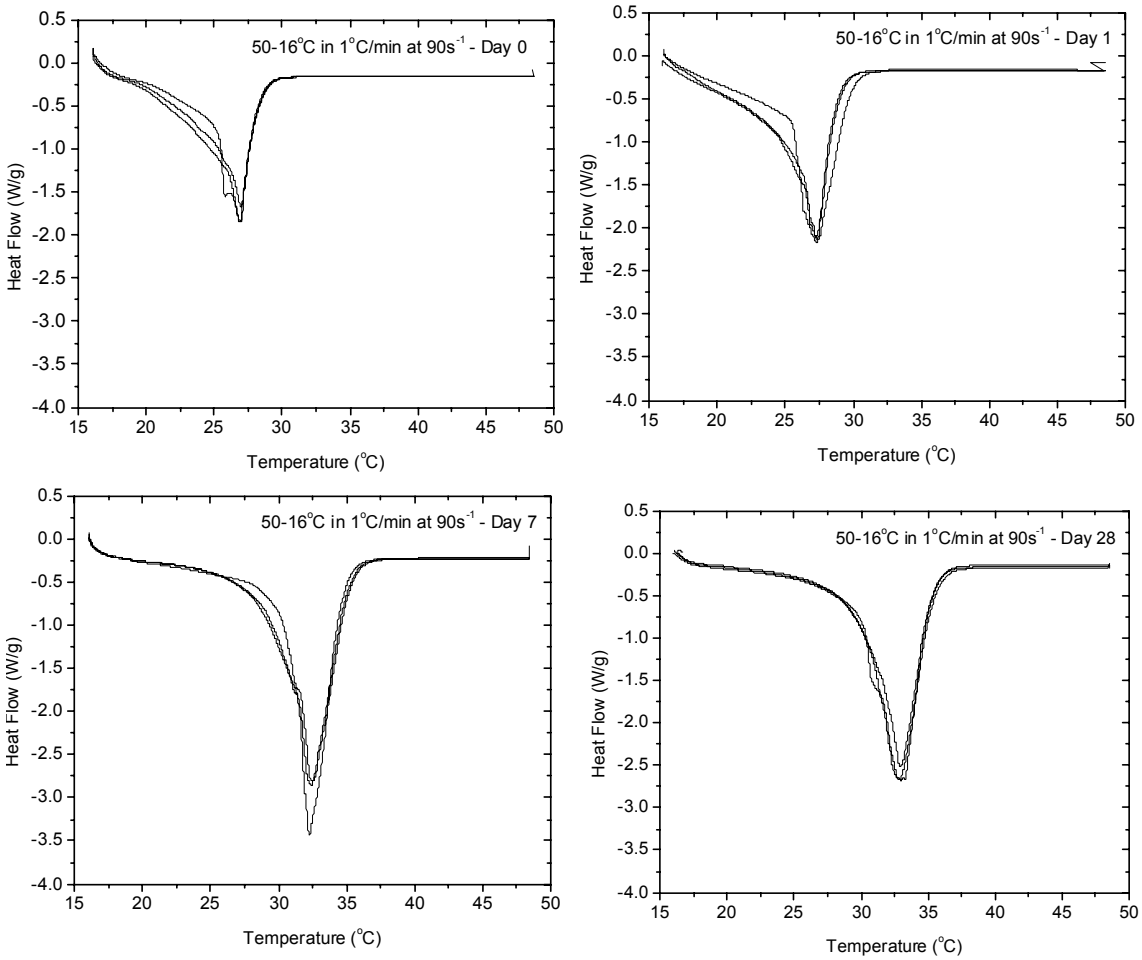

Figure 90: Heat flow curves of samples created by being cooled from 50 to 16°C at 1°C/min whilst shearing at a rate of $90s^{-1}$. The four graphs shown are sample repetitions carried out on day 0, day 1, day 7 and day 28.

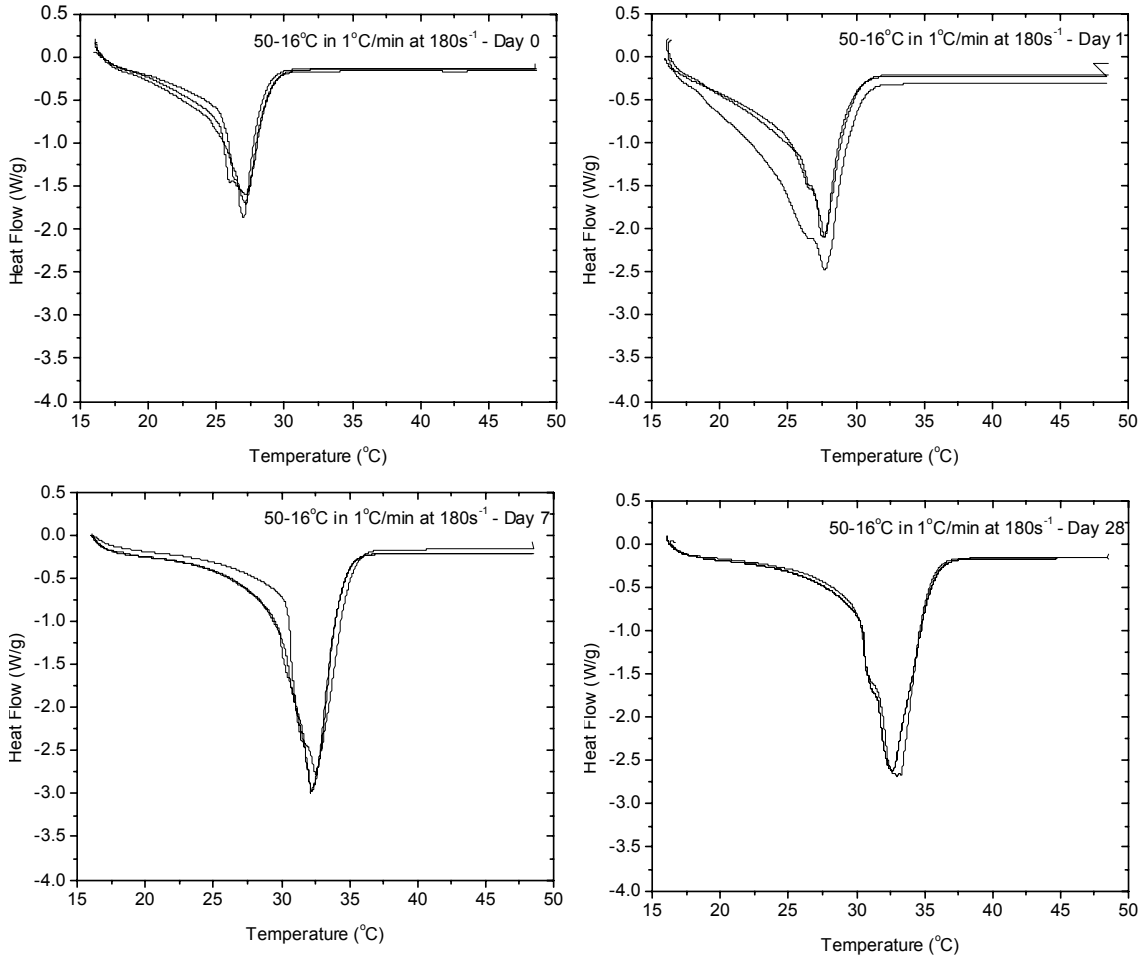

Figure 91: Heat flow curves of samples created by being cooled from 50 to 16°C at 1°C/min whilst shearing at a rate of $180s^{-1}$. The four graphs shown are sample repetitions carried out on day 0, day 1, day 7 and day 28.

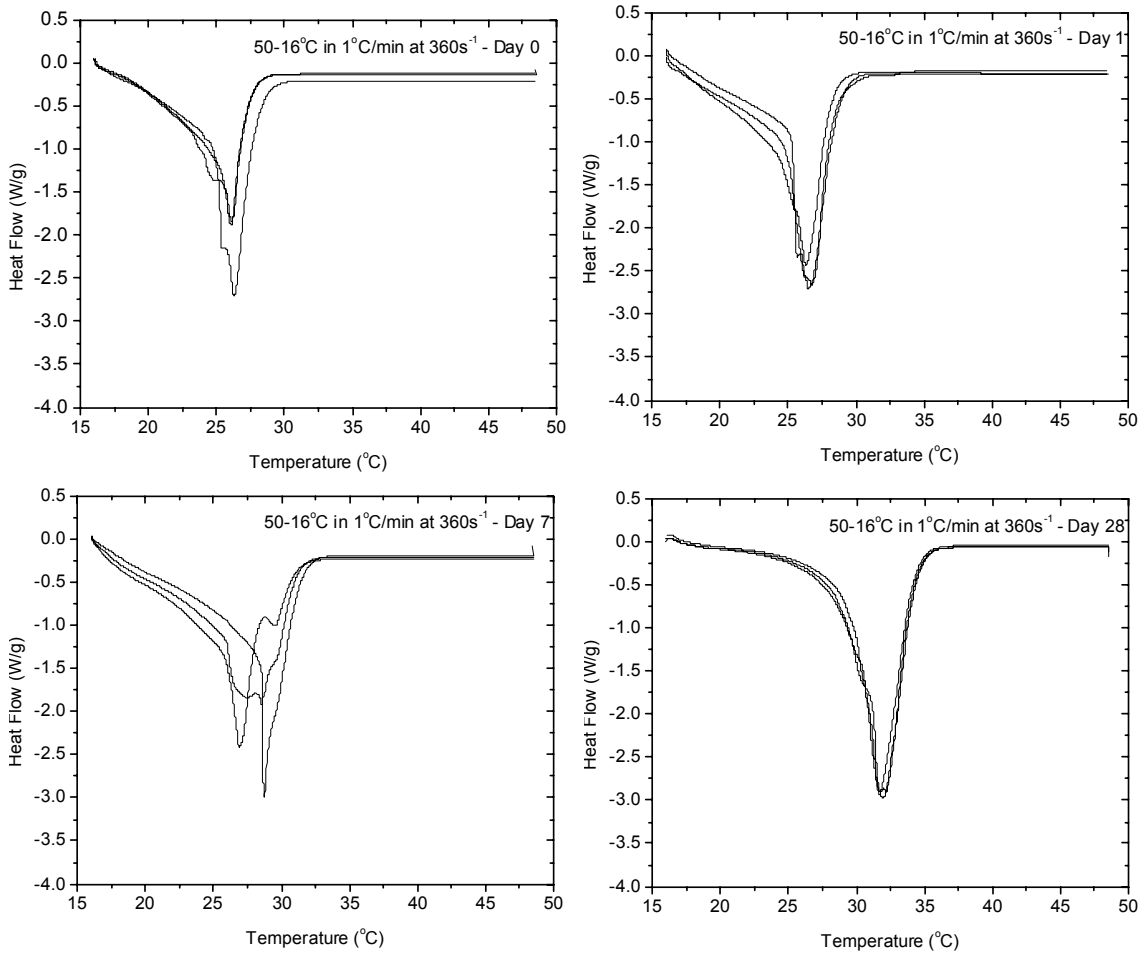

Figure 92: Heat flow curves of samples created by being cooled from 50 to 16°C at 1°C/min whilst shearing at a rate of $360s^{-1}$. The four graphs shown are sample repetitions carried out on day 0, day 1, day 7 and day 28.

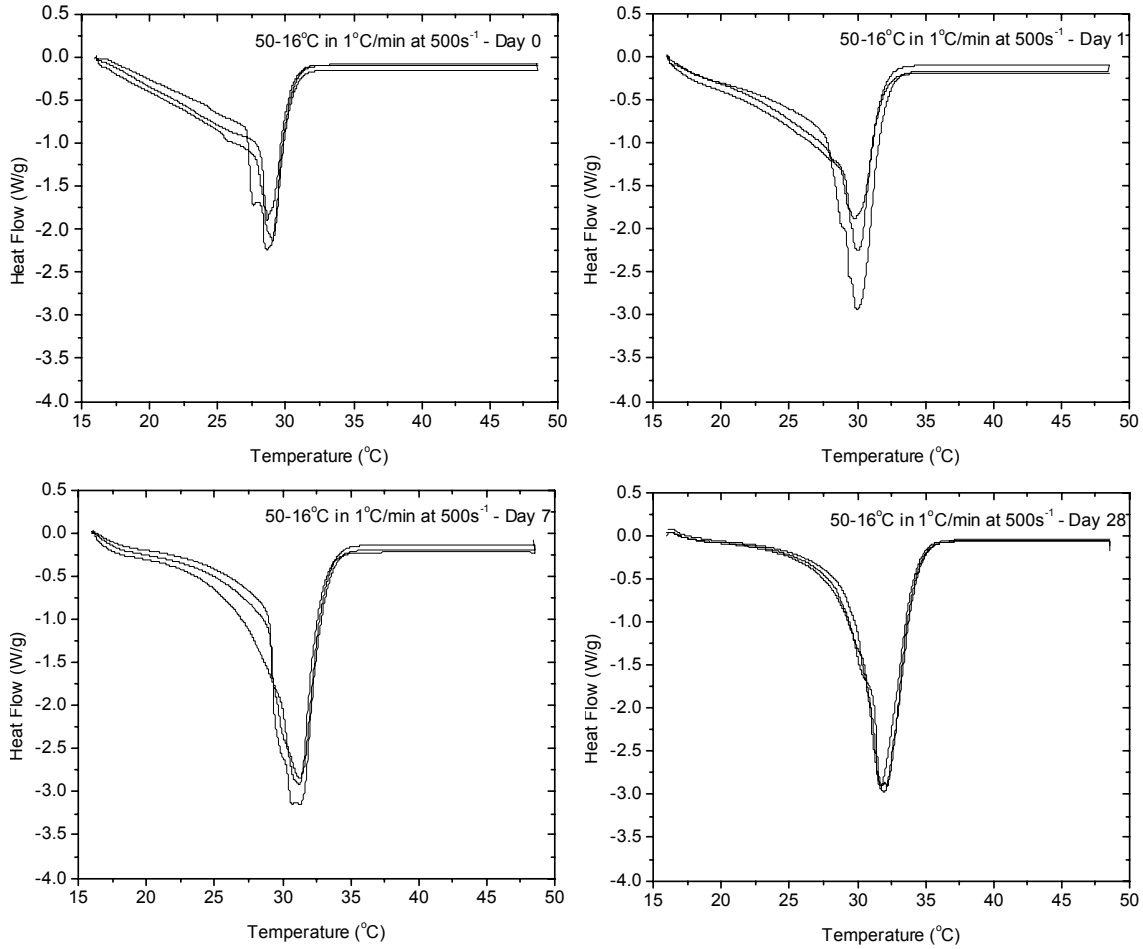

Figure 93: Heat flow curves of samples created by being cooled from 50 to 16°C at 1°C/min whilst shearing at a rate of $500s^{-1}$. The four graphs shown are sample repetitions carried out on day 0, day 1, day 7 and day 28.

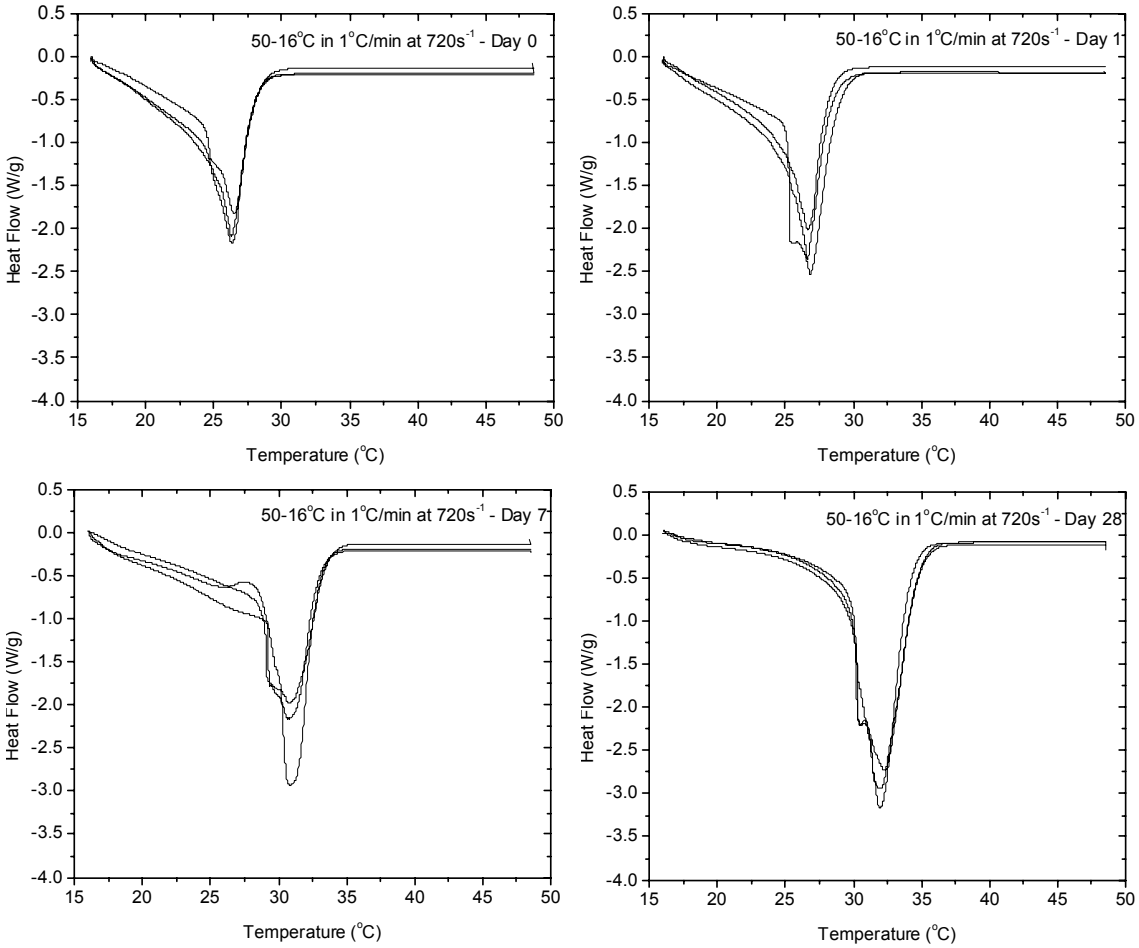

Figure 94: Heat flow curves of samples created by being cooled from 50 to 16°C at 1°C/min whilst shearing at a rate of $720s^{-1}$. The four graphs shown are sample repetitions carried out on day 0, day 1, day 7 and day 28.

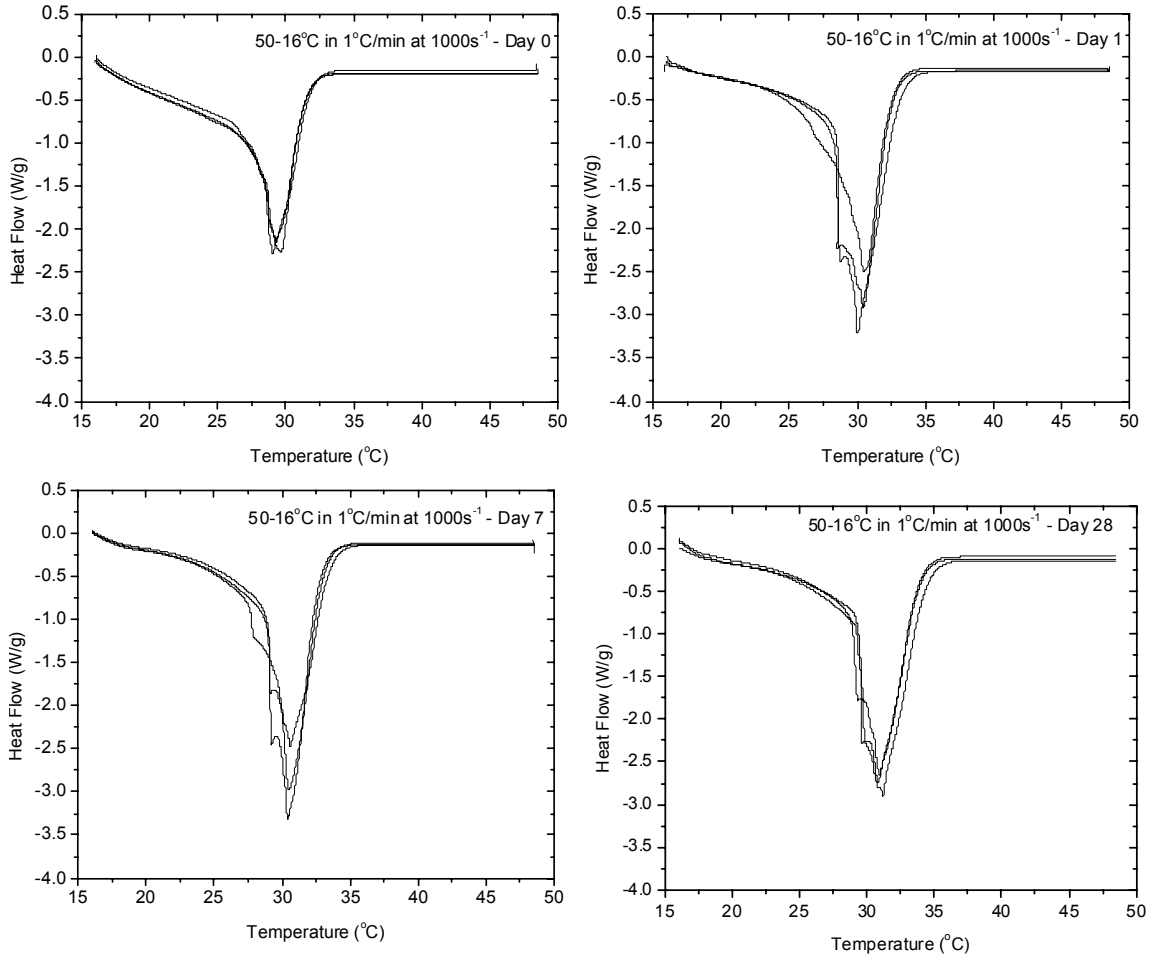

Figure 95: Heat flow curves of samples created by being cooled from 50 to 16°C at 1°C/min whilst shearing at a rate of $1000s^{-1}$. The four graphs shown are sample repetitions carried out on day 0, day 1, day 7 and day 28.

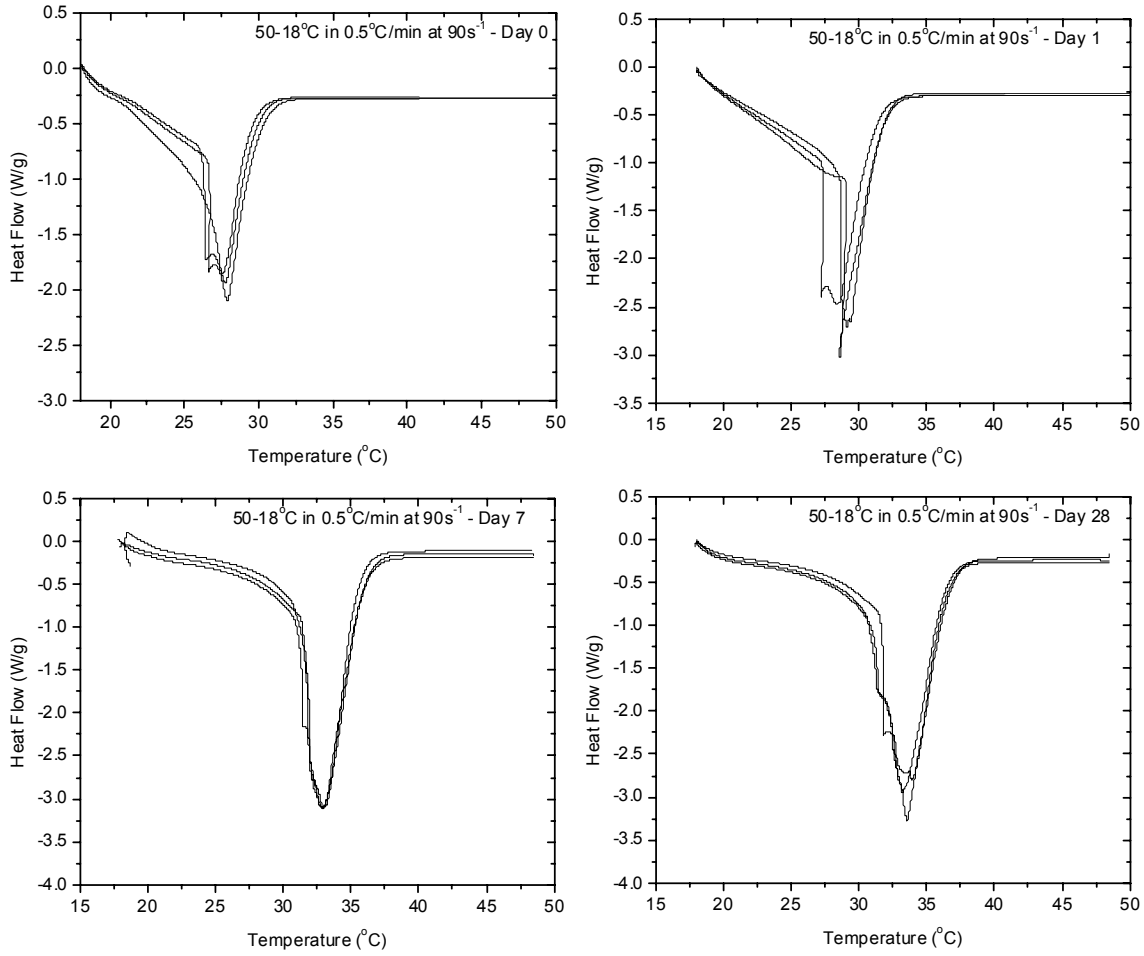

Figure 96: Heat flow curves of samples created by being cooled from 50 to 18°C at 0.5°C/min whilst shearing at a rate of $90s^{-1}$. The four graphs shown are sample repetitions carried out on day 0, day 1, day 7 and day 28.

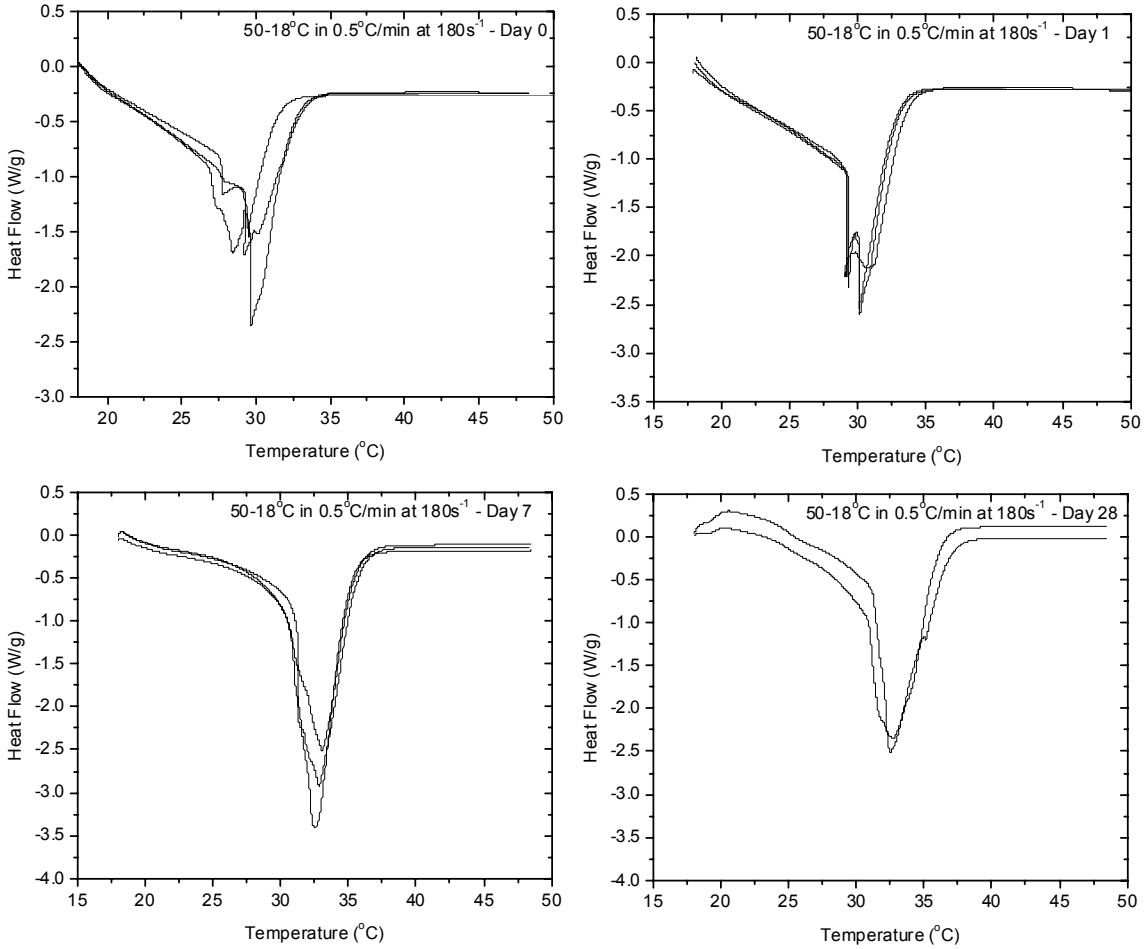

Figure 97: Heat flow curves of samples created by being cooled from 50 to 18°C at 0.5°C/min whilst shearing at a rate of $180s^{-1}$. The four graphs shown are sample repetitions carried out on day 0, day 1, day 7 and day 28.

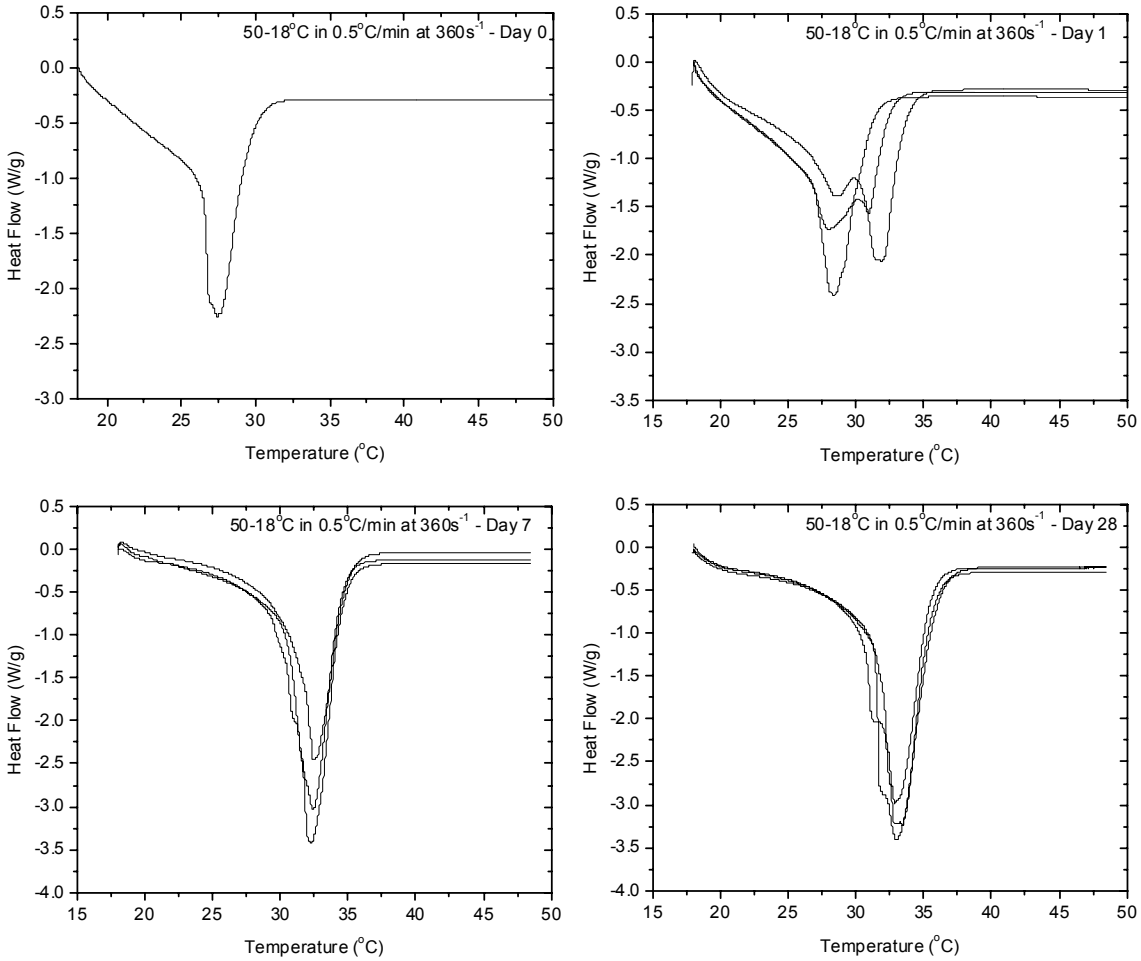

Figure 98: Heat flow curves of samples created by being cooled from 50 to 18°C at 0.5°C/min whilst shearing at a rate of $360s^{-1}$. The four graphs shown are sample repetitions carried out on day 0, day 1, day 7 and day 28.

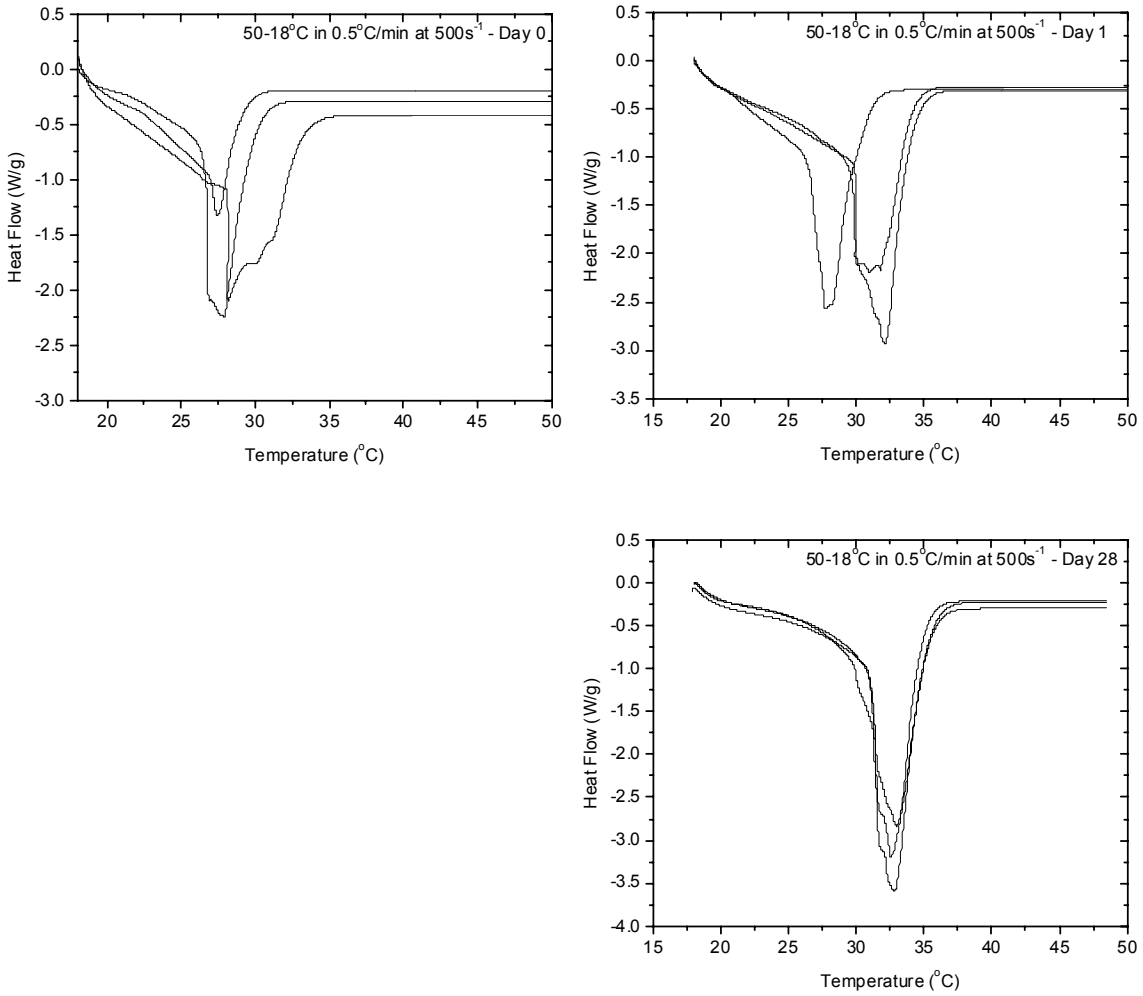

Figure 99: Heat flow curves of samples created by being cooled from 50 to 18°C at 0.5°C/min whilst shearing at a rate of $500s^{-1}$. The four graphs shown are sample repetitions carried out on day 0, day 1 and day 28.

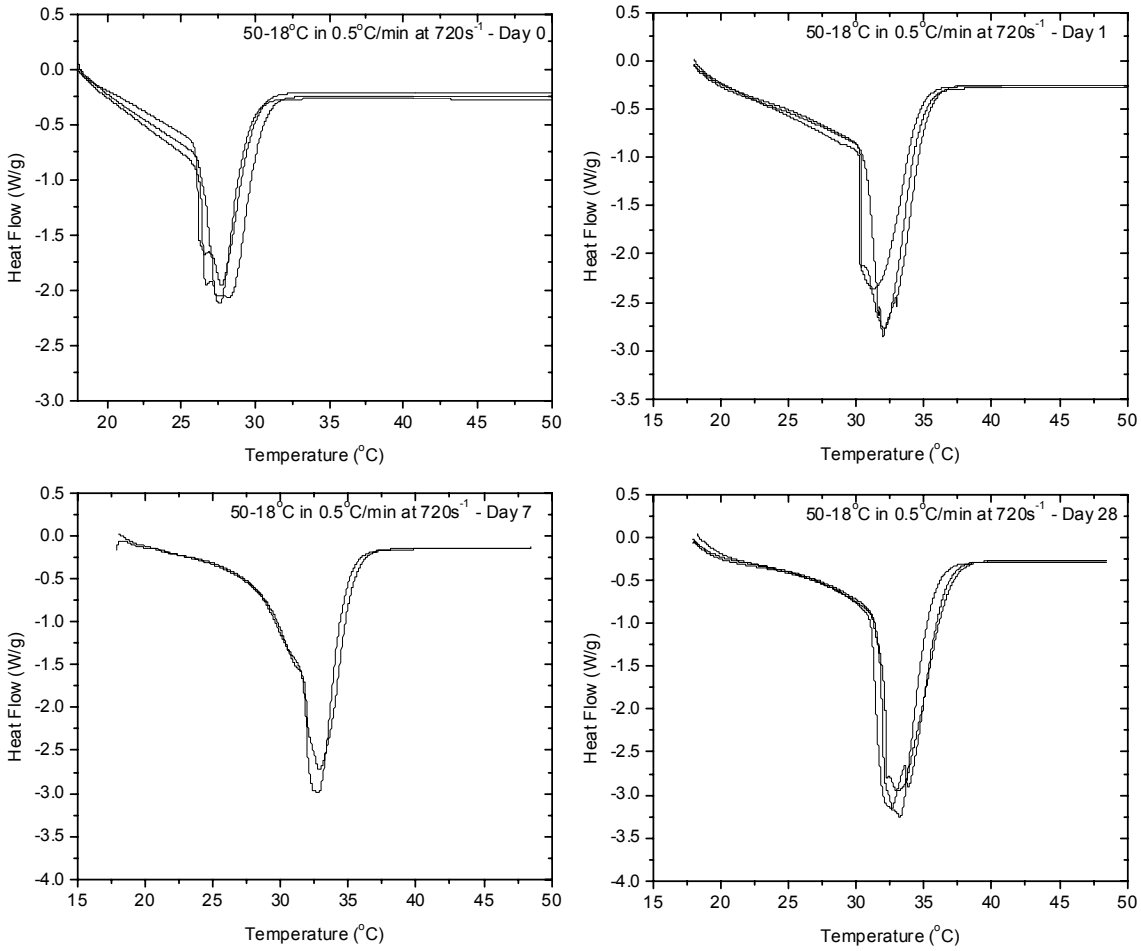

Figure 100: Heat flow curves of samples created by being cooled from 50 to 18°C at 0.5°C/min whilst shearing at a rate of $720s^{-1}$. The four graphs shown are sample repetitions carried out on day 0, day 1, day 7 and day 28.

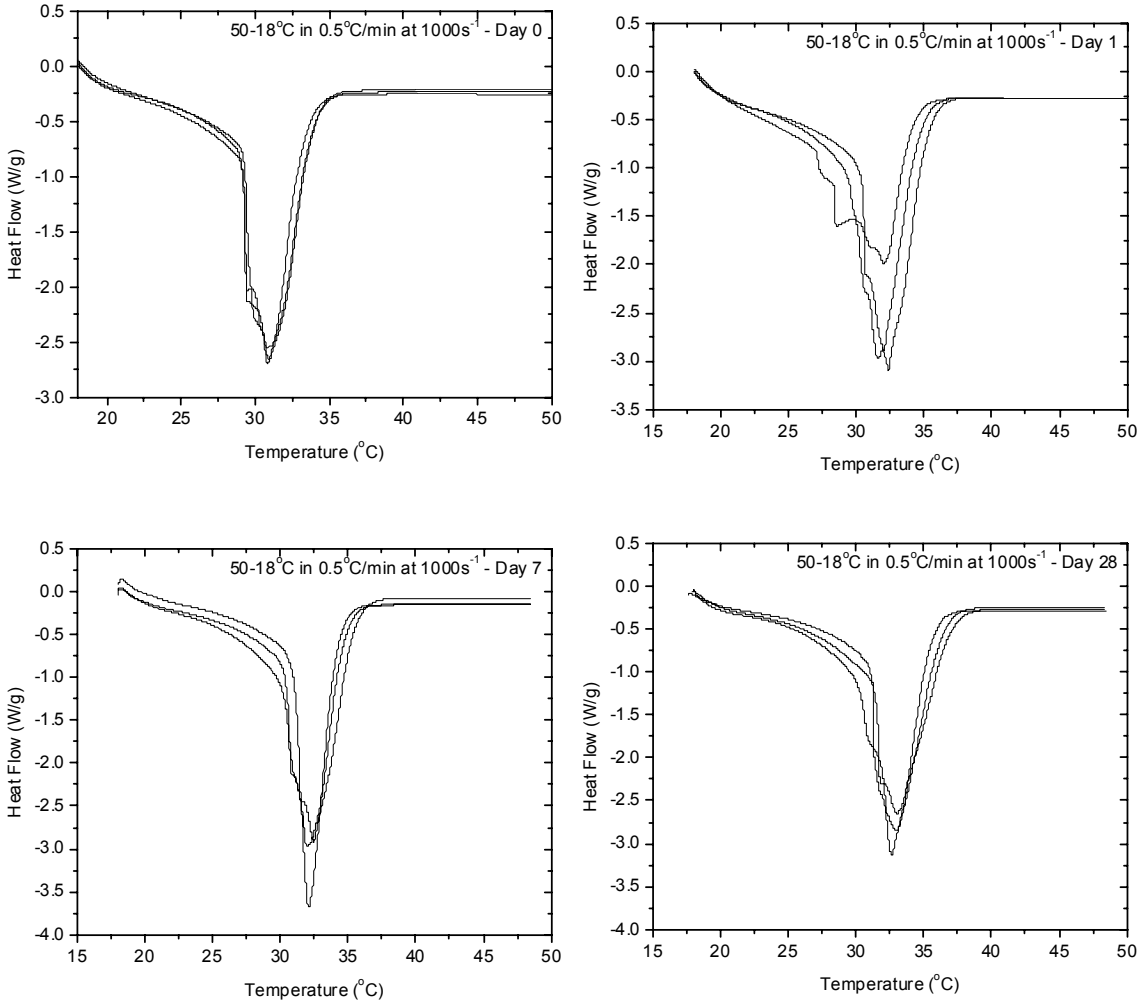

Figure 101: Heat flow curves of samples created by being cooled from 50 to 18°C at 0.5°C/min whilst shearing at a rate of $1000s^{-1}$. The four graphs shown are sample repetitions carried out on day 0, day 1, day 7 and day 28.

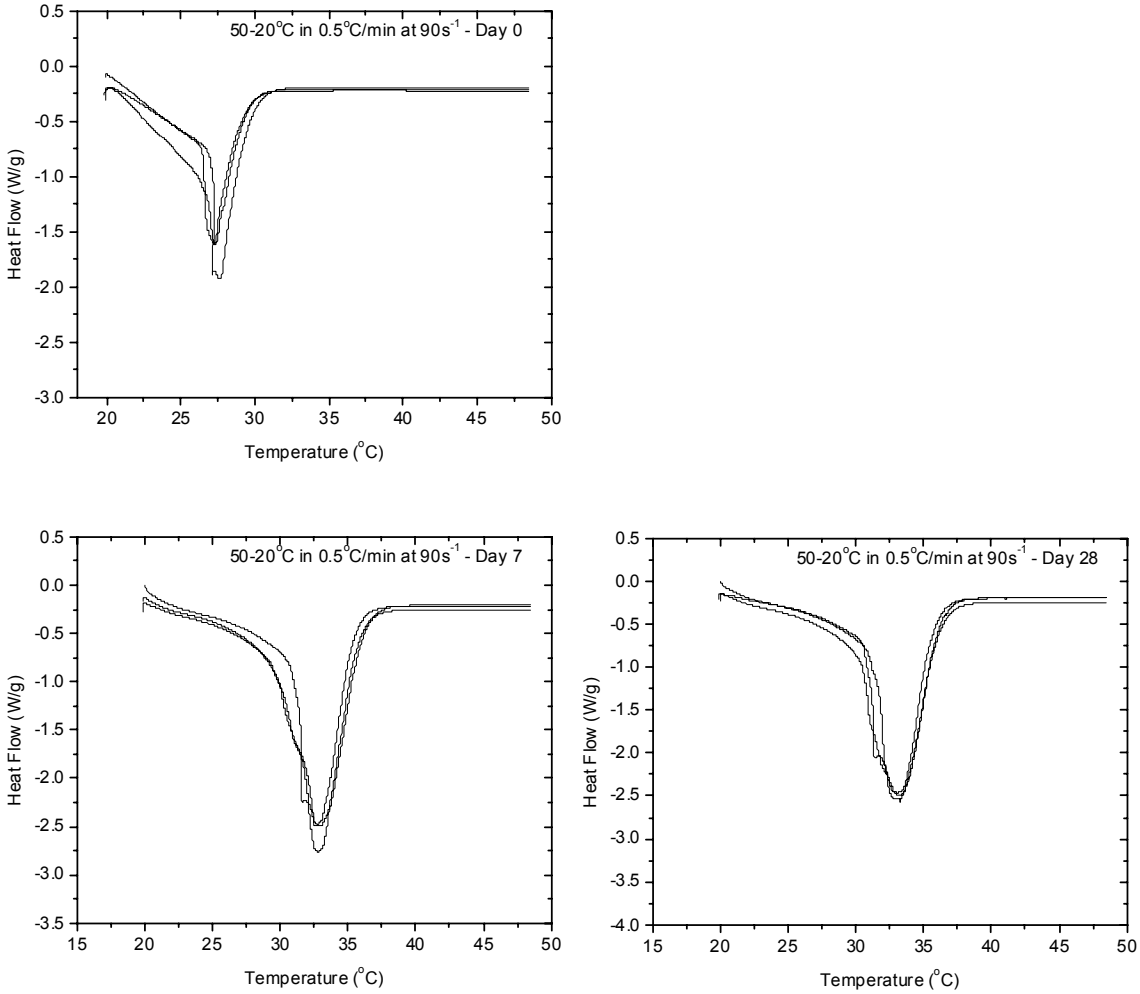

Figure 102: Heat flow curves of samples created by being cooled from 50 to 20°C at 0.5°C/min whilst shearing at a rate of $90s^{-1}$. The four graphs shown are sample repetitions carried out on day 0, day 7 and day 28.

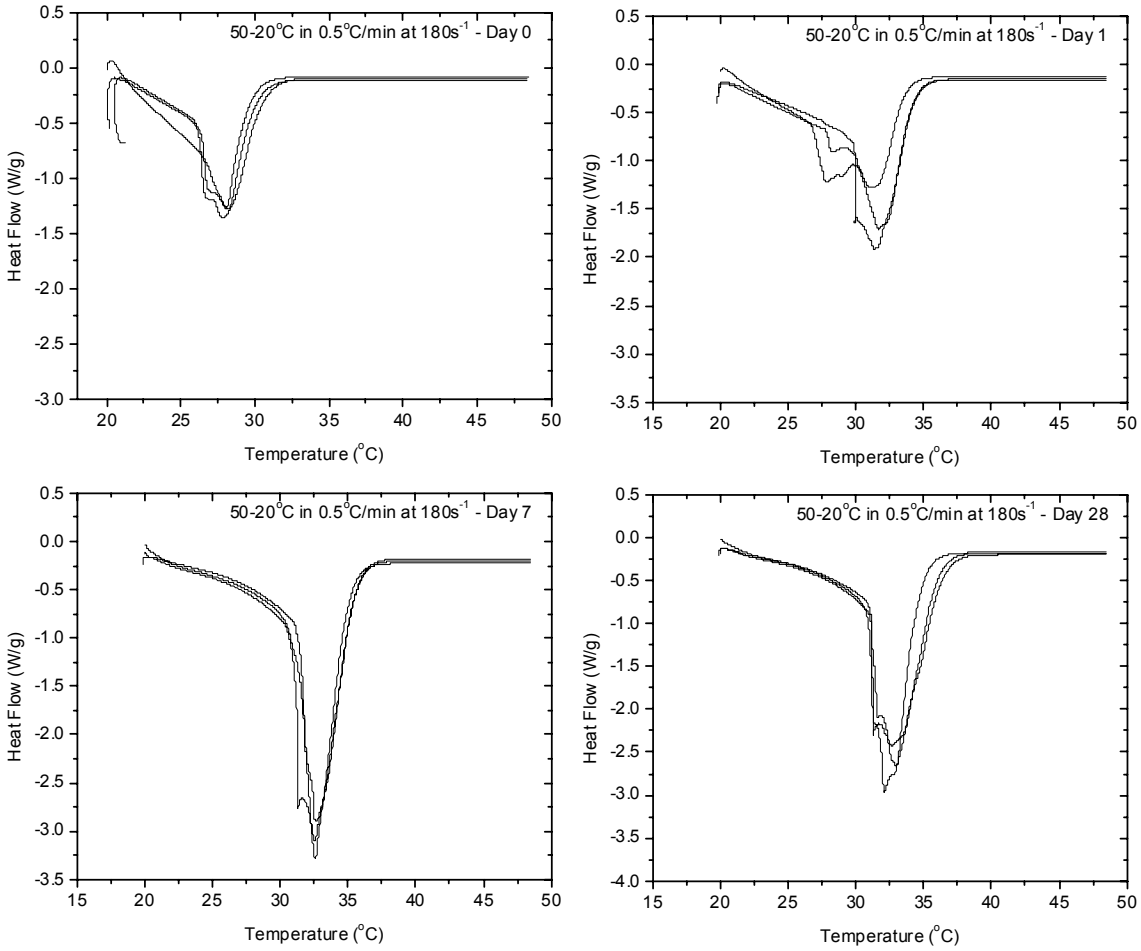

Figure 103: Heat flow curves of samples created by being cooled from 50 to 20°C at 0.5°C/min whilst shearing at a rate of $180s^{-1}$. The four graphs shown are sample repetitions carried out on day 0, day 1, day 7 and day 28.

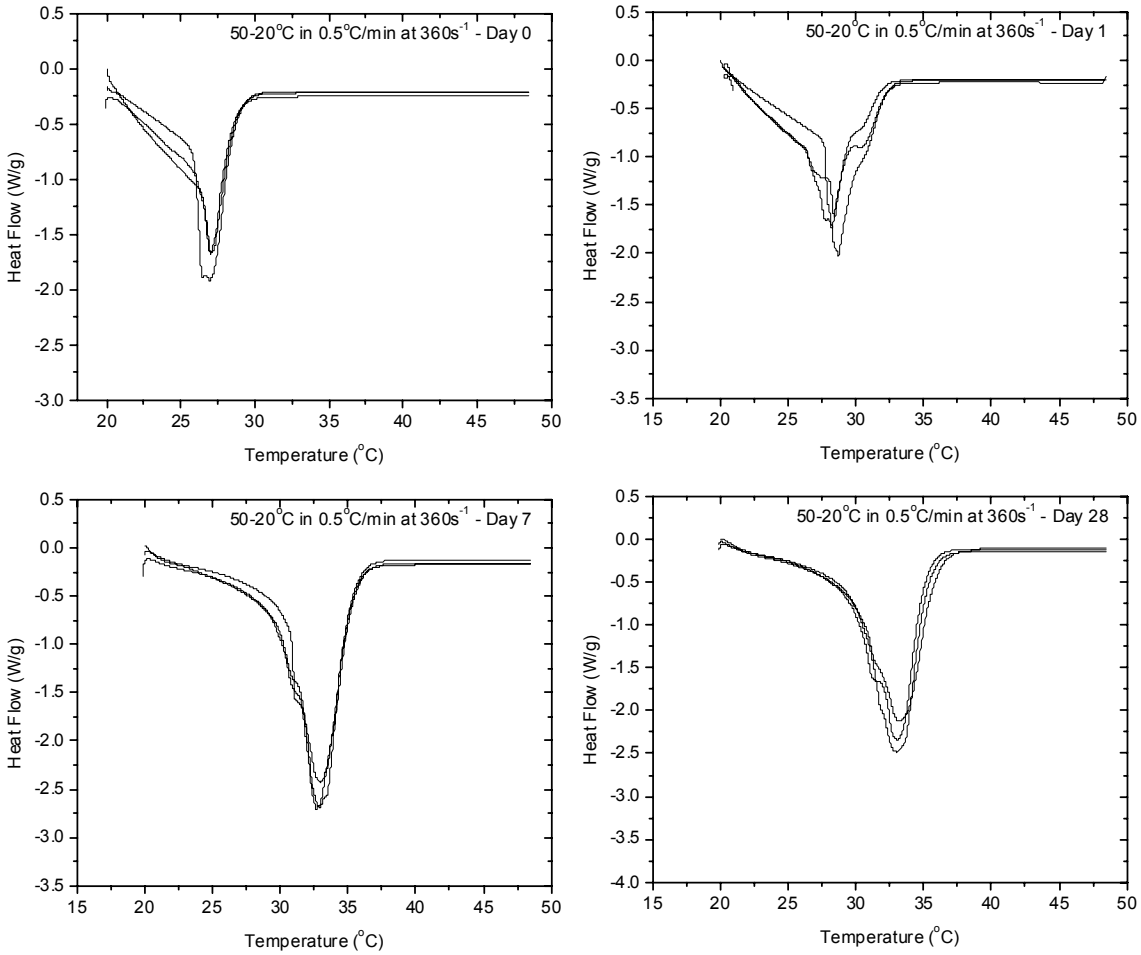

Figure 104: Heat flow curves of samples created by being cooled from 50 to 20°C at 0.5°C/min whilst shearing at a rate of $360s^{-1}$. The four graphs shown are sample repetitions carried out on day 0, day 1, day 7 and day 28.

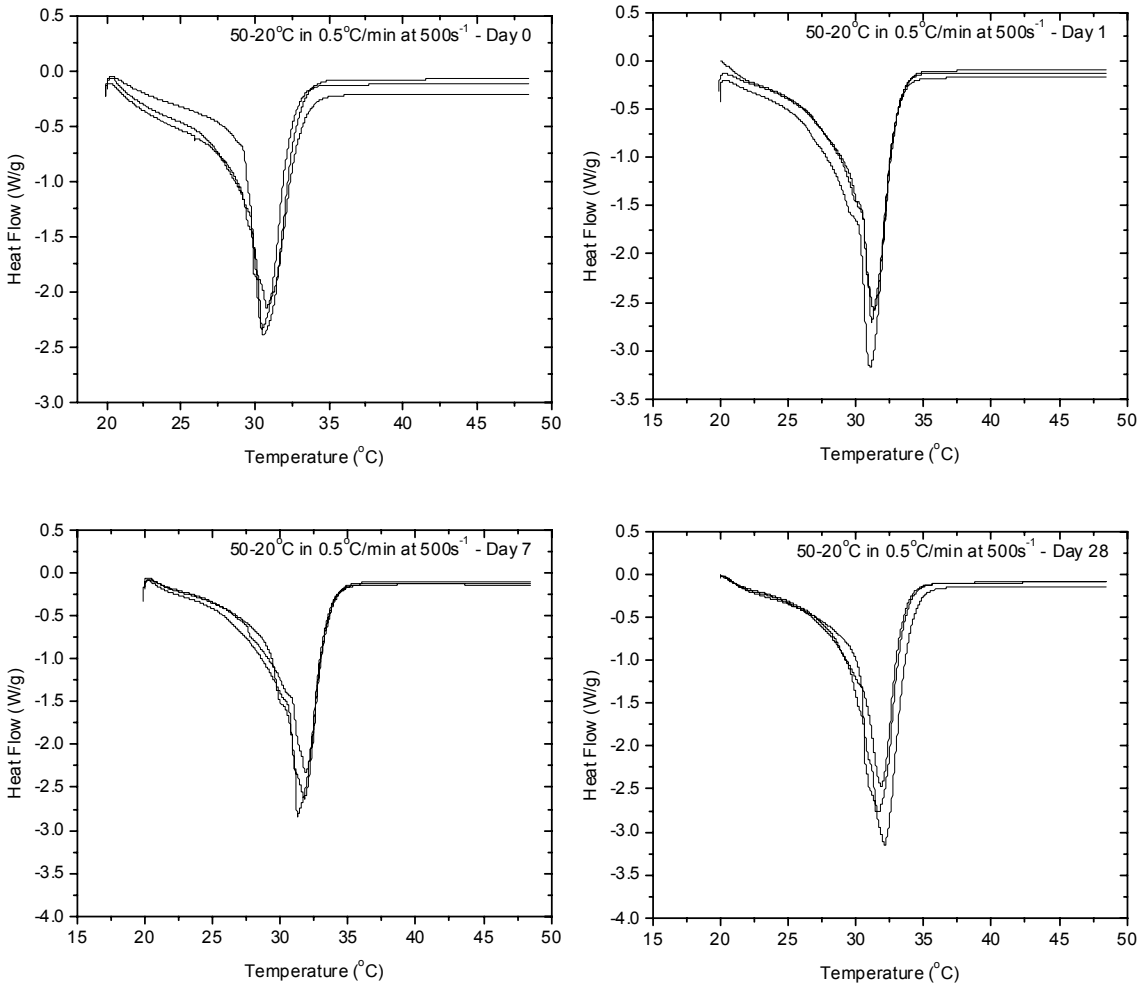

Figure 105: Heat flow curves of samples created by being cooled from 50 to 20°C at 0.5°C/min whilst shearing at a rate of $500s^{-1}$. The four graphs shown are sample repetitions carried out on day 0, day 1, day 7 and day 28.

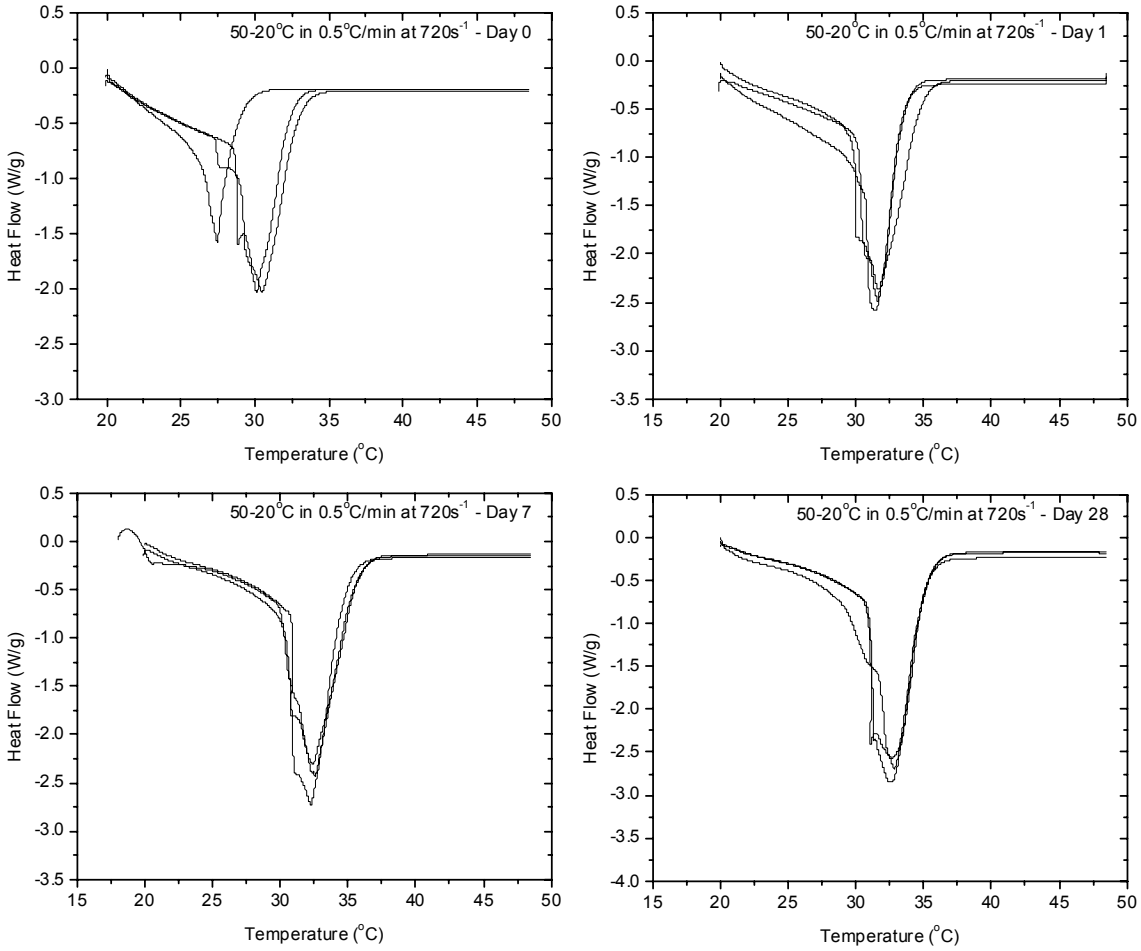

Figure 106: Heat flow curves of samples created by being cooled from 50 to 20°C at 0.5°C/min whilst shearing at a rate of $720s^{-1}$. The four graphs shown are sample repetitions carried out on day 0, day 1, day 7 and day 28.

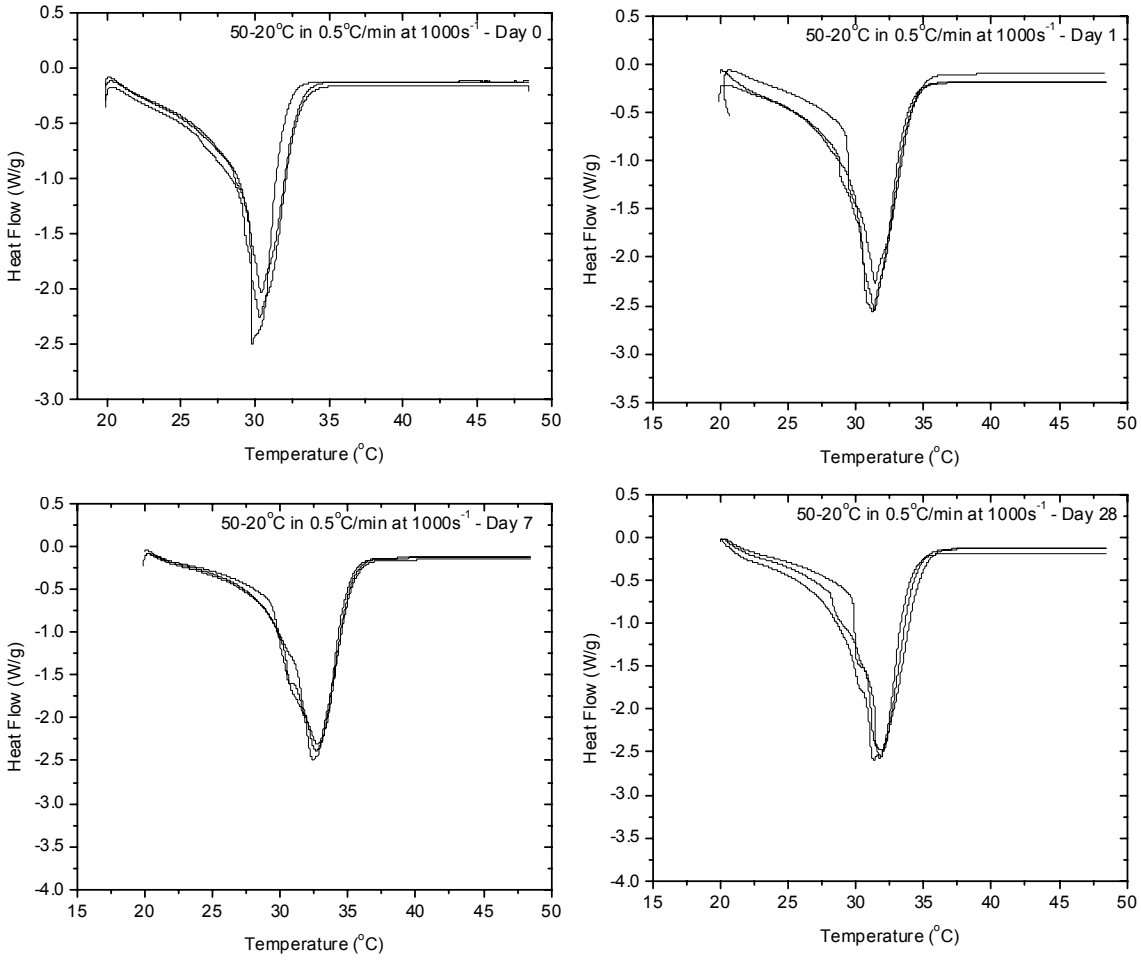

Figure 107: Heat flow curves of samples created by being cooled from 50 to 20°C at 0.5°C/min whilst shearing at a rate of $1000s^{-1}$. The four graphs shown are sample repetitions carried out on day 0, day 1, day 7 and day 28.

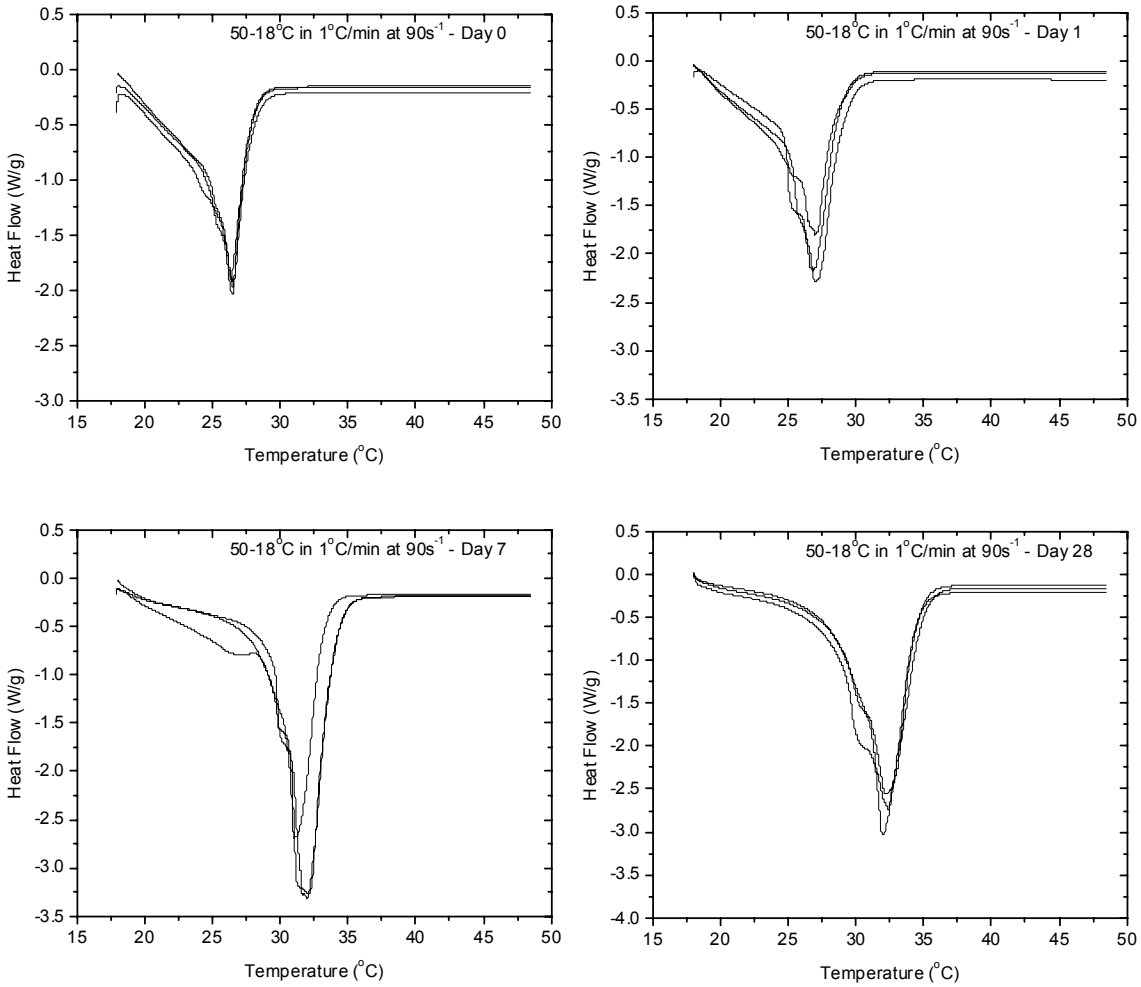

Figure 108: Heat flow curves of samples created by being cooled from 50 to 18°C at 1°C/min whilst shearing at a rate of $90s^{-1}$. The four graphs shown are sample repetitions carried out on day 0, day 1, day 7 and day 28.

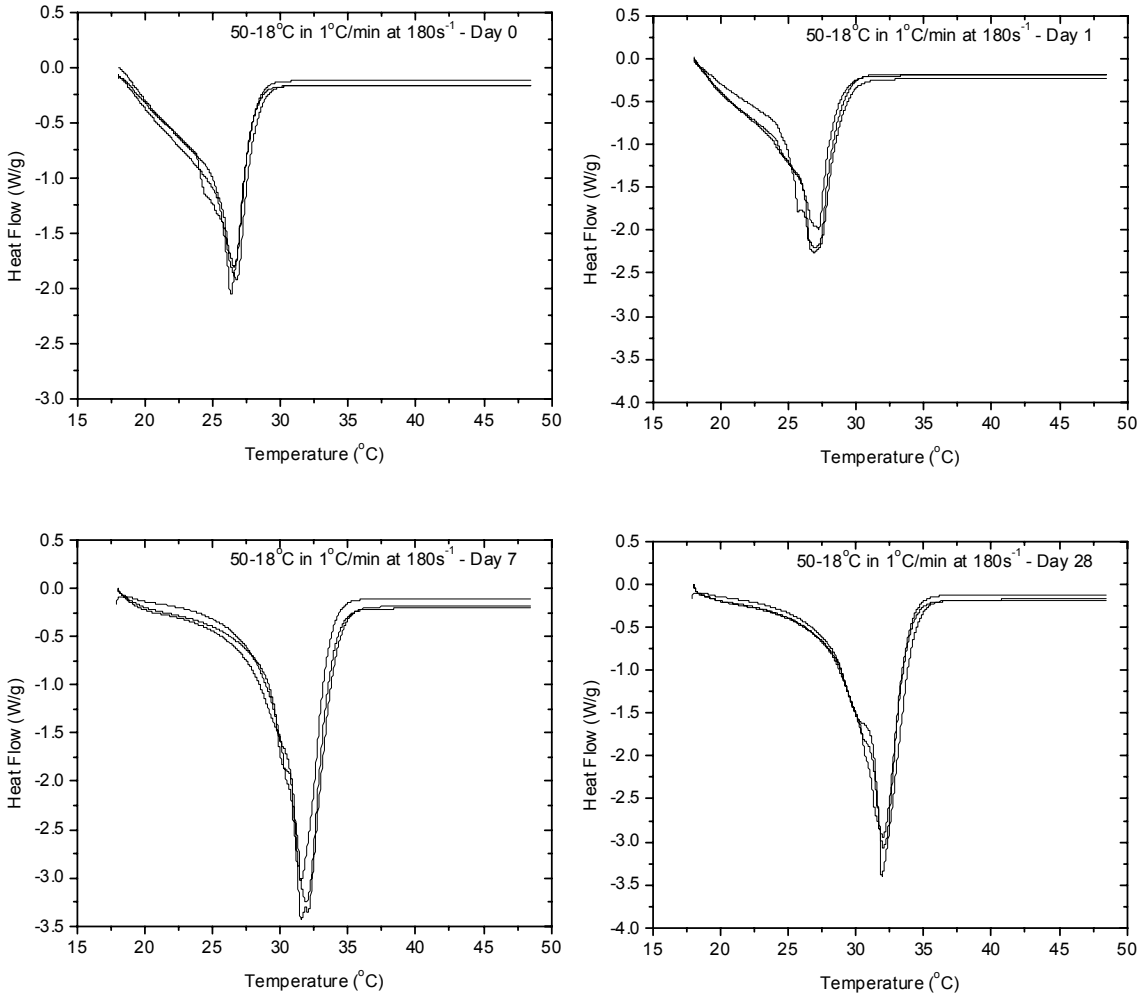

Figure 109: Heat flow curves of samples created by being cooled from 50 to 18°C at 1°C/min whilst shearing at a rate of $180s^{-1}$. The four graphs shown are sample repetitions carried out on day 0, day 1, day 7 and day 28.

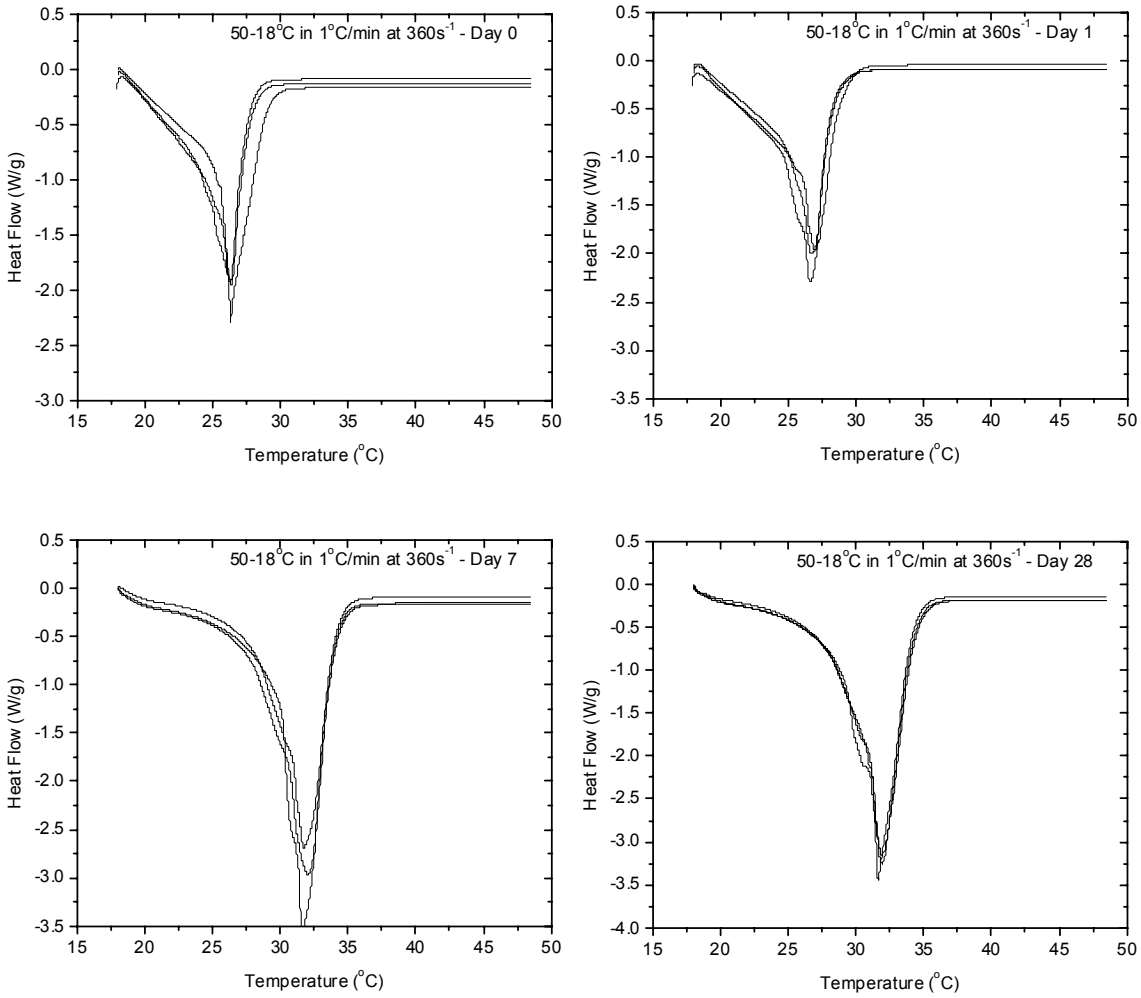

Figure 110: Heat flow curves of samples created by being cooled from 50 to 18°C at 1°C/min whilst shearing at a rate of $360s^{-1}$. The four graphs shown are sample repetitions carried out on day 0, day 1, day 7 and day 28.

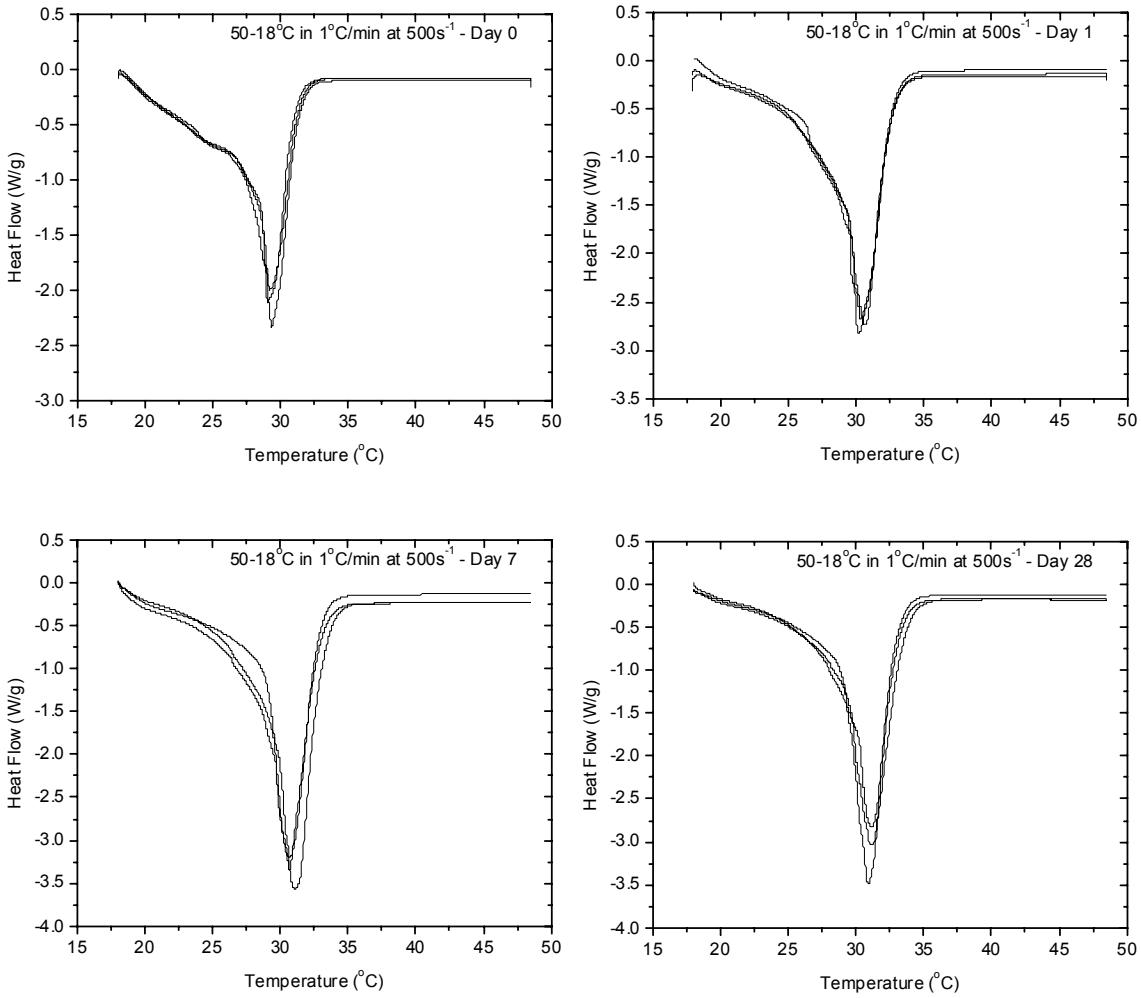

Figure 111: Heat flow curves of samples created by being cooled from 50 to 18°C at 1°C/min whilst shearing at a rate of $500s^{-1}$. The four graphs shown are sample repetitions carried out on day 0, day 1, day 7 and day 28.

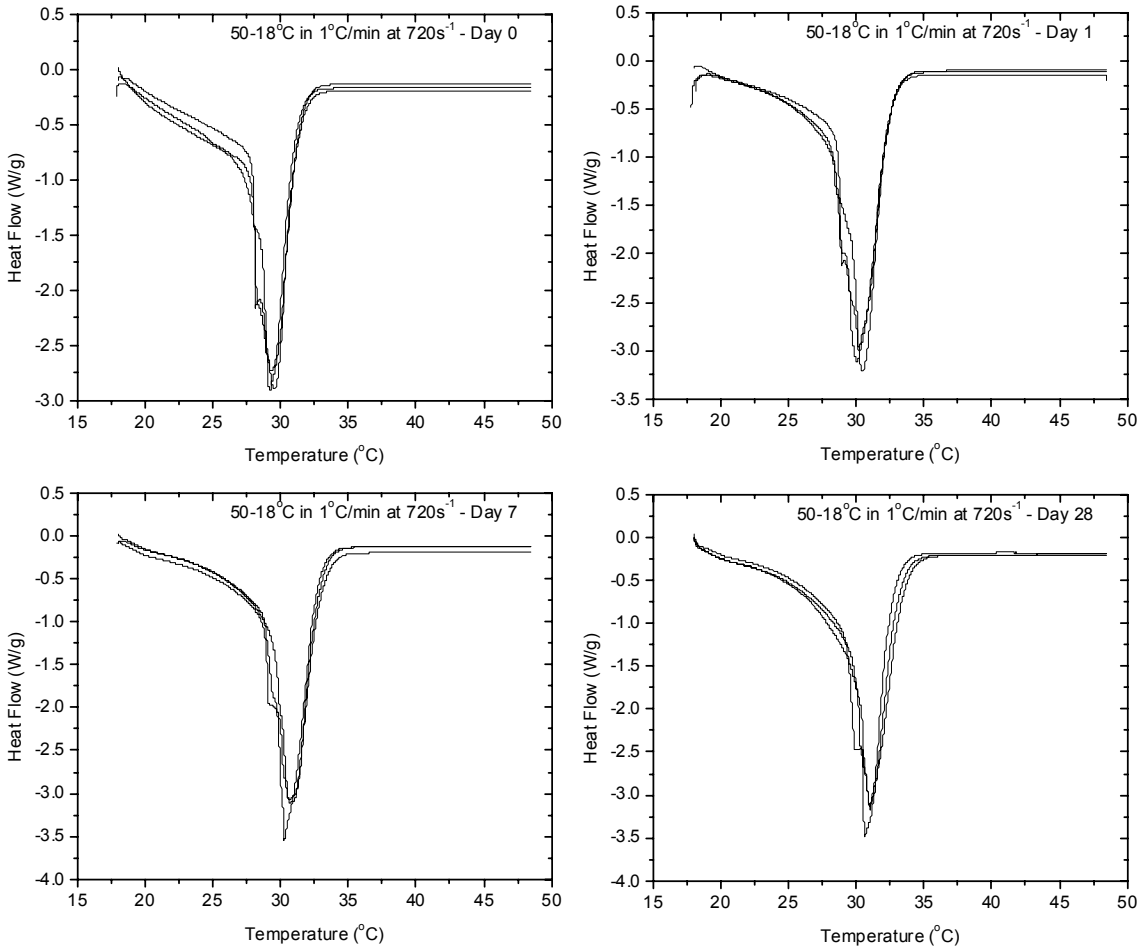

Figure 112: Heat flow curves of samples created by being cooled from 50 to 18°C at 1°C/min whilst shearing at a rate of $720s^{-1}$. The four graphs shown are sample repetitions carried out on day 0, day 1, day 7 and day 28.

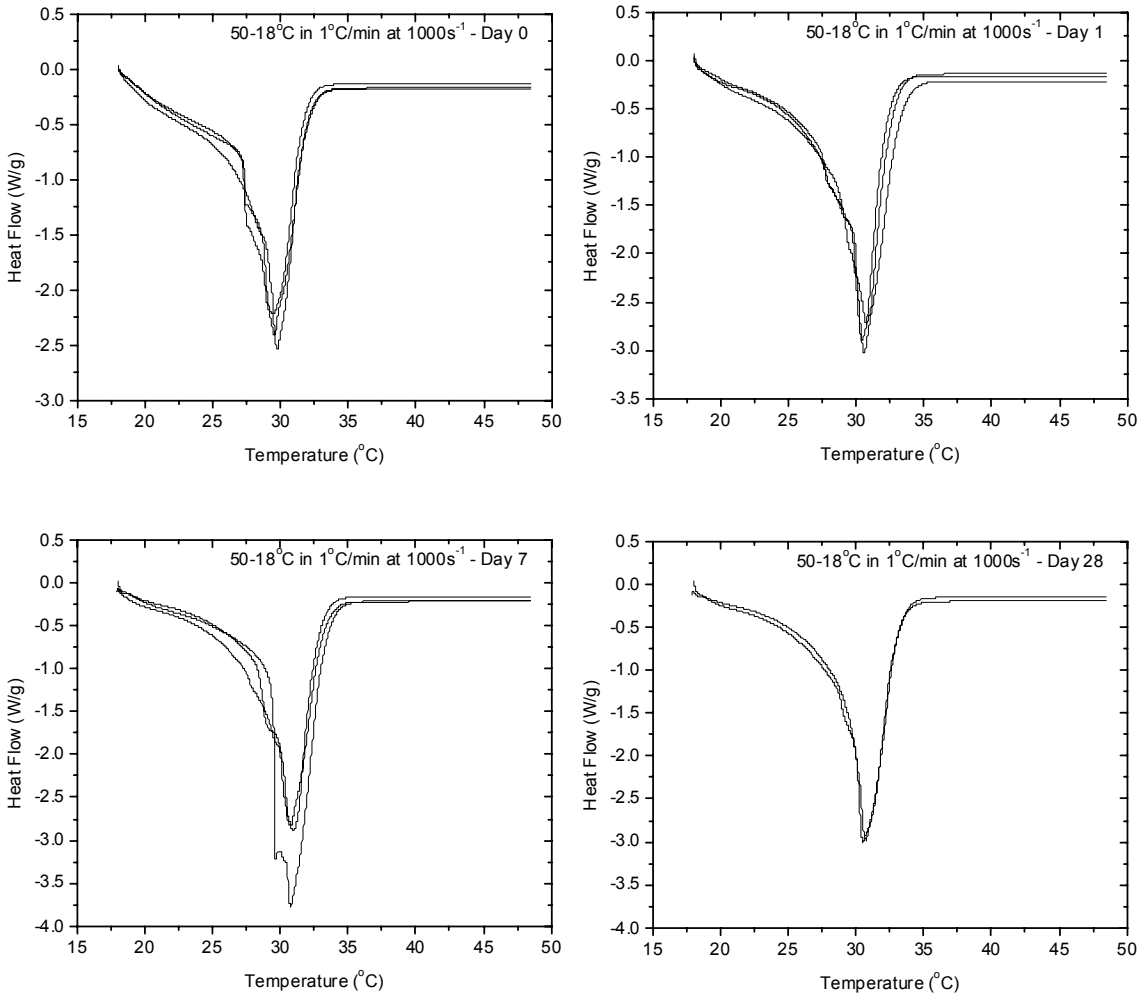

Figure 113: Heat flow curves of samples created by being cooled from 50 to 18°C at 1°C/min whilst shearing at a rate of $1000s^{-1}$. The four graphs shown are sample repetitions carried out on day 0, day 1, day 7 and day 28.

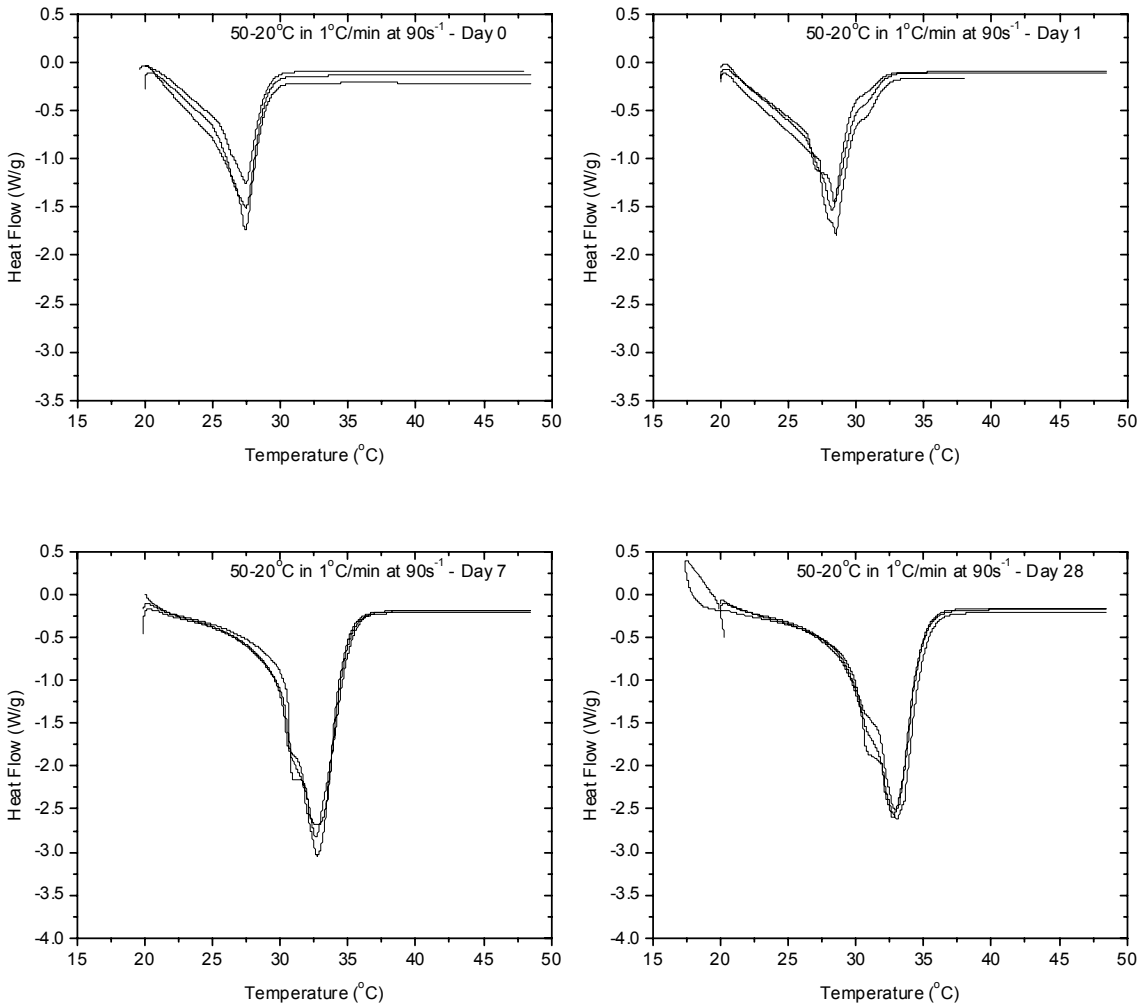

Figure 114: Heat flow curves of samples created by being cooled from 50 to 20°C at 1°C/min whilst shearing at a rate of $90s^{-1}$. The four graphs shown are sample repetitions carried out on day 0, day 1, day 7 and day 28.

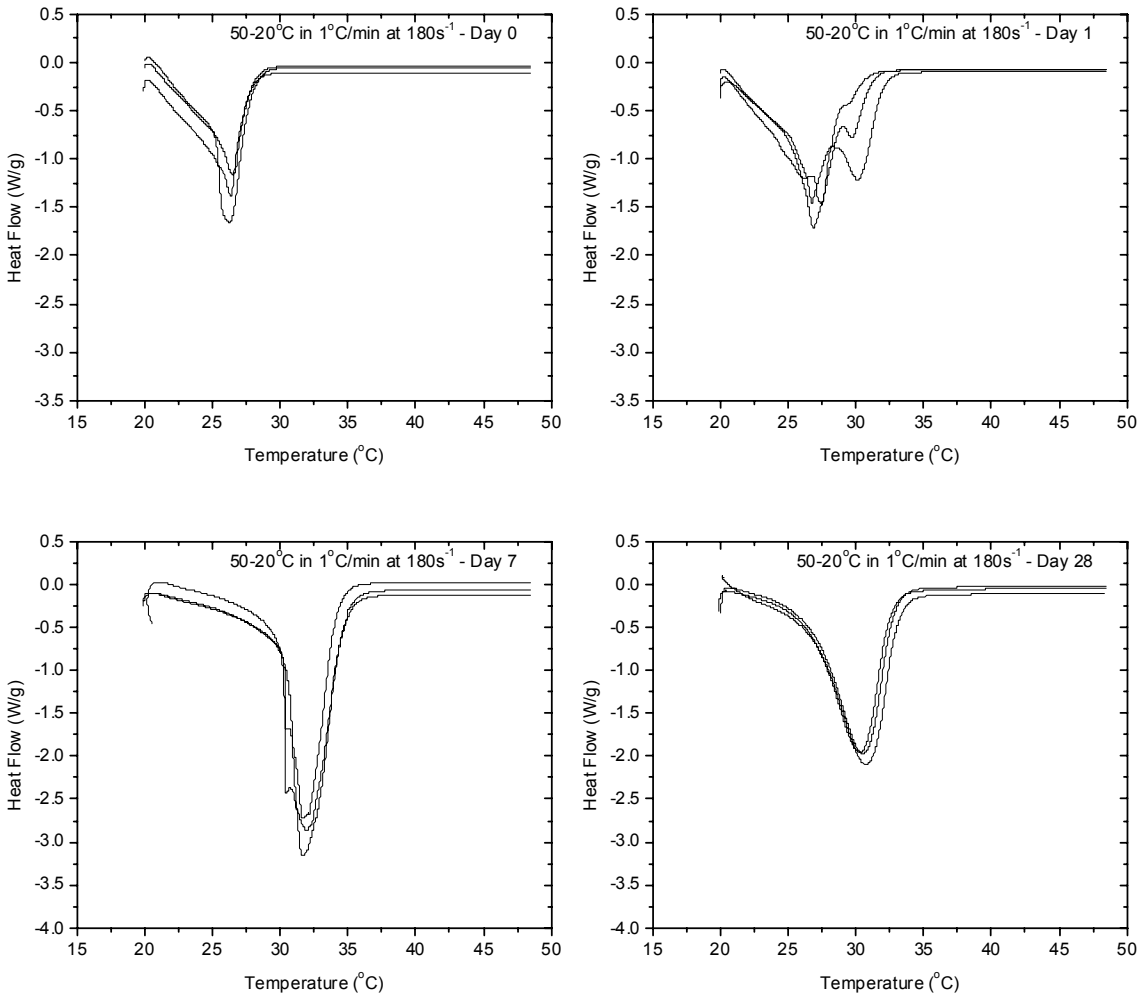

Figure 115: Heat flow curves of samples created by being cooled from 50 to 20°C at 1°C/min whilst shearing at a rate of $180s^{-1}$. The four graphs shown are sample repetitions carried out on day 0, day 1, day 7 and day 28.

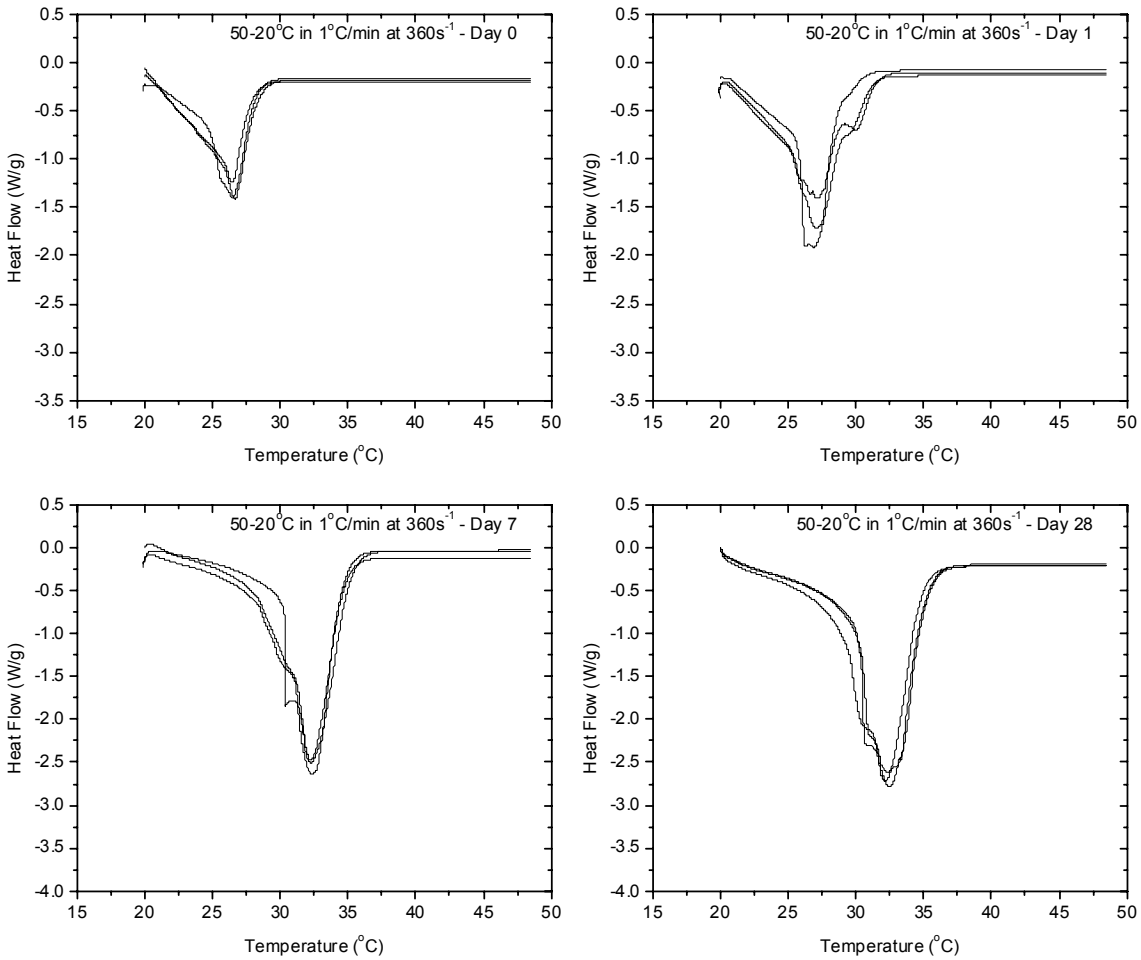

Figure 116: Heat flow curves of samples created by being cooled from 50 to 20°C at 1°C/min whilst shearing at a rate of $360s^{-1}$. The four graphs shown are sample repetitions carried out on day 0, day 1, day 7 and day 28.

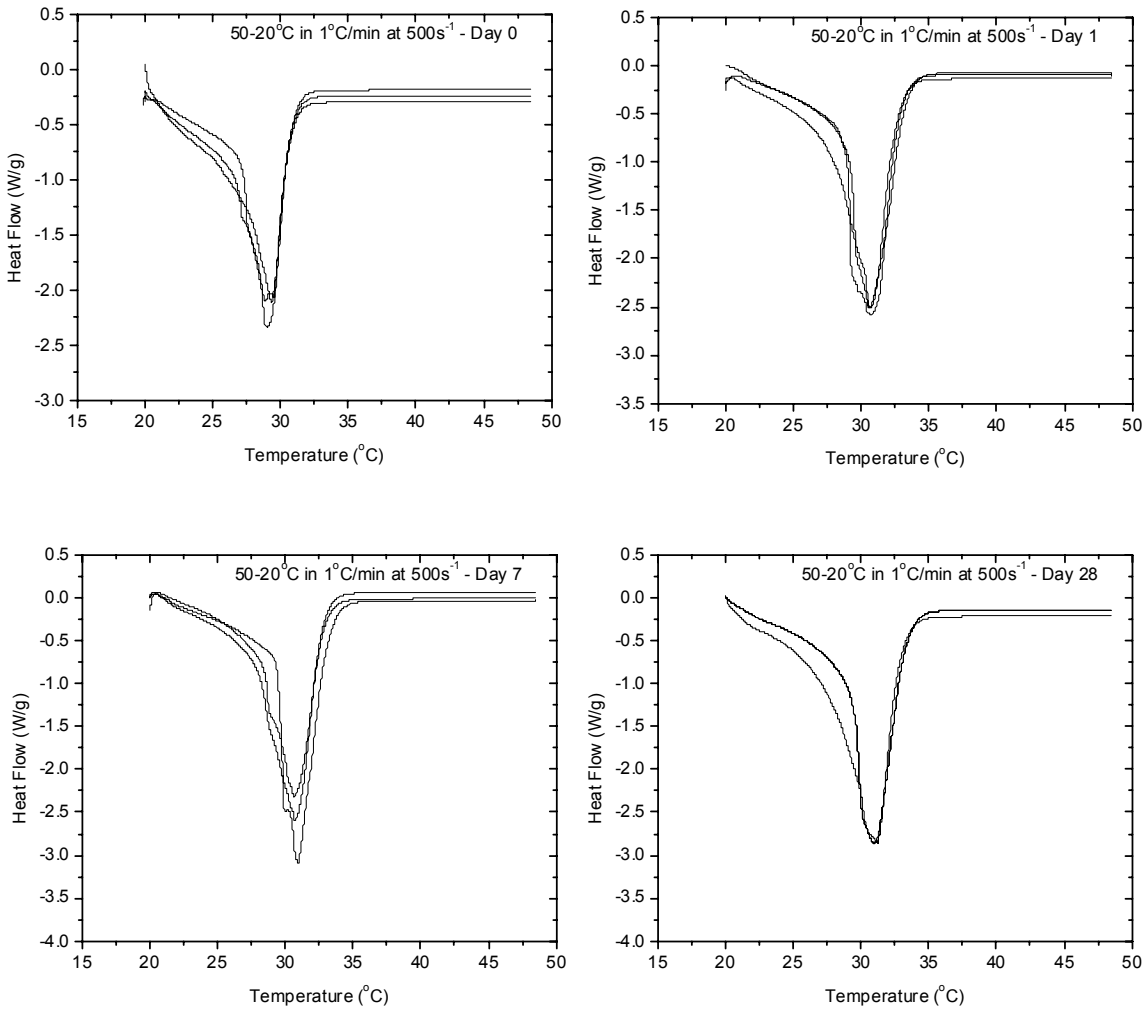

Figure 117: Heat flow curves of samples created by being cooled from 50 to 20°C at 1°C/min whilst shearing at a rate of $500s^{-1}$. The four graphs shown are sample repetitions carried out on day 0, day 1, day 7 and day 28.

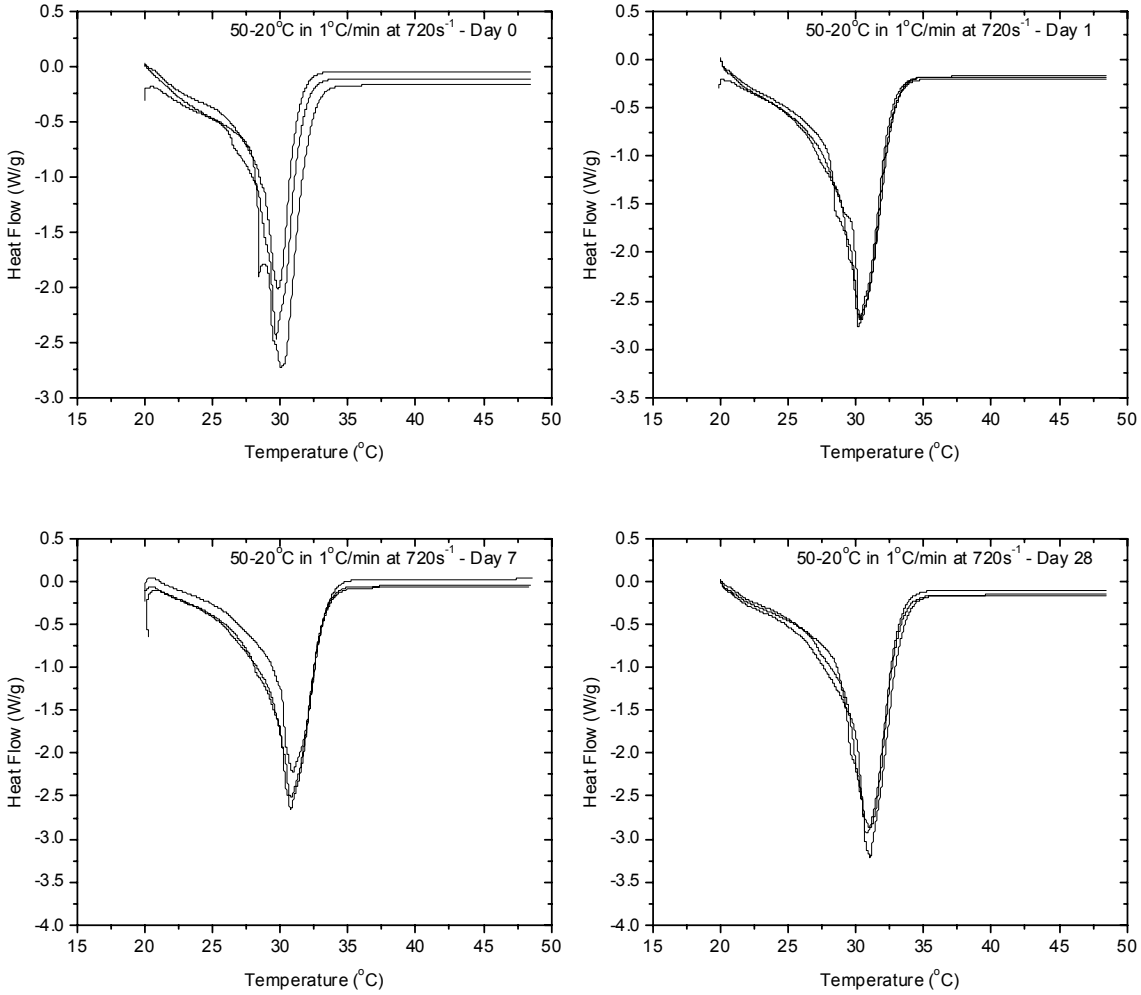

Figure 118: Heat flow curves of samples created by being cooled from 50 to 20°C at 1°C/min whilst shearing at a rate of $720s^{-1}$. The four graphs shown are sample repetitions carried out on day 0, day 1, day 7 and day 28.

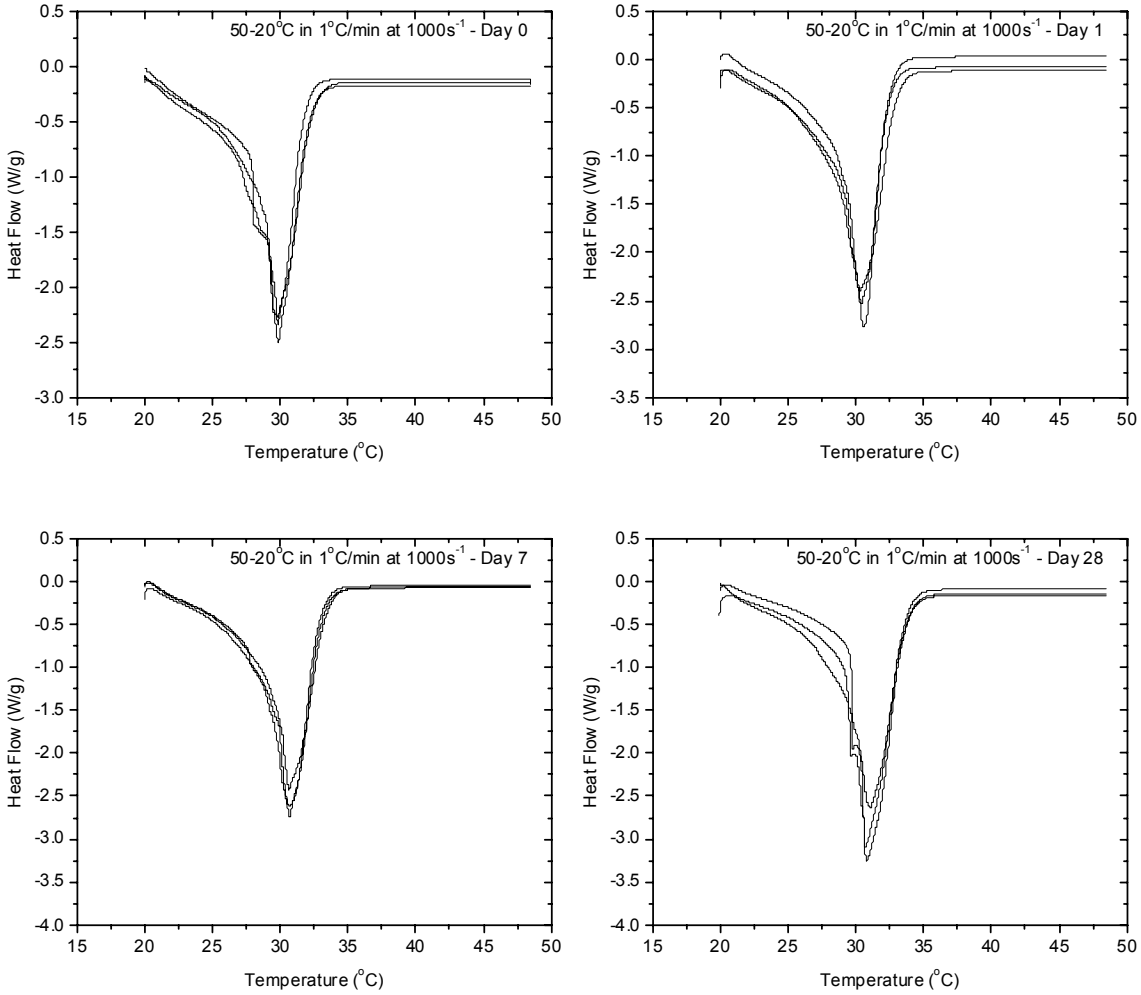

Figure 119: Heat flow curves of samples created by being cooled from 50 to 20°C at 1°C/min whilst shearing at a rate of $1000s^{-1}$. The four graphs shown are sample repetitions carried out on day 0, day 1, day 7 and day 28.

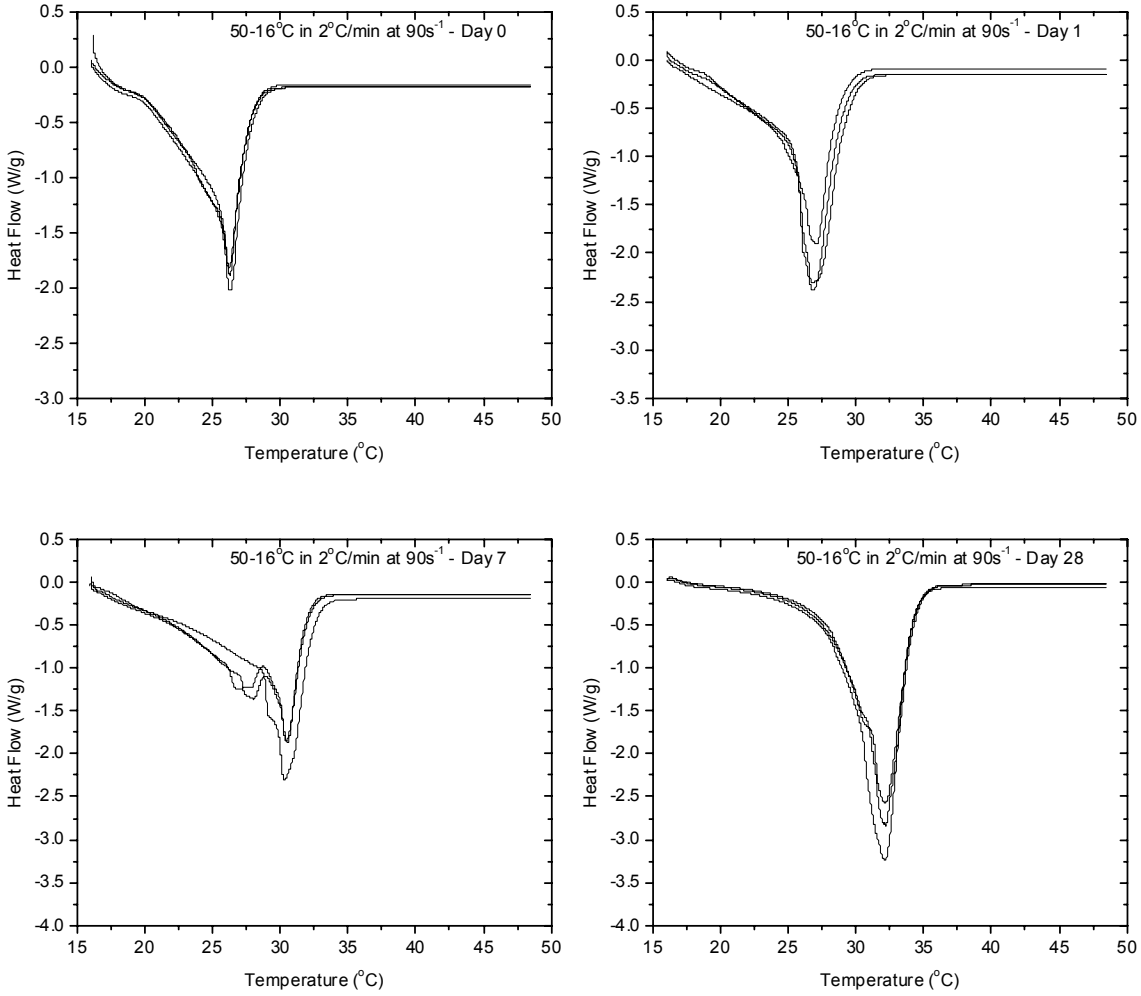

Figure 120: Heat flow curves of samples created by being cooled from 50 to 16°C at 2°C/min whilst shearing at a rate of $90s^{-1}$. The four graphs shown are sample repetitions carried out on day 0, day 1, day 7 and day 28.

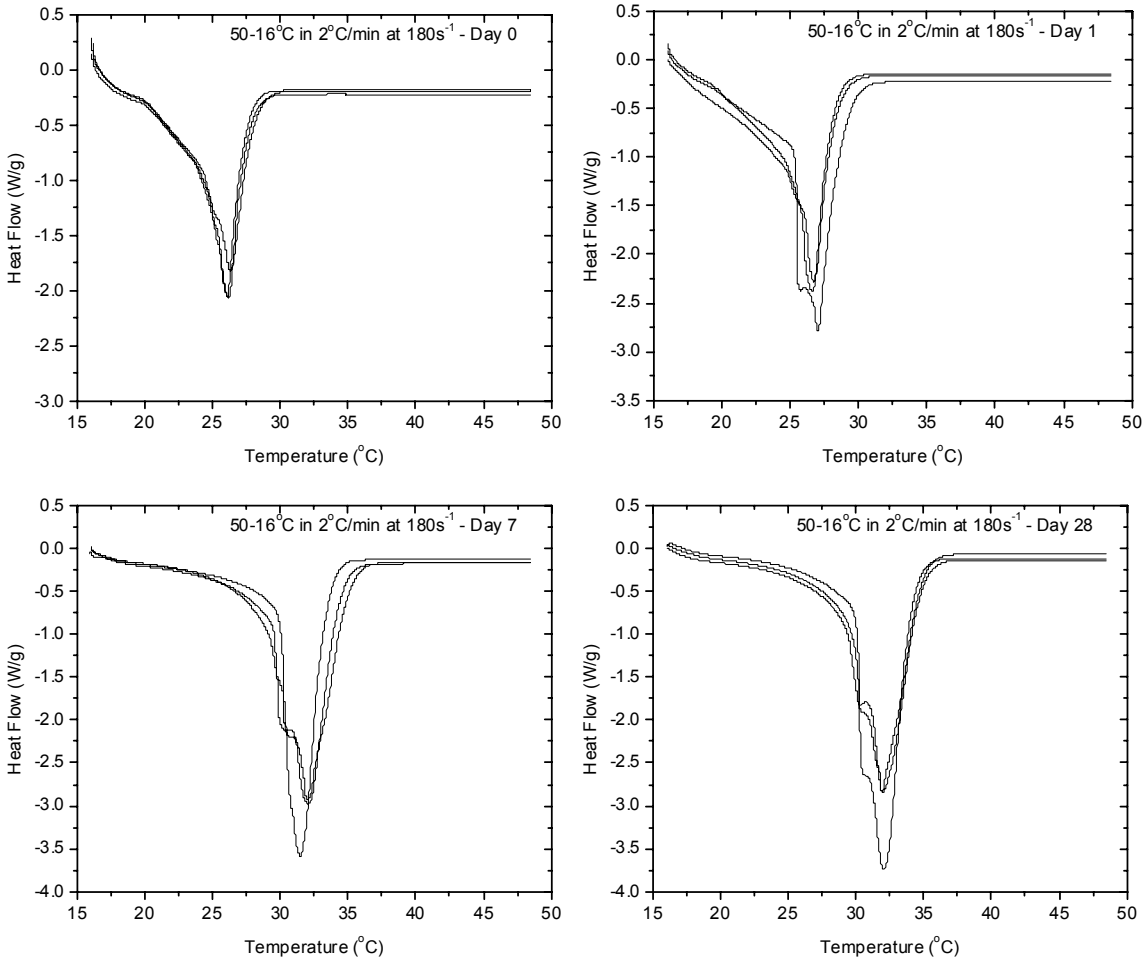

Figure 121: Heat flow curves of samples created by being cooled from 50 to 16°C at 2°C/min whilst shearing at a rate of $180s^{-1}$. The four graphs shown are sample repetitions carried out on day 0, day 1, day 7 and day 28.

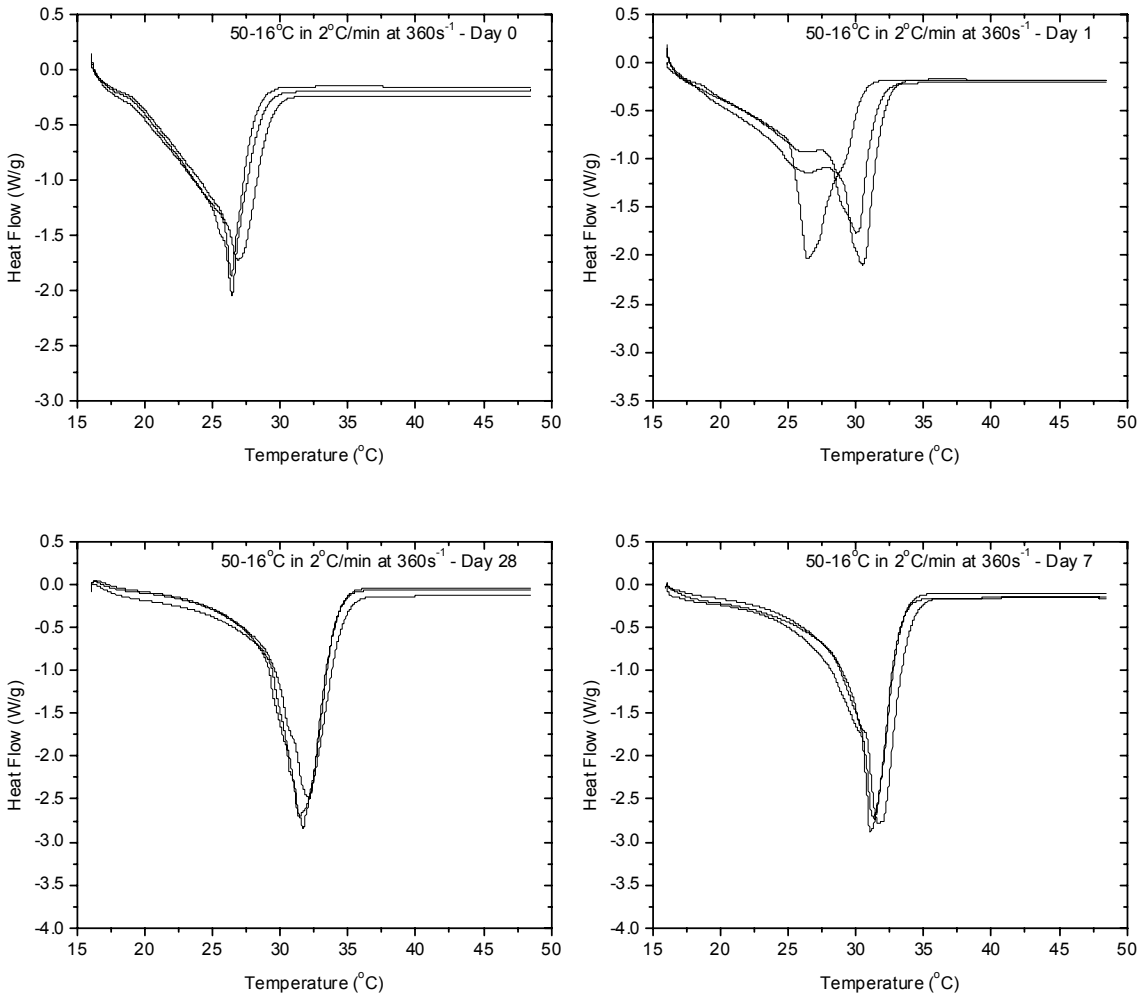

Figure 122: Heat flow curves of samples created by being cooled from 50 to 16°C at 2°C/min whilst shearing at a rate of $360s^{-1}$. The four graphs shown are sample repetitions carried out on day 0, day 1, day 7 and day 28.

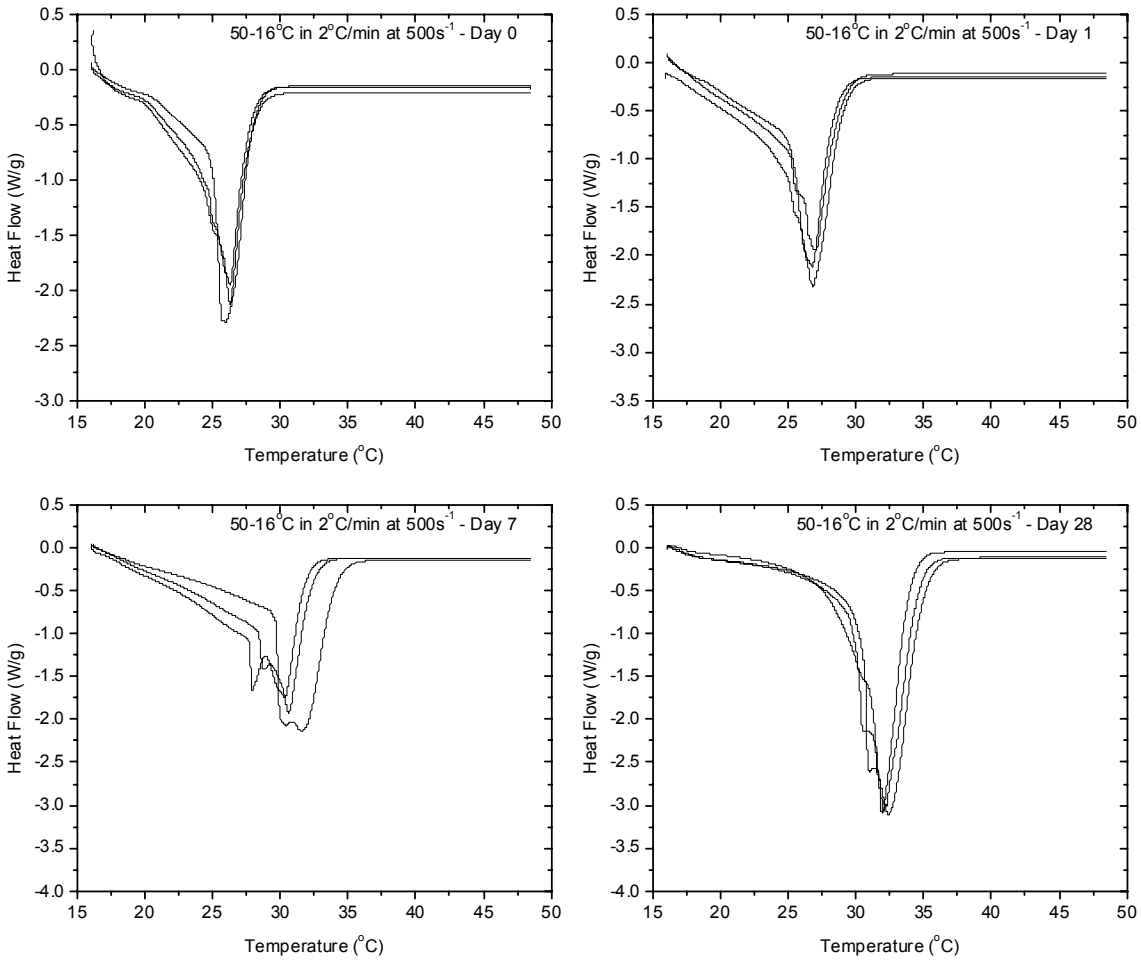

Figure 123: Heat flow curves of samples created by being cooled from 50 to 16°C at 2°C/min whilst shearing at a rate of $500s^{-1}$. The four graphs shown are sample repetitions carried out on day 0, day 1, day 7 and day 28.

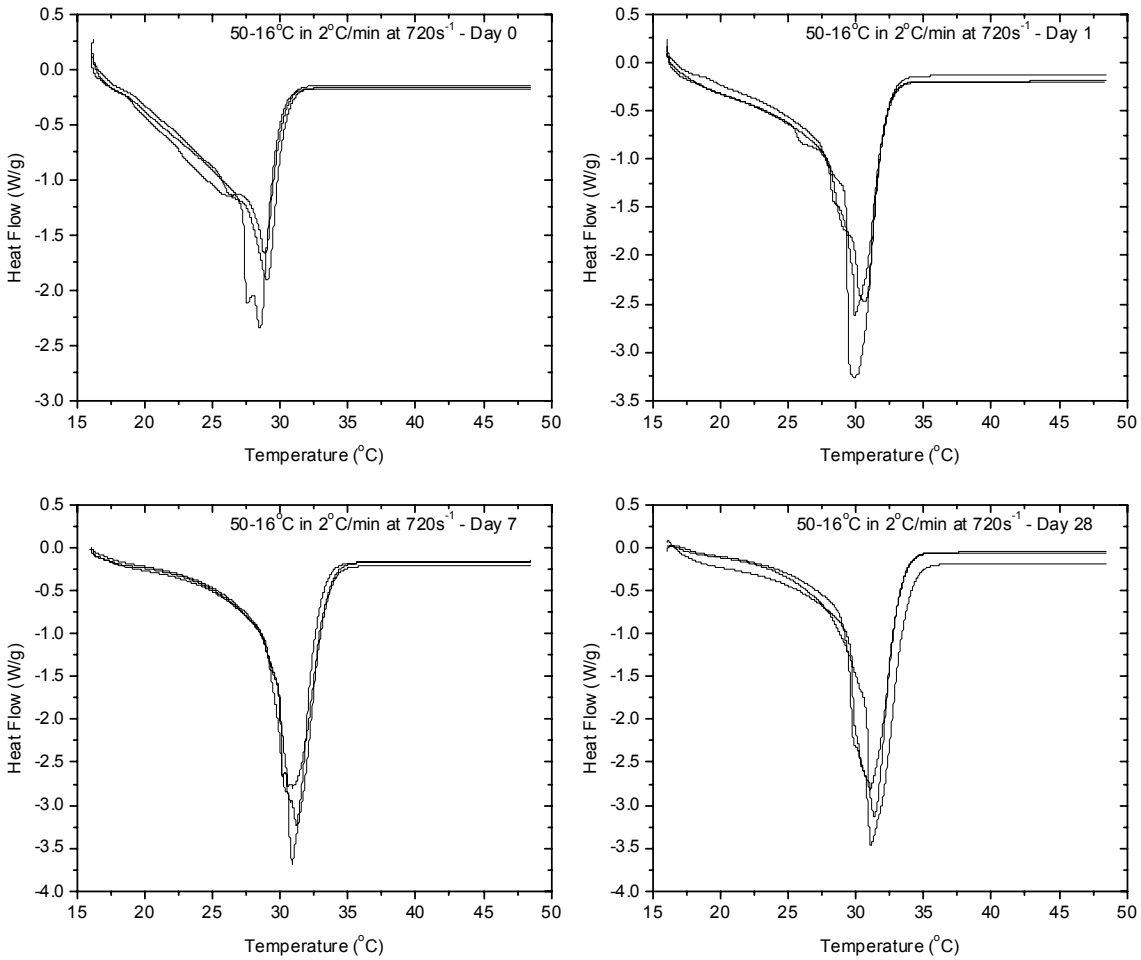

Figure 124: Heat flow curves of samples created by being cooled from 50 to 16°C at 2°C/min whilst shearing at a rate of $720s^{-1}$. The four graphs shown are sample repetitions carried out on day 0, day 1, day 7 and day 28.

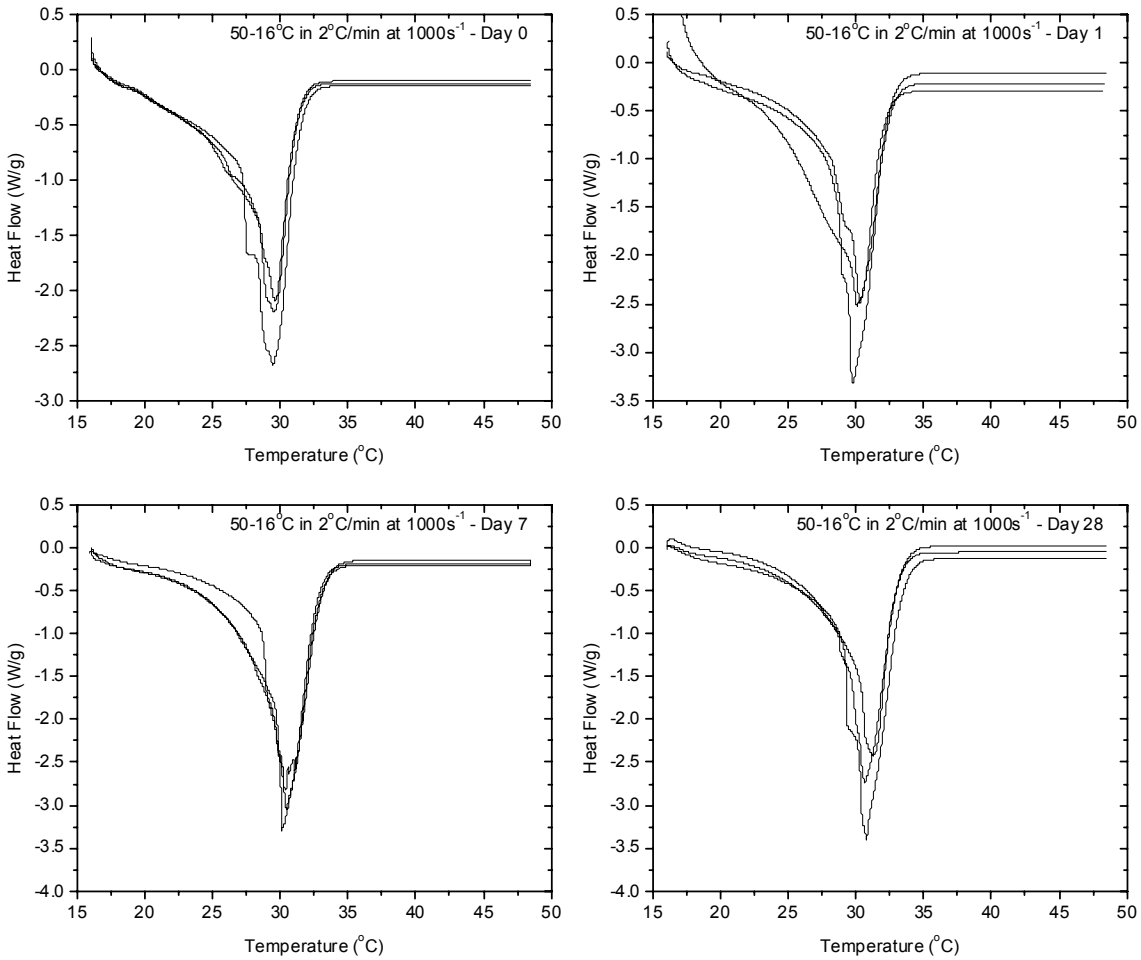

Figure 125: Heat flow curves of samples created by being cooled from 50 to 16°C at 2°C/min whilst shearing at a rate of $1000s^{-1}$. The four graphs shown are sample repetitions carried out on day 0, day 1, day 7 and day 28.

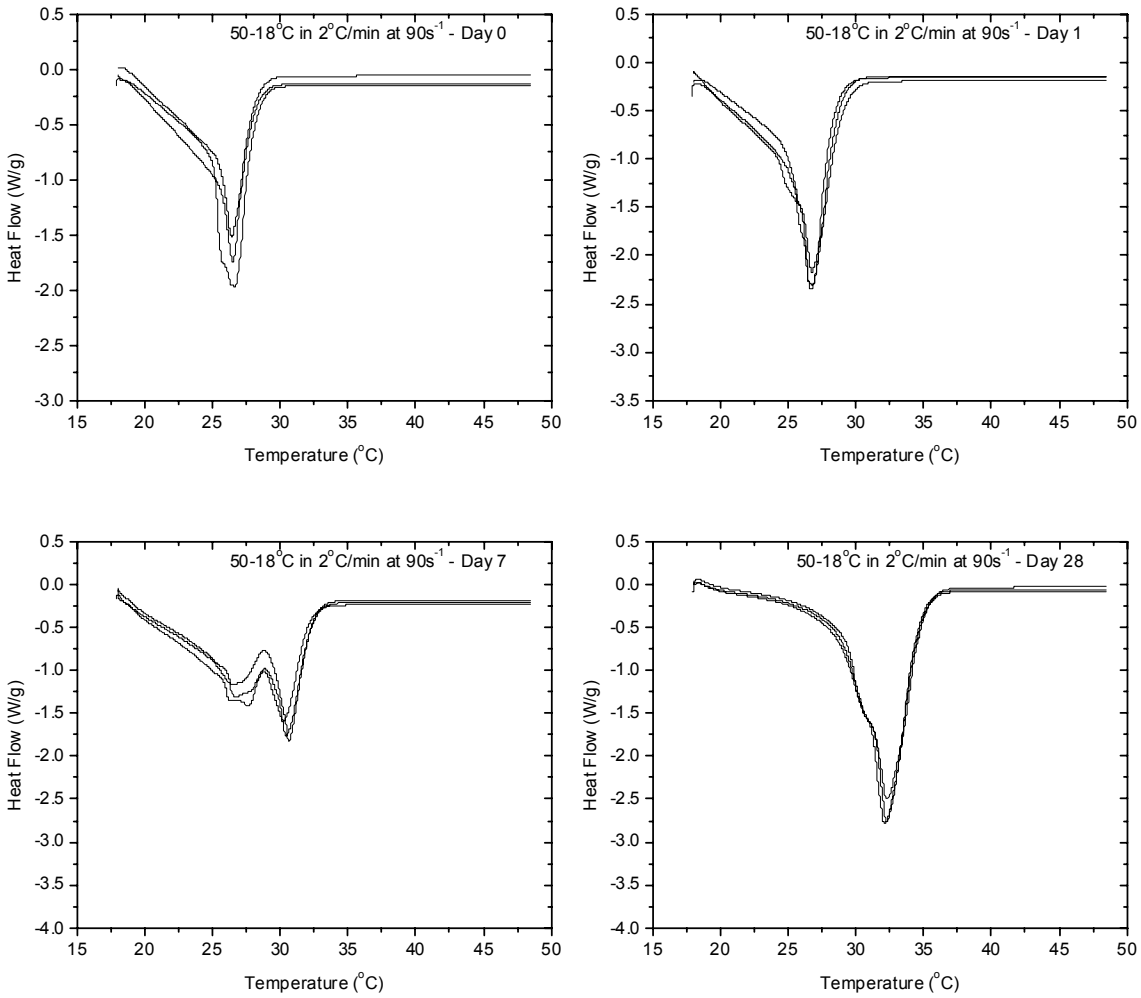

Figure 126: Heat flow curves of samples created by being cooled from 50 to 18°C at 2°C/min whilst shearing at a rate of $90s^{-1}$. The four graphs shown are sample repetitions carried out on day 0, day 1, day 7 and day 28.

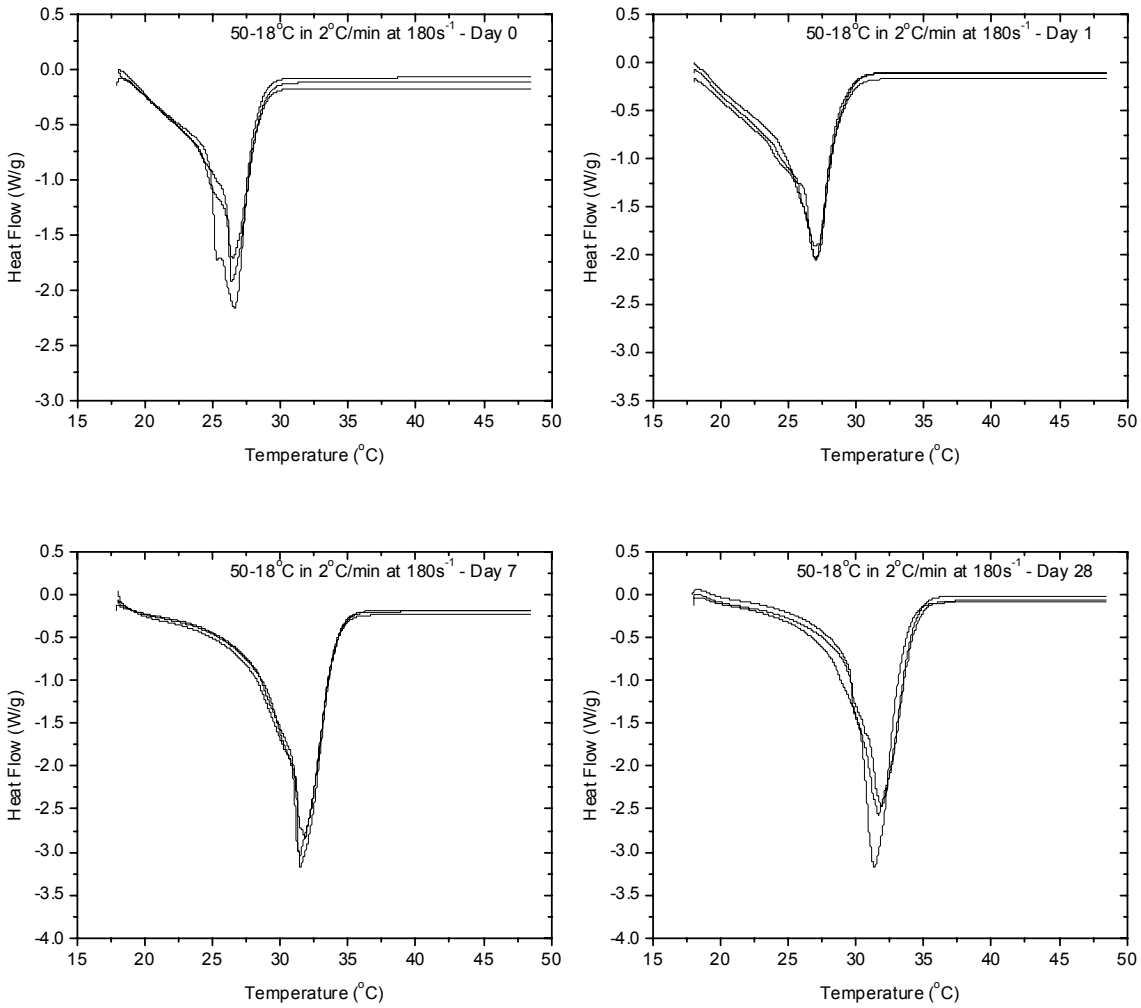

Figure 127: Heat flow curves of samples created by being cooled from 50 to 18°C at 2°C/min whilst shearing at a rate of $180s^{-1}$. The four graphs shown are sample repetitions carried out on day 0, day 1, day 7 and day 28.

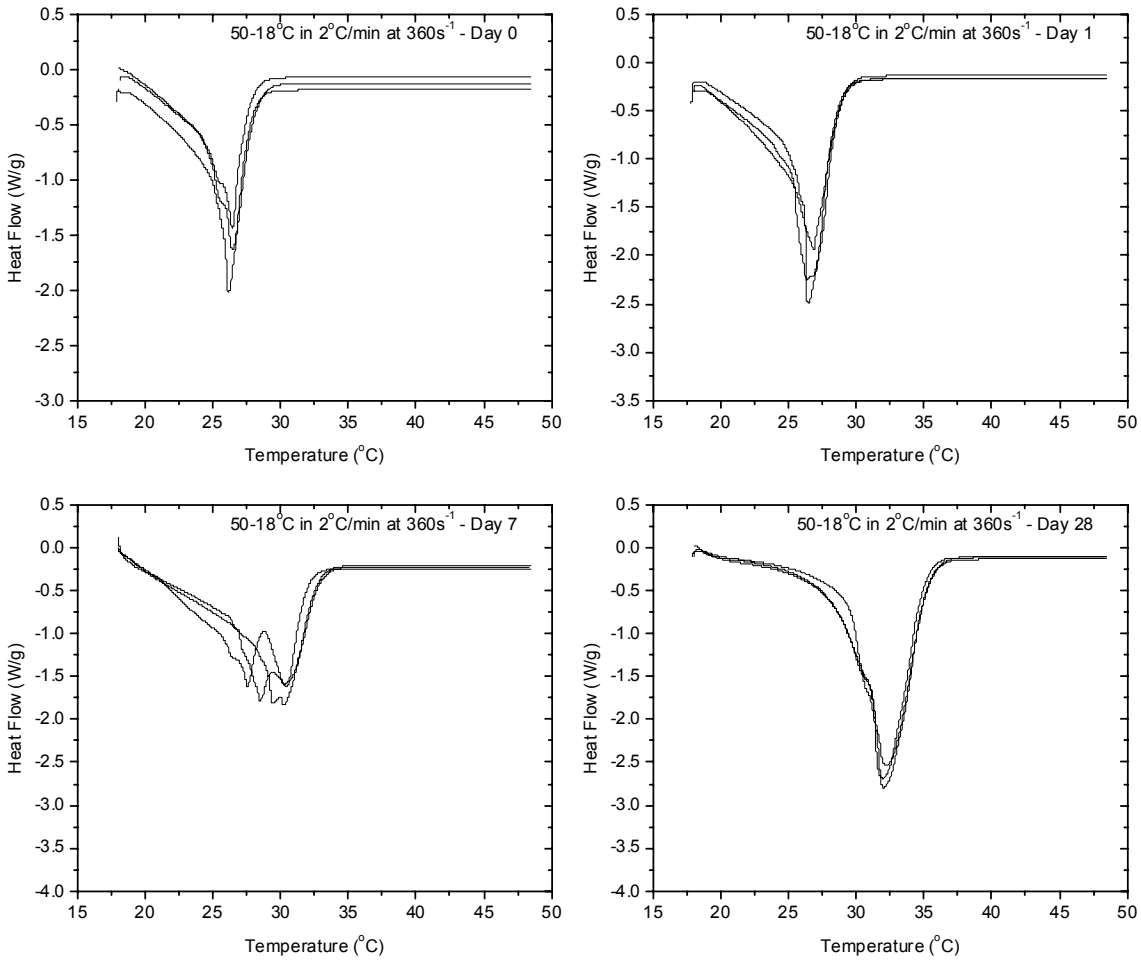

Figure 128: Heat flow curves of samples created by being cooled from 50 to 18°C at 2°C/min whilst shearing at a rate of $360s^{-1}$. The four graphs shown are sample repetitions carried out on day 0, day 1, day 7 and day 28.

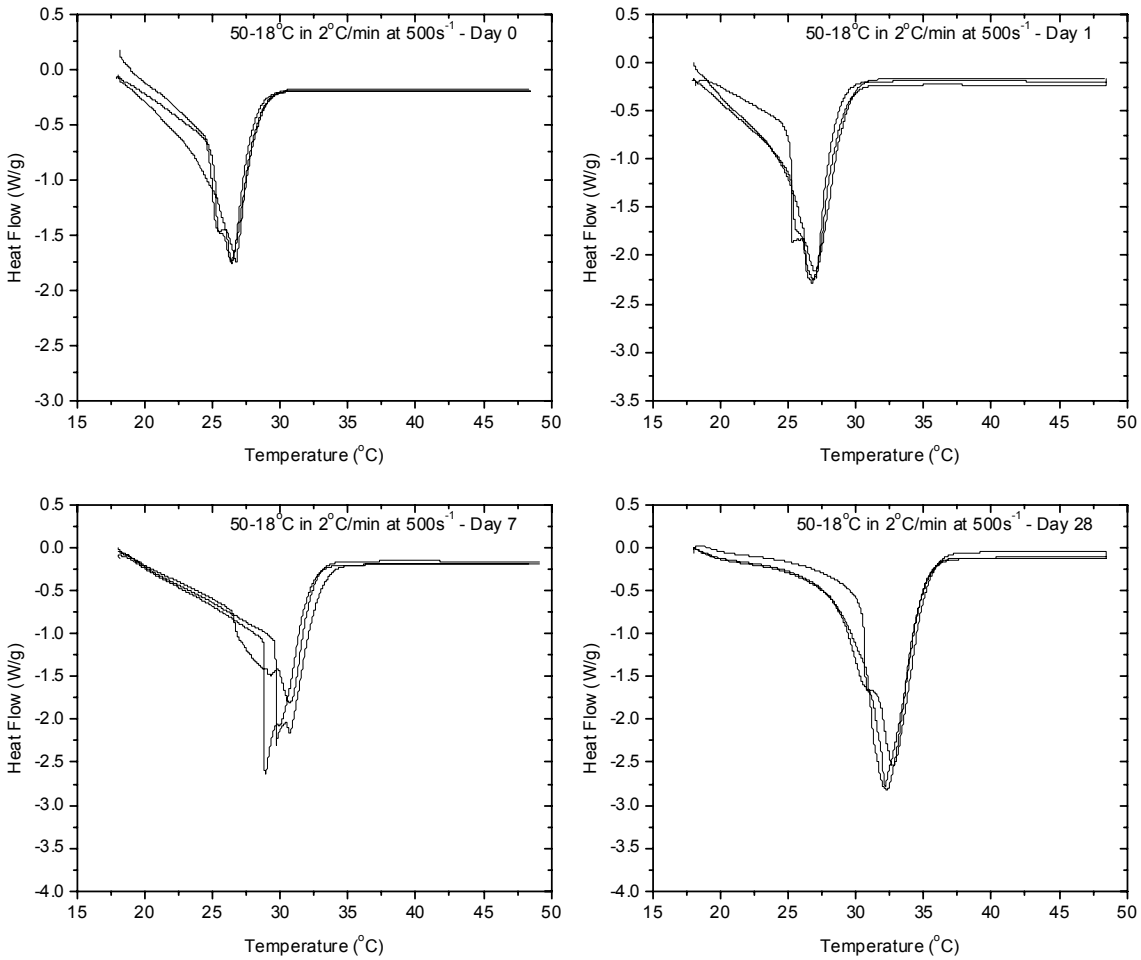

Figure 129: Heat flow curves of samples created by being cooled from 50 to 18°C at 2°C/min whilst shearing at a rate of $500s^{-1}$. The four graphs shown are sample repetitions carried out on day 0, day 1, day 7 and day 28.

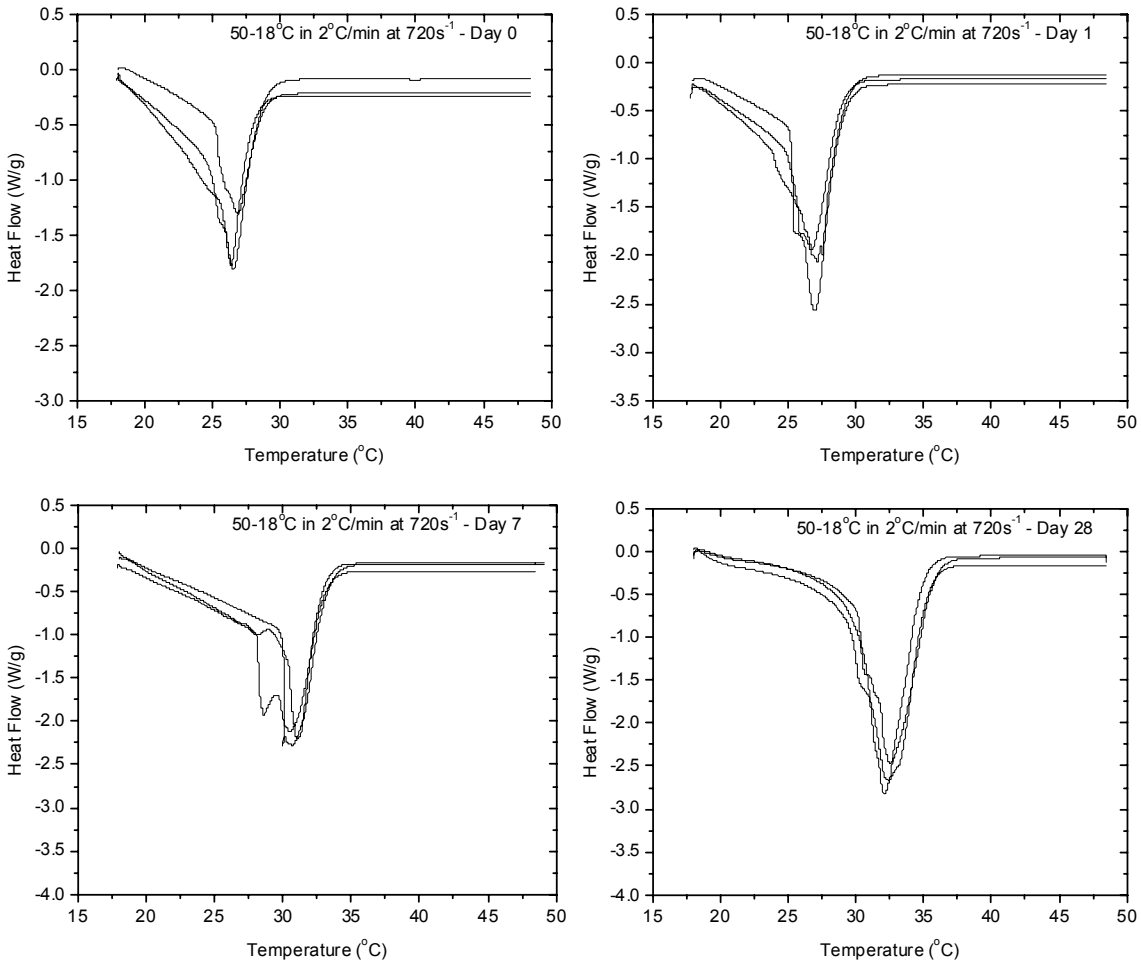

Figure 130: Heat flow curves of samples created by being cooled from 50 to 18°C at 2°C/min whilst shearing at a rate of $720s^{-1}$. The four graphs shown are sample repetitions carried out on day 0, day 1, day 7 and day 28.

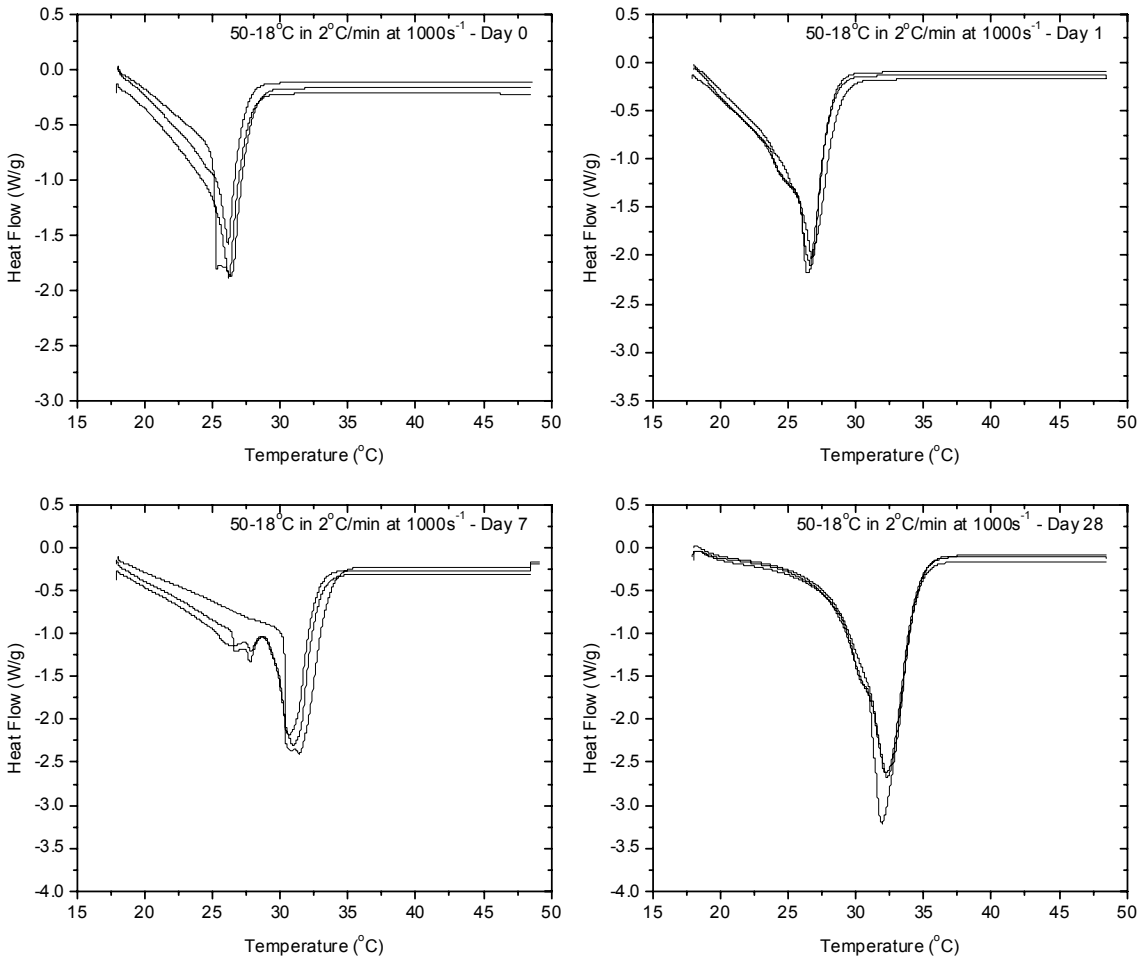

Figure 131: Heat flow curves of samples created by being cooled from 50 to 18°C at 2°C/min whilst shearing at a rate of $1000s^{-1}$. The four graphs shown are sample repetitions carried out on day 0, day 1, day 7 and day 28.

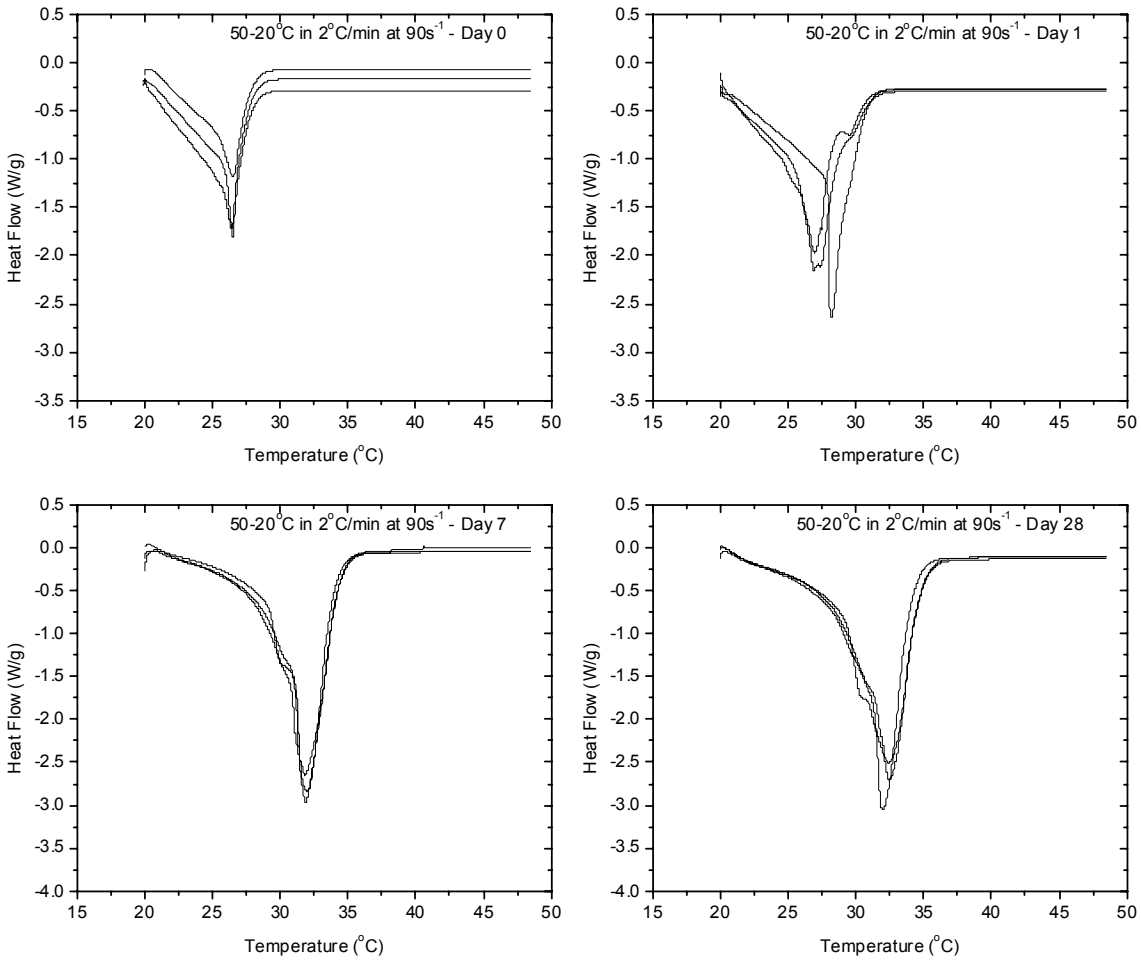

Figure 132: Heat flow curves of samples created by being cooled from 50 to 20°C at 2°C/min whilst shearing at a rate of $90s^{-1}$. The four graphs shown are sample repetitions carried out on day 0, day 1, day 7 and day 28.

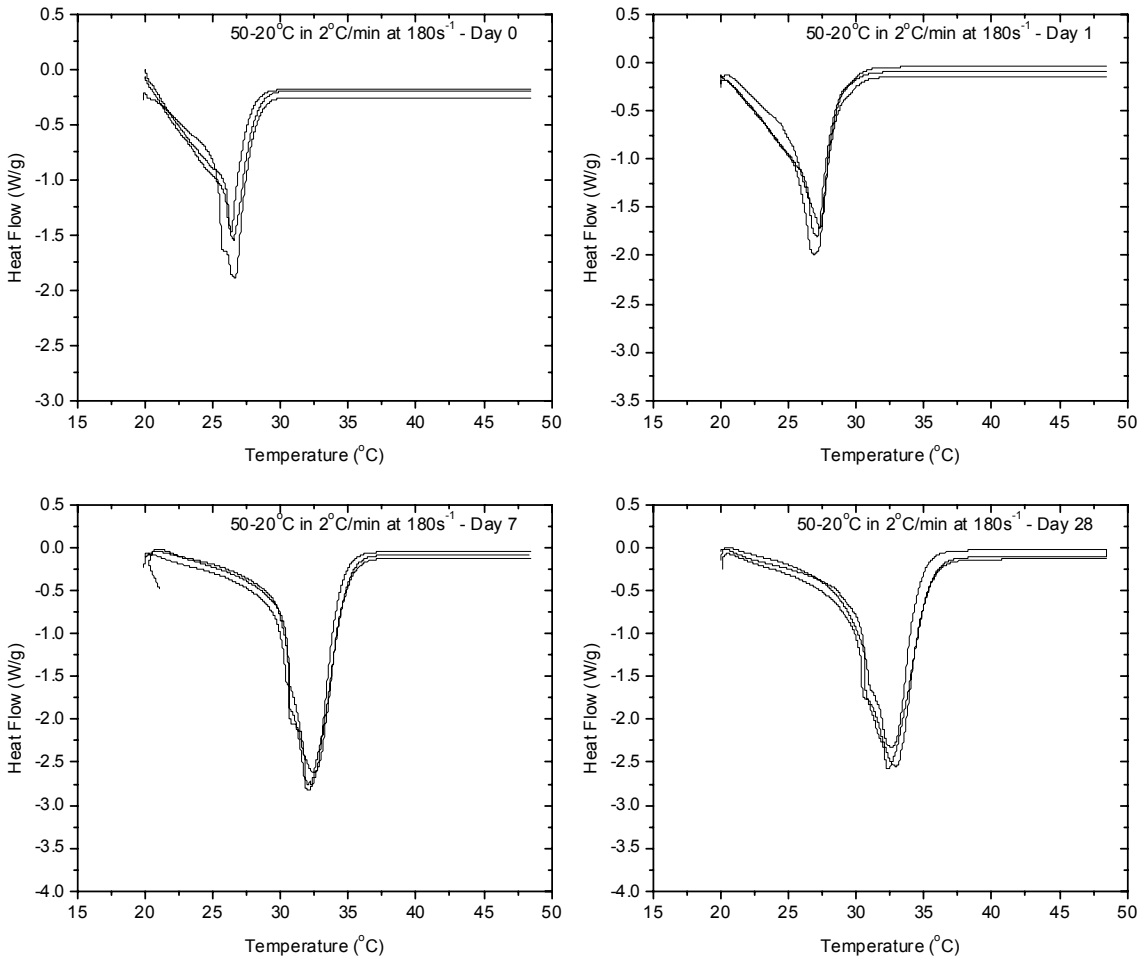

Figure 133: Heat flow curves of samples created by being cooled from 50 to 20°C at 2°C/min whilst shearing at a rate of $180s^{-1}$. The four graphs shown are sample repetitions carried out on day 0, day 1, day 7 and day 28.

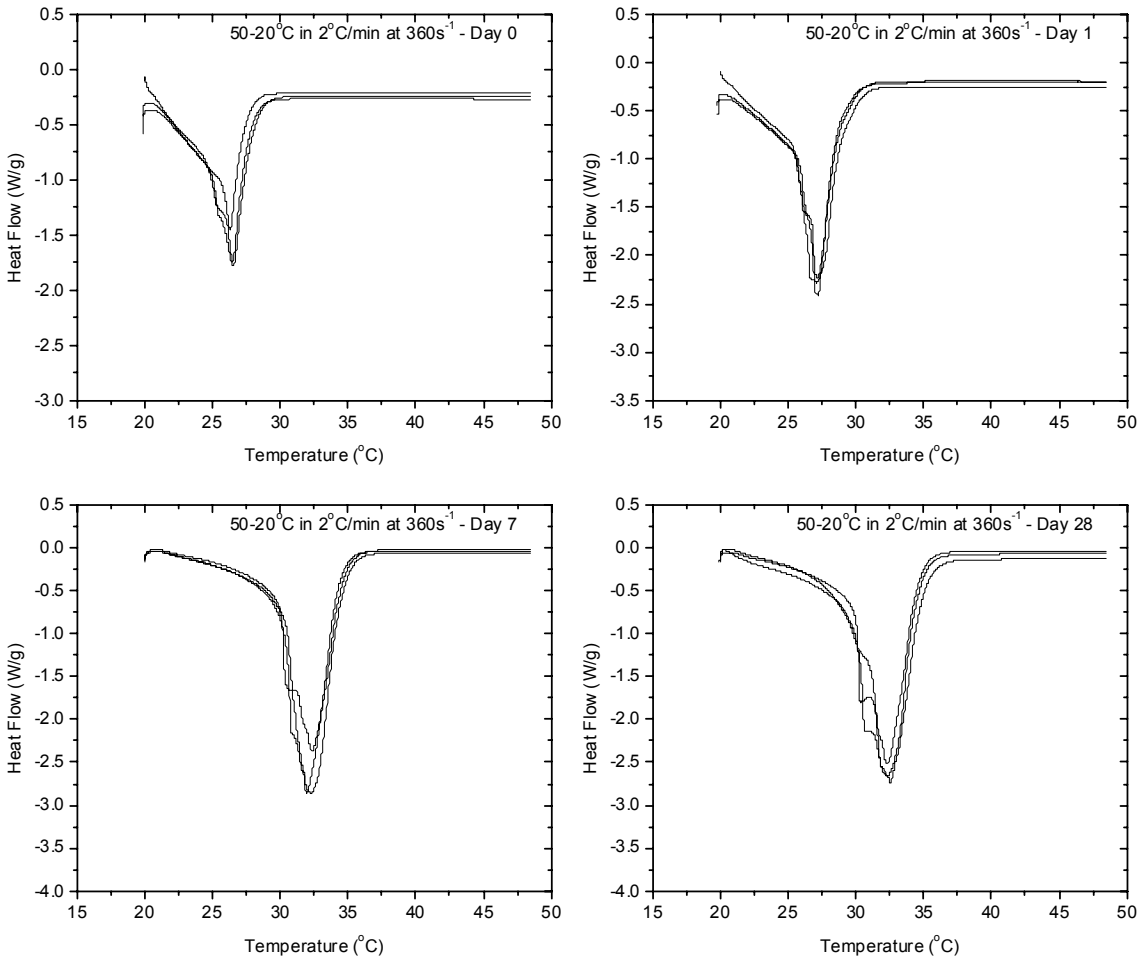

Figure 134: Heat flow curves of samples created by being cooled from 50 to 20°C at 2°C/min whilst shearing at a rate of $360s^{-1}$. The four graphs shown are sample repetitions carried out on day 0, day 1, day 7 and day 28.

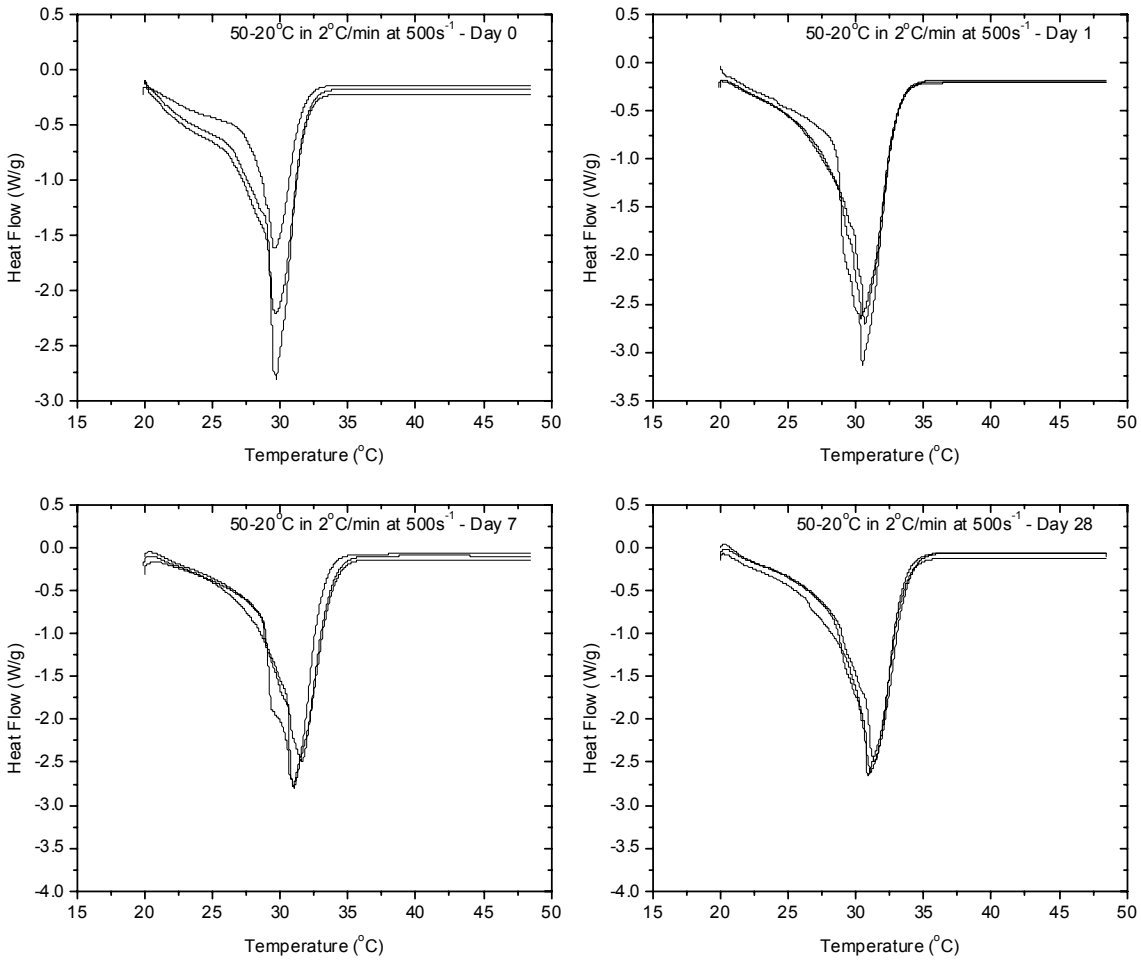

Figure 135: Heat flow curves of samples created by being cooled from 50 to 20°C at 2°C/min whilst shearing at a rate of $500s^{-1}$. The four graphs shown are sample repetitions carried out on day 0, day 1, day 7 and day 28.

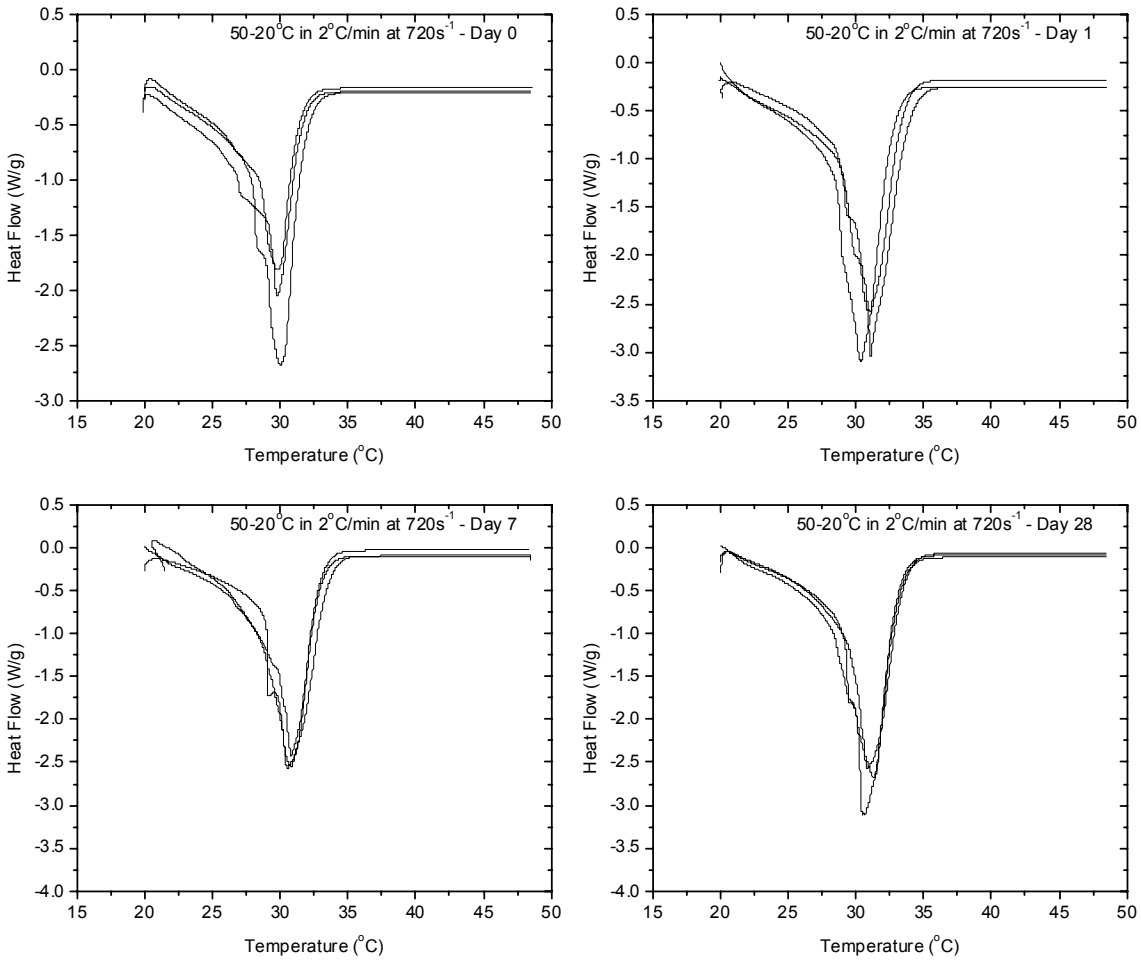

Figure 136: Heat flow curves of samples created by being cooled from 50 to 20°C at 2°C/min whilst shearing at a rate of $720s^{-1}$. The four graphs shown are sample repetitions carried out on day 0, day 1, day 7 and day 28.

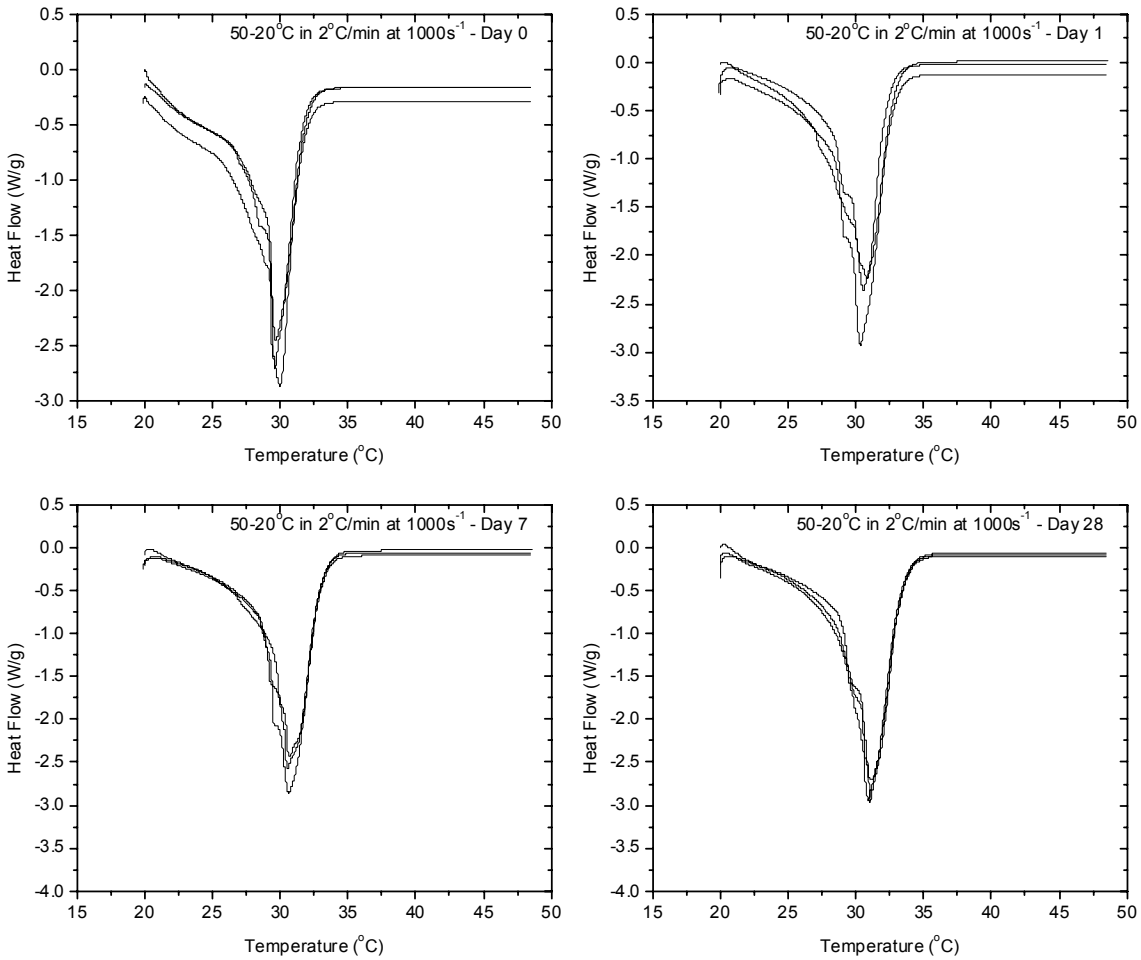

Figure 137: Heat flow curves of samples created by being cooled from 50 to 20°C at 2°C/min whilst shearing at a rate of $1000s^{-1}$. The four graphs shown are sample repetitions carried out on day 0, day 1, day 7 and day 28.

Appendix 5:

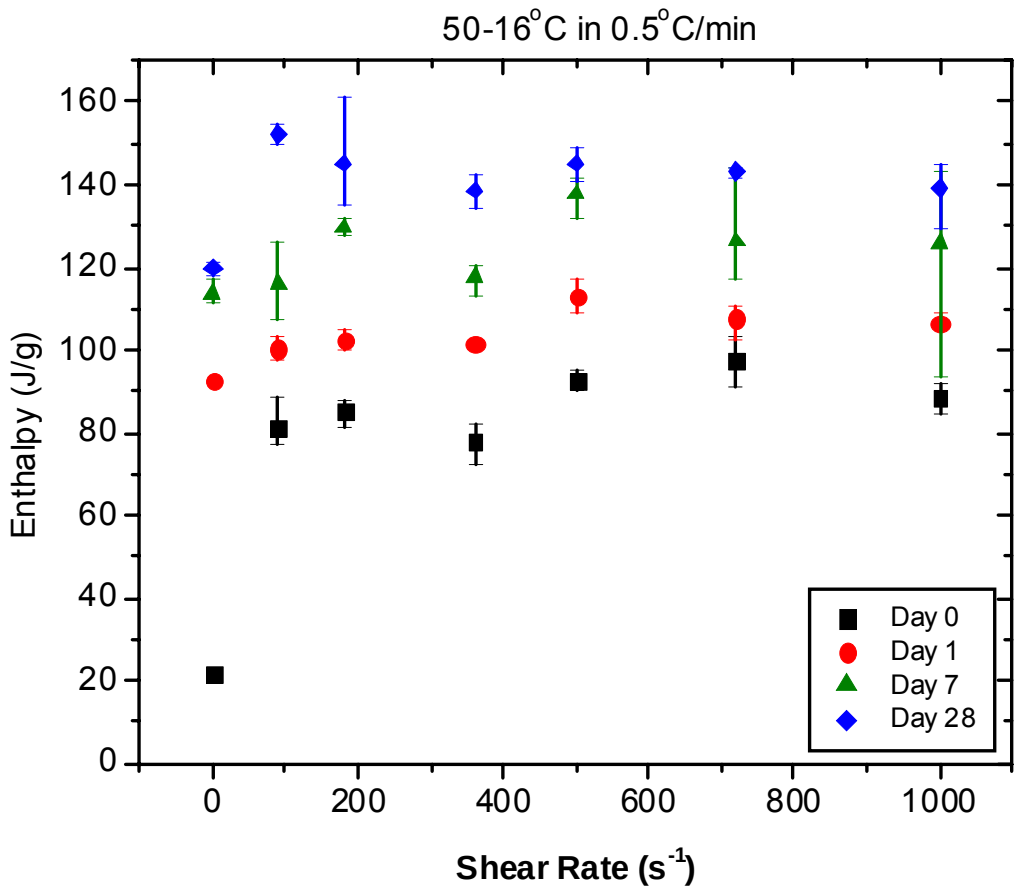

Figure 138: Graph showing enthalpy values extracted from DSC melting curves for a sample of cocoa butter created under shear rates of 0-1000s^{-1} whilst cooled from 50-16°C in 0.5°C/min

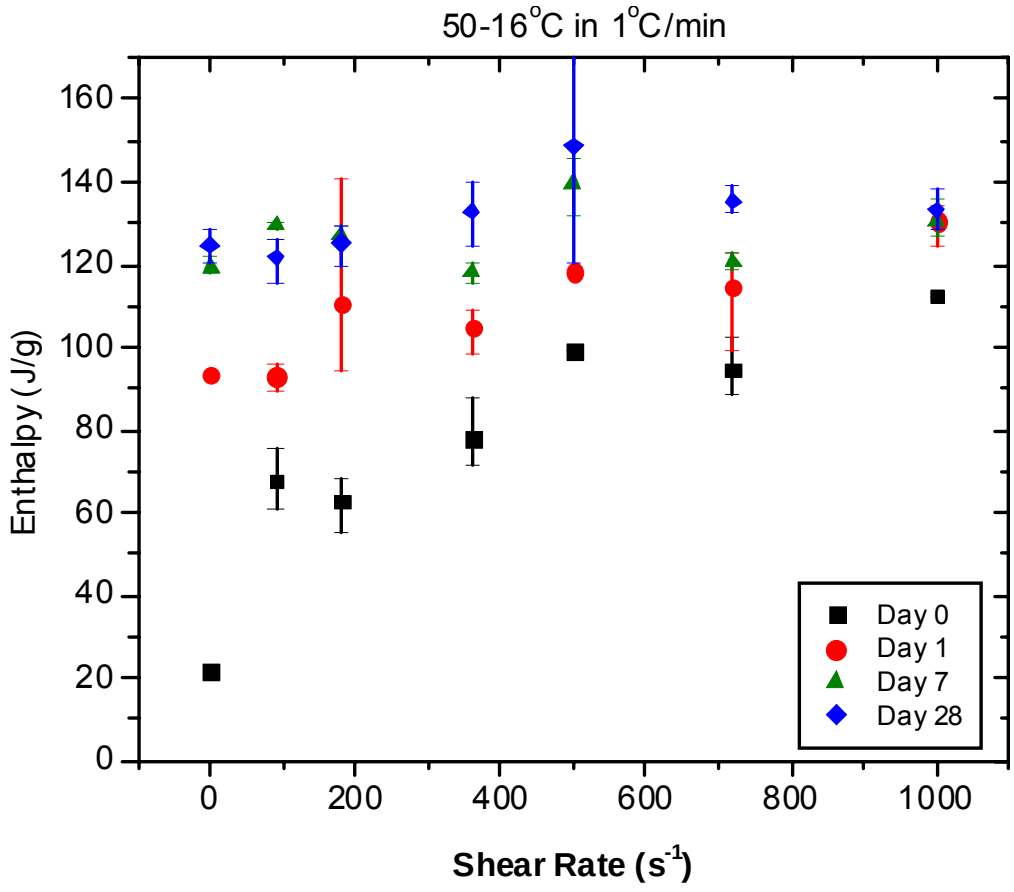

Figure 139: Graph showing enthalpy values extracted from DSC melting curves for a sample of cocoa butter created under shear rates of 0-1000s^{-1} whilst cooled from 50-16°C in 1°C/min

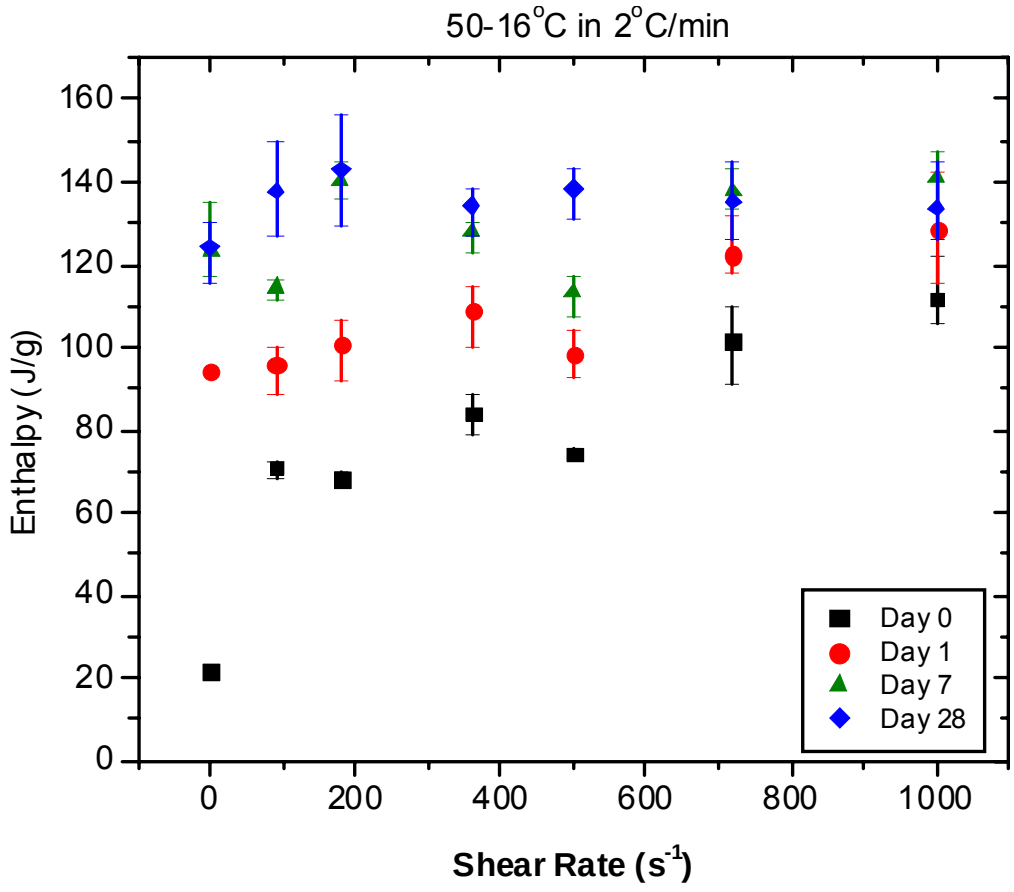

Figure 140: Graph showing enthalpy values extracted from DSC melting curves for a sample of cocoa butter created under shear rates of 0-1000s^{-1} whilst cooled from 50-16°C in 2°C/min

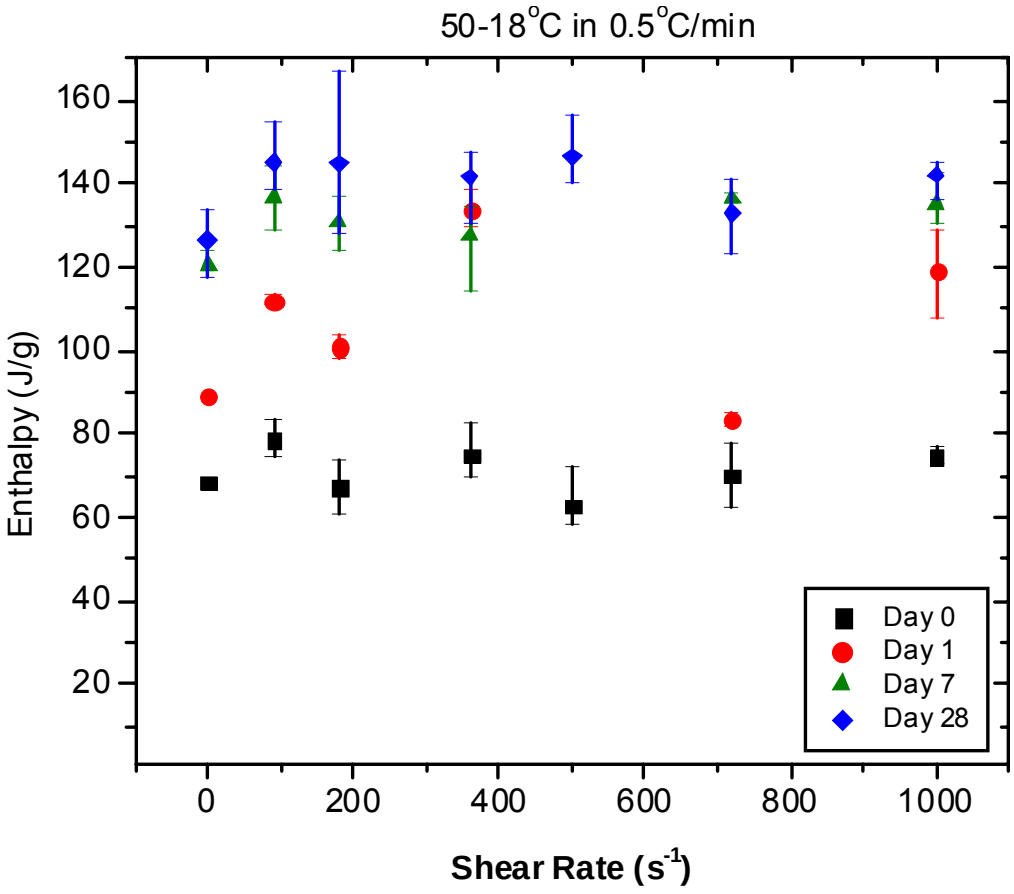

Figure 141: Graph showing enthalpy values extracted from DSC melting curves for a sample of cocoa butter created under shear rates of 0-1000s^{-1} whilst cooled from 50-18°C in 0.5°C/min

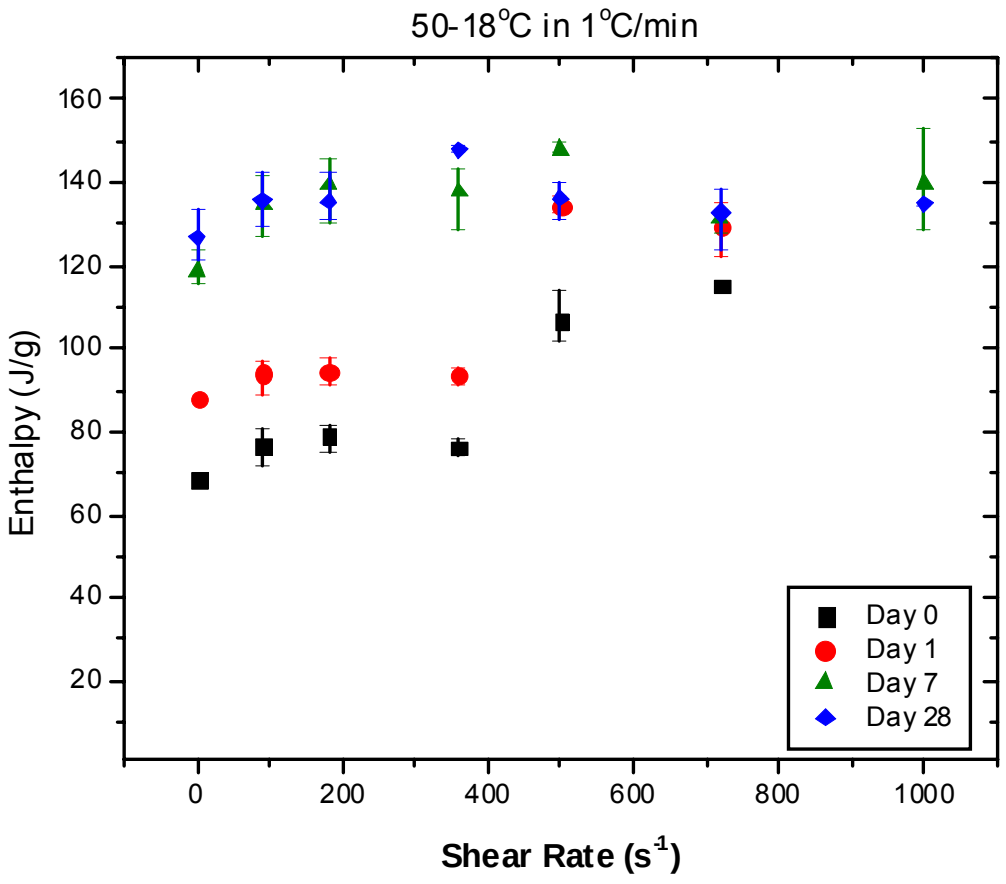

Figure 142: Graph showing enthalpy values extracted from DSC melting curves for a sample of cocoa butter created under shear rates of 0-1000s^{-1} whilst cooled from 50-18°C in 1°C/min

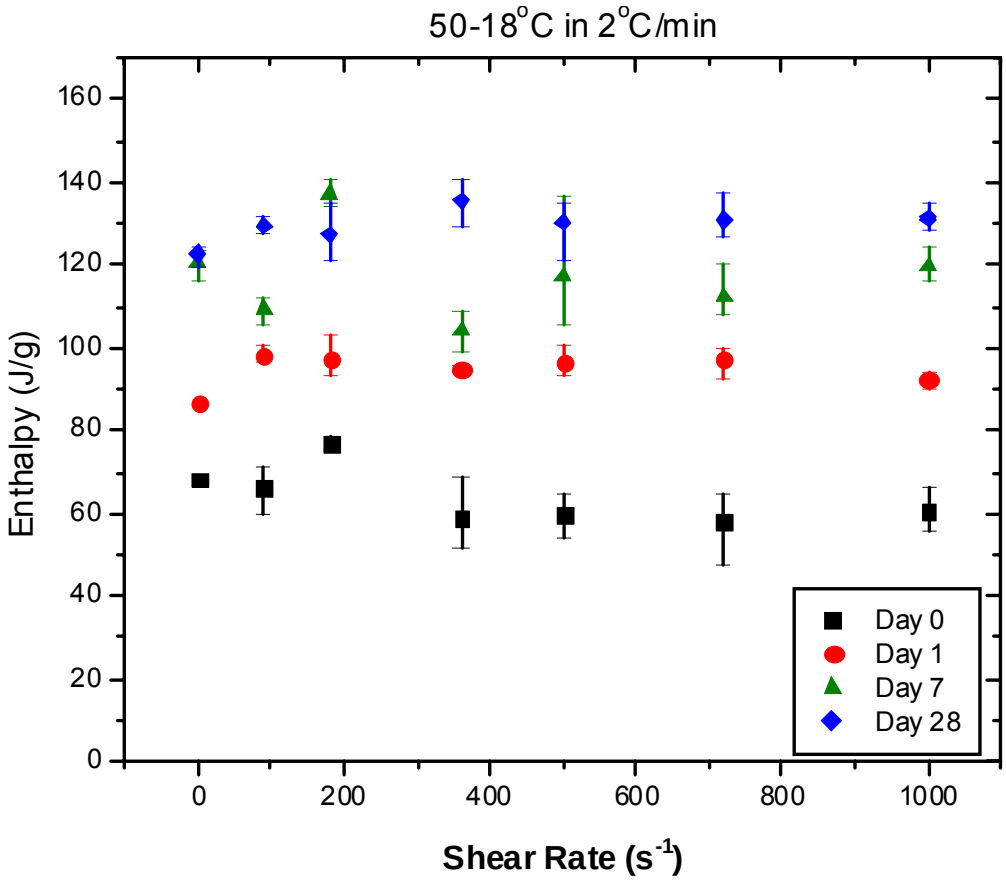

Figure 143: Graph showing enthalpy values extracted from DSC melting curves for a sample of cocoa butter created under shear rates of 0-1000s^{-1} whilst cooled from 50-18°C in 2°C/min

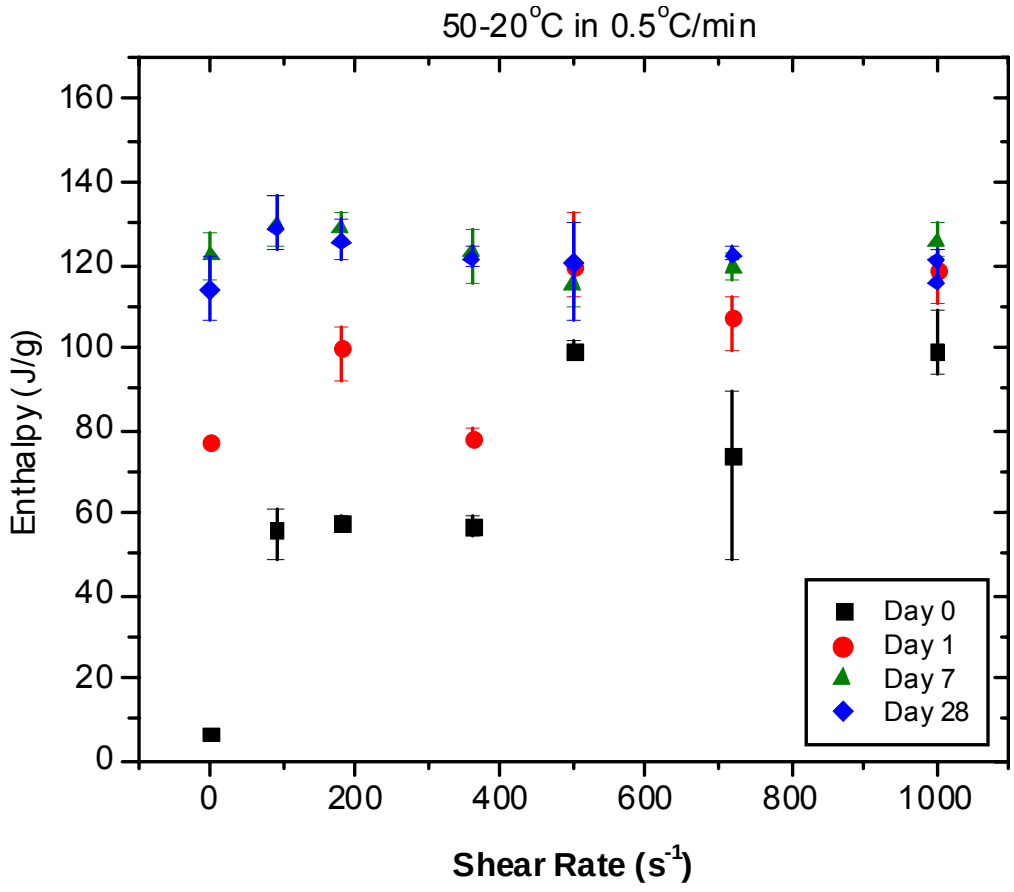

Figure 144: Graph showing enthalpy values extracted from DSC melting curves for a sample of cocoa butter created under shear rates of 0-1000s^{-1} whilst cooled from 50-20°C in 0.5°C/min

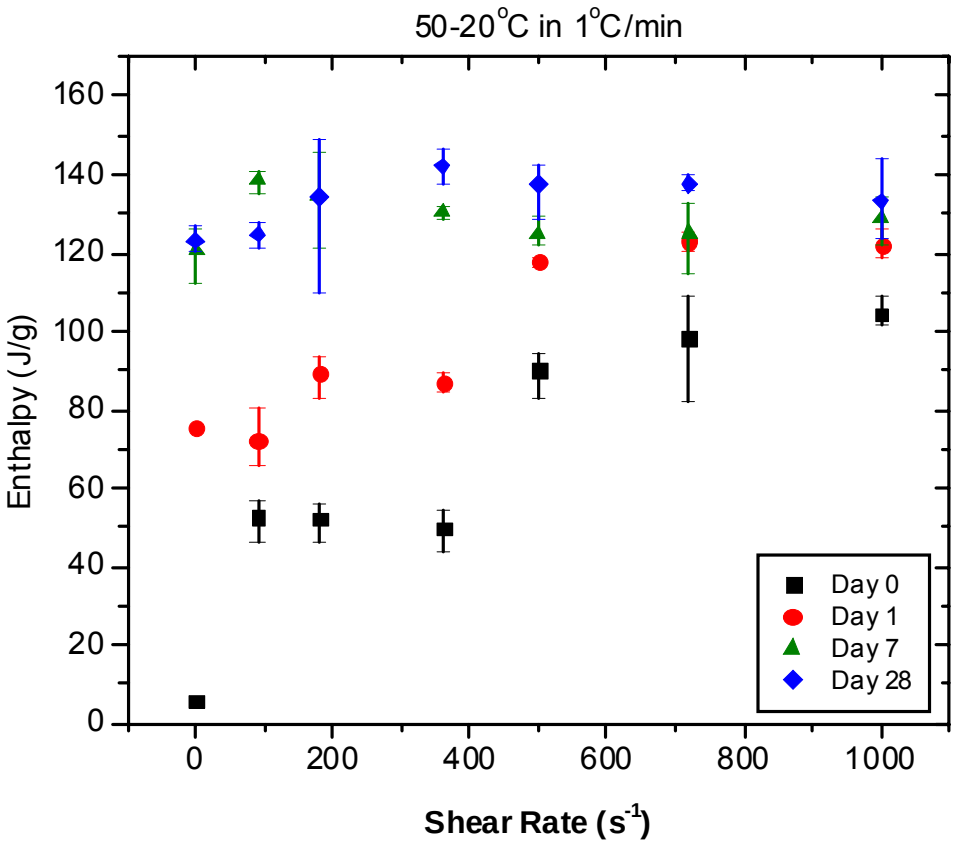

Figure 145: Graph showing enthalpy values extracted from DSC melting curves for a sample of cocoa butter created under shear rates of 0-1000s^{-1} whilst cooled from 50-20°C in 1°C/min

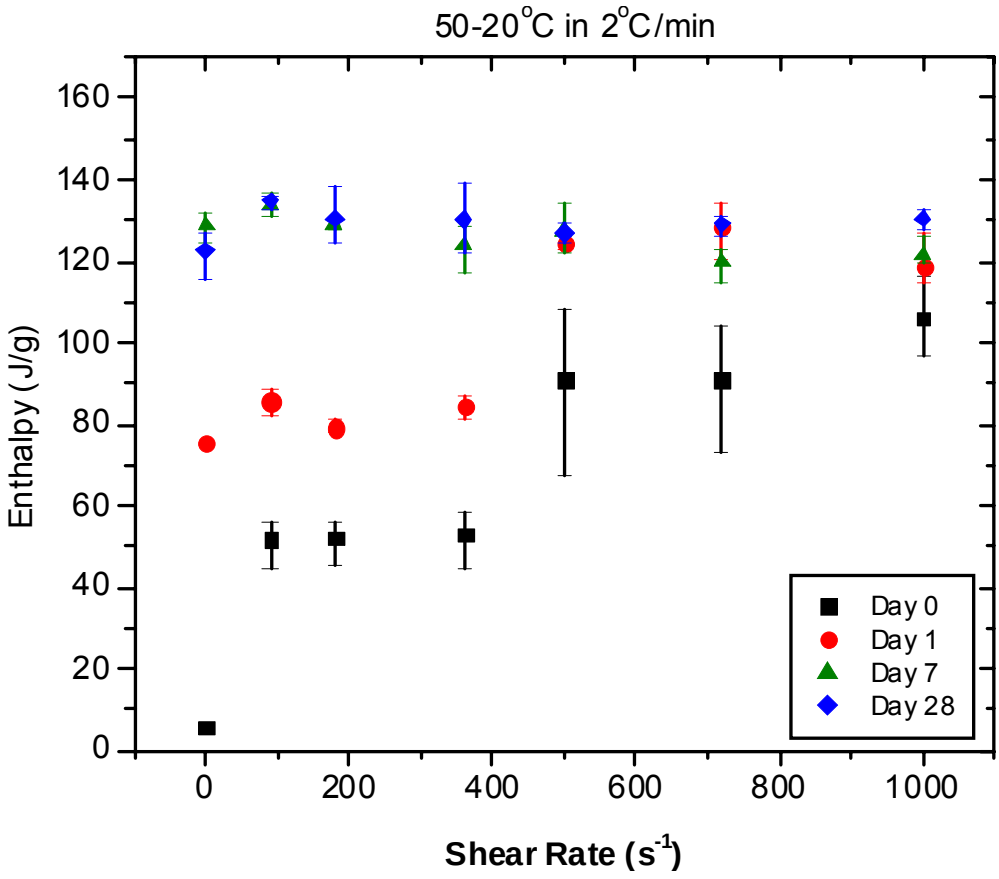

Figure 146: Graph showing enthalpy values extracted from DSC melting curves for a sample of cocoa butter created under shear rates of 0-1000s^{-1} whilst cooled from 50-20°C in 2°C/min

References

1. Guthrie, S.E. and S.H.J. Idziak, *Split rheometer Couette attachment to enable sample extraction.* Review of Scientific Instruments, 2005. **76**(2): p. 026110-1 - 026110-3.
2. Vaeck, S.V., *Die Polymorphie (Vielgestaltigkeit) einiger Naturfette.* International Chocolate Review, 1951. **6**: p. 100-113.
3. Giddey, C. and E. Clerc, *Polymorphism of Cocoa Butter and its Importance in the Chocolate Industry.* International Chocolate Review, 1961. **16**: p. 548-554.
4. Wille, R.L. and E.S. Lutton, *Polymorphism of Cocoa Butter.* Journal of the American Oil Chemists Society, 1966. **43**(8): p. 491-496.
5. Witzel, H. and K. Becker, *Crystalline Structure of Cocoa Butter.* Fette Seifen Anstrichmittel, 1969. **71**(6): p. 507-516.
6. Riiner, U., *Investigation of the Polymorphism of Fats and Oils by Temperature Programmed X-Ray Diffraction.* Lebensmittel-Wissenschaft & Technologie, 1970. **3**(6): p. 101-106.
7. Chapman, G.M., E.E. Akehurst, and W.B. Wright, *Cocoa Butter and Confectionery Fats - Studies Using Programmed Temperature X-Ray Diffraction and Differential Scanning Calorimetry.* Journal of the American Oil Chemists Society, 1971. **48**(12): p. 824-830.
8. Beckett, S.T., *The Science of Chocolate*. 2000, Cambridge, UK: Royal Society of Chemistry.
9. MacMillan, S.D., et al., *In situ small angle x-ray scattering (SAXS) studies of polymorphism with the associated crystallization of cocoa butter fat using shearing conditions.* Crystal Growth & Design, 2002. **2**: p. 221-226.
10. Mazzanti, G., et al., *Orientation and phase transitions of fat crystals under shear.* Crystal Growth & Design, 2003. **3**(5): p. 721-725.
11. Mazzanti, G., et al., *Novel shear-induced phases in cocoa butter.* Crystal Growth & Design, 2004. **4**(3): p. 409-411.
12. Stapley, A.G.F., H. Tewkesbury, and P.J. Fryer, *The effects of shear and temperature history on the crystallization of chocolate.* Journal of the American Oil Chemists Society, 1999. **76**(6): p. 677-685.
13. Ziegleder, G., *Verbessertes Kristallisationsverhalten von Kakaobutter unter dem Einfluss eines Schergefalles.* ZFL, 1985. **6**: p. 412-416.
14. Bolliger, S., et al., *Comparison of precrystallization of chocolate.* Journal of Food Engineering, 1998. **35**(3): p. 281-297.
15. Bolliger, S., Y.T. Zeng, and E.J. Windhab, *In-line measurement of tempered cocoa butter and chocolate by means of near-infrared spectroscopy.* Journal of the American Oil Chemists Society, 1999. **76**(6): p. 659-667.
16. Toro-Vazquez, J.F., et al., *Rheometry and polymorphism of cocoa butter during crystallization under static and stirring conditions.* Journal of the American Oil Chemists Society, 2004. **81**(2): p. 195-202.
17. Dhonsi, D. and A.G.F. Stapley, *The effect of shear rate, temperature, sugar and emulsifier on the tempering of cocoa butter.* Journal of Food Engineering, 2006. **77**: p. 936-942.

18. Sonwai, S. and M.R. Mackley, *The Effect of Shear on the Crystallization of Cocoa Butter.* JAOCS, 2006. **83**(7): p. 583-596.
19. Welmans, P., Pharm. Ztg., 1900. **45**: p. 959.
20. Vaeck, S.V., *Cocoa Butter and Fat Bloom.* Manufacturing Confectioner, 1960. **40**: p. 35-46, 71-74.
21. Duffy, P., *On certain Isomeric Transformations of Fats.* Journal of the Chemical Society, 1852. **5**(3): p. 197-210.
22. Sato, K., *Crystallization behavior of fats and lipids - a review.* Chemical Engineering Science, 2001. **56**: p. 2255-2265.
23. van Mechelen, J.B., R. Peschar, and H. Schenk, *Structure of mono-unsaturated tracylglycerols. II. The β_2 polymorph.* Acta Crystallographica Section B, 2006. **62**(6): p. 1131-1138.
24. van Mechelen, J.B., R. Peschar, and H. Schenk, *Structures of mono-unsaturated triacylglycerols. I. The β_1 polymorph.* Acta Crystallographica Section B, 2006. **62**(6): p. 1121-1130.
25. Mazzanti, G., *X-Ray Diffraction Study on the Crystallization of Fats Under Shear*, in *Food Science*. 2004, University of Guelph: Guelph. p. 233.
26. Huyghebaert, A. and H. Hendrickx, *Polymorphism of Cocoa Butter, shown by Differential Scanning Calorimetry.* Lebensmittel-Wissenschaft & Technologie, 1971. **79**: p. 59-63.
27. Lovegren, N.V., M.S. Gray, and R.O. Feuge, *Polymorphic Changes in Mixtures of Confectionery Fats.* Journal of the American Oil Chemists Society, 1976. **53**(2): p. 83-88.
28. Hicklin, J.D., G.G. Jewell, and J.F. Heathcock, *Combining Microscopy and Physical Techniques in the Study of Cocoa Butter Polymorphs and Vegetable Fat Blends.* Food Microstructure, 1985. **4**: p. 241-248.
29. Loisel, C., et al., *Phase transitions and polymorphism of cocoa butter.* Journal of the American Oil Chemists Society, 1998. **75**(4): p. 425-439.
30. Merken, G.V. and S.V. Vaeck, *A Study of the polymorphism of cocoa butter by means of DSC calorimetry.* Lebensmittel-Wissenschaft & Technologie, 1980. **13**: p. 314-317.
31. Schlichter-Aronhime, J. and N. Garti, *Solidification and Polymorphism in Cocoa Butter and the Blooming Problem*, in *Crystallization and Polymorphism of Fats and Fatty Acids*, K. Sato, Editor. 1988, Marcel Dekker, Inc.: New York. p. 363-393.
32. Schlichter-Aronhime, J., S. Sarig, and N. Garti, *Reconsideration of Polymorphic Transformations in Cocoa Butter Using the DSC.* Journal of the American Oil Chemists Society, 1988. **65**(7): p. 1140-1143.
33. van Langevelde, A., et al., *Cocoa-butter long spacings and the memory effect.* Journal of the American Oil Chemists Society, 2001. **78**(9): p. 911-918.
34. van Malssen, K., et al., *Phase behavior and extended phase scheme of static cocoa butter investigated with real-time X-ray powder diffraction.* Journal of the American Oil Chemists Society, 1999. **76**(6): p. 669-676.
35. van Malssen, K.F., et al., *Real-time X-ray powder diffraction investigations on cocoa butter. III. Direct $\beta-$ crystallization of cocoa butter: Occurence of a*

memory effect. Journal of the American Oil Chemists Society, 1996. **73**: p. 1225-1230.
36. van Malssen, K.F., R. Peschar, and H. Schenk, *Real-time X-ray powder diffraction investigations on cocoa butter. I. Temperature-dependent crystallization behavior.* Journal of the American Oil Chemists Society, 1996. **73**: p. 1209-1251.
37. Davis, T.R. and P.S. Dimick, *Isolation and Thermal Characterization of High-Melting Seed Crystals Formed During Cocoa Butter Solidification.* Journal of the American Oil Chemists Society, 1989. **66**(10): p. 1488-1493.
38. Merken, G.V., S.V. Vaeck, and D. Dewulf, *Determination of the Technological Properties of Cocoa Butter by Means of Differential Scanning Calorimetry.* Lebensmittel-Wissenschaft & Technologie, 1982. **15**(4): p. 195-198.
39. Narine, S.S. and A.G. Marangoni, *Fractal Nature of Fat Crystal Networks.* Physical Review E, 1999. **59**(2): p. 1908-1920.
40. Spigno, G., C. Pagella, and D.M. De Faveri, *DSC characterisation of cocoa butter polymorphs.* Italian Journal of Food Science, 2001. **13**(3): p. 275-284.
41. Marangoni, A.G. and S.E. McGauley, *Relationship between crystallization behavior and structure in cocoa butter.* Crystal Growth & Design, 2003. **3**(1): p. 95-108.
42. Chaiseri, S. and P.S. Dimick, *Dynamic Crystallization of Cocoa Butter. II. Morphological, Thermal, and Chemical Characteristics During Crystal Growth.* Journal of the American Oil Chemists Society, 1995. **72**(12): p. 1497-1504.
43. Cebula, D.J. and G. Ziegleder, *Studies of Bloom Formation Using X-Ray-Diffraction from Chocolates after Long-Term Storage.* Fett Wissenschaft Technologie-Fat Science Technology, 1993. **95**(9): p. 340-343.
44. Marangoni, A. and S.E. McGauley, *Relationship between Crystallization Behavior and Structure in Cocoa Butter.* Crystal Growth & Design, 2003. **3**(1): p. 95-108.
45. van Langevelde, A., et al., *Effect of temperature on recrystallization behavior of cocoa butter.* Journal of the American Oil Chemists Society, 2001. **78**(9): p. 919-925.
46. van Gelder, R.N.M.R., et al., *Crystallization and Polymorphism in Cocoa Butter Fat: In-situ Studies Using Synchrotron Radiation X-Ray Diffraction*, in *Crystal Growth of Organic Materials*, P. Meenan, Editor. 1996, American Chemical Society: Washington, DC. p. 209-215.
47. Manning, D.M. and P.S. Dimick, *Crystal Morphology of Cocoa Butter.* Food Microstructure, 1985. **4**: p. 249-265.
48. Forsterling, G., et al., *New Understandings about the Crystal Structure of Cocoa Butter.* Fette Seifen Anstrichmittel, 1981. **83**(7): p. 249-254.
49. Bricknell, J. and R.W. Hartel, *Relation of Fat Bloom in Chocolate to Polymorphic Transition of Cocoa Butter.* Journal of the American Oil Chemists Society, 1998. **75**(11): p. 1609-1615.
50. Adenier, H., et al., *Le blanchiment gras I. Observations et commentaires.* Chocolaterie Confiserie de France, 1975. **315**: p. 7-14.

51. Schlichter-Aronhime, J., N. Garti, and S. Sarig, *The Bleaching of Chocolate Relating to Polymorphism of Cocoa Butter.* Industrie alimentari, 1984. **23**(11): p. 871-877.
52. Chaiseri, S. and P.S. Dimick, *Dynamic crystallization of cocoa butter .1. Characterization of simple lipids in rapid- and slow-nucleating cocoa butters and their seed crystals.* Journal of the American Oil Chemists Society, 1995. **72**(12): p. 1491-1986.
53. Savage, C.M. and P.S. Dimick, *Influence of Phospholipids During Crystallization of Hard and Soft Cocoa Butters.* The Manufacturing Confectioner, 1995. **75**: p. 127-132.
54. Brunello, N., S.E. McGauley, and A. Marangoni, *Mechanical Properties of cocoa butter in relation to its crystallization behavior and microstructure.* Lebensmittel-Wissenschaft & Technologie, 2003. **36**: p. 525-532.
55. Walter, P. and P. Cornillon, *Influence of Thermal Conditions and Presence of Additives on Fat Bloom in Chocolate.* Journal of the American Oil Chemists Society, 2001. **78**(9): p. 927-932.
56. Keller, G., et al., *Investigation of the complex thermal behavior of fats - Combined DSC and X-ray diffraction techniques.* Journal of Thermal Analysis, 1996. **47**(5): p. 1545-1565.
57. Arruda, D.H. and P.S. Dimick, *Phospholipid Composition of Lipid Seed Crystal Isolates from Ivory Coast Cocoa Butter.* Journal of the American Oil Chemists Society, 1991. **68**(6): p. 385-390.
58. Hachiya, I., T. Koyano, and K. Sato, *Seeding Effects on Crystallization Behavior of Cocoa Butter.* Agricultural and Biological Chemistry, 1989. **53**(2): p. 327-332.
59. Hindle, S.A., M.J.W. Povey, and K.W. Smith, *Characterizing cocoa-butter seed crystals by the oil-in-water emulsion crystallization method.* Journal of the American Oil Chemists Society, 2002. **79**(10): p. 993-1002.
60. Koyano, T., I. Hachiya, and K. Sato, *Fat Polymorphism and Crystal Seeding Effects on Fat Bloom Stability of Dark Chocolate.* Food Structure, 1990. **9**(3): p. 231-240.
61. Davis, T.R. and P.S. Dimick, *Lipid-Composition of High-Melting Seed Crystals Formed During Cocoa Butter Solidification.* Journal of the American Oil Chemists Society, 1989. **66**(10): p. 1494-1498.
62. Feuge, R.O., et al., *Tempering Triglycerides by Mechanical Working.* Journal of the American Oil Chemists Society, 1962. **39**(7): p. 310-&.
63. MacMillan, S.D., et al., *Identification of the initial nucleating form involved in the thermal processing of cocoa butter fat as examined using wide angle X-ray scattering (WAXS).* Crystal Growth & Design, 2003. **3**(2): p. 117-119.
64. Ziegleder, G., *Vorkristallisation von Schokoladen.* Susswaren, 1993. **1-2**: p. 54-58.
65. Windhab, E., E. Niediek, A,, and L. Rolfes, *Tieftemperature-Scherkristallisation.* Susswaren, 1993. **3**: p. 32-37.
66. Mazzanti, G., et al., *A conceptual model for shear-induced phase behavior in crystallizing cocoa butter.* Crystal Growth & Design, 2007. **7**(7): p. 1230-1241.

67. Higaki, K., et al., *Effects of ultrasonic irradiation on crystallization behavior of tripalmitoylglycerol and cocoa butter.* Journal of the American Oil Chemists Society, 2001. **78**(5): p. 513-518.
68. Dimick, P.S. and D.M. Manning, *Thermal and Compositional Properties of Cocoa Butter During Static Crystallization.* Journal of the American Oil Chemists Society, 1987. **64**(12): p. 1663-1669.
69. Narine, S.S. and A.G. Marangoni, *Relating the structure of fat crystal networks to mechanical properties : a review.* Food Research International, 1999. **32**(4): p. 227-248.
70. Hodge, S.M. and D. Rousseau, *Fat bloom formation and characterization in milk chocolate observed by atomic force microscopy.* Journal of the American Oil Chemists Society, 2002. **79**(11): p. 1115-1121.
71. Tietz, R.A. and R.W. Hartel, *Effects of minor lipids on crystallization of milk fat-cocoa butter blends and bloom formation in chocolate.* Journal of the American Oil Chemists Society, 2000. **77**(7): p. 763-771.
72. Vaeck, S.V., *Kakaobutter und Fettreif.* International Chocolate Review, 1961. **16**: p. 442-459.
73. Vaeck, S.V., *Uber Kakaobutter und den Fettreif von Kakao-Erzeugnissen.* Fette Seifen Anstrichmittel, 1960. **62**(8): p. 709-722.
74. Brunello, N., *The Rheology of Cocoa Butter in Relation to its Crystallization Behaviour and Microstructure*, in *Department of Food Science*. 2002, University of Guelph: Guelph. p. 128.
75. Narine, S.S. and A.G. Marangoni, *Relating structure of fat crystal networks to mechanical properties: a review.* Food Research International, 1999. **32**(4): p. 227-248.
76. Narine, S.S. and A.G. Marangoni, *Mechanical and structural model of fractal networks of fat crystals at low deformations.* Physical Review E, 1999. **60**(6): p. 6991-7000.
77. deMan, J.M., *Relationship amoung chemical, physical and textural properties of fats*, in *Physical properties of fats, oils and emulsions*, N. Widlak, Editor. 1999, AOCS Press: Champaign, IL USA. p. 79-95.
78. deMan, J.M., *Texture of fats and fat products*, in *Rheology and texture in food quality*, D.W. Stanley, Editor. 1976, AVI Press: Westport, CT. p. 355-381.
79. Campos, R., S.S. Narine, and A.G. Marangoni, *Effect of cooling rate on the structure and mechanical properties of milk fat and lard.* Food Research International, 2002. **35**(10): p. 971-981.
80. Hohne, G.W.H., W.F. Hemminger, and H.-J. Flammersheim, *Differential Scanning Calorimetry*. 2nd ed. 2003, Berlin Heidelberg New York: Springer-Verlag. 298.
81. Höhne, G., *Differential scanning calorimetry : an introduction for practitioners*. 2nd rev. and enl. ed. ed. 2003, New York: Springer. 298.
82. Fang, T.N., et al., *Rheological Behaviour of Cocoa Dispersions.* Journal of Texture Studies, 1995. **26**(2): p. 203-215.
83. Olhero, S.M. and J.M.F. Ferreira, *Influence of particle size distribution on rheology and particle packing of silica-based suspensions.* Powder Technology, 2004. **139**(1): p. 69-75.

84. Guthrie, S.E., G. Mazzanti, and S.H.J. Idziak, *X-ray phase identification of chocolate is possible without the removal of sugar.* European Journal of Lipid Science and Technology, 2005. **107**(9): p. 656-659.
85. Press, W.H., et al., *Numerical recipes example book (C)*. 2nd ed. 1992, Cambridge, England: Cambridge University Press.
86. Rabinovich, M.K., V.G. Kudryashov, and M.V. Markushev, *Effect of grain size on the structural strength of the aluminum alloy AMg6.* Metal Science and Heat Treatment, 1988. **30**(8): p. 609-612.
87. Kirchner, H.P. and R.M. Gruver, *Strength-Anisotropy-Grain Size Relations in Ceramic Oxides.* Journal of the American Ceramic Society, 1970. **53**(5): p. 232-236.
88. Matsuo, Y., et al., *Magnetic properties and mechanical strength of MnZn ferrite.* IEEE Transactions on Magnetics, 2001. **37**(4): p. 2369-2372.